Contribution to the biochemical characterization of astrocytes expressing a mitochondrial-tagged form of catalase

Nicoló Bonora

Director: Prof. Dr. D. Juan Pedro Bolaños Hernández

Salamanca, 2018

Juan Pedro Bolaños Hernández, Catedrático de Bioquímica y Biología Molecular de la Universidad de Salamanca,

Autoriza:

La presentación de la Tesis Doctoral titulada "Contribution to the biochemical characterization of astrocytes expressing a mitochondrial-tagged form of catalase", que ha sido realizada bajo mi dirección por el Licenciado en Farmacia D. Nicoló Bonora, en el Departamento de Bioquímica y Biología Molecular y en el Instituto de Biología Funcional y Genómica, de la Universidad de Salamanca. En mi opinión, reúne todos los requisitos científicos y formales para ser defendida y optar al Título de Doctor Internacional.

Salamanca, a 20 de marzo 2018

Fdo.: Juan Pedro Bolaños Hernández

What made Galileo point his telescope to the sky,

Lavoisier develop new techniques to investigate matter,

and Einstein spend sleepless nights wondering

about the ultimate law of the Universe?

Curiosity, yes, and a sense of beauty.

ABBREVIATIONS

6PGD: 6-phosphogluconate dehydrogenase

AMC: 7-amino-4-methylcoumarin

ARE: Antioxidant response element

ATP: Adenosine triphosphate

APN: Aminopeptidase N

BSA: Bovine serum albumine

CAT: Catalase

cDNA: complementary DNA

CO_2: Carbon dioxide

CSP-3: Caspase-3

C_t: Threshold cycle

Cul3: Culin 3

Cys: Cysteine

Cyt c: Cytochrome c

DAPI: 4',6-Diamidino-2-phenylindole

DIV: Days *in vitro*

DMEM: Dulbecco's Modified Eagle Medium

DNA: Deoxiribonucleic acid

DNL: *de novo* lipogenesis

$\Delta\Psi_m$: Mitochondrial membrane potential

ETC: Electron transport chain

G6PD: Glucose-6-phosphate dehydrogenase

GAPDH: Glyceraldehyde-3-phosphate dehydrogenase

GCL_c: Glutamate cysteine ligase catalytic subunit

GCL_m: Glutamate cysteine ligase modifier subunit

γ-GC: Gamma glutamylcysteine

γ-GT: Gamma glutamyltranspeptidase

GPx: Glutathione peroxidase

GSH: Reduced glutathione

GSSG: Glutathione disulphide

GS: Glutathione synthetase

HA: Hemagglutinin

HDAC4: Histone deacetylase 4

HIF-1α: Hypoxia-inducible factor 1α

HO-1: Heme oxygenase 1

KEAP1: Kelch like ECH associated protein 1

KRPG: Krebs-Ringer phosphate buffer

mCAT: Mitochondrial Catalase

MEFs: Murine embryonic fibroblasts

miRNA: Micro ribonucleic acid

mRNA: Messenger ribonucleic acid

mROS: Mitochondrial reactive oxygen species

MRP1: Multidrug resistance-associated proteine 1

$NAPD^+$: Nicotinamide adenine dinucleotide phosphate oxidized form

NADPH: Nicotinamide adenine dinucleotide phosphate reduced form

NOX: NADPH oxidase

NQO1: NADPH quinone dehydrogenase 1

NRF1: Nuclear factor (erythroid-derived 2)-like 1

NRF2: Nuclear factor (erythroid-derived 2)-like 2

NRF2 PM: NRF2 phosphomimetic form

NRF3: Nuclear factor (erythroid-derived 2)-like 3

PBS: Phosphate buffer saline

PCR: Polimerase chain reaction

PPP: Pentose phosphate pathway

Prx: Peroxiredoxin

ROS: Reactive oxygen species

RT-qPCR: Real time quantitative polimerase chain reaction

S. E. M.: Standard error of the mean

Ser: Serine

SOD1 or Cu/ZnSOD: Superoxide dismutase 1

SOD2 or MnSOD: Superoxide dismutase 2

SOD3: Superoxide dismutase 3

Thr: Threonine

Trx: Thioredoxin

TKT: Transketolase

VDAC: Voltage-dependent anion channel

WT or +/+: Wild type

INTRODUCTION 1

1. REACTIVE OXYGEN SPECIES (ROS) 3

1.1. Intracellular sources of ROS 4

1.1.1 Mitochondria 4

1.1.2 NADPH oxidases 5

1.1.3 Other intracellular sources of ROS 6

1.1.4 ROS production in the brain 7

1.2. Antioxidant systems in the central nervous system 7

1.3. ROS functions in cellular signaling 9

1.3.1 ROS chemistry sets target specificity 10

1.3.2 ROS modulate crucial pathways 12

1.3.2.1. ROS modulate the HIF-1α pathway 12

1.3.2.2. ROS modulate the NRF2 pathway 13

1.3.2.3. ROS modulate the cellular growth 13

1.3.2.4. ROS modulate cellular differentiation 13

1.3.2.5. ROS and aging 14

2. NRF2 PATHWAY 16

2.1. Structure and functions of NRF2 17

2.1.1 Structure of NRF2 17

2.1.2 Functions of NRF2 18

2.2. Regulation of the NRF2 pathway 19

2.2.1 Models of NRF2-KEAP1 regulation 20

2.2.2 Non-canonical regulation of the NRF2 pathway 21

2.2.3 The NRF2 pathway in the central nervous system 22

3. GLUTATHIONE IN THE BRAIN 23

3.1. Functions of glutathione 24

3.2. Synthesis of glutathione 25

3.3. Regulation of glutathione biosynthesis 27

3.4. Astrocyte-neuron glutathione shuttle 27

4. PENTOSE PHOSPHATE PATHWAY (PPP) 30

4.1. Functions of the PPP in the brain 33

4.2. Regulation of the PPP 34

HYPOTHESIS AND OBJECTIVES 37

1. HYPOTHESIS 39

2. OBJECTIVES 40

MATERIAL AND METHODS 43

1. ANIMALS 45

1.1. +/mCAT mouse line generation 45

1.2. Tissue extraction 47

1.3. DNA extraction 47

1.4. Genotyping 48

1.5. Gel electrophoresis 49

2. CELL CULTURES 49

2.1. Mouse embryonic fibroblasts (MEFs) immortalization 49

2.2. Neurons in primary cultures 49

2.3. Astrocytes in primary culture 51

2.4. Astrocyte-neuronal co-culture 51

3. CELL TRANSFECTION 52

4. ROS MEASUREMENTS 53

4.1. Hydrogen peroxide 53

4.2. mROS 54

4.3. Extracellular superoxide 55

5. MITOCHONDRIAL MEMBRANE POTENTIAL MEASUREMENT 55

6. PROTEIN EXTRACTION 56

6.1. Total protein extraction 56

6.2. Cytosolic and nuclear fractionation *in vitro* 56

6.3. Cytosolic and nuclear fractionation *ex vivo* 58

6.4. Cytosolic and mitochondrial fractionation 59

6.5. Protein concentration determination 60
7. ELECTROPHORESIS AND PROTEIN IMMUNODETECTION (WESTERN BLOT) 61
8. MITOCHONDRIA ISOLATION 63
9. mCAT ACTIVITY MEASUREMENT 64
10. IMMUNOCYTOCHEMISTRY 66
11. RNA PURIFICATION 67
12. REAL TIME QUANTITATIVE POLYMERASE CHAIN REACTION 68
13. miRNA EXPRESSION ANALYSIS 70
13.1. miRNA reverse transcription 70
13.2. Pre-PCR amplification 70
13.3. miRNA expression analysis using 48.48 dynamic array 71
14. GLUTATHIONE CONCENTRATION DETERMINATION 71
15. CASPASE-3 ACTIVITY DETERMINATION 73
16. PENTOSE-PHOSPHATE PATHWAY (PPP) FLUX MEASUREMENT 73
17. NADPH/NADP$^+$ RATIO DETERMINATION 78
18. *de novo* LIPOGENESIS FLUX MEASUREMENT 78
19. STATISTICAL ANALYSIS 79

RESULTS 81

1. mCAT expression down-modulates endogenous mROS in MEFs 83
2. Endogenous mROS modulate NRF2 abundance and activity in immortalized MEFs 86
3. mCAT expression down-modulates physiological endogenous mROS in primary astrocytes 88
4. Generation of constitutive +/mCAT mouse 89
5. mCAT constitutive expression in MEFs down-modulates hydrogen peroxide release 90
6. mCAT constitutive expression in primary astrocytes 91

7. Constitutive expression of mCAT efficiently detoxifies hydrogen peroxide and down-modulates endogenous ROS in primary astrocytes 93
8. Down-modulation of endogenous mROS does not affect astrocytic survival 96
9. Endogenous mROS modulate nuclear accumulation of NRF2 in primary astrocytes and *in vivo* 97
10. Endogenous mROS modulate NRF2 functional activity in primary astrocytes 101
11. Down-modulation of endogenous mROS increases the abundance of pentose phosphate pathway (PPP)-related enzymes 102
12. Down-modulation of endogenous mROS increases miR-1 and miR-206 expression in astrocytes 104
13. Down-modulation of endogenous mROS increases glucose flux through PPP 106
14. Endogenous mROS modulate extracellular superoxide production in primary astrocytes 107
15. Rescue of the NRF2 levels decreases extracellular superoxide release by primary astrocytes 109
16. Endogenous mROS modulate glutathione abundance in primary astrocytes *via* NRF2 111
17. Neurons co-cultured with mROS-weakened astrocytes show less antioxidant defenses, and higher ROS release and apoptosis 114
18. Expression of NRF2 PM in mCAT astrocytes rescues the antioxidant defenses and survival of neurons 117

DISCUSSION 120

1. Expression of a mitochondrial form of catalase allows to investigate physiological roles of mROS 121
2. Endogenous mROS modulate redox homeostasis in primary astrocytes *via* the NRF2 pathway 122

3. Endogenous mROS modulate glucose flux through the pentose phosphate pathway (PPP)..... 123
4. Endogenous mROS are neuroprotective 123

CONCLUSIONS 127

RESUMEN EN ESPAÑOL 133

1. INTRODUCCIÓN..... 135
2. HIPÓTESIS 137
3. OBJETIVOS..... 138
4. RESULTADOS..... 139
1. Generación del ratón +/mCAT constitutivo..... 139
2. Expresión constitutiva de la mCAT en los astrocitos primarios..... 139
3. La mCAT constitutiva destoxifica eficientemente el peróxido de hidrogeno y disminuye los niveles de los ROS endógenos en los astrocitos primarios..... 141
4. Los mROS endógenos modulan la acumulación nuclear y la actividad funcional de NRF2 en astrocitos primarios..... 144
5. La disminución de los niveles de mROS endógenos aumenta la abundancia de los enzimas de la PPP..... 145
6. La disminución de los niveles de los mROS endógenos aumenta la expresión de miR-1 y miR-206 147
7. La disminución de los niveles de los mROS endógenos aumenta el flujo de glucosa hacia la PPP 148
8. Los mROS endógenos modulan la producción de superóxido extracelular en los astrocitos 149
9. El rescate de los niveles de NRF2 disminuye la liberación de superóxido en los astrocitos 151
10. Los mROS endógenos modulan la abundancia del glutatión en astrocitos primarios a través de la vía NRF2 153
11. Las neuronas co-cultivadas con astrocitos +/mCAT presentan menos defensas antioxidantes, un aumento de la liberación de ROS y más apoptosis .. 156

12. La expresión de NRF2 PM en los astrocitos +/mCAT restablece las defensas antioxidantes y la supervivencia de las neuronas 157

5. DISCUSIÓN 159

6. CONCLUSIONES 164

REFERENCES 169

ACKNOWLEDGEMENTS 193


INTRODUCTION

1. REACTIVE OXYGEN SPECIES (ROS)

The advent of oxygen into the Earth's atmosphere was a crucial event that promoted the evolution of aerobic organisms, which are able to produce energy in a very efficient manner. One of the consequences of this improvement was the appearance of novel reactive molecules derived from oxygen, the reactive oxygen species (ROS) (**Figure I**).

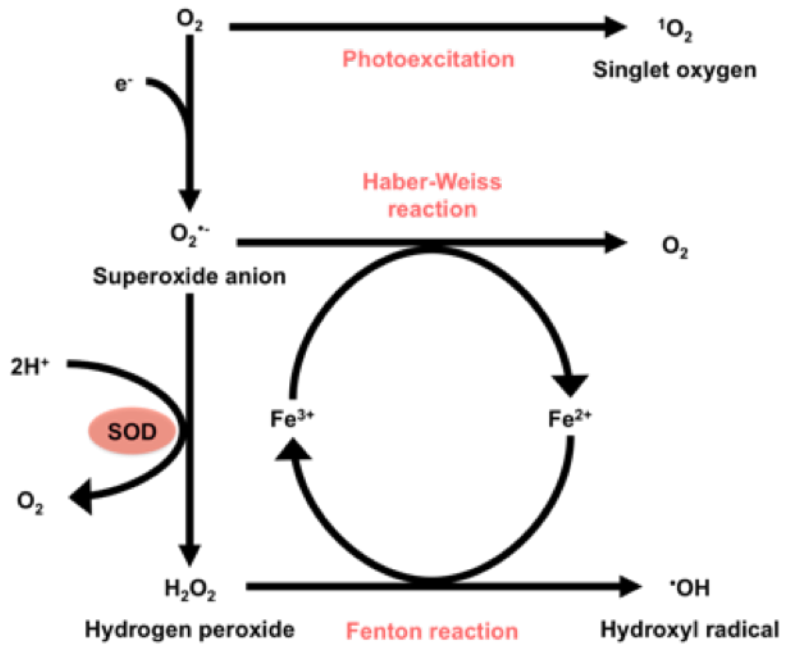

Figure I: Main mechanisms of cellular ROS production. Due to the high ROS reactivity, the interaction between different pathways is possible, in which the product of a reaction is used to generate new ROS. SOD: superoxide dismutase.

ROS include the superoxide ($O_2^{\bullet-}$), hydrogen peroxide (H_2O_2) and hydroxyl radical ($^\bullet OH$). These species present higher chemical reactivity than oxygen and they are able to trigger both physiological and pathological processes. In general terms, under normal conditions, the level of cellular ROS is constant in a dynamic equilibrium, and this balance is modulated by cellular processes that produce ROS and eliminate them (Zhang *et al.*, 2016). However, under certain circumstances,

the rate of ROS production exceeds the ability of the antioxidant systems to eliminate them. This excess ROS, commonly called "oxidative stress", results in the oxidation of proteins, nucleic acids and lipids (Poyton *et al*., 2009; Temple *et al*., 2005). Oxidative stress can trigger damage that can lead to the activation of autophagy of certain organelles, even leading to cell death (Brand, 2010). Indeed, in *post-mortem* brain samples of neurological diseases, there are signs of oxidative stress in neurons within the degenerating brain areas (Cannon and Greenamyre 2013; Federico *et al*., 2012). Thus, oxidative stress appears to be associated with the cause of neurodegenerative diseases. However, all clinical trials based on an antioxidant strategy performed so far in several neurodegenerative diseases were not conclusive (Halliwell 2013; Heyland *et al*., 2013; Kamat *et al*., 2008; Snow *et al*., 2010), hence arguing against a pathological role of ROS. The reason is yet unknown, although has been suggested to be ascribed to the wrong design of the treatment with the antioxidants (Halliwell 2013; Kamat *et al*., 2008). However, the option that ROS physiologically modulate survival pathways, hence antioxidant will be deleterious, has received none or very little attention.

1.1. Intracellular sources of ROS

Various organelles within the cell can generate ROS physiologically. These include mitochondria, the endoplasmic reticulum and peroxisomes. In addition, various enzymes, including oxidases and oxygenases, generate ROS as part of their reaction cycles (Holmström and Finkel, 2014). Furthermore, ROS generation is species-, cell- and tissue-specific and also depends on the physiopatological state of the cells. For these reasons, defining the major intracellular source of ROS is complex. The best-characterized intracellular sources of ROS are described in the successive sections.

1.1.1 Mitochondria

From a quantitative perspective, mitochondria are the largest sources of ROS within most mammalian cells (Murphy, 2009). These organelles generate ATP in an oxygen-dependent manner, during which the flow of electrons

culminates at complex IV of the electron transport chain (ETC), with the reduction of oxygen to water. Throughout this process, 1-3% oxygen can also undergo a one-electron reduction to generate superoxide (Green *et al.*, 2011; Murphy, 2009). Within the mitochondria eight sites of superoxide production have been identified (**Figure II**). The major sites of superoxide production are complexes I and III of the ETC (Brand, 2010). Superoxide is rapidly converted into hydrogen peroxide by superoxide dismutase 2 (SOD2 or MnSOD), located within the mitochondria.

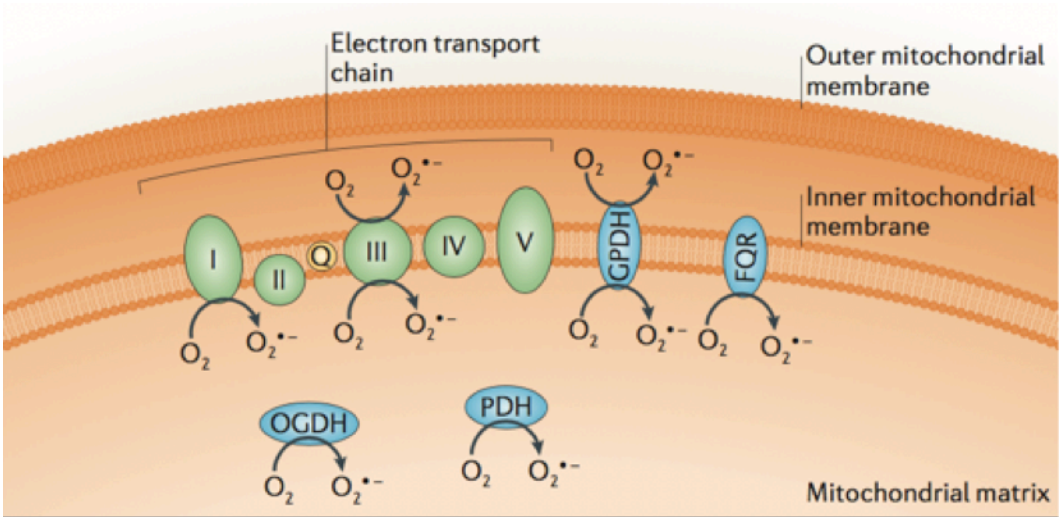

Figure II: Superoxide production within the mitochondria. Mitochondria are the largest source of ROS in most of mammalian cell types. Complexes I and III are the major sites of superoxide production. Other contributors include metabolic enzymes in the mitochondrial matrix, such as OGDH (2-oxoglutarate dehydrogenase) and PDH (pyruvate dehydrogenase), and the mitochondrial membrane forms of GPDH (Glycerol 3-phosphate dehydrogenase) and the FQR (electron transfer flavoprotein-ubiquinone oxidoreductase, mitochondrial) system. Obtained from Holmström and Finkel, 2014.

1.1.2 NADPH oxidases

The family of the NADPH oxidases is another important intracellular source of ROS. NADPH oxidases, known as NOX enzymes, are multi-subunit enzymes which primary catalytic function is the generation of ROS (Belarbi *et al.*, 2017). The major source of ROS generation is a flavin- and haem-containing protein complex that transfer electrons from cytosolic NADPH to oxygen to

purposely produce superoxide or hydrogen peroxide (Holmström and Finkel, 2014).

Seven members of the NOX family were described in humans, NOX1-5 and Duox1-2, which they differ for the specific ROS produced and for the sub-cellular localization. NOX1, -2, -3 and -5 and Duox1 and -2 are anchored to the plasma membrane and they release superoxide in the extracellular space, participating in processes like the innate immunity (NOX2) or in the control of the arterial pressure (NOX1) (Altenhöfer *et al*., 2012). NOX4 mainly produce hydrogen peroxide and is localized in the mitochondrial and endoplasmic reticulum membranes (Block *et al*., 2009; Petry *et al*., 2006). Therefore, depending on the cell state, the subcellular localization, the cell type and the specific NOXs isoforms expressed, NOX-derived ROS could participate differently in redox signaling (Lambeth and Neish, 2014). The distribution of NOXs in the brain shows that neurons express NOX1, -2 and -4, whereas astrocytes mostly NOX2, but also NOX1 and -4 (Belarbi *et al*., 2017; Nayernia and Jaquet, 2014). The majority of studies on the physiological roles of NOXs in the central nervous system have focused on their participation in the host defense. However, under basal conditions, NADPH oxidases produce small amounts of ROS, which the most probable function is redox signaling (Nayernia and Jaquet, 2014).

1.1.3 Other intracellular sources of ROS

In addition to mitochondria and the NOX family, there are a wide range of enzymes, such as xanthine oxidase, nitric oxide synthase, cyclooxygenases, cytochrome P450 enzymes and lipoxygenases, that are able to produce ROS (Holmström and Finkel, 2014). Furthermore, organelles like peroxisome and the endoplasmic reticulum can produce oxidants. The relative contribution of these additional sources of ROS varies according to cell type, but, in basal conditions, they are usually smaller compared to mitochondria or NOXs (Holmström and Finkel, 2014).

1.1.4 ROS production in the brain

Within the central nervous system the production of ROS differs between the cell types. Neurons and astrocytes, the two most abundant cell types in the brain, present a differential pattern of mitochondrial ROS (mROS) production, with glial cells producing mROS severalfold faster than neurons (Lopez-Fabuel *et al*., 2016). However, the physiological role of this major mROS production by astrocytes is still elusive. These differences are explained by the different organization of the mitochondrial respiratory chain between the two cell types. Astrocytes present less complex I assembled in supercomplexes and more free complex I compared to neurons (Lopez-Fabuel *et al*., 2016). These data confirm the higher mROS production by free complex I, compared to the complex I assembled in supercomplexes, previously seen in liposomes (Maranzana *et al*., 2013). Furthermore, this different assembly of complex I into supercomplexes between neuronal and glial cells could explain their bioenergetic differences. Neurons present a higher respiration rate compared with astrocytes (Lopez-Fabuel *et al*., 2016), which is consistent with the dependency of neural cells on oxidative phosphorylation for neurotransmission and survival (Almeida *et al*., 2001; Almeida *et al*., 2004; Herrero-Mendez *et al*. 2009) and with the glycolytic metabolism of astrocytes (García-Nogales *et al*., 2003; Herrero-Mendez *et al*., 2009).

1.2. Antioxidant systems in the central nervous system

To maintain the redox homeostasis, and therefore to counteract the deleterious effects of excess ROS, brain cells have developed several enzymatic antioxidant systems (**Figure III**). Superoxide is rapidly inactivated and converted to hydrogen peroxide by superoxide dismutase (SOD). There are three isoform of this enzyme, depending on its localization: SOD1 or Cu/Zn-SOD (cytosolic), SOD2 or Mn-SOD (mitochondrial) and SOD3 (extracellular).

Considering its pro-oxidant properties and its role in cell signaling, the levels of hydrogen peroxide need to be tightly regulated, for which cells use different enzymatic systems that neutralize it to water. The most important are peroxiredoxins (Prxs), glutathione peroxidases (GPxs) and catalase.

Catalase is an haem-containing enzyme localized in the peroxisomes that converts hydrogen peroxide to water in a direct manner (Dringen *et al*., 2005). Peroxiredoxins are a family of peroxidases that contribute to the elimination of organic hydroperoxides and hydrogen peroxides (Circu and Aw, 2010). To do so, peroxiredoxins posess an active site containing cysteines able to oxidize themselves at sulphenic acid (Cys-SOH) and subsequently to condense with a cysteine localized in the C-terminal subunit to form a disulphide (D'Autréaux and Toledano, 2007). This disulphide is then reduced by the thioredoxin (Trx)/thioredoxin reductase (TrxR) system at the expense of an equivalent of NADPH to regenerate cysteine moieties of peroxiredoxin (Patenaude *et al*., 2005). Glutathione peroxidases (GPx) convert hydrogen peroxide to water at the expense of the tripeptide glutathione (GSH, γ-glutamyl-cysteinyl-glicine) which become oxidized to its disulphide form GSSG (Flohé *et al*., 2011). GSH is then regenerated by glutathione reductase (GR), which transfers electrons from NADPH to GSSG (Dringen *et al*., 2005). Since it provides reducing equivalents for the regeneration of GSH, NADPH plays a pivotal role in the redox homeostasis of the brain, especially in neurons (Bouzier-Sore and Bolaños, 2015). These cells contains very low amounts of glutathione (Bolaños *et al*., 1995; Dringen *et al*., 1999), hence the recycling of GSH from GSSG is critical for their survival. Most of the cytosolic pool of NADPH is produced in the pentose phosphate pathway (PPP) (Wamelink *et al*., 2008), underlying the interconnections between the glucose metabolism and redox homeostasis within the central nervous system.

Considering that the hydrogen peroxide concentration needs to be strictly regulated spatially and temporarily, mammalian cells express several isoforms of peroxiredoxins, thioredoxins and glutathione peroxidases in the cytosol, nucleus, endoplasmic reticulum and mitochondria (Hekimi *et al*., 2011; Marí *et al*., 2009; Perkins *et al*., 2015).

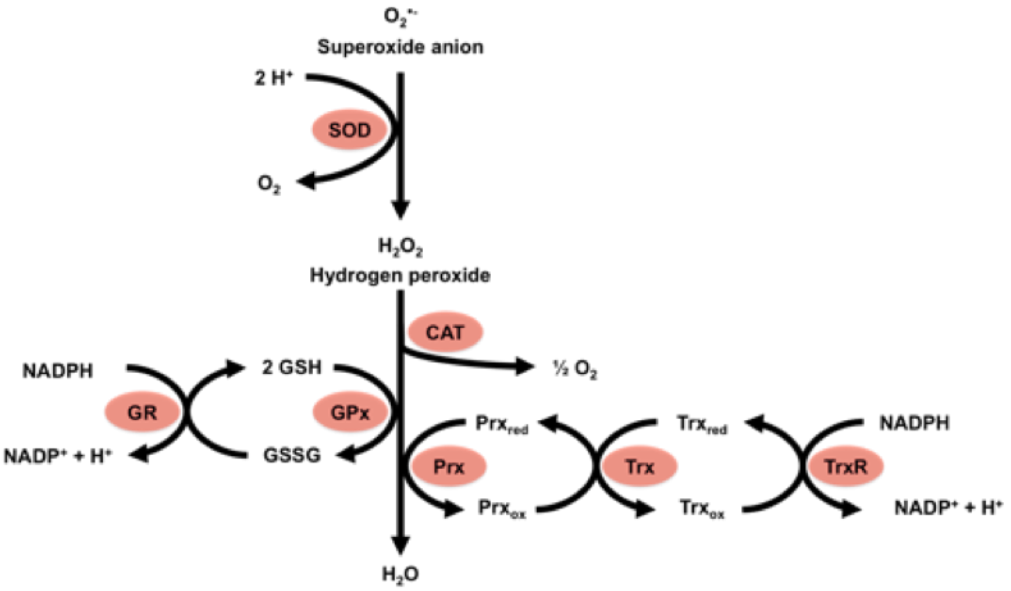

Figure III: Main antioxidant systems within the cell. Superoxide is converted to hydrogen peroxide by superoxide dismutase (SOD). Hydrogen peroxide is neutralized to water by several enzymes, including catalase (CAT), peroxiredoxins (Prx) or glutathione peroxidase (GPx). The thioredoxin (Trx) / thioredoxin reductase (TrxR) system regenerates the reduced form of peroxiredoxin (Prx_{red}). GR: glutathione reductase, GSH: glutathione reduced form, GSSG: glutathione disulphide form, $NADP^+$: nicotinamide adenine dinucleotide phosphate oxidized form, NADPH: nicotinamide adenine dinucleotide phosphate reduced form.

It is a remarkable fact that numerous antioxidant enzymes depend on GSH and other thiols as cofactors. Considering that glutathione is the most abundant mammalian thiol-containing antioxidant (Dringen, 2000), its importance in the redox homeostasis is crucial. For this reason, glutathione metabolism receives a detailed analysis in successive sections.

Besides the enzymatic antioxidant systems, the brain contains ascorbic acid and vitamin E, which act as direct radical scavengers through their hydroxyl moieties. The ascorbate is especially abundant in neurons (Shimizu *et al.*, 1960). Nevertheless, astrocytes possess more vitamin E, compared with neurons, which protects glial cells against mitochondrial oxidative damage (Heales *et al.*, 1994).

1.3. ROS functions in cellular signaling

Traditionally ROS are considered as harmful and unregulated agents, with random intracellular targets. Indeed, due to their greater chemical reactivity, ROS oxidize

lipids, DNA and proteins and this may lead to the accumulation of damaged biomolecules, and contribute to a range of pathologies. Although this nonspecific, random and damaging aspect of ROS biology persists, a growing body of evidence now suggests that ROS act as signaling molecules in several physiological processes (D'Autréaux and Toledano, 2007; Holmström and Finkel, 2014; Wang and Hai, 2016). However, this view is not free from controversy.

1.3.1 ROS chemistry sets target specificity

The scepticism about the physiological functions of ROS as second messenger stems from the idea that they lack of the specificity required for signaling processes. While this might be true for hydroxyl radical, which has indiscriminate reactivity toward biomolecules (D'Autréaux and Toledano, 2007), superoxide and hydrogen peroxide have specific biological targets. This specificity comes from their chemical proprieties, which include reactivity, half-life and lipid solubility (D'Autréaux and Toledano, 2007).

The instability of superoxide and its inability to cross membranes make this ROS a poor signaling molecule (D'Autréaux and Toledano, 2007). In contrast to superoxide, the chemical characteristics of hydrogen peroxide make this ROS more suitable for signaling. First of all, hydrogen peroxide is able to cross membranes by diffusion or, more rapidly, transported by a specific aquaporin, the peroxiporin (Bienert *et al*., 2007). Moreover, its relative stability compared to other ROS (cellular half life ~1 ms, *in vivo* concentration ~10^{-7} M) supports its role in redox signaling (Giorgio *et al*., 2007). Last, but not less important, hydrogen peroxide is a poor oxidant and reacts mildly with [Fe-S] clusters, very slowly with glutathione and free cysteine (Cys) and methionine (Met), and it loosely binds metals. However, its reactivity towards Cys residues can significantly increase, depending on the protein environment (D'Autréaux and Toledano, 2007). In addition, the ability of Cys residues to cycle between different stable redox forms, makes them the ideal hydrogen peroxide target for redox signaling (Holmström and Finkel, 2014). It should to be noted that only the forms of Cys that can be reversibly oxidized operate in redox signaling. An

irreversible oxidation of Cys result in permanent protein damage that might lead to oxidative stress (Schieber and Chandel, 2014).

Cysteines residues are not equally reactive, providing the basis for selectivity and specificity. Their reactivity is dictated by their solvent-exposed localization, ionization state and protein environment (D'Autréaux and Toledano, 2007). Depending on their pK_a, Cys might exist as a thiolate anion (Cys-S^-) at physiological pH and they are more susceptible to oxidation compared with the protonated cysteine thiol (Cys-SH) (Finkel, 2012). During redox signaling, hydrogen peroxide oxidizes the thiolate anion to the sulphenic form (Cys-SOH), causing allosteric changes within the protein that modulates its function (Holmström and Finkel, 2014) (**Figure IV**).

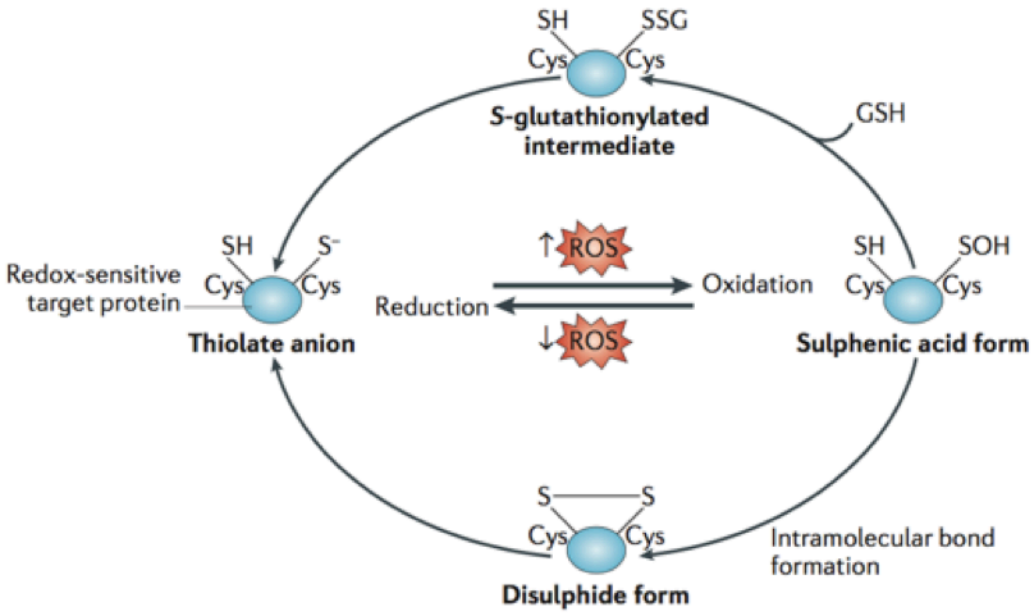

Figure IV: Reversible modulation of reactive Cys residues. Redox-sensitive target proteins present reactive Cys residues that could form thiolate anions (-S^-) at physiological pH. Oxidation of this residue results in a sulphenic acid moiety (-SOH) that leads to a change in function of the target protein. The sulphenic acid form could form an intramolecular disulphide bond or conjugate with glutathione (GSH) to form an S-glutathionylated (-SSG) intermediate. Obtained from Holmström and Finkel, 2014.

Aside from the specificity and selectivity of ROS on their targets, the compartmentalization of ROS production within cells is an important determinant of whether damage or redox signaling occurs. In order to obtain an effective redox

signaling, the hydrogen peroxide-dependent oxidation of a given protein is likely to occur close to the source of hydrogen peroxide production (Schieber and Chandel, 2014). For example, mitochondria are very dynamic organelles that move to their targets, allowing mitochondrially generated hydrogen peroxide to activate specific pathways (Al-Mehdi *et al.*, 2012).

1.3.2 ROS modulate crucial pathways

Reactive oxygen species, in particular hydrogen peroxide, are second messengers able to modulate pathways involved in nuclear transcription, cellular differentiation, cell death and ageing, among others.

1.3.2.1. ROS modulate the HIF-1α pathway

Mammalian cells possess several redox-sensitive transcription factors, which modulate the transcription of genes involved in different biological processes following a ROS-mediated activation. The family of the hypoxia-inducible factors (HIFs) orchestrates the transcriptional response to hypoxia, promoting expression of erythropoietin to enhance red blood cell production, vascular endothelial growth factor to promote new blood vessel formation, and glycolytic enzymes to maintain ATP levels. Under normal oxygen conditions, prolyl hydroxylase domain protein 2 (PHD2) hydroxylates HIF-1α at two proline residues (Pro402 and Pro564), which targets the transcription factor for pVHL-dependent proteasomal degradation (Kaelin and Ratcliffe, 2008). When oxygen levels decrease below 5%, PHD2 is inhibited, allowing the HIF-1α stabilization and its translocation to the nucleus where it forms a heterodimer with HIF-1β, which binds the hypoxia response elements (HRE) to initiate gene transcription. Early evidences that suggest that mROS modulate HIF-transcription activity came from the observations that cells depleted of mitochondrial DNA (ρ^o cells) do not stabilize HIF-1α during hypoxia (Chandel *et al.*, 1998). These ρ^o cells lack a functional electron transport chain (ETC) and could not increase mROS under hypoxia. Wild type cells treated with ETC inhibitors phenocopied the ρ^o cells (Chandel *et al.*, 2000). The critical experiment that demonstrates that mROS, and not oxidative phosphorylation, stabilize HIF-1α under hypoxia was performed in

cells lacking the complex III subunit *cytochrome b* (Bell *et al*., 2007). These *cytochrome b* null cells cannot perform oxidative phosphorylation but can produce mROS and stabilize HIF-1α during hypoxia.

1.3.2.2. ROS modulate the NRF2 pathway

The transcriptional activity of the nuclear factor (erythroid-derived-2)-like 2 (NRF2), the master regulator of the antioxidant response, is modulated similarly to HIF-1α. Under basal conditions, NRF2 is kept in the cytosol by associating with Kelch-like ECH-associated protein 1 (KEAP1) and the E3 ubiquitin ligase cullin 3 (CUL3), forming a complex that facilitates the ubiquitination and the subsequent proteasomal degradation of NRF2 (Kobayashi *et al*., 2004). Acting as a stress sensor, KEAP1 presents multiple thiols, which are direct targets of oxidants and electrophiles. Modifications of these thiols result in a conformational change of KEAP1 leading to the nuclear accumulation of NRF2 (Taguchi *et al*., 2011). Once in the nucleus, NRF2 binds the antioxidant response element (ARE, 5'-TGACnnnGC-3') and promotes the transcription of a plethora of genes involved in the response to different cellular stresses (Taguchi *et al*., 2011). Considering the crucial role of this pathway in the redox homeostasis, NRF2 receives a detailed analysis in successive sections.

1.3.2.3. ROS modulate the cellular growth

Hydrogen peroxide is required for activation of a number of cellular pathways involved in physiological and oncogenic cellular growth. The induction of cell proliferation by several growth factors (such as epidermal growth factor, platelet-derived growth factor, nerve growth factor and insulin) correlates with a transient increase of intracellular hydrogen peroxide, whereas antioxidant treatments prevent DNA synthesis (Finkel, 2000). Similarly, cellular transformation following the expression of activated oncogenes (such as Ras or overexpressed *myc*) is associated with increased intracellular hydrogen peroxide and is prevented by antioxidants (Giorgio M, *et al*., 2007).

1.3.2.4. ROS modulate cellular differentiation

ROS are also essential for stem-cell differentiation. Scavenging ROS by overexpression of glutathione peroxidase retards differentiation of *Drosophila* multipotent hematopoietic progenitors, while increasing mROS by depletion of the mitochondrial complex I protein ND75 or deletion of SOD2 increased differentiation (Owusu-Ansah and Banerjee, 2009). Another evidence of the importance of redox signaling in stem-cell differentiation comes from the observation that in murine cardiomyocytes the arrest of the cell-cycle through activation of the DNA damage response, was subsequent of a mROS rise (Puente *et al*., 2014). This increase of mROS is consequent of a shift from glycolytic to oxidative metabolism, which occurs within the first week of the mouse life. Scavenging ROS by expressing a mitochondrial form of catalase (mCAT) specifically in cardiomyocites increases the undifferentiated cell number, confirming the critical role of mROS in cell differentiation (Puente *et al*., 2014). Another study shows that the increase of ROS early in neuronal development, due to a NRF2 decline, helps to establish a mildly oxidant environment, which is permissive for signaling pathways sensible to redox modulation involved in neuronal maturation, such as the Wnt pathway (Bell *et al*., 2015).

1.3.2.5. ROS and aging

In the middle of the past century, Denham Harman proposed the "Free radical theory of aging" as a molecular explanation why aging occurs (Harman, 1956). The theory proposes that free radicals, as by-product of oxidative metabolism, cause cumulative cellular damage resulting in overall loss of organismal fitness over time. However, longevity studies in multiple model organisms have not consistently demonstrated that antioxidants prevent aging. Early studies in *Drosophila* suggested that increasing SOD and catalase activity in the cytosol extend longevity (Orr and Sohal, 1994), although other investigators could not replicate these results (Mockett *et al*., 2010). Furthermore, careful measurements of ROS in *Drosophila* have not found any correlation between ROS levels and longevity (Schieber and Chandel, 2014). In mice, overexpression of SOD1 together with catalase or SOD2, does not increase lifespan (Pérez *et al*., 2009). By contrast, the expression of mCAT, but not cytosolic or nuclear catalase, extends the longevity in mice (Schriner *et al*., 2005). The conventional interpretation is

that mCAT detoxifies mitochondrial matrix-generated hydrogen peroxide, preventing hydrogen peroxide-induced damage to mitochondria. An alternative explanation is that detoxification of matrix-generated hydrogen peroxide prevents leakage of hydrogen peroxide into the cytosol, interfering with normal ROS signaling pathways that prevent pathologies such as cancer, a major cause of death in laboratory mice (Schieber and Chandel, 2014). Studies carried out in several model organisms show that a mild increase of ROS could extend lifespan. In yeast, inhibition of target of rapamycin (mTOR) or caloric restriction extends chronological lifespan by increasing mROS (Mesquita *et al*., 2010; Pan *et al*., 2011). In *C. elegans*, loss of mitochondrial SOD but not cytosolic SOD, extend lifetime (Schaar *et al*., 2015). The increased lifespan ROS-mediated has been found also in mammals. Mice heterozygous for *mclk1*, which is required for proper electron transport, show increased mROS (Lapointe *et al*., 2009). Furthermore, these mice present less oxidative damage to cytosolic proteins, supporting a model whereby elevated ROS levels are paradoxically protective through the induction of stress response pathways (Liu *et al*., 2005).

ROS signaling is essential for homeostasis and adaption to stress. Hence, ROS concentration needs to be tightly regulated to maintain an optimal oxidative environment for cellular signaling which is ideal to maintain homeostasis. ROS levels below this range lead to a disruption on redox signaling and loss of homeostasis; by contrast, ROS level above the optimal range cause oxidative stress and aberrant cell signaling, that might results in pathologies such as cancer or neurodegenerative diseases (**Figure V**).

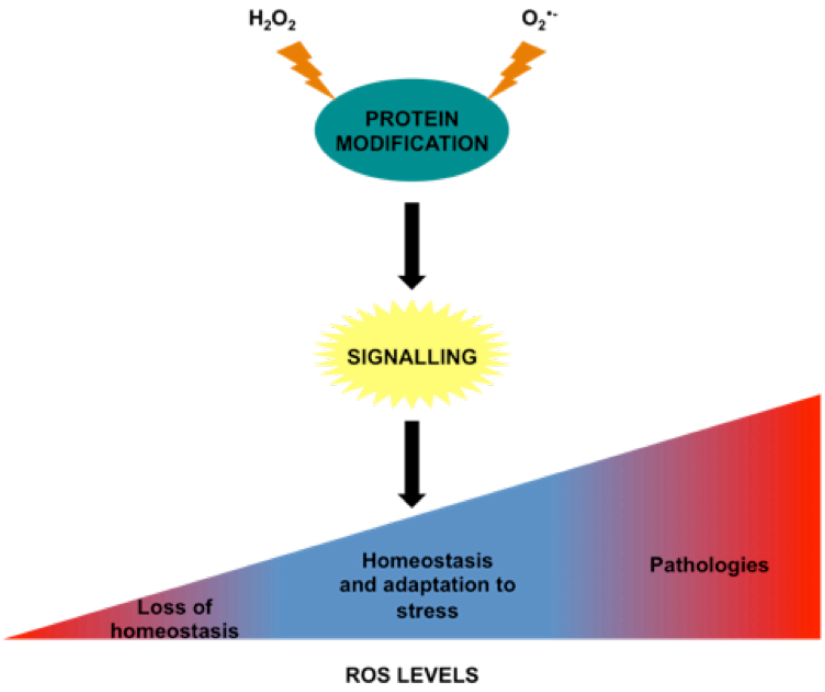

Figure V: ROS signaling. Depending on the ROS levels, redox signaling could be ideal to maintain homeostasis and to adapt to stress. ROS levels above the optimal range cause oxidative stress and aberrant cell signaling resulting in pathologies;, however, ROS levels below this optimal range lead to a disruption of redox signaling resulting in loss of homeostasis.

2. NRF2 PATHWAY

During its life, every organism is challenged to fight against a variety of stressors, both endogenous (such as mROS) and exogenous (such as toxins), that disrupt cellular homeostasis. With the purpose to counteract these insults and survive, organisms evolved several mechanisms to maintain ROS homeostasis. One example is NRF2 or NFE2L2 (Nuclear factor erythroid-derived 2 like 2) pathway, which regulates more than 1% of the human genome encoding metabolic, detoxification, antioxidant and anti-inflammatory cytoprotective proteins (Malhotra *et al.*, 2010).

2.1. Structure and functions of NRF2

NRF2 is encoded by the gene *NFE2L2* and belongs to the family of basic leucine zipper (bZIP) transcription factors (Moi *et al*., 1994). In vertebrates, other members of the CNC-bZIP family include the nuclear factor erythroid-derived 2 like 1 (NRF1) and the nuclear factor erythroid-derived 2 like 3 (NRF3) (Andrews *et al*., 1993; Chan *et al*., 1993; Kobayashi *et al*., 1999) In mammals, NRF1 and NRF2 are well known for their role in the transcriptional modulation of cytoprotective genes in response to stress (Biswas and Chan, 2010; Venugopal and Jaiswal, 1998), although NRF2 appears to be more potent in activating ARE-regulated genes that NRF1 (Jaiswal, 2004). In contrast, NRF3 has been linked to differentiation, inflammation and carcinogenesis (Chevillard and Blank, 2011).

2.1.1 Structure of NRF2

The NRF2 protein in humans is 605 amino acids long and contains seven highly conserved regions known as NRF2-ECH homology (Neh) domains (**Figure VI**), where each fulfills distinct functions:

- Neh2 contains two degrons, DLG and ETGE motifs, essential for the interaction with KEAP1 (Tong *et al*., 2006).
- Neh4 and Neh5 are transcriptional activation domains that cooperatively bind to the co-activator cAMP-responsive element-binding protein and facilitate NRF2 transcription (Xiang *et al*., 2014).
- Neh7 is involved in the NRF2 repression by linking up with the retinoic X receptor α (Wang *et al*., 2013).
- Neh6 contains two further redox-independent degrons, DSGIS and DSAPGS, which are targeted for degradation by the E3 ubiquitin ligase β-TrCP (McMahon *et al*., 2004).
- Neh1 mediates the dimerization with Maf (musculoaponeurotic fibrosarcoma oncogene homolog) necessary for the NRF2 transactivation function (Motohashi *et al*., 2004).

- Neh3 interacts with the co-activator known as CHD6, which is critical for the transactivation of ARE-dependent genes (Namani *et al*., 2014).

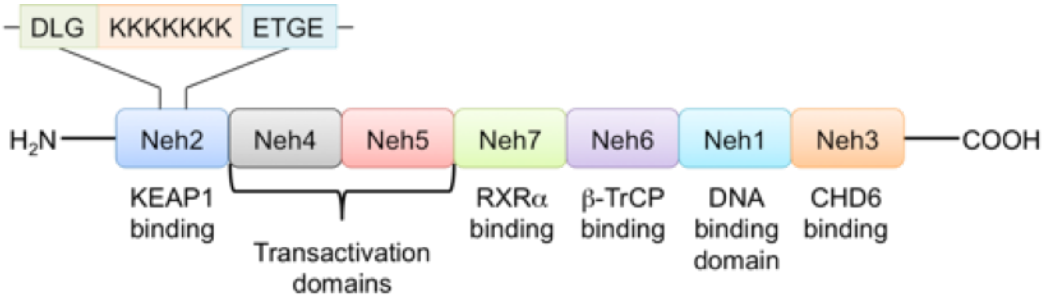

Figure VI: NRF2 structure. NRF2 contains seven domains, called Neh, where each fulfils distinct functions. It should be noted that the Neh2 domain contains two motifs, DLG and ETGE, necessaries for the interaction with KEAP1. Between them there are seven lysine residues (K), which are required for the NRF2 ubiquitination.

2.1.2 Functions of NRF2

The NRF2 pathway modulates the transcription of a large number of genes involved in metabolism, detoxification, antioxidant defenses and anti-inflammatory processes (Hayes and Dinkova-Kostova, 2014). Considering its role in the modulation of key genes involved in the antioxidant defenses, such as thioredoxines, peroxiredoxins and genes involved in the glutathione homeostasis, NRF2 is defined as the master regulator of the antioxidant response (Hayes and Dinkova-Kostova, 2014). Besides the up-regulation of the antioxidant defenses, it was recently reported that NRF2 modulates the redox environment repressing the expression of the ROS producer NOX2, while enhances the expression of NOX4 (Kovac *et al*., 2015; Wei *et al*., 2016), although the mechanisms are still elusive.

In addition to its importance in the redox and xenobiotic response, NRF2 modulates the metabolism and the mitochondrial function (Esteras *et al*., 2016), up-regulating the transcription of enzymes such as the malic enzyme 1 (Wu *et al*., 2011) or the Peroxisome Proliferator-Activated Receptor γ (PPARγ) (Pi *et al*., 2010). Another important mechanism by which NRF2 can modulates metabolism

or mitochondrial function is by preventing the oxidative thiol modifications, through the expression of several antioxidant enzymes, that can modulate the function of proteins implicated in metabolic pathways. mROS can reversibly modify thiol groups present in several enzymes implicated in carbohydrates and lipid metabolism, regulating their activity (Hurd *et al*., 2007). Most of these enzymes are involved in fatty acid oxidation (carnitine acetyltransferase, very long chain acyl CoA dehydrogenase, propionyl-CoA carboxylase) and in the regulation of the pyruvate dehydrogenase, through the pyruvate dehydrogenase kinase 2 (Hurd *et al*., 2007). Furthermore, transcription of PPP-related genes are indirectly regulated by NRF2 through an epigenetic mechanism that involves the oxidation of Cys of a specific redox-sensitive histone deacetylase, HDAC4 (Singh *et al*., 2013).

Besides the modulation of its target genes, NRF2 regulates itself, both directly and indirectly. The *NFE2L2* gene contains two ARE-like sequences, which enable NRF2 to modestly auto up-regulates its own expression (Kwak *et al*., 2002). Moreover, KEAP1, the major NRF2 repressor, contains an ARE domain (Lee *et al*., 2007), creating a tight auto-regulatory loop necessary to avoid an aberrant activation of the NRF2 pathway, which could be lethal (Wakabayashi *et al*., 2003).

Furthermore, the role of the NRF2 pathway in cancer is dual: although the activation of cytoprotective genes can suppress carcinogenesis in the earliest stages (Hayes *et al*., 2010; Hu *et al*., 2010; Kensler and Wakabayashi, 2010), the aberrant up-regulation of its target genes cause chemotherapy resistance (Ohta *et al*., 2008; Shibata *et al*., 2017; Zhang *et al*., 2010) and a more favourable intracellular environment for the survival of tumour cells (DeNicola *et al*., 2011; Ohta *et al*., 2008; Singh *et al*., 2008).

2.2. Regulation of the NRF2 pathway

Considering the crucial role of NRF2 in maintaining the cellular homeostasis and how its aberrant activation might be lethal, the NRF2 pathway has to be very tightly regulated. The canonical regulation of the NRF2 pathway involves the complex formed by Kelch-like ECH-associated protein 1 (KEAP1), Cullin 3

(Cul3), an E3 ubiquitin ligase, and RING (really interesting new gen)-box protein 1 (Rbx1).

2.2.1 Models of NRF2-KEAP1 regulation

Under basal conditions, NRF2 is constitutively expressed but its intracellular levels are kept low by the KEAP1-Cul3 complex, which degrades it rapidly, with a half-life of less than 20 minutes (Katoh *et al*., 2005). The homodimer KEAP1 binds NRF2 sequestering it in the cytoplasm, inhibiting its activation and its nuclear translocation (Kang *et al*., 2004). Moreover, KEAP1 regulates the turnover of NRF2 interacting with the Cul3-Rbx1 complex, which ubiquitinates and targets the transcription factor for its degradation by the 26S proteasome (Itoh *et al*., 1999). This mechanism ensures low intracellular levels of NRF2 in unstressed conditions. Nevertheless, under stress conditions, NRF2 can rapidly accumulate in the nucleus where it up-regulates the expression of its target genes. The prevailing model by which KEAP1 regulates NRF2 is called the "Hinge and Latch model" (Tong *et al*., 2006). However, live cell imaging based on the Förster resonance energy transfer (FRET) system suggests a new model called "Cyclic sequential attachment and regeneration model of KEAP1-mediated degradation of NRF2" (Baird *et al*., 2013). *De novo* synthetized NRF2 binds to a single member of a free KEAP1 homodimer through its ETGE (high affinity) motif to form the open conformation. When the ETGE domain alone is bound to KEAP1, NRF2 is not ubiquitinated (McMahon *et al*., 2006). After a period in the open conformation, the cycle progresses to form the closed conformation through the binding of the low affinity motif DLG to the other member of the KEAP1 homodimer. In the closed conformation, the Cul3-Rbx1 complex polyubiquinates seven lysines located between the ETGE and DLG motifs of NRF2, which is subsequently released for the proteasomal degradation (**Figure VII A**). The regenerated free KEAP1 dimer is then able to bind to a *de novo* synthetized NRF2 to start a new cycle (Baird *et al*., 2013). In presence of inducers (i.e. compounds that modifies the reactive Cys of KEAP1, such as oxidants or electrophiles), Cys151, Cys273 and Cys288 are chemically modified resulting in a conformational change in the KEAP1-Cul3-NRF2 complex, blocking it in the

induced closed conformation and preventing the regeneration of free KEAP1. This allows the *de novo* synthetized NRF2 to translocate to the nucleus and to start the transcription of its target genes (**Figure VII B**).

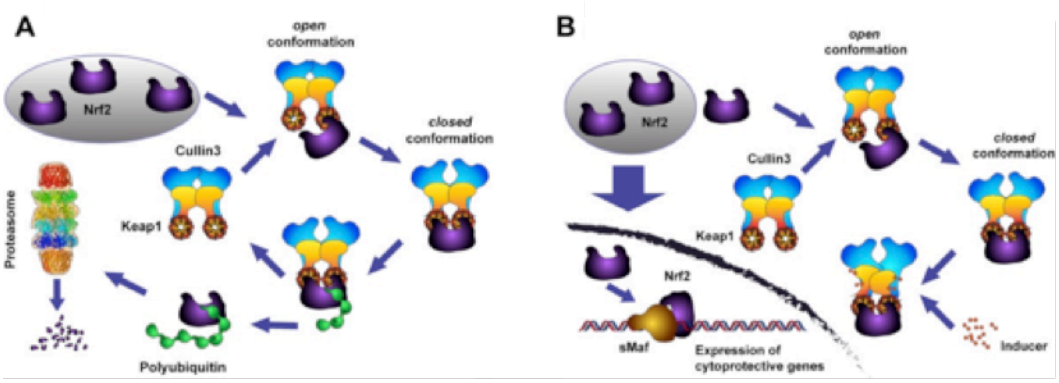

Figure VII: Cyclic sequential attachment and regeneration model of KEAP1-mediated degradation of NRF2. A) In unstressed conditions, *de novo* synthetized NRF2 first interacts with one member of the KEAP1 homodimer through its ETGE (high affinity) motif and forms the open conformation. Subsequently, the low affinity DLG motif binds the other KEAP1 member to form the close conformation, which allows the NRF2 polyubiquitination and its proteasomal degradation. Free KEAP1 homodimer is regenerated, allowing the cycle to start again. **B)** Inducers (such as oxidants or electrophiles) block the cycle of KEAP1-mediated degradation of NRF2 by chemically modifying cysteine sensors of KEAP1 and disabling its substrate adaptor function, leading to accumulation of the protein complex in the closed conformation. As a result, NRF2 is not released for its degradation and KEAP1 is not regenerated. This allows the *de novo* synthesized NRF2 to accumulate, to translocate to the nucleus, to bind a small Maf protein and to initiate the transcription of its downstream target genes. Obtained from Dinkova-Kostova *et al.*, 2016.

It was suggested that this induced closed conformation orientates the lysines moieties in a manner that they are no longer aligned with the Cul3-Rbx complex, thus the ubiquitination does not occurs (Baird *et al.*, 2013).

This model suggests that the KEAP1-NRF2 complex might exist in the open conformation, which is compatible with other types of regulation of the NRF2 pathway, called non-canonical regulation of the NRF2 pathway.

2.2.2 Non-canonical regulation of the NRF2 pathway

In addition to the canonical regulation, the NRF2 pathway could be modulated through different mechanisms. Recent studies have identified numerous proteins with motifs that are very similar to the ETGE present in NRF2.

These proteins can compete with NRF2 for KEAP1 binding, thus stabilizing NRF2 (Hast *et al*., 2013). The most recognized positive regulator of NRF2 is SQSTM1/p62, an autophagosome cargo protein, which binds KEAP1 through its (E/S)TGE motif stabilizing NRF2 (Lau *et al*., 2010). Furthermore, the directly repression of the NRF2 activity is obtained by the phosphorylation of the Neh6 domain mediated by the glycogen synthase kinase-3β (GSK-3β) (Chowdhry *et al*., 2013; Rada *et al*., 2011; Rada *et al*., 2012). This phosphorylation of NRF2 leads to its recognition by an E3 ligase receptor, its subsequent ubiquitination and its proteasomal degradation. This regulation has been largely overlooked because GSK-3β is inhibited under conventional cell culture conditions (i.e. in medium containing 10% fetal bovine serum) by growth factor signaling (Hayes and Dinkova-Kostova, 2014). Nevertheless, NRF2 phosphorylation not only represses its activity. Active protein kinase Cδ (PKCδ) in astrocytes promotes, by phosphorylation, the stabilization of p35, a cyclin-dependent kinase-5 (Cdk5) co-factor. Active p35/Cdk5 complex phosphorylates NRF2 at Thr395, Ser433 and Thr439 which is sufficient to promote the NRF2 nuclear translocation (Jimenez-Blasco *et al*., 2015).

2.2.3 The NRF2 pathway in the central nervous system

The NRF2 pathway plays a crucial role maintaining the cellular homeostasis and in the pathogenesis of several diseases, hence it needs to be tightly regulated at different levels. This implies that, depending on the cell type, there are different patterns of the NRF2 modulation. In the brain, neurons and astrocytes express different activity of the NRF2 pathway (Bell *et al*., 2015; Jimenez-Blasco *et al*., 2015). The transcription of antioxidant genes in neurons is repressed as a consequence of the continuous protein destabilization of NRF2 by the high levels of its repressors KEAP1 and Cul3 (Jimenez-Blasco *et al*., 2015). Furthermore, there is an epigenetic repression of the NRF2 promoter in neurons (Bell *et al*., 2015), that maintains low levels of functional NRF2 pathway. Forcing the expression of NRF2 resulted in an impaired neuronal development (Bell *et al*., 2015).

The extreme neuronal vulnerability to oxidative damage and the need to maintain low levels of NRF2 for their proper development, explain the neuronal reliance on astrocytic support to maintain the redox homeostasis (Bolaños, 2016).

3. GLUTATHIONE IN THE BRAIN

The tripeptide γ-L-glutamyl-L-cysteinylglycine (glutathione or GSH) (**Figure VIII**) is the most abundant mammalian thiol-containing antioxidant (Dringen, 2000). Its concentration varies in the range of 1–10 mM, depending on the cell type. The highest levels of glutathione are found in liver, spleen, kidney, lens, erythrocytes and leukocytes (Njålsson, 2005). Concentrations in brain are on the order of 1–3 mM (Dringen, 2000), however its distribution in brain cells is not uniform. *In vivo* measurement of intracellular levels of glutathione show that in neurons its concentration is estimated to be 2.5 mM, whereas astrocytes have a higher intracellular concentration estimated at 3.8 mM (Rice and Russo-Menna, 1997).

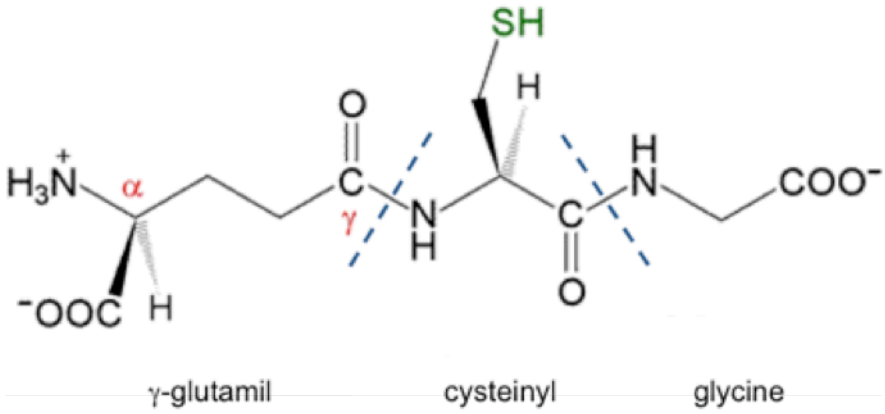

Figure VIII: Glutathione structure. The tripeptide glutathione consists of an unusual gamma peptide linkage between the carboxyl group of the glutamate side-chain and the amine group of the cysteine, and a usual peptide bond among cysteine and glycine. Adapted from Lash, 2006.

Most of the intracellular GSH is localized in the cytosol (80–85%), where it presents a half-life of 2-3 hours. The rest of the glutathione is present in the

mitochondria (10–15%) and a small percentage in the endoplasmic reticulum, peroxisomes and nucleus (Lu, 2009; Meredith and Reed, 1982; Wu *et al.*, 2004). The glutathione exists mainly in its reduced form (GSH); only about 1-5% is in the oxidized form as glutathione disulphide (GSSG) (Lu, 2009), or as mixed disulphide with xenobiotic (GSSX) or thiol-containing protein (GSSPr) (Njålsson, 2005).

3.1. Functions of glutathione

Glutathione serves several crucial functions including antioxidant defense, detoxification of xenobiotics and/or their metabolites, modulation of redox signaling, regulation of cell cycle progression and cell death, storage of cysteine, among the others.

The most important cellular function of GSH is the antioxidant defense, accomplished largely by GPx-catalyzed reactions, which reduce hydrogen peroxide and lipid peroxides as GSH is oxidized to GSSG. In turn, GSH is regenerated by glutathione reductase at the expenses of NADPH, forming a redox circle (**Figure III**) (Lu, 2009). Besides the antioxidant function, glutathione is involved in several crucial processes to maintain the cellular viability. The main functions of GSH are resumed in the **Table I**.

Main functions of glutathione
• **Antioxidant defense** (Dringen, 2000)
• **Detoxification of electrophiles and xenobiotics** (Lu, 2009; Meister, 1988)
• **Modulation of intracellular thiols** (Kumar *et al.*, 2011; Lu, 2009)
• **Post-translational modifications of proteins** (Ballatori *et al.*, 2009; Wu *et al.*, 2004)
• **Cysteine reservoir** (Lu, 2009; Meister, 1988)
• **Modulation of cellular growth** (Holmgren, 1981; Lu, 2009)
• **Modulation of cellular death** (Anathy *et al.*, 2009; Ballatori *et al.*, 2009; Diaz-Hernandez *et al.*, 2005; Garcia-Ruiz and Fernández-Checa, 2007; Huang *et al.*, 2008)

Table I: Functions of glutathione. The main functions directly or indirectly modulated by the GSH are resumed in this table.

3.2. Synthesis of glutathione

The synthesis of glutathione from its constituent amino acid involves two ATP-requiring enzymatic steps: formation of γ-glutamylcysteine (γ-GC) from glutamate and cysteine and formation of GSH from γ-GC and glycine (**Figure IX**) (Lu, 2013). The first step of GSH biosynthesis is rate limiting and catalysed by γ-glutamylcysteine synthetase or glutamate-cysteine ligase (GCL), while the second step is catalysed by glutathione synthetase (GS).

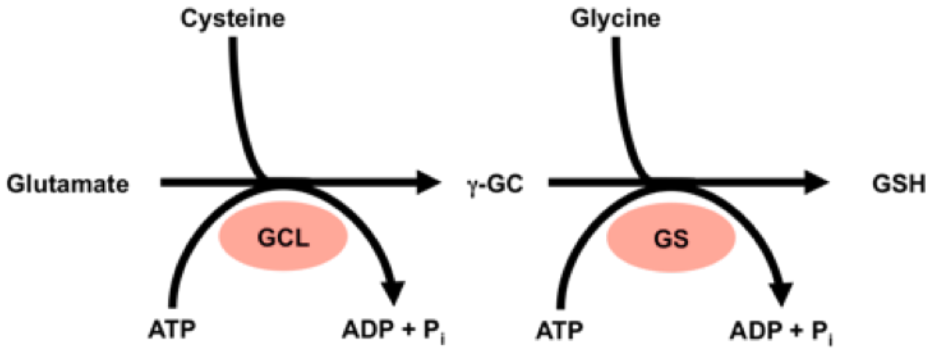

Figure IX: Glutathione synthesis. GSH is synthesized in the cytosol from its constituent amino acids by the sequential action of two ATP-requiring enzymes: γ-glutamylcysteine synthetase (GCL) and glutathione synthetase (GS).

GCL is an heterodimer composed of a heavy or catalytic (GCL_C, ~73 kDa) and a light or modifier (GCL_M, ~31 kDa) subunit, which are encoded by different genes in *Drosophila*, rodents and humans (Dalton *et al*., 2004; Gipp *et al*., 1992; Huang *et al*., 1993; Yan and Meister, 1990). GCL_C exhibits all of the catalytic activity of the isolated enzyme and feedback inhibition by GSH (Seelig *et al*., 1984). GCL_M is enzymatically inactive, however plays an important regulatory function by lowering the K_m of GCL for glutamate and raising the K_i for GSH (Huang *et al*., 1993a; Huang *et al*., 1993b).

The GS is an homodimer and is not subject to feedback inhibition by GSH (Oppenheimer *et al*., 1979). Considering that γ-GC, the product of GCL, is present exceedingly low concentrations when GS is present, GCL is considered rate limiting (Dalton *et al*., 2004). Supporting this evidence, the overexpression of GS failed to increase GSH levels, whereas overexpression of GCL does it (Grant *et al*., 1997).

The structure of glutathione is unique (**Figure VIII**). The peptide bond linking glutamate and cysteine, formed in the first step catalized by GCL, is through the γ-carboxyl group of glutamate rather than the conventional α-carboxyl group. This characteristic confers intracellular stability to GSH, considering that the only enzyme that can hydrolyses this unusual bond is the γ-glutamyltranspeptidase (γ-GT), which is only present on the external surfaces of specific cell types (Meister and Anderson, 1983), such as astrocytes (Cambier *et al*., 2000).

3.3. Regulation of glutathione biosynthesis

The glutathione biosynthesis occurs in the cytoplasm and it is regulated by three major factors: a) the expression of the rate-limiting enzyme GCL, b) the availability of L-cysteine, and c) the nonallosteric feedback competitive inhibition (with glutamate) by GSH (Lu, 2013; Meister and Anderson, 1983; Richman and Meister, 1975).

The expression of many genes involved in the GSH homeostasis is regulated by several transcription factors. Among all, NRF2 up-regulates the expression of genes involved in the supply of precursors (x_c^-), the biosynthesis (GCL_C, GCL_M and GS), the recycling (GR), the transport (MRP1), and the specific extracellular hydrolization (γ-GT) of glutathione (Hayes and Dinkova-Kostova, 2014). The promoter region of these genes contains an ARE sequence, which allows NRF2 to increase their expression, both in basal and stressed conditions (Hayes and Dinkova-Kostova, 2014; Lee *et al*., 2004).

Post-transcriptional regulation of GCL is mainly based on its mRNA stabilization and post-translational modifications. The directly phosphorylation of GCL_C, mediated by protein kinase A (PKA), protein kinase C (PKC) or Ca^{2+}-calmodulin kinase II (CAMK), decrease its activity (Sun *et al*., 1996). Furthermore, GCL could be inhibited by nitric oxide through nitrosylation (Griffith, 1999). Another post-translational modification of GCL is the cleavage mediated by caspase-3 (Franklin *et al*., 2002), which regulates GSH biosynthesis during apoptosis.

3.4. Astrocyte-neuron glutathione shuttle

Oxidative stress is a hallmark of neurodegenerative diseases, stroke and traumatic brain injuries, highlighting the particularly susceptibility of the brain to oxidative damage (Dringen, 2000; Bélanger *et al*., 2011). Paradoxically, despite the fact that the greater part of the brain's oxidative metabolism occurs in neurons and the neurotransmission unavoidably increases mROS, the neuronal antioxidant machinery is generally weak (Bolaños *et al*., 1995; Bolaños *et al*., 1996), dues to the continuous NRF2 degradation (Bell *et al*., 2015; Jimenez-Blasco, *et al*., 2015). In contrast, NRF2 is highly stable in neighbor astrocytes, which present a greater

antioxidant potential compared to neurons (Jimenez-Blasco *et al*., 2015). Accordingly, astrocytes are much more resistant than neurons to cellular damage induced by pro-oxidant compounds (Almeida *et al*., 2001; Bolaños *et al*., 1995; Dringen, 2000; Wilson, 1997). One reason for the higher vulnerability of neurons appears to be a lower glutathione content compared to astrocytes (Bolaños *et al*., 1995; Dringen *et al*., 1999).

Evidence is growing that especially between neurons and astrocytes, intensive metabolic and redox exchanges occur, both *in vitro* and *in vivo* (Bolaños, 2016; Fernandez-Fernandez *et al*., 2012; Mächler *et al*., 2016; Pellerin and Magistretti, 2012). In co-culture systems, astrocytes protect neighbour neurons from harmful doses of hydrogen peroxide, nitric oxide iron or hydroxydopamine (Bélanger and Magistretti, 2009; Dringen, 2000; Vargas and Johnson, 2009; Wilson, 1997), suggesting that neural cells are dependent upon the high antioxidant potential of astrocytes for their own defense against oxidative stress.

To prevent competition, neurons and astrocytes display differential preference for extracellular GSH precursors. Neural cells rely on the presence of extracellular cysteine for GSH synthesis, since they cannot use cystine (Dringen *et al*., 1999; Kranich *et al*., 1996; Sagara *et al*., 1993), while the best extracellular precursor for the glutamate moiety of glutathione is glutamine (Kranich *et al*., 1996). In contrast, astrocytes prefer glutamate and cystine as extracellular GSH precursors (Dringen and Hamprecht, 1998; Kranich *et al*., 1996; Kranich *et al*., 1998). However, since neurons cannot use extracellular cystine, they depend for their glutathione synthesis on the supply of cysteine or a cysteine precursor from neighbour astrocytes (Dringen *et al*., 2000). The presence of astrocytes increases glutathione levels in co-cultured neurons (Bolaños *et al*., 1996; Dringen *et al*., 1999), suggesting the existence of a GSH precursors supply from astrocytes to neurons (Dringen *et al*., 1997), called astrocyte-neuron glutathione shuttle (ANGS) (**Figure X**) (Bolaños, 2016).

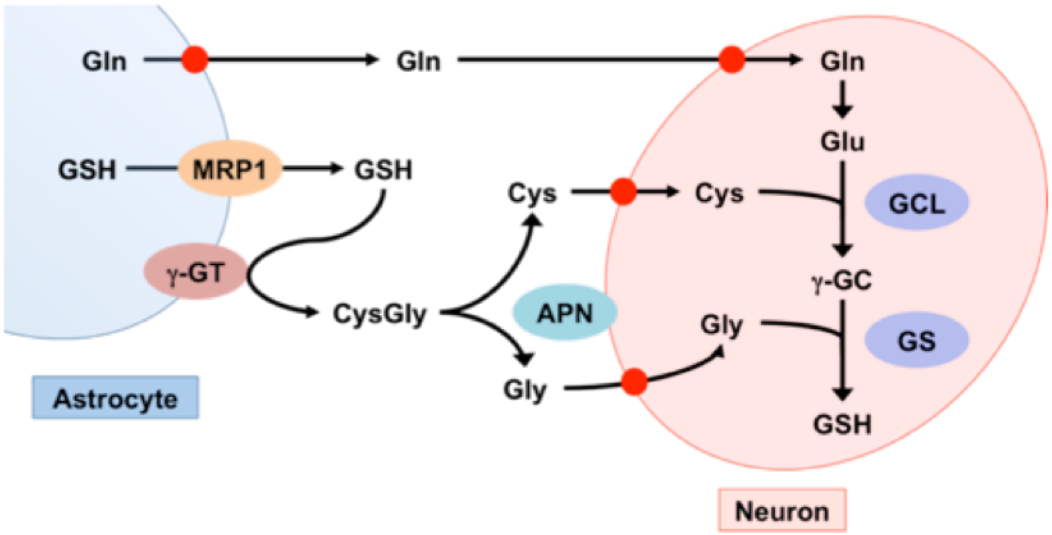

Figure X: Astrocyte-neuron glutathione shuttle (ANGS). Astrocytes export, through MRP1, up to 10% about their intracellular GSH per hour, which is cleaved into CysGly by the γ-GT. The APN on the neuronal surface cleaves CysGly into cysteine and glycine, which are uptake by neurons. Meanwhile, astrocytes also export glutamine, which is uptake by neurons and converted to glutamate. Modified from Fernandez-Fernandez *et al*., 2012.

Cultured astrocytes export about 10% of their intracellular GSH per hour (Dringen *et al*., 1997), which has continuously to be resynthesized from its precursors in order to maintain a constant cellular concentration. These data and the reported half life of about 5 hours for astroglial GSH (Devesa *et al*., 1993) indicate that the export of GSH is quantitatively the most important process consuming astrocytic glutathione. Indeed, treatments that increase the glutathione concentration in glial cells lead to an increase in the rate of cellular GSH export (Dringen *et al*., 2015). The GSH export from astrocytes is predominately mediated by multidrug resistance-associated protein 1 (MRP1) (Minich *et al*., 2006). GSH that has been exported from astrocytes is a substrate of the γ-glutamyl transpeptidase (γ-GT) (Dringen *et al*., 1997). One product of this reaction is the dipeptide CysGly, which is cleaved by the neuronal aminopeptidase N (APN) (Dringen *et al*., 2001) to provide cysteine and glycine to neurons.

Astrocytes are therefore necessary for maintaining neuronal GSH through the ANGS; however, they may not be sufficient. Knockdown of GCL in neurons triggers GSH depletion and neuronal death, both *in vitro* and *in vivo* (Chinta *et al*., 2007; Diaz-Hernandez *et al*., 2005; Garrido *et al*., 2011). Hence, intact

biosynthetic enzymatic machinery for *de novo* synthesis of glutathione in neurons is necessary for their survival, even in presence of neighbour astrocytes.

4. PENTOSE PHOSPHATE PATHWAY (PPP)

The vast majority of glucose that enters in the cells is oxidized by glycolysis to provide ATP and metabolic intermediates. However, a percentage of glucose that varies from 5 to 30% in a tissue-dependent manner, is oxidized through the PPP to yield ribose-5-phosphate for nucleic acid synthesis and NADPH for redox homeostasis or biosynthetic processes (Riganti *et al.*, 2012). The basal flux through the PPP reaches the maximal percentage in lipid- and steroid-synthetizing tissues (such as liver, white adipose tissue, lactating mammary glands, adrenal glands and gonads) and in erythrocytes. Nevertheless, the rate of PPP may widely vary. Cells exposed to oxidative stress increase the PPP activity in order to regenerate GSH and restore the redox homeostasis (Riganti *et al.*, 2012). Moreover, PPP sustains glycolytic cancer cells to meet their anabolic demands and combat oxidative stress increasing their survival (Patra and Hay, 2014).

The PPP can be divided into two branches: the oxidative and the non-oxidative phase (**Figure XI**) (Wamelink *et al.*, 2008).

The oxidative branch of the PPP starts with the dehydrogenation of glucose-6-phosphate, catalysed by the rate limiting enzyme glucose-6-phosphate dehydrogenase (G6PD). The product 6-phosphogluconolactone is rapidly and irreversibly hydrolysed by the 6-phosphogluconolactonase to yield 6-phosphogluconate. The lately is oxydatively decarboxylated by the 6-phosphogluconate dehydrogenase (6PGD) to produce ribulose-5-phosphate and CO_2. The effectiveness of the oxidative branch of the PPP is favored by the localization of G6PD and 6PGD next to the glucose transporters (Kletzien *et al.,* 1994). The net result of the oxidative phase of the PPP is the formation of one mole of ribulose-5-phosphate, two moles of NADPH and one mole of CO_2 per mole of glucose-6-phosphate.

In the non-oxidative branch of the PPP, ribulose-5-phosphate can be epimerized to xylulose-5-phosphate by ribulose-5-phosphate epimerase, or isomerized by the

ribulose-5-phosphate isomerase to ribose-5-phosphate and incorporated into nucleotides (Wamelink *et al*., 2008). Depending on the cellular requirements, the pentose phosphates generated in the non-oxidative branch could be transformed in the glycolytic intermediates glycealdehyde-3-phosphate and fructose-6-phosphate (Baquer *et al*., 1988), or can be recycled into glucose-6-phosphate and re-enter in the oxidative branch to generate more NADPH (Wamelink *et al*., 2008).

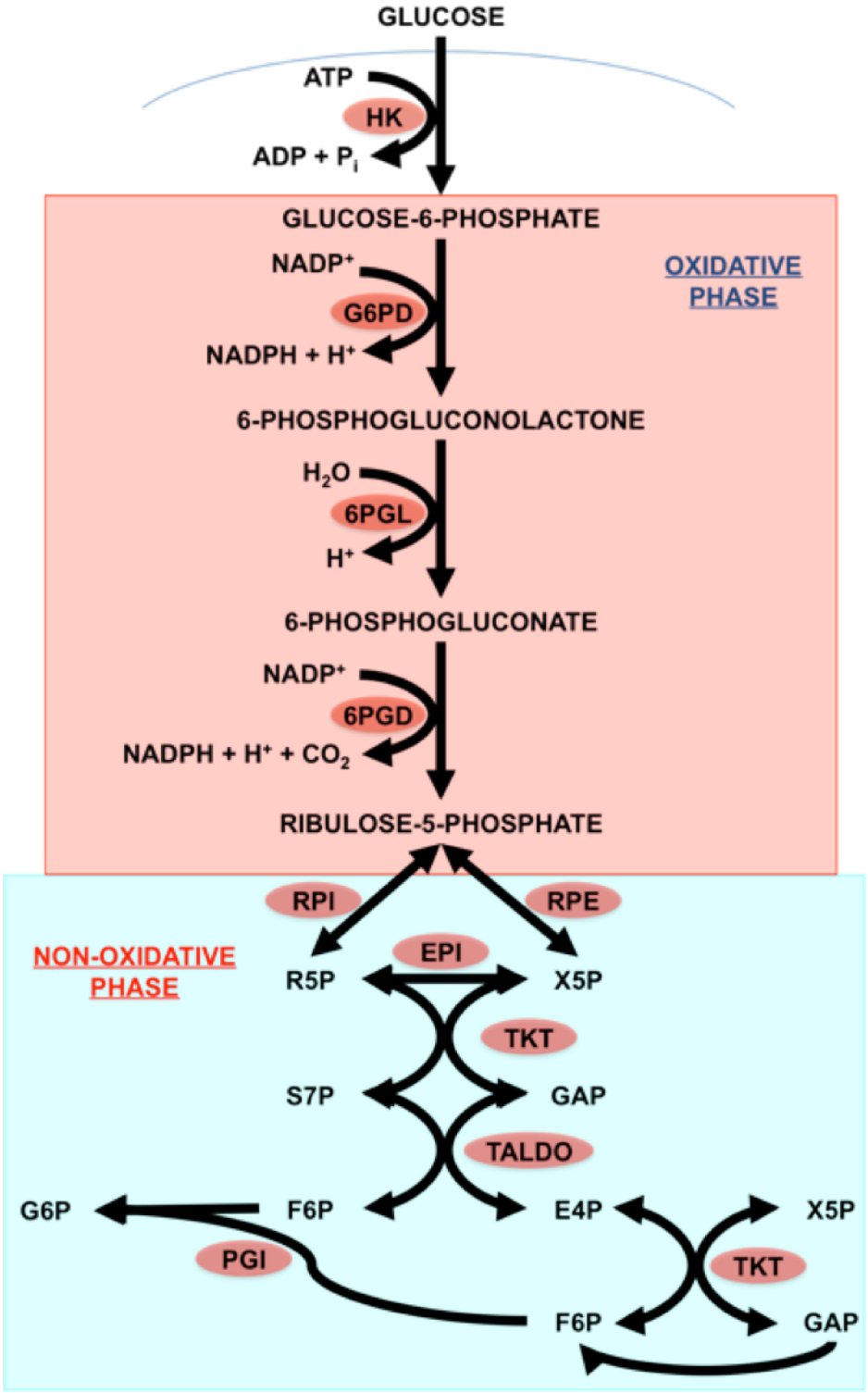

Figure XI: Pentose phosphate pathway. Abbreviations used: HK: hexokinase; G6PD: glucose-6-phosphate dehydrogenase; 6PGL: 6-phosphoglucolactonase; 6PGD: 6-phosphogluconate dehydrogenase; RPI: ribulose-5-phosphate isomerase; RPE: ribulose-5-phosphate epimerase; R5P: ribose-5-phosphate; EPI: epimerase; X5P: xilulose-5-phosphate; TKT: transketolase; S7P: sedoheptulose-7-phosphate; GAP: glyceraldehyde-3-phosphate; TALDO: transaldolase; F6P: fructose-6-phosphate; E4P: erythrose-4-phosphate; PGI: phosphoglucose isomerase; G6P: Glucose-6-phosphate.

4.1. Functions of the PPP in the brain

The two major functions of the PPP are the production of NADPH and the synthesis of ribose-5-phosphate. Most of the cytosolic NADPH is produced by G6PD and 6PGD (Wamelink *et al*., 2008). This coenzyme plays a pivotal role in redox homeostasis, since it provides reduced equivalents for the GSH and thioredoxin regeneration (Stincone *et al*., 2015). Besides its importance in the antioxidant systems, NADPH is required as electron donor in many anabolic pathways, such as fatty acid oxidation, lipid and cholesterol synthesis (Dringen *et al*., 2007). Among the various NADPH-consuming processes in the adult brain, the regeneration of GSH is likely to be quantitatively the most important one, especially in neurons (Bouzier-Sore and Bolaños, 2015). These cells contains very low amounts of glutathione (Bolaños *et al*., 1995; Dringen *et al*., 1999), hence it regeneration is critical for their survival. Since NADPH is essential for this process, the re-cycling version of the PPP, which recovers a considerable proportion of glucose-6-phosphate, explains both the low glucose consumption and the efficient GSH regenerating activity of neurons compared to astrocytes (Bouzier-Sore and Bolaños, 2015). Metabolic switch from PPP to glycolysis overexpressing 6-phosphofructo-2-kinase/fructose-2,6-biphosphatase 3 (PFKFB3), cause neuronal death by nitrosative stress (Herrero-Mendez *et al*., 2009), confirming the importance of the PPP in the redox homeostasis of neurons. In contrast, astrocytes express higher PPP-rate limiting enzyme G6PD, have higher basal PPP activity rate and a better capability to stimulate this pathway in response to oxidative stress, compared to neurons (Ben-Yoseph *et al.,* 1996; García-Nogales *et al*., 1999; Herrero-Mendez *et al*., 2009). However, the production of NADPH by G6PD and 6PGD plays a dual role in the regulation of the redox homeostasis: on the one hand, these enzymes supply reducing equivalent for the glutathione regeneration, but on the other hand, they provide cytoplasmic substrate for ROS generation by NADPH-oxidases (Park *et al*., 2005).

The synthesis of ribose-5-phosphate, fundamental for dividing cells, occurs both in the oxidative and in the non-oxidative branch of PPP (Wamelink *et al*., 2008). With the exception of processes such as DNA repair (Brooks, 2002)**,** proliferation

of stem cells (Baizabal *et al*., 2003) and the growth of brain tumors (Loreck *et al*., 1987; Spence *et al*., 1997), low amounts of ribose-5-phosphate are required for the generation of nucleotides in the adult brain. Hence, synthesis of ribose-5-phosphate does not appear to be a major function of the PPP in the central nervous system (Dringen *et al*., 2007).

4.2. Regulation of the PPP

The activity of the PPP varies in a tissue-specific manner. Moreover, the basal flux of PPP depends on the cell state. The activity of G6PD, the rate limiting enzyme of the PPP, is directly related to the NADPH/$NADP^+$ ratio (Barcia-Vieitez and Ramos-Martínez, 2014). Situations in which this ratio drops, boost the activity of the G6PD enzyme increasing the glucose flux through the PPP, with the aim to restore physiological values of the NADPH/$NADP^+$ ratio (Stincone *et al*., 2015).

Besides the post-translational regulation of the G6PD enzyme, there is a transcriptional regulation of several enzymes involved in the PPP. The rate limiting enzyme, G6PD, is transcriptionally induced upon oxidative stress and by the need for NADPH and PPP intermediates for anabolic reactions such as lipid and nucleotide synthesis (Stincone *et al*., 2015). A recent study suggests that the mRNA levels of the *G6pd*, *6Pgd* and transketolase (*Tkt*) were indirectly regulated by NRF2 (Singh *et al*., 2013). The targeted deletion of the ARE sequence from these genes demonstrates that they are not directly regulated by NRF2 (Singh *et al*., 2013). The suggested indirect modulation of several PPP-related genes by NRF2, involves an epigenetic mechanism. Histone deacetylase 4 (HDAC4) is a redox-sensitive protein which nuclear localization depends on the reduced state of two cysteines, Cys-667 and Cys-669 (Ago *et al*., 2008). In its reduced state, HDAC4 accumulates in the nucleus, deacetylates chromatin causing its compaction and represses the transcription of two micro-RNAs, miR-1 and miR-206. These two micro-RNAs target the newly synthesized *G6pd*, *6Pgd, Tkt* and *Hdac4* mRNA interfering with their ribosomic translation (Chen *et al*., 2010; Coda *et al*., 2015; Hak *et al*., 2006; Singh *et al*., 2013). Decreased antioxidant potential results in the oxidation of the Cys residues, nuclear exportation of

HDAC4 and increased transcription of miR-1 and miR-206, which in turn leads to lower levels of G6PD, 6PGD, TKT and HDAC4 itself (Singh *et al*., 2013) (**Figure XII**). Thioredoxin-1 (Trx-1) overexpression preserves the Cys moieties in their reduced state, maintaining HDAC4 in the nucleus repressing the transcription of miR-1 and miR-206 (Ago *et al*., 2008). Modulating the redox environment through the transcription of several antioxidant genes, among them Trx-1, NRF2 indirectly controls the HDAC4 subcellular localization.

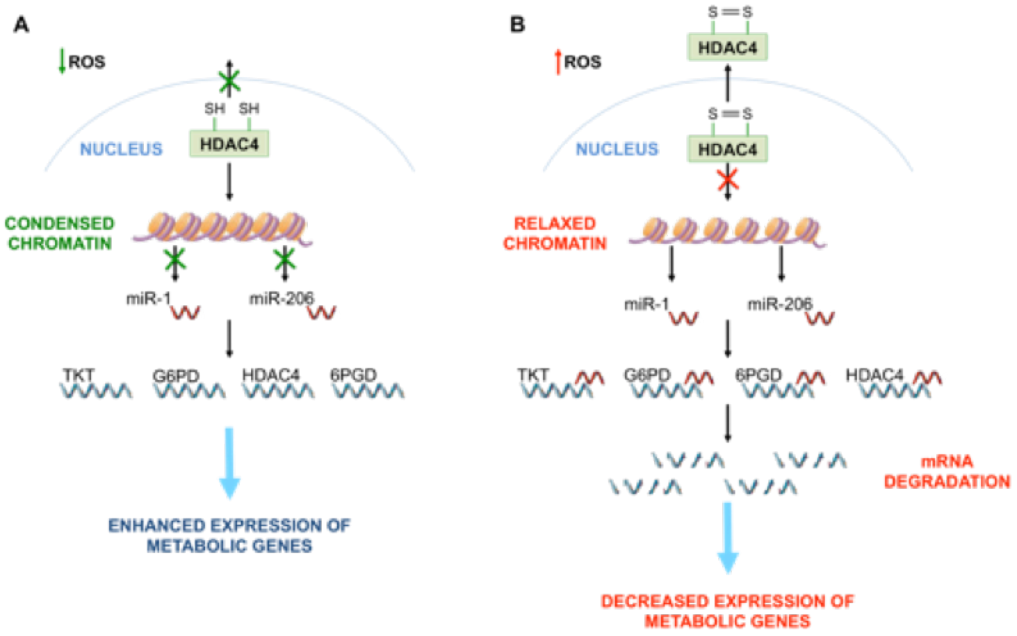

Figure XII: Epigenetic model of PPP-related genes modulation by a ROS-mediated mechanism. A mechanism involving ROS, HDAC4 and miRNAs modulates the expression of several PPP genes. **A**) With low ROS levels, the two Cys residues of HDAC4 are in their reduced state. HDAC4 could accumulate in the nucleus, deacetylates the chromatin causing its condensation and suppresses miR-1 and miR-206 gene expression, leading to an enhanced expression of metabolic genes. **B**) A ROS increase causes the Cys oxidation leading to nuclear export of HDAC4 and relaxation of chromatin, which leads to miR-1 and miR-206 expression. Newly formed miRNAs target specific mRNAs (G6PD, 6PDG, TKT and HDAC4) leading to a decreased gene expression. Abbreviations used: HDAC4: histone deacetylase-4; G6PD: glucose-6-phosphate dehydrogenase; 6PGD: 6-phosphogluconate dehydrogenase; TKT: transketolase.

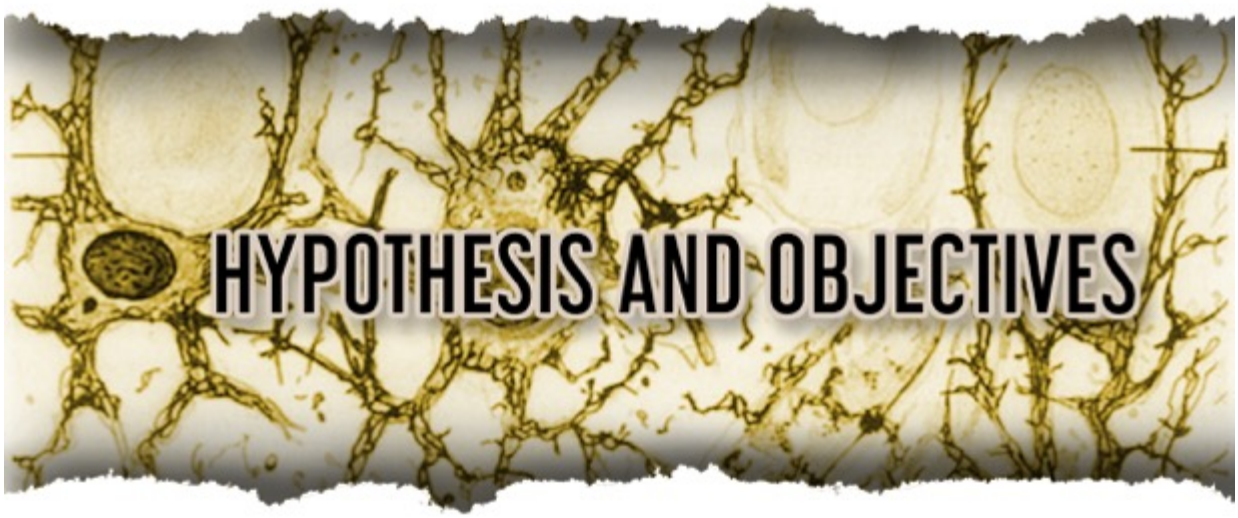
HYPOTHESIS AND OBJECTIVES

1. HYPOTHESIS

Reactive oxygen species (ROS) have been associated with oxidative stress conditions and to participate in the etiology of human pathologies, including neurodegenerative diseases. Whilst antioxidant treatments in *in vitro* and *in vivo* models of neurodegenerative diseases have shown neuronal protection, translation to human has not been conclusive (Halliwell 2013; Heyland *et al*., 2013; Kamat *et al*., 2008; Snow *et al*., 2010), which argues against the notion of a pathological role for ROS.

Recent evidences from our laboratory show that, under basal conditions, astrocytes produce higher mitochondrial ROS (mROS) compared to neurons (Lopez-Fabuel *et al*., 2016). This seems to be paradoxical, considering that astrocytes express a robust antioxidant machinery, reliable to a major NRF2 activity, compared to neurons (Jimenez-Blasco *et al*., 2015). Furthermore, astrocytes support neuronal antioxidant defenses by shutting glutathione (GSH) precursors. This shuttle is maintained by NRF2 activity in astrocytes. However, the factor(s) responsible for such a high NRF2 activity in astrocytes is unknown.

In the view of the previously described premises, we hypothesize that endogenous mROS maintain active the NRF2 pathway in astrocytes. If so, mROS-NRF2 pathway should contribute to neuronal survival.

2. OBJECTIVES

To address the above-mentioned hypotheses, we planned the following objectives:

1. To generate a mouse model able to down modulate endogenous mROS in astrocytes.

2. To investigate whether endogenous mROS modulate the redox homeostasis in astrocytes.

3. To investigate whether astrocytic mROS modulate neuronal redox homeostasis and survival.

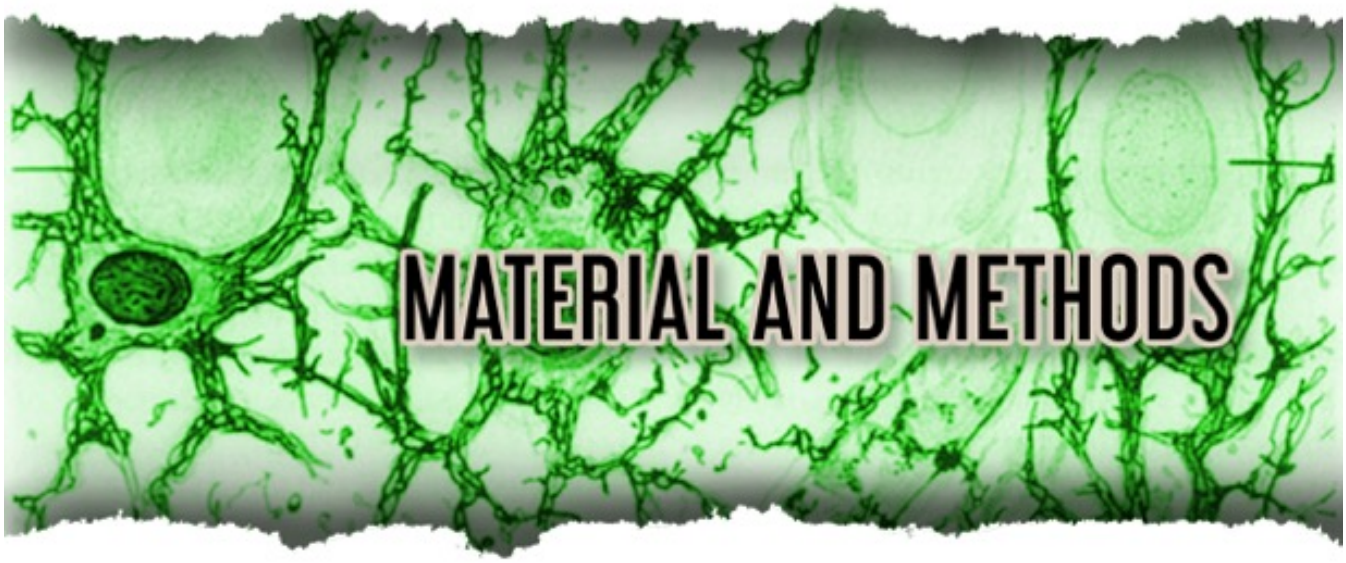
MATERIAL AND METHODS

1. ANIMALS

1.1. +/mCAT mouse line generation

To down-modulate endogenous mitochondrial ROS (mROS) abundance, a knock-in mouse model harbouring a mitochondrial-tagged form of Catalase (mCAT) was generated (Genoway, France).

The mCAT cDNA, generously supplied by J.A. Enríquez (CNIC, Madrid), contains the N-terminal mitochondrial-leading cDNA sequence of cytochrome c oxidase VIII (C8), followed by the full-length cDNA sequence of catalase and the cDNA sequence of the human influenza hemagglutinin (HA) (**Scheme 1**).

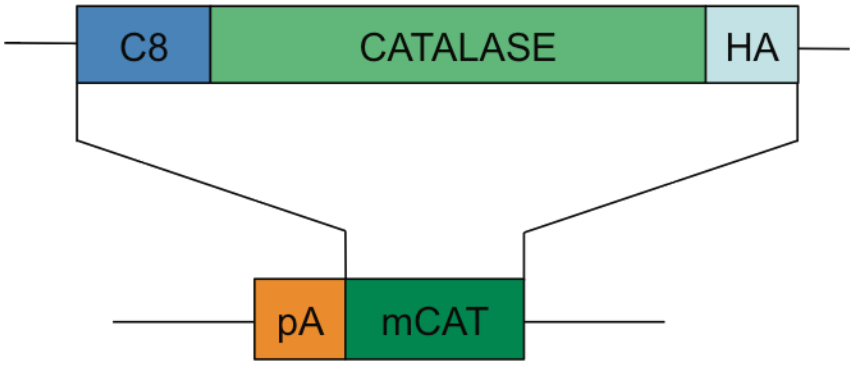

Scheme 1: mitochondrial catalase (mCAT) construction. C8: cytochrome c oxidase VIII; HA: human influenza hemagglutinin tag; pA: poly-A tail; mCAT: mitochondrial catalase.

The mCAT construct was inserted in the *Rosa26* locus of C57Bl/6 embryonic stem cells by homologous recombination. The *Rosa26* locus strategy has several advantages over random integration transgenesis:

- Only one copy of the transgene is inserted in a defined locus
- A reliable and predictable expression pattern of the transgene
- The endogenous (cytosolic) catalase is kept intact.

Furthermore, a floxed (loxP flanked) transcriptional STOP cassette was

incorporated between mCAT and the CAG promoter, in order to eventually obtain tissue- and time-specific expression of mCAT *in vivo*. This strategy allows the P1 phage-derived Cre recombinase to site-specifically recombine DNA flanked by LoxP sites (5'-ATAACTTCGTATAATGTATGCTATACGAAGTTAT-3') (Branda and Dymecki, 2004).

Thus, the mouse line harbouring the floxed mCAT construct does not express mitochondrial catalase unless Cre recombinase is present. This can be obtained by crossbreeding the floxed mCAT mice with mice harbouring the Cre recombinase gene.

To obtain ubiquitous constitutive mCAT expression, the floxed mCAT mice were crossbred with the human cytomegalovirus minimal promoter (CMV)-Cre recombinase mice under a C57Bl/6 genetic background (C57Bl/$6^{+/mCAT}$, henceforth +/mCAT). (**Scheme 2**). +/mCAT was bred in heterozygosis.

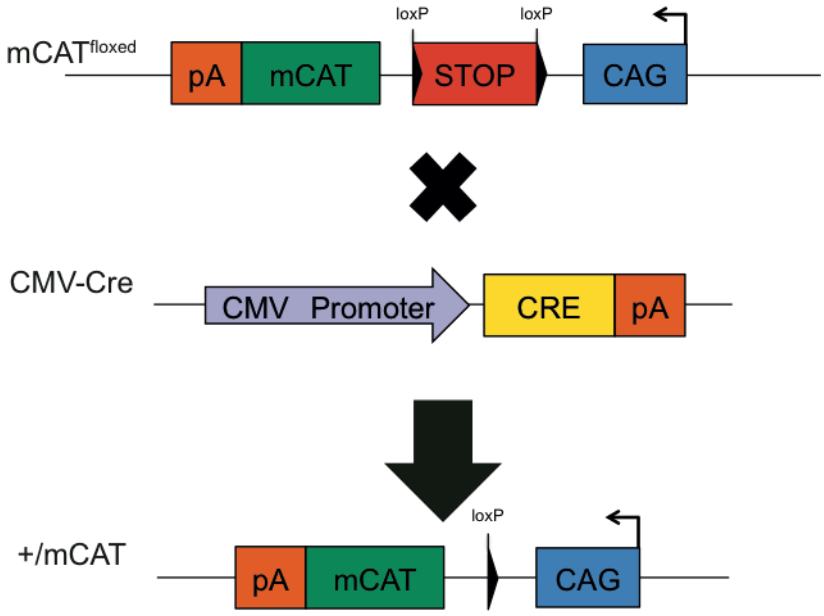

Scheme 2: Strategy used to express ubiquitously the mCAT. pA: poly-A tail; mCAT: mitochondrial catalase; CAG: cytomegalovirus enhancer fused to chicken β-actin promoter; CMV: cytomegalovirus.

Animals were bred at the Animal Experimentation Facility of the University of Salamanca in cages (maximum 5 animals/cage) and a light-dark cycle was maintained for 12 hours. Humidity was between 45% and 65% and temperature

between 20ºC and 25ºC. Animals were fed *ad libitum* with a standard solid diet (17% proteins, 3% lipids, 58.7% glucidic component, 4.3% cellulose, 5% minerals and 12% humidity) with free access to water.

Gestational stage was controlled by limiting the cohabitation of female mice with males to one night. At 9:00 hours of the following day, mice that had the presence of spermatozoids in the vaginal smear accompanied by epithelial cells from the vagina (indicator of the successful copulation) were isolated. Under these conditions, gestational period of the mouse is assumed to be 19.5 days.

All animal handlings and procedures are in agreement with the current and Spanish legislation (Law 6/2013) related to accommodation and experimental animals care. All the protocols performed in this thesis were approved by Bioethics Committee of the University of Salamanca.

1.2. Tissue extraction

Mice were anesthetized with CO_2, euthanized by cervical dislocation and the brain, liver, heart and kidney were extracted within the following 5 min and processed to obtain a cytosolic and nuclear fractionation (see Section 7.3).

1.3. DNA extraction

DNA was extracted from tails (2-5 mm long) of newborn mice. Tails were incubated with 120 µl of TENS buffer (100 mM Tris, 5 mM EDTA, 200 mM NaCl, 0.2% SDS, pH 8) and 1.2 µl of Proteinase K (800 U/µl; Sigma-Aldrich) and left overnight at 55ºC for complete digestion. Subsequently, 410 µl of Phenol-Chloroform-Isoamilic acid (PCI) mix (25:24:1) was added and centrifuged at 13,000 rpm for 5 minutes. The aqueous phase was transferred to a new tube, to which an equal volume of isopropanol was added, kept at 4 ºC for at least 30 minutes, and centrifuged at 13,000 rpm for 5 minutes at 4 ºC. Tubes were left to dry for no more than 5 minutes, and 50 µl of TE buffer solution (10 mM Tris-HCl, 1 mM EDTA, pH 8) was added. Tubes were left 24 hours at room temperature, and DNA concentrations were measured using NanoDrop 2000 (Thermo Fisher).

1.4. Genotyping

mCAT mice were genotyped by PCR. Forward (124540-BOL1) and reverse (124541-BOL1) oligonucleotides used were, respectively, 5'-CTCCCAAAGTCGCTCTGAGTTGTTATCA-3' and 5'-CGATTTGTGGTGTATGTAACTAATCTGTCTGG-3', which generated a 778 bp band in the wild type allele and a 5949 bp band in the mCAT allele (due to the large size of this PCR product, the amplification will not occur). Hence, to detect the mCAT construction, a third oligonucleotide (0034-Kin-ROSA) was used, 5'-GCAGTGAGAAGAGTACCACCATGAGTCC-3', which generated a 245 bp band (**Scheme 3**).

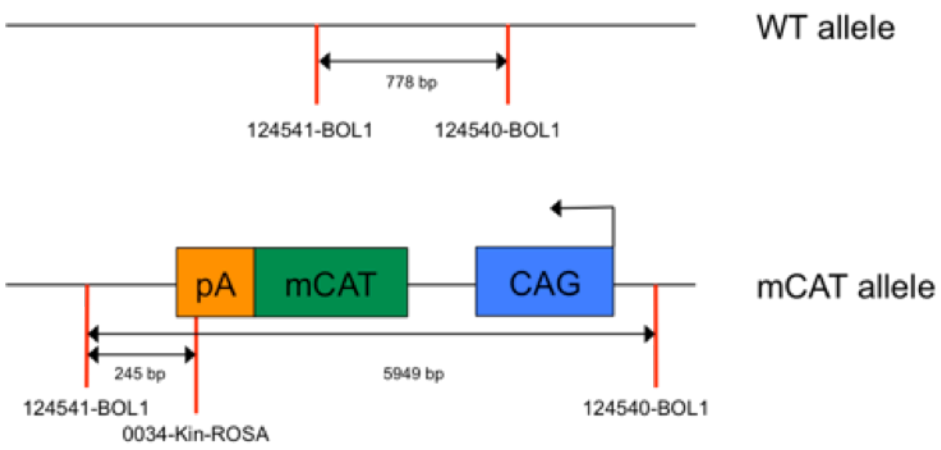

Scheme 3: +/mCAT identification strategy by PCR. Red lines illustrate the primers localization

PCR conditions were: 5 minutes at 94°C, 35 cycles of 30 seconds at 94°C followed by 30 seconds at 65°C and 3 minutes at 60°C and a final step 8 minutes at 68°C. Final concentrations of PCR components were 0.5 mM dNTPs mix (Roche), 0.3 µM of primers (Sigma-Aldrich), 0.042 U/µl of Taq polymerase (Biotools) and 1X reaction buffer containing $MgCl_2$. The total amount of DNA added was 30 ng.

1.5. Gel electrophoresis

PCR products were run in a 2% (w/v) agarose gels (Sigma-Aldrich). Gels were pre-stained with MidoriGreen (1:20,000) and run in TAE buffer (200 µM Trizma-Base, 100 mM Glacial Acetic Acid, 5 mM $Na_2EDTA{\cdot}2H_2O$), using a 6X loading dye (10 mM Trizma-Base, 0.03% Bromophenol blue, 0.03% (v/v) Xylene cyanole, 60% (v/v) Glycerol, 60 mM $Na_2EDTA{\cdot}2H_2O$, pH 7.6) for DNA input. Images were taken using Bio-Rad Chemidoc.

2. CELL CULTURES

2.1. Mouse embryonic fibroblasts (MEFs) immortalization

MEFs were prepared from fetal +/mCAT mice (E13.5), using the wild type (WT or +/+) littermates as control. Embryos were processed individually, and the liver and brain tissue were disregarded. The carcass was mechanically disaggregated in 0.25 g/ml of trypsin/1 mM EDTA and seeded in a 60 cm^2 cell culture dish containing Dulbecco's Modified Eagle's Medium (DMEM, Sigma-Aldrich) supplemented with 10% v/v fetal bovine serum (FBS, GE Healthcare Life Sciences) and 25 mM D-glucose. Confluent cells were split 1:3 during 2 weeks, until the immortalization crisis occurred, which lasted for a further 2 weeks. During this period, medium was renewed every 3 days. One week after the immortalization crisis, single cell colonies were spotted, picked and grew. Cells were placed in a thermostatized cell-culture incubator at 37ºC (Thermo Forma 310, Thermo Fisher) and 5% CO_2 atmosphere. MEFs were frozen in a mixture of FBS and DMSO (9:1).

2.2. Neurons in primary cultures

Neurons in primary culture were obtained from fetal embryos of 15.5 days (E15.5) C57Bl/6 mice according to standard procedure (Almeida *et al.,* 1998). In brief, pregnant mice were anesthetized with CO_2, euthanized by cervical dislocation and the embryos were removed by hysterectomy. Embryos were transferred to a laminar flux cabin (TC48, Gelaire Flow Laboratories) in order to maintain the sterile conditions of the culture. Cerebral hemispheres were removed

using scissors, forceps and 70% ethanol impregnates handkerchiefs. The brain tissue was then placed in a polystyrene Petri plate containing the disintegration solution (EBSS (Eagle's Basal Salt Solution): 116 mM NaCl, 5.4 mM KCl, 1.01 mM NaH_2PO_4, 1.5 mM $MgSO_4$, 26 mM $NaHCO_3$, 4 mM glucose, 10 mg/ml phenol red, with 2.94 mg/ml BSA (Bovine Serum Albumin) and 20 μg/ml DNAse, pH 7.15) and very smoothly chopped with a scalpel. After this, it was placed in a tube and left for 4 minutes for sedimentation. The pellet was re-suspended in trypsinization solution (EBSS; 50 μg/ml DNAse, 3.15 mg/ml BSA, 10mg/ml trypsin, pH 7.15) and incubated at 37ºC for 15 minutes in a thermostatic bath. Trypsinization was stopped by adding FBS at a final concentration of 10 % v/v, and the tissue was centrifuged at 500 *g* for 5 minutes (Eppendorf 5702R, Eppendorf). The pellet was re-suspended in 12 ml of disintegration solution and triturated with a silicon-coated Pasteur pipette for 9 strokes. After letting the cellular solution stand for 4 minutes, the supernatant containing the dissociated cells was carefully removed and placed in a fresh tube. This process was repeated once more in order to increase yield. The supernatants were then centrifuged at 500 *g* for 5 minutes. The cellular sediment was re-suspended in specific medium for neuronal growth (Neurobasal-A (Life Technologies) supplemented with 2% B27 MAO (Minus AntiOxidants, Life Technologies), 2 mM glutamine, 5.5 mM glucose, 0.22 mM pyruvate, 100 U/ml penicillin, 100 μg/ml streptomycin and 0.25 μg/ml amphotericin B (Sigma Aldrich). 10 μl of the cellular suspension was diluted four times and mixed with an equal volume of trypan blue 0.4 % (Sigma-Aldrich) for alive cellular counting using a Neubauer chamber (Zeiss) and a phase contrast microscope (CK30 model, Olympus). The cell suspension was diluted in culture medium and seeded at 200,000 cells/cm^2 in plastic culture plates (Corning Incorporate), previously coated with poly-D-lysine (10 μg/ml; Sigma-Aldrich). Plates were placed in a thermostatized cell-culture incubator at 37ºC and 5% CO_2 atmosphere. The medium was renewed at DIV3 (days *in vitro*). Neurons were used for experiments at DIV7.

2.3. Astrocytes in primary culture

Astrocytes in primary culture were obtained from +/mCAT newborn mice (from 0 to 24 hours of age), using the WT littermates as control (Almeida *et al.,* 1998). Animals were cleaned with 70% ethanol, decapitated and the whole brain was removed under a laminar flux cabin. Cerebellum and olfactory bulb were removed using forceps and cerebral hemispheres were cleaned from meninges and blood vessels. The tissue was then placed in a Petri dish with the disintegration solution. Every brain was processed individually. Cellular suspension was obtained as previously described for neurons.

Individual cellular suspension was seeded in DMEM supplemented with 10% v/v FBS in a 75 cm^2 culture flask. Cells were incubated in a thermostatic cell-culture incubator at 37 ºC and 5% CO_2 atmosphere. Culture medium was renewed twice per week. To detach non-astrocytic cells, at DIV7 the flasks were shaken at 180 rpm overnight. The supernatant was discarded, and the attached, astrocyte-enriched cells, were reseeded at 100,000 cells/cm^2 in DMEM supplemented with 10% v/v FBS in different plate size. At DIV11 the medium was replaced with Neurobasal A supplemented with 2% B27 MAO, 2 mM glutamine, 5.5 mM glucose, 0.22 mM pyruvate. A glucose control was made at DIV13 with a glucometer (Glucocard G+ meter, Angelini) and the glucose concentration was adjusted to 5.5 mM. Astrocytes were used for experiments at DIV15.

2.4. Astrocyte-neuronal co-culture

To obtain astrocyte-neuronal co-culture, the cells were obtained as previously described. Neurons were seeded on plastic culture plates (Corning) previously coated with poly-D-lysine. At DIV8, astrocytes were re-seeded on semipermeable inserts (0.4 μm pore size, Corning). At DIV11 of astrocytes, corresponding at DIV3 for neurons, medium was renewed and the inserts were placed over the neurons. Cells were co-cultured and harvested at DIV7 of neurons, corresponding at DIV15 for astrocytes.

3. CELL TRANSFECTION

Cells were transfected with the aim to overexpress cDNA (complementary DNA) 24 or 96 hours before cell recollection. Transfection of cells with plasmid vectors was carried out using a final concentration of 1.6 μg/ml of DNA.

To transfect MEFs, a previously described protocol (Boussif *et al.,* 1995) with some variations was used. Thus, after incubation of the plasmid with 1 μM polyethylenimine (PEI, Sigma-Aldrich) for 10 min at room temperature, the mixture was added to the cells, which were incubated in OptiMEM medium (Invitrogen) for 1h. After washing with phosphate buffer saline (PBS, 136 mM NaCl, 2.7 mM KCl, 7.8 mM $Na_2HPO_4 \cdot 2H_2O$, 1.7 mM KH_2PO_4, pH 7.4) the cells were incubated in DMEM with 10% v/v FBS and 25 mM D-glucose.

Astrocytes were transfected using the cationic reagent Lipofectamine LTX with Plus Reagent™ (Invitrogen), following manufacturer's instructions. The protocol is based on the incubation of the plasmid DNA with Lipofectamine and the Plus Reagent in OptiMEM medium. The expression of the proteins encoded by the plasmid DNA was confirmed by immunoblotting.

Plasmid vectors used (**Table 1**) were obtained following transformation of *E. coli* competent cells, strain DH-5α, by heat shock. Bacteria culture mediums (LB, LB-agar and 2 x YT) were prepared with bactotriptone, yeast extract and agar from DIFCO Laboratories. Extraction and purification of the plasmids after the amplification in bacteria was performed using the Wizard plus Midipreps system (Promega).

Plasmid	Protein	Brand
pIRES2eGFP		Invitrogen
pIRES2eGFP-mitoCatalase	mitoCatalase	Supplied from J. A.Enríquez (CNIC, Madrid)
pEGFP-C1		Invitrogen
pEGFP-C1-NRF2 PM	NRF2 PM	Published by Jimenez-Blasco et al. 2015

Table 2: Plasmid vectors used. Name of the plasmid vector, protein encoded and origin are specified. NRF2 PM: Nuclear factor (erythroid-derived 2)-like 2 phosphomimetic, published by Jimenez-Blasco et al. (Jimenez-Blasco, *et al.,* 2015).

4. ROS MEASUREMENTS

4.1. Hydrogen peroxide

The production of hydrogen peroxide (H_2O_2) in whole cells or in fresh isolated mitochondria was assessed using the Amplex Red™ dye (Life Technologies). In presence of horseradish peroxidase (HRP), the Amplex Red™ reagent reacts with hydrogen peroxide in a 1:1 stoichiometry to produce the red-fluorescent oxidation product, resorufin (λ_{exc} 538 nm; λ_{em} 604 nm), as indicated in the **Scheme 4.**

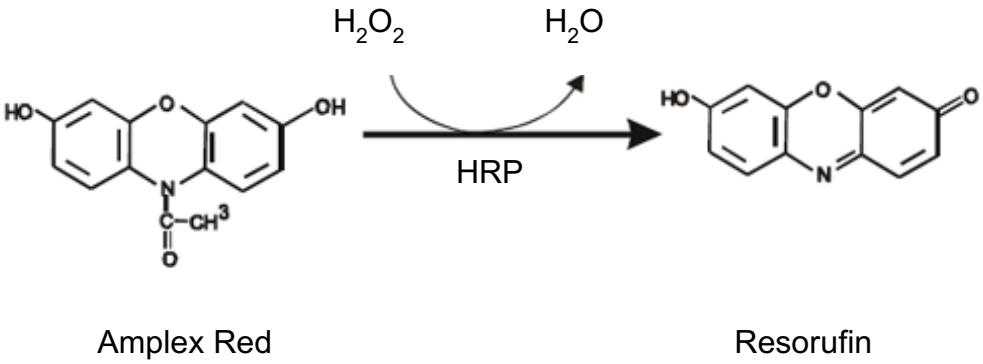

Scheme 4: Amplex Red™ reaction. Amplex Red™ dye is oxidized by H_2O_2 in presence of the horseradish peroxidase, liberating the fluorescent molecule Resorufin.

For the hydrogen peroxide measurement, cells or fresh isolated mitochondria were incubated with the Amplex Red™ dye (9.45 μM) in Krebs Ringer Phosphate Glucose Buffer (KRPG: 145 mM NaCl, 5.7 mM Na_2HPO_4, 4.86 mM KCl, 0.54 mM $CaCl_2$, 1.22 mM $MgSO_4$, 5.5 mM glucose, pH 7.35) in presence of HRP (0.1 U/ml). Luminescence was recorded for 2 hours at 30 minutes intervals using a Fluoroskan Ascent FL (Thermo Fisher) (λ_{exc} 538 nm; λ_{em} 604 nm). Hydrogen peroxide release rate was calculating extrapolating the slopes to those obtained from a hydrogen peroxide standard curve and the results were expressed as arbitrary unit (fold) between the control, to which is assigned the value of 1, and the sample condition.

4.2. mROS

mROS were measured using the fluorescent probe MitoSOX™ Red (Life Technologies). This probe is live-cell permeant and is rapidly and selectively targeted to the mitochondria. Once in the mitochondria, MitoSOX™ Red reagent is oxidized by mROS and it exhibits red fluorescence. The oxidation product becomes highly fluorescent upon binding to nucleic acids. Cells were incubated with 2 μM MitoSOX™ Red for 30 min at 37°C in a 5% CO_2 atmosphere in Hank's Balanced Salt Solution (HBSS) (134.2 mM NaCl, 5.26 mM KCl, 0.43 mM KH_2PO_4, 4.09 mM $NaHCO_3$, 0.33 mM $Na_2HPO_4 \cdot 2H_2O$, 5.44 mM glucose, 20 mM HEPES (4-(2-hydroxyethyl)-1-piperazineethanesulfonic acid), 4 mM

$CaCl_2 \cdot 2H_2O$, pH 7.4). Cells were then washed with PBS and trypsinized. MitoSOX™ red fluorescence was detected in channel FL3 in a FACScalibur (BD, Biosciences) flux cytometer equipped with a 15 mW argon ion laser tuned at 488 nm and analysed using CellQuest™ PRO and Paint-a-Gate™ PRO (BD, Biosciences) software. Results were expressed in arbitrary units.

4.3. Extracellular superoxide

The production of extracellular superoxide was measured following a previous published protocol (Li *et al.*, 2016) with some modifications. This method is based on the reduction of the oxidized cytochrome C (Cyt C) to its reduced form by the superoxide. Reduced Cyt C absorbs light at λ=550 nm and the value of absorbance is directly proportional to its concentration. To determine the extracellular superoxide production, intact astrocytes in a 96-well plate were washed twice with KRPG and incubated with 120 µM oxidized Cyt C (Sigma-Aldrich), for 4 hours at 37°C. Thus, absorbance at 550 nm was recorded using a Fluoroskan Ascent FL (Thermo Fisher). Superoxide concentration was calculated using the extinction coefficient of the reduced form of Cyt C and normalized to the amount of proteins. Results are expressed as arbitrary unit (fold) between the control, to which is assigned the value of 1, and the sample condition.

5. MITOCHONDRIAL MEMBRANE POTENTIAL MEASUREMENT

The mitochondrial membrane potential ($\Delta\Psi_m$) was assessed using the cyanine dye DiIC1(5) (1,1′,3,3,3′,3′-hexamethylindodicarbo-cyanine iodide) (Life Technologies). DiIC1(5) is a cationic probe that accumulates primarily in mitochondria with active membrane potentials, hence the fluorescence intensity is directly proportional to the $\Delta\Psi_m$. Cells were incubated with DiIC1(5) dye (50 nM) in PBS at 37°C for 30 minutes in a bath with soft agitation. $\Delta\Psi_m$ intensity signal was detected in channel FL4 in a FACScalibur (BD, Biosciences) flux cytometer and analysed using CellQuest™ PRO and Paint-a-Gate™ PRO (BD, Biosciences) software. Once analysed, cells were incubated for 15 minutes with the

mitochondrial uncoupler CCCP (carbonyl cyanide *m*-chlorophenyl hydrazone) (10 mM) to define the depolarized value. Results were expressed in arbitrary units.

6. PROTEIN EXTRACTION

6.1. Total protein extraction

To obtain total cell protein extracts, cells were washed with cold PBS and lysed in RIPA buffer (1% sodium dodecylsulphate, 10 mM ethylene diamine tetraacetic acid (EDTA), 1 % v/v Triton Tx-100, 150 mM NaCl, 10 mM Na_2HPO_4 , pH 7.0), supplemented with phosphatase (1 mM Na_3VO_4 , 50 mM NaF) and protease (100 µM phenylmethylsulfonyl fluoride (PMSF), 50 µg/ml aprotinine, 50 µg/ml leupeptine, 50 µg/ml pepstatin, 50 µg/ml anti-papain, 50 µg/ml amastatin, 50 µg/ml bestatin and 50 µg/ml soybean trypsin inhibitor) inhibitor cocktail, and boiled for 5 minutes. Extracts were then centrifuged at 13,000 *g* for 10 minutes and the supernatant transferred to a new tube.

6.2. Cytosolic and nuclear fractionation *in vitro*

To obtain cytosolic and nuclear fractions from cell cultures, a previously reported protocol (Zancai *et al.,* 2005) was used, with some modifications. This method first uses a mildly aggressive solution (Cytosolic buffer) that fragmentises cellular membranes maintaining the integrity of the nuclei, which are lysed using a more aggressive solution (Nuclear buffer) to obtain nuclear proteins exclusively (**Scheme 5**).

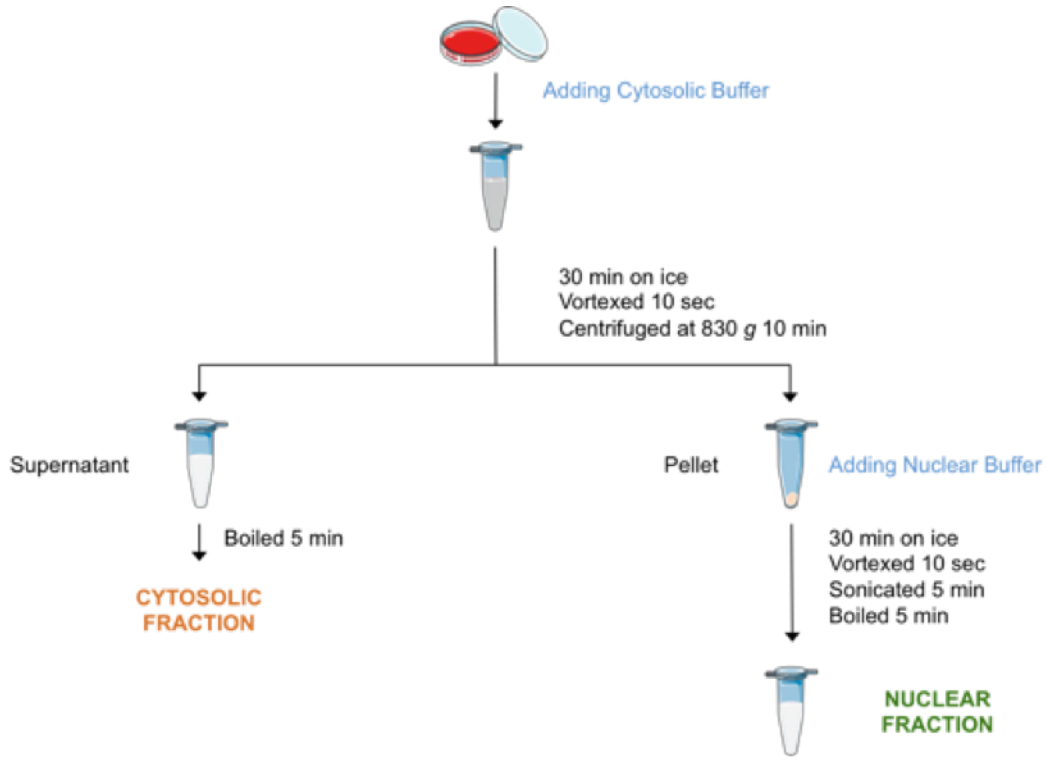

Scheme 5: Cytosolic and nuclear fractionation *in vitro*. Cytosolic and nuclear fractions were obtained following a differential centrifugation protocol.

Cells were washed with cold PBS containing 1 mM $MgCl_2$, harvested with Cytosolic buffer (10 mM HEPES, 1.5 mM $MgCl_2$, 10 mM KCl, 1 mM EDTA, NP-40 0.1%, v/v, 1.5 M sucrose and protease and phosphatase inhibitor cocktail, pH 7.9), triturated with a micropipette to promote cell lysis, left on ice for 30 minutes and vortexed for 10 seconds. After checking the cell lysis under a light microscope, extracts were centrifuged at 830 *g* for 10 minutes and the cytosolic fraction (supernatant) was removed and boiled for 5 minutes. Lysis of the nuclei was performed by re-suspending the nuclear pellet in Nuclear buffer (50 mM HEPES, 1.5 mM $MgCl_2$, 10 mM KCl mM, 0.5 mM NaCl, 1 mM EDTA, NP-40 1%, v/v, and protease and phosphatase inhibitor cocktail, pH 7.9), triturated with a micropipette, left on ice for 1 hour, vortexed at maximum speed for 10 seconds, boiled for 5 minutes and sonicated for 5 minutes.

6.3. Cytosolic and nuclear fractionation *ex vivo*

To obtain cytosolic and nuclear fractions from brain, liver, heart and kidney tissue, a previously reported protocol (Dimauro *et al.,* 2012) was used. Fresh tissue (approximately 50 mg) was washed with cold PBS, minced on ice using sharp scissor and re-suspended in 500 µl of STM buffer (250 mM sucrose, 50 mM Tris-HCl, 5 mM $MgCl_2$, protease and phosphatase inhibitor cocktail, pH 7.4) and homogenized for 1 minute on ice using a Teflon pestle attached to a Potter-Elvehjem homogeniser set to 1,000 rpm. The homogenate was then inspected and if intact tissue was still evident, the homogenisation was repeated. The homogenate was decanted into a centrifuge tube and maintained on ice for 30 minutes, vortexed at maximum speed for 15 seconds and then centrifuged at 800 *g* for 15 minutes. The pellet was labelled as P_0 and kept on ice, the supernatant was labelled as S_0 ad used for subsequent isolation of cytosolic fraction (**Scheme 6**).

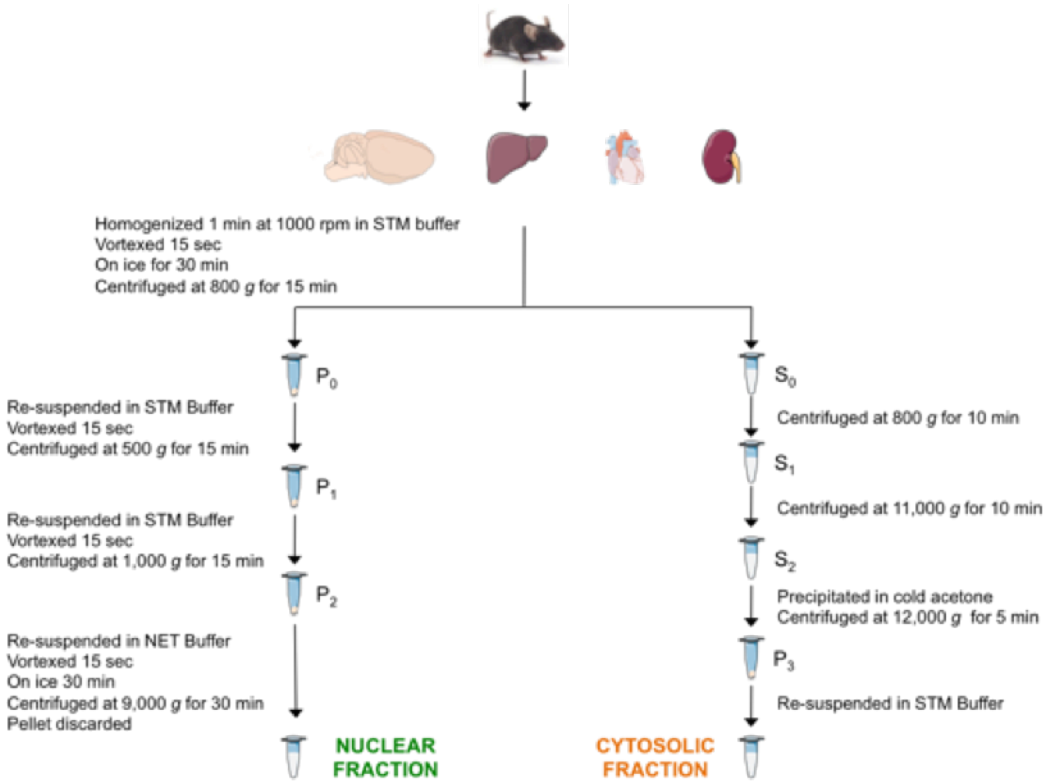

Scheme 6: Cytosolic and nuclear fractionation *ex vivo*. Cytosolic and nuclear fractions were obtained following a differential fractionation protocol.

The pellet P_0 (containing nuclei and debris) was re-suspended in 500 µl of STM buffer, vortexed at maximum speed for 15 seconds and then centrifuged at 500 *g* for 15 minutes. Subsequently the above step, the nuclear pellet was labelled as P_1 and kept on ice, while the supernatant S_1 (containing cell debris) was discarded. To further increase the purity, P_1 fraction was washed in 500 µl of STM buffer, vortexed at maximum speed for 15 seconds and then centrifuged at 1,000 *g* for 15 minutes. The supernatant was discarded and the pellet was labelled as P_2 and re-suspended in 300 µl of NET buffer (20 mM HEPES, 1.5 mM $MgCl_2$, 0.2 mM EDTA, 20% glycerol, 1% Triton-X-100, protease and phosphatase inhibitor cocktail, pH 7.9) using a pipette to triturate until homogeneous. Pellet P_5 was vortexed at maximum speed for 15 seconds and incubated on ice for 30 minutes. This fraction containing the nuclei were lysed with 20 passages through a micropipette and sonicated for 5 minutes. The lysate was centrifuged at 9,000 *g* for 30 minutes and the resulting supernatant was the nuclear fraction.

Cytosolic fraction was extracted from S_0 by centrifugation at 800 *g* for 10 minutes. The pellet was discarded and the supernatant S_1 was centrifuged at 11,000 *g* for 10 minutes. The pellet was discarded and the supernatant S_2 (containing cytosol and microsomal fraction) was precipitated in 500 µl of 100% cold acetone at -20ºC for at least 1 hour, followed by centrifugation at 11,000 *g* for 10 minutes. The supernatant was discarded and the pellet P_3 was re-suspended in 300 µl of STM buffer and labelled as cytosolic fraction.

6.4. Cytosolic and mitochondrial fractionation

To obtain cytosolic and mitochondrial fractions from cell culture, a differential centrifugation protocol was used (Almeida *et al.,* 1998). Cells grown in 145 cm^2 plates were collected in Mitochondria Isolation Buffer (MIB, 320 mM sucrose, 1 mM potassium EDTA, 10 mM Tris-HCl and the protease and phosphatase inhibitor cocktail, pH 7.4). Cells were centrifuged at 600 *g* for 5 minutes and the pellet re-suspended in MIB. After a 18 stroke homogenization step in a Teflon pestle attached to a Potter-Elvehjem homogeniser, homogenate was centrifuged three times at 1,300 *g* for 10 minutes, keeping the supernatants in every step. The mitochondrial pellet resulted from the final centrifugation (at 17,000 *g* for 12

minutes) was re-suspended in RIPA buffer, and the supernatant, containing the cytosolic fraction, was kept on ice (**Scheme 7**).

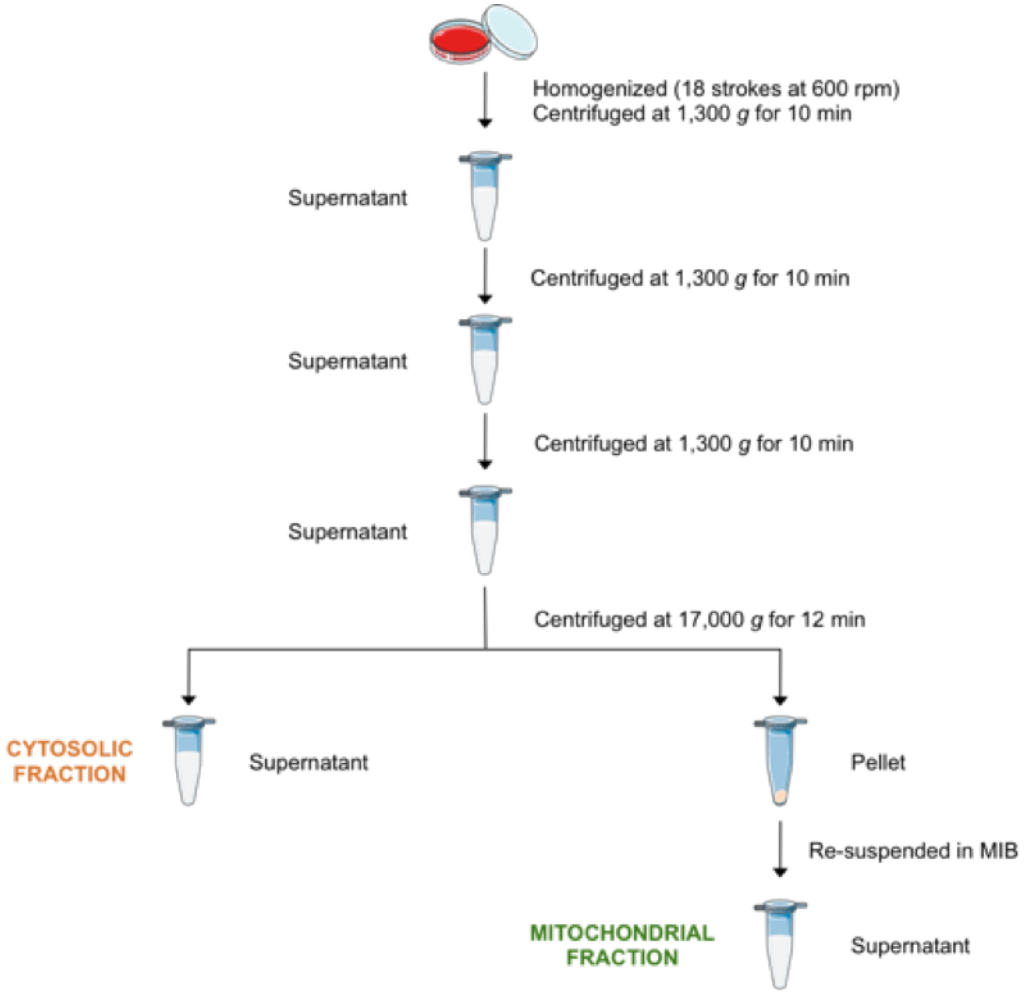

Scheme 7: Cytosolic and mitochondrial fractionation *in vitro*. Cytosolic and mitochondrial fraction were obtained following a differential fractionation protocol.

6.5. Protein concentration determination

Protein concentration in samples was determined using the commercially available BCA (bicinchoninic acid) protein assay kit (Pierce). This method is based on the reduction of Cu^{2+} (blue) to Cu^{+} by the peptide bond. The amount of Cu^{2+} reduced is proportional to the amount of protein present in the solution. Next, two molecules of BCA chelate with each Cu^{+} ion, forming a purple-colored

complex that strongly absorbs light at wavelength of 562 nm that was measured with a Multiskan Ascent (Thermo Electron Corp) spectrophotometer. Protein concentration was determined using a BSA standard curve.

7. ELECTROPHORESIS AND PROTEIN IMMUNODETECTION (WESTERN BLOT)

Extract of whole cells, cytosolic-, nuclear- and mitochondrial-fraction were obtained as previously described (see Section 6). Aliquots of the samples and a molecular weight marker (PageRuler^{TM} Plus Prestained Protein Ladder, Thermo Scientific) were loaded in a sodium dodecyl sulfate (SDS) polyacrylamide gel (acrilamide/bisacrilamide 29/1; BioRad Laboratories S.A.) and subjected to vertical electrophoresis (MiniProtean, Bio-Rad). Proteins were transferred to nitrocellulose membranes (Hybond®, Amersham Biosciences), blocked with 5% w/v low-fat milk in TTBS (20 mM Tris, 500 mM NaCl, 0.1 % v/v Tween 20, pH 7.5) for 1 hour at room temperature, and incubated with the primary antibody (**Table 2**) over night at 4ºC. As loading control β-Actin was used for whole cells, GAPDH for cytosolic fraction, Lamin-B for nuclear fraction and VDAC for mitochondrial fraction.

The following day, membranes were washed 3 times with TTBS and incubated with the secondary antibody (**Table 2**), conjugated with the horseradish peroxidase (HRP), in 2% w/v BSA in TTBS for 1 hour at room temperature. Signal was detected with the enhanced chemiluminescence kit (Pierce, Thermo Scientific) by exposing membranes on a Fuji Medical X-Ray Film (Fujifilm). For quantification, auto radiographies were scanned and the bands were analyzed using image treatment software (NIH Image, Wayne Rasband, National Institutes of Health). Values were expressed as the target protein/loading control band intensities ratio.

Antibody	Host	Dilution	Reference	Brand
Primary antibodies				
6-phosphogluconate dehydrogenase (6PGD)	Rabbit	1:2,000	ab129199	Abcam
β-Actin	Mouse	1:30,000	A5441	Sigma
Cleaved Caspase-3 (Asp-175)	Rabbit	1:1,000	9661	Cell Signaling
Catalase	Rabbit	1:1,000	PA5-23246	Thermo Scientific
Gliceraldehide 3-phosphate dehydrogenase (GAPDH)	Mouse	1:40,000	4300	Ambion
Glucose-6-phosphate dehydrogenase (G6PD)	Rabbit	1:1,000	A9521	Sigma
Glutamate cysteine ligase (Catalytic subunit, GCL)	Rabbit	1:1,000	sc-22755	Santa Cruz
Human influenza hemagglutinin (HA)-tag	Mouse	1:10,000	26183	Thermo Scientific
Histone deacetylase 4 (HDAC4)	Rabbit	1:1,000	2072	Cell Signaling
Lamin B	Mouse	1:500	sc-374015	Santa Cruz
Nuclear factor (erythroid-derived-2)-like 2 (Nrf2)	Rabbit	1:1,000	ab62352	Abcam
Voltage-dependent anion channel (VDAC)	Rabbit	1:1,000	PC548	Calbiochem
Secondary antibodies				
Anti-Mouse IgG (H+L)-HRP Conjugate	Goat	1:10,000	170-6516	BioRad
Anti-Rabbit IgG-HRP conjugate	Goat	1:10,000	sc-2030	Santa Cruz

Table 3 Antibodies employed for Western Blot immunodetection. Dilutions used, references and suppliers are specified.

8. MITOCHONDRIA ISOLATION

To obtain large quantities of isolated mitochondria in order to measure mCAT activity (see Section 9), a different centrifugation protocol was used (Acín-Pérez *et al.,* 2008). Cells grown in 145 cm^2 plates were washed with cold PBS, collected and centrifuged at 500 *g* for 5 minutes. The supernatant was discarded and the pellet was re-suspended in 1 ml of Buffer A (83 mM sucrose, 10 mM MOPS (3-(N-morpholino)propanesulfonic acid, pH 7.2) and homogenized (10 strokes) in a Teflon pestle attached to a Potter-Elvehjem homogeniser. The same volume of Buffer B (250 mM sucrose, 30 mM MOPS, pH 7.2) was added to the sample and the homogenate was centrifuged at 1,000 *g* for 5 minutes to remove unbroken cells and nuclei. The pellet was discarded and the supernatant was centrifuged at 12,000 *g* for 2 minutes. The supernatant was discarded and the pellet, which contains the mitochondrial fraction, was washed in 200 µl of Buffer C (320 mM sucrose, 1 mM EDTA, 10 mM Tris-HCl, pH 7.4) and centrifuged at 12,000 *g* for 2 minutes. The supernatant was discarded and the pellet, containing the washed mitochondria, was re-suspended in 200 µl of Buffer D (1 M 6-aminohexanoic acid, 50 mM Bis-Tris HCl, pH 7.0) (**Scheme 8**). Protein concentration was determined using the BCA method, as previously described (see Section 6.5).

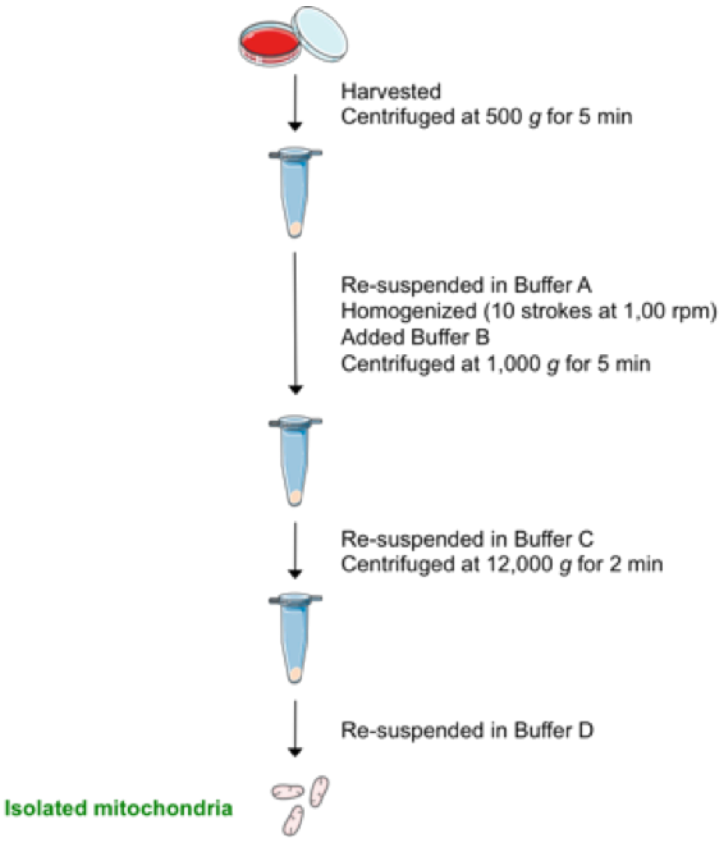

Scheme 8: Isolation of mitochondria. Large quantities of mitochondria were isolated following a previously published protocol (Acín-Pérez et al. 2008) based on centrifugal differentiation.

9. mCAT ACTIVITY MEASUREMENT

mCAT activity was measured from isolated mitochondria according to a previously published protocol (Quintana-Cabrera and Bolaños 2013), with some modifications. The assay is based on the ability of mCAT to neutralize the exogenous hydrogen peroxide. Mitochondria were incubated with different hydrogen peroxide concentrations for different times; once the reactions were stopped, samples were incubated with a solution containing Fe^{2+}, which is oxidized by hydrogen peroxide at Fe^{3+}. The incubation solution also contains SCN^-, which reacts with Fe^{3+} to form the orange complex $FeSCN^{2+}$, which absorbs light at wavelength of 492 nm (**Scheme 9**). The value of the absorbance is directly proportional to the residual hydrogen peroxide concentration.

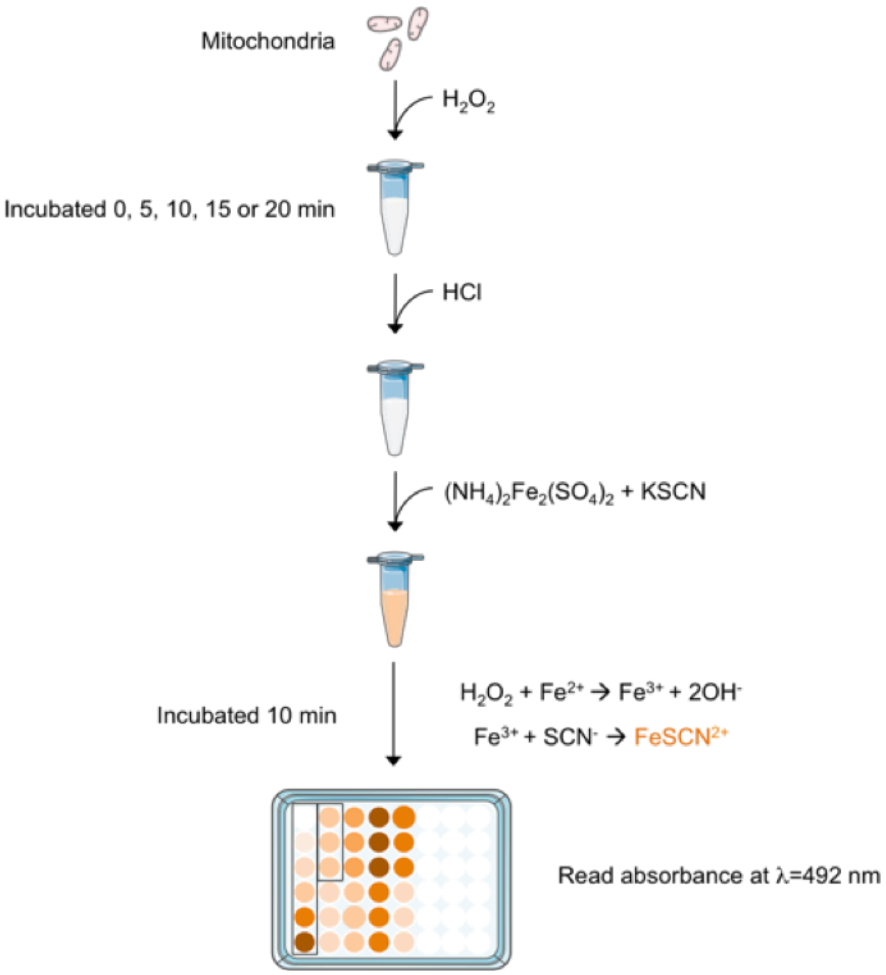

Scheme 9: Evaluation of the mCAT activity. To determine the mCAT activity, a colorimetric assay based on the formation of the orange complex $FeSCN^{2+}$ was used.

To determine the mCAT activity, 5 µg of mitochondria were incubated in a final volume of 50 µl of 0.1 M Phosphate Buffer (PB) pH 7.4 with 0, 25, 50 and 100 µM hydrogen peroxide for 0, 5, 10, 15 and 20 minutes. Reactions were stopped using 37% HCl. Then, 3.2 mM $(NH_4)_2Fe(SO_4)_2$ (ammonium ferrous sulfate hexahydrate) and 180 mM KSCN (potassium thiocyanate) were added and the samples were incubated for 10 minutes at room temperature in the dark. The absorbance at 492 nm was measured using a Fluoroskan Ascent FL (Thermo Fisher) and the concentration of the residual hydrogen peroxide was calculated using a standard curve.

10. IMMUNOCYTOCHEMISTRY

Astrocytes were grown on glass coverslips. At DIV15 they were fixed with 4% paraformaldehyde (v/v) in PBS for 20 minutes and washed with PBS. Subsequently, astrocytes were incubated in 5% goat serum, 1% BSA PBS-Tx 0.2% for 1 hour at room temperature. Afterwards, they were incubated with the primary antibody (**Table 3**) in 2% goat serum, 1% BSA, PBS-Tx 0.2% overnight at 4ºC. The following day astrocytes were washed with PBS-Tx 0.2% and incubated with the secondary antibody (**Table 3**) and the nuclear marker DAPI (Sigma, Ref D9542, 1/10,000) in 2% goat serum, 1% BSA, PBS-Tx 0.2% for 1 hour at room temperature. Subsequently, glass coverslips were placed on a glass slide using SlowFade® (Molecular Probes) in order to avoid fluorescence loss. Confocal microscopy images were obtained using a spinning disk confocal microscopy Olympus IX81 and processed with Adobe Photoshop cs5.5 software.

Antibody	Host	Dilution	Reference	Brand
Primary antibodies				
Heat shock protein 60 (HSP60)	Rabbit	1:500	ab46798	Abcam
Human influenza hemagglutinin (HA)-tag	Mouse	1:100	2367	Cell Signaling
Nuclear factor (erythroid-derived-2)-like 2 (Nrf2)	Rabbit	1:500	ab62352	Abcam
Secondary antibodies				
Cy™2-conjugated AffiniPure Goat Anti Mouse IgG (H+L)	Goat	1:500	115-225-003	Jackson ImmunoResearch
Cy™2-conjugated AffiniPure Goat Anti Rabbit IgG (H+L)	Goat	1:500	111-225-144	Jackson ImmunoResearch
Cy™3-conjugated AffiniPure Goat Anti Rabbit IgG (H+L)	Goat	1:500	111-165-003	Jackson ImmunoResearch

Table 3: Antibodies employed for immunocytochemistry. Dilutions used, references and suppliers are specified.

11. RNA PURIFICATION

To obtain a total RNA fraction, the Genelute™ Mammalian Total RNA kit (Sigma-Aldrich) was used.

Cells were lysed with a solution of β-mercaptaethanol:Lysis Solution in 1:100 proportion. The lysates were filtered through a Genelute Filtration Column and centrifuged at 16,000 *g* in order to eliminate cellular debris and discard the DNA. An equivalent 70% ethanol volume (prepared in DEPC (dyethyl pyrocarbonate) water RNase free) was added and the samples were vortexed. After that, the samples were passed to a Genelute Binding Column, which retains the RNA. The filtered was discarded and the column was washed with the Wash Solution 1.

Once the RNA was separated, the column was treated with 100 U of DNAse I (Roche) for 15 minutes at room temperature in a buffer containing 400 mM Tris-HCl, 100 mM NaCl, 60 mM $MgCl_2$, 10 mM $CaCl_2$, pH 7.9. To eliminate residual DNA, column was washed first with the Wash Solution 1 and then with the Wash Solution 2 Concentrate/ethanol. Finally, the total RNA was eluted with 50 µl of Elution Solution through a centrifugation at 16,000 *g* for 1 minute.

To obtain a micro-RNA (miRNA) enriched fraction, the miRNeasy kit (Qiagen) was used. Cells were lysed with QIAzol Lysis reagent, homogenized by vortexing for 1 minute and left at room temperature for 5 minutes to promote the dissociation of nucleoprotein complexes. Subsequently, chloroform was added, the tube was vortexed for 15 seconds and left at room temperature for 3 minutes. After that, the tube was centrifuged at 12,000 *g* at 4ºC, The aqueous phase was transferred to a new tube and mixed with an equivalent 70% ethanol volume (prepared in DEPC water RNase free) and the tube was vortexed. The sample was then passed to an RNeasy Mini spin column, which retains the larger RNAs. The filtered containing the miRNA was passed to a new tube and mixed with 0.65 volumes of 100% ethanol. The sample was passed to a RNeasy Mini spin column and the filtered was discarded. To eliminate residual impurities, the column was washed first with RWT buffer, then with RPE buffer and finally with 80% ethanol (prepared in DEPC water RNAse free). The spin column membrane was dried by centrifugation at 8,000 *g* for 2 minutes and the miRNA-enriched fraction was

eluted in 14 µl of RNAse free water through a centrifugation at 8,000 *g* for 1 minute.

Purified RNA concentration was measured using the UV-Vis Nanodrop 2000 (Thermo Scientific). The absorbance ratio calculated between 260 and 280 nm (A_{260}/A_{280}), which determines the RNA purity, was 1.8 – 2.

12. REAL TIME QUANTITATIVE POLYMERASE CHAIN REACTION

Real Time quantitative Polymerase Chain Reaction (RT-qPCR) was used to evaluate the relative gene expression. This method compares target genes versus a housekeeping gene (*β-actin* in this case) of constant expression in the samples studied, at the same time that relativizes this expression to a control condition.

Concentration of primers for the RT-qPCR was optimized, calculating the efficiency for every pair of primers. Efficiencies in the range 90-110% were considered optimal conditions. To achieve this, serial RNA dilutions were incubated with different primers concentrations. In the **Table 4** they are shown the concentrations and the sequences of the primers used, following their optimization, for the different mRNA. This step is necessary to compare the different gene expression using the comparative method of C_t ($\Delta\Delta C_t$).

Gene	Forward sequence 5'→ 3'	Reverse sequence 5'→ 3'	Concentration (μM)
6pgd	5'-ATCTCCTACGCCCAAGGCTTTATG-3'	5'-AATTGAGGGTCCAGCCAAACTCAG-3'	0.3
β-Actin	5'-AGAGTCATGAGCTGCCTGAC-3'	5'-CAACGTCACACTTCATGATG-3'	0.4
G6pd	5'-ATGCAGGCCAACCGTCTATT-3'	5'-TGTCTGACTCATGCAGGTCT-3'	0.3
Gcl_c	5'-GGCACAAGGACGTGCTCAAGT-3'	5'-TTTGTCCTCTCCCCCTTCTC-3'	0.3
Gpx2	5'-CGGGACTACAACCAGCTCAAT-3'	5'-TCCGAACTGGTTGCAAGGGAA-3'	0.4
Ho-1	5'-AGCACAGGGTGACAGAAGAG-3'	5'-GAGGGACTCTGGTCTTTGTG-3'	0.4
Nox1	5'-AAATTCCAGCGTGCCGACAA-3'	5'-AACCAGGCAAAGGCACCTGT-3'	0.1
Nox2	5'-ATGCAGGAAAGGAACAATGC-3'	5'-GTGCACAGCAAAGTGATTGG-3'	0.1
Nox4	5'-TGCAGAGATATCCAGTCCTTCC-3'	5'-TCCCATCTGTTTGACTGAGG-3'	0.1
Nqo1	5'-GGGGACATGAACGTCATTCTCT-3'	5'-TTCTAAGACCTGGAAGCCAC-3'	0.4
Nrf2	5'-GCAGGACATGGATTTGATTGA-3'	5'-GTCAAACACTTCTCGACTTAC-3'	0.4
Prdx1	5'-CAAGTGATTGGCGCTTCTGT-3'	5'-TGTTCATGGGTCCCAATCCT-3'	0.4
Trx1	5'-GGTGTGGACCTTGCAAAATG-3'	5'-GGCAGTCATCCACATCCACTT-3'	0.4

Table 4: Sequences and concentrations of primers used for the RT-qPCR. *6pgd*: 6-phosphogluconate dehydrogenase; *G6pd:* Glucose-6-phoshate dehydrogenase; Gcl_c*:* Glutamate cysteine ligase, catalytic subunit; Gpx2: Glutathione peroxidase-2; *Ho-1:* Heme oxygenase-1; *Nqo1:* NAD(P)H dehydrogenase quinone-1; *Nox1*: NADPH-oxidase-1; *Nox2*: NADPH-oxidase-2; *Nox4*: NADPH-oxidase-4; *Nrf2:* Nuclear factor (erythroid-derived 2)-like 2; *Prdx1*: Peroxiredoxin-1; *Trx1:* Thioredoxin-1.

To perform the RT-qPCR the commercial kit Power Sybr Green RNA-to-C_t 1-Step kit (Applied Biosystems) was used, following the manufacture's protocol. This kit allows the reverse transcription of the mRNA to cDNA and the following PCR in a unique step. 100 ng of purified RNA in a final volume of 20 μl were used. Every determination was performed in triplicate using the thermocycler Mastercycler ep Realplex (Eppendorf).

RT-qPCR conditions were: 30 minutes at 48ºC (reverse transcription step), 10 minutes at 95ºC (DNA polymerase activation step), 40 cycles of 15 seconds at 95ºC (denaturalization step) followed by 1 minute at 60ºC (annealing and elongation steps).

The value obtained for every reaction was the C_t (threshold cycle), which represents the cycle number at which the fluorescence generated within a reaction crosses the fluorescence threshold, a fluorescent signal significantly above the background fluorescence. For every gene studied, including the housekeeping

gene (*β-actin*), a C_t is obtained. ΔC_t sample is the Ct value for any sample normalized to the endogenous housekeeping gene (*β-actin*).

Comparative method of C_t ($\Delta\Delta C_t$) relates the number of copies of mRNA between different conditions, which is obtained using the formula:

$$2^{-[(C_t \text{ sample} - C_t \text{ housekeeping gene}) - (C_t \text{ control} - C_t \text{ housekeeping gene})]}$$

Results are expressed as arbitrary unit (fold) between the control, to which is assigned the value of 1, and the sample condition. Expression levels equal to 1 indicate no differences between the two conditions; lower levels to 1 indicate a decreased gene expression in the sample compared to the control condition; on the contrary, higher levels to 1 indicate an increased gene expression in the sample compared to the control.

13. miRNA EXPRESSION ANALYSIS

All the following techniques have been performed at the ADN Sequencing service of NUCLEUS, University of Salamanca.

13.1. miRNA reverse transcription

To perform the miRNA reverse transcription, 50 ng of miRNA-enriched fraction was mixed with 0.1 µl of 100 nM dNTP, 0.14 µl of RNase inhibitor (20 U/ µl), 0.67 µl of reverse transcriptase (50 U/ µl), 1 µl RT-Buffer 1X and 4.5 µl of primer pool (mixed to allow a final concentration of 0.05X for hsa-miR-1 and hsa-miR-206 and 0.5X for mmu-miR-202-5p) in a final volume of 10 µl. All reagents were purchased from Applied Biosystems. Samples were incubated for 5 minutes on ice, 30 minutes at 16ºC, 30 minutes at 42ºC and finally 5 minutes at 85ºC.

13.2. Pre-PCR amplification

Before the expression analysis of miRNA, the cDNA was pre-amplified. To do so, pre-PCR amplification reaction was done at 5 µl containing 2.5 µl TaqMan PreAmp Master Mix (2X), 1.25 µl of pooled TaqMan assay mix (0.2X each assay) and 1.25 µl of cDNA. The pre-amplification PCR was performed at one

cycle 95ºC for 10 minutes, 10 cycles at 95ºC for 15 seconds followed by 4 minutes at 60ºC. All reagents were purchased from Applied Biosystems.

13.3. miRNA expression analysis using 48.48 dynamic array

Relative miRNA expression was evaluated using a 48.48 dynamic array (Fluidigm Corporation). This method compares target miRNA versus a miRNA endogenous control (mmu-miR-202-5p in this case) of constant expression in the samples studied, at the same time that relativizes this expression to a control condition.

miRNA expression analysis was carried out using the 48.48 dynamic array (Fluidigm Corporation) following the manufacturer's protocol. Specifically, a 5 µl of sample mixture was prepared for each sample containing 2.5 µl TaqMan Universal Master Mix (No UNG) (Life Technologies), 0.25 µl of 20X GE Sample Loading Reagent (Fluidigm Corporation) and 2.25 µl of pre-amplified cDNA. Then, 5 µl of Assay mix was prepared with 2.5 µl of 20X TaqMan miRNA assay (Thermo Scientific) and 2.5 µl of 2X Assay Loading Reagent (Fluidigm Corporation). An integrated fluidic circuit (IFC) controller was used to prime the fluidic array (chip) with control line fluid and then with samples and assay mixes in the appropriate inlets. After loading, the chip was placed in the BioMark HD Instrument for PCR at 96.5ºC for 10 minutes, followed by 40 cycles at 96ºC for 15 seconds and 60ºC for 1 minute. Different miRNA expression was calculated using the comparative method of C_t ($\Delta\Delta C_t$), as previously described in Section 12. Data were analysed with Fluidigm Real-Time PCR Software (Fluidigm Corporation). TaqMan assays used were mmu-miR-202-5p, hsa-miR-1 and hsa-miR-206 (Thermo Scientific).

14. GLUTATHIONE CONCENTRATION DETERMINATION

To determinate the glutathione concentration, cells were washed with cold PBS and rapidly harvested with 1% w/v 5-sulfosalicylic acid with a cell scraper. An equal volume of 0.1 M NaOH was added to the same amount of cells for protein quantification. Cell lysates were centrifuged at 13,000 *g* for 5 minutes and the total glutathione concentration, which is the sum of reduced glutathione plus two-

fold the oxidized (GSx = GSH + 2GSSG), was measured in the supernatant using a previously described protocol (Tietze 1969). The assay is based on the GSH (reduced glutathione) oxidation at expense of the DTNB (5,5'-dithiobis-(2-nitrobenzoic acid) (Sigma-Aldrich) reduction to TNB (λ_{max}=405 nm). The newly formed GSSG (oxidized glutathione) is regenerated to GSH through the enzymatic activity of the glutathione reductase, which need NADPH (H^+) as a co-factor. This is a cyclic reaction (**Scheme 10**), whose reaction rate is directly proportional to the GSx (total glutathione) concentration.

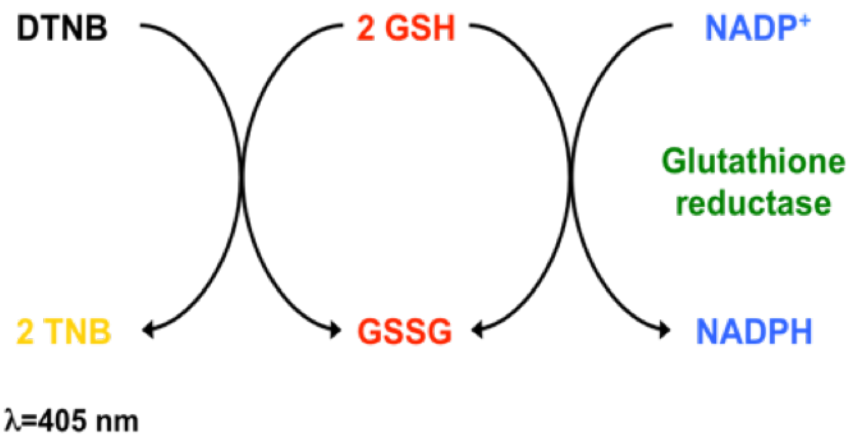

Scheme 10: GSx enzymatic determination. DTNB: 5,5'-dithiobis-(2-nitrobenzoic acid); GSH: reduced glutathione; $NADP^+$: Nicotinamide Adenine Dinucleotide Phosphate; TNB: 5'-thio-2-nitrobenzoic acid; GSSG: oxidized glutathione; NADPH: Nicotinamide Adenine

This determination was realized in a 96-wells plate mixing 10 µl of the sample, 90 µl of water and 100 µl of the buffer reaction (1 mM EDTA, 0.3 mM DTNB, 0.4 mM NADPH, 1 U/ml glutathione reductase, prepared in 0.1 mM PB, pH 7.5). Increases of absorbance, following the reaction between GSH and DTNB, was measured using a Fluoroskan Ascent FL (Thermo Fisher) at 405 nm, every 15 seconds during 2.5 minutes (10 iterations).

GSx concentration was determined extrapolating the slopes to those obtained from a GSSG standard curve (0-50 µM) and the results were expressed as nmol GSx / mg protein.

15. CASPASE-3 ACTIVITY DETERMINATION

To evaluate cellular apoptosis, the activity of the enzyme Caspase-3 (CSP-3) was chose as apoptotic marker. For this purpose, Caspase 3 Assay Kit, Fluorimetric (Sigma-Aldrich) was used following the manufacture's protocol. This assay is based on the hydrolysis of the peptide substrate Ac-DEVD-AMC (acetyl-Asp-Glu-Val-Asp-7-amino-4-methylcoumarin) by CSP-3, resulting in the release of the fluorescent AMC (7-amino-4-methylcoumarin) moiety (**Scheme 11**).

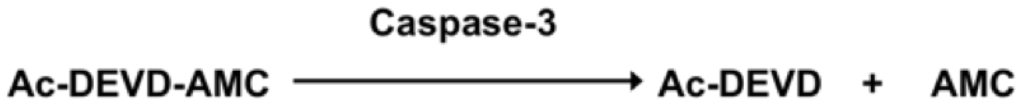

Scheme 11: Caspase-3 activity determination. Ac-DEVD-AMC: acetyl-Asp-Glu-Val-Asp-7-amino-4-methylcoumarin; Ac-DEVD: acetyl-Asp-Glu-Val-Asp; AMC: 7-amino-4-methylcoumarin.

The excitation and emission wavelengths of AMC are 360 nm and 460 nm, respectively. The concentration of the AMC released can be calculated from a standard curve determined with defined AMC solutions.

Cells were lysed with a Lysis Buffer (50 mM HEPES, 5 mM CHAPS, 5 mM DTT, pH 7.4) for 20 minutes on ice. Successively, Assay Buffer containing the Ac-DEVD-AMC substrate (20 mM HEPES, 2 mM EDTA, 0.1% CHAPS, 5 mM DTT, 16 µM Ac-DEVD-AMC, pH 7.4) was added, the solution was mixed well by pipetting and 200 µl was transferred to a 96 wells plate. The fluorescence was recorded for 2 hours at 20 minutes intervals at 37 ºC using a Fluoroskan Ascent FL (Thermo Scientific) (λ_{exc}=360 nm, λ_{em}=460 nm). CSP-3 activity was determined as AMC release rate extrapolating the slopes to those obtained from a AMC standard curve and the results were expressed as arbitrary unit (fold) between the control, to which is assigned the value of 1, and the sample condition.

16. PENTOSE-PHOSPHATE PATHWAY (PPP) FLUX MEASUREMENT

The PPP flux was measured in attached cells following a previously published protocol (Rodriguez-Rodriguez *et al.,* 2013). This method determines the PPP

flux by determining the difference of $^{14}CO_2$ produced from D-[1-^{14}C]-glucose, metabolized both in the tricarboxylic acid cycle and in the PPP, and the $^{14}CO_2$ produced from D-[6-^{14}C]-glucose, metabolized only in the tricarboxylic acid cycle, in the reactions catalyzed by isocitrate dehydrogenase and α-ketoglutarate dehydrogenase (**Scheme 12A and 12B**).

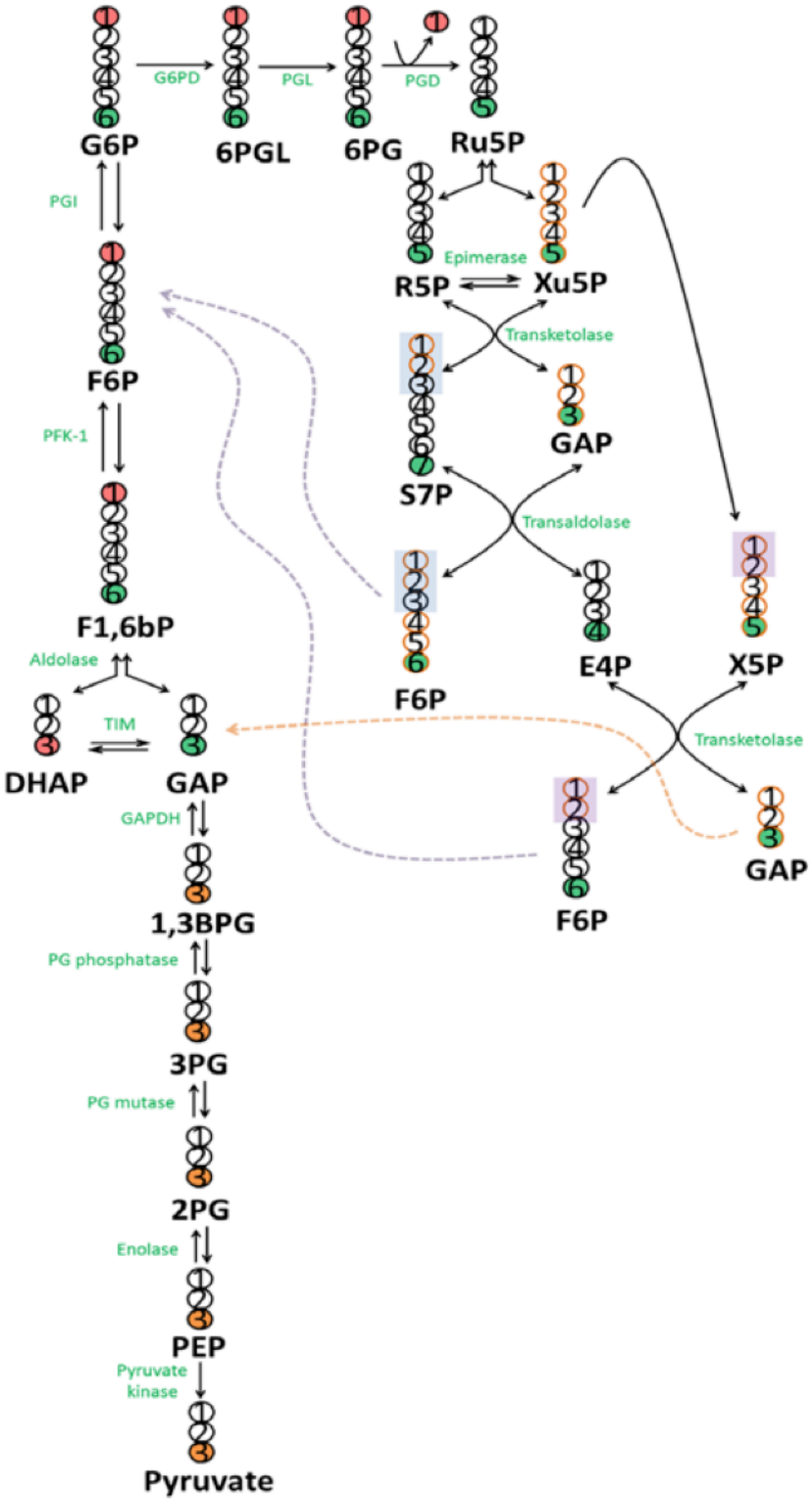

Scheme 12A: Schematic representations of the fate of the radiolabeled carbons used for the PPP flux assessment. D-[1-^{14}C]-glucose is decarboxylated in the reaction catalysed by 6-phosphogluconate dehydrogenase. D-[6-^{14}C]-glucose that enters PPP is transformed back into GAP or F6P in the non-oxidative branch of PPP. D-[6-^{14}C]-glucose and D-[1-^{14}C]-glucose can also enter glycolysis. After their transformation in DHAP and GAP they are indistinguishable.

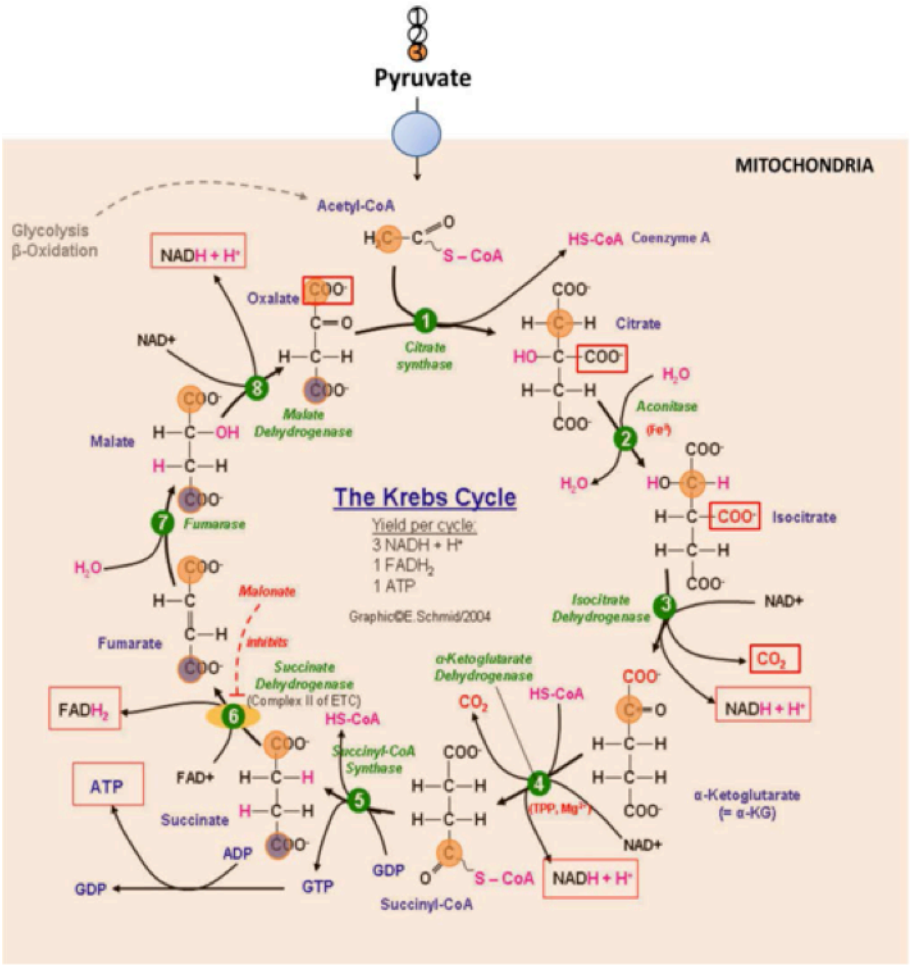

Scheme 12B: Schematic representations of the fate of the radiolabeled carbons used for the PPP flux assessment. Radiolabeled pyruvate, proceeding from D-[1-^{14}C]-glucose or D-[6-^{14}C]-glucose enters TCA and is decarboxylated in the different turns of the cycle in the reactions catalysed by isocitrate dehydrogenase and α-ketoglutarate dehydrogenase.

To do so, cells were seeded in the bottom of 25 cm^2 flasks. At DIV15 in culture, medium was replaced by 1.5 ml KRPG in presence of 0.5 µCi/ml of either D-[1-^{14}C]-glucose or D-[6-^{14}C]-glucose. Before sealing the flask with a rubber cap, a 1.5-ml Tube containing 0.8 ml of benzetonium hydroxide (Sigma-Aldrich) for $^{14}CO_2$ trapping was fixed inside the flask by holding it from the flask tab using a rib (**Scheme 13**).

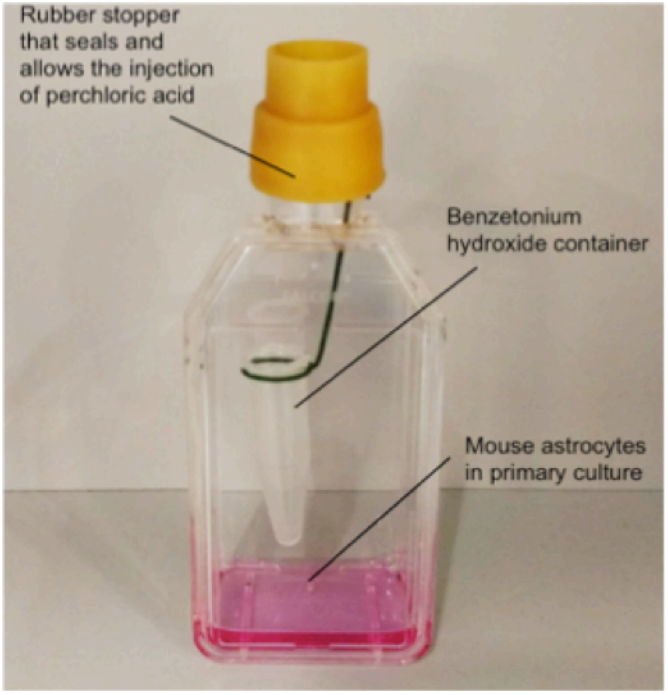

Scheme 13: Schematic representation of the method for PPP flux determination in attached cells.

In order to ensure an adequate O_2 supply throughout incubation period, the atmosphere of the flasks was gassed with an O_2:CO_2 (95:1) mixture for 20 seconds, before the flasks were sealed and incubated in a thermostatic orbital shaker for 90 minutes. After the incubation period, reaction was stopped by adding 0.15 ml of 20% w/v perchloric acid and flasks were incubated for another 90 minutes to allow $^{14}CO_2$ trapping by the benzetonium hydroxide. The tubes were placed in a vial containing Optiphase HiSafe III (PerkinElmer) scintillating liquid, vortexed at maximum speed for 20 seconds and left to equilibrate overnight. The following day, counts per minute was measured using a Tri-Carb 4810 TR (PerkinElmer) liquid scintillating analyser and results were expressed as nmol of glucose turned into $^{14}CO_2$ per hour and per mg protein.

The efficiency of $^{14}CO_2$ trappping by the benzetonium hydroxide was determined to be a 75% (Rodriguez-Rodriguez *et al.,* 2013). Total µCi in the tube where then measured for calculating the percentage of $^{14}CO_2$ trapped, which was taken in account for the calculations.

17.NADPH/NADP$^+$ RATIO DETERMINATION

To determine the concentration of the nucleotides NADPH and NADP$^+$, the commercial kit NADP/NADPH Assay Kit (Colorimetric) (Abcam) was used. The enzymes in the system specifically recognize NADP and NADPH in an enzyme cycling reaction.

Cells were trypsinized and centrifuged at 500 *g* for 5 minutes. The supernatant was discarded and the pellet was re-suspended in 500 µl of NADP/NADPH Extraction Buffer and kept on ice for 10 minutes. Samples were then vortexed for 10 seconds and centrifuged at 14,000 rpm for 5 minutes to remove insoluble material. The extracted NADP/NADPH supernatant was transferred to a new tube, labelled as NADPt (total NADP, containing NADPH and NADP$^+$) and kept on ice. To determine NADPH only, 200 µl of NADPt was separated into a new tube and heated at 60 ºC for 30 minutes to decompose NADP$^+$. The samples containing only NADPH were then cooled on ice and centrifuged 1 minute at 14,000 rpm.

The determination was realized in a 96-wells plate mixing 50 µl of the sample in presence of 100 µl of the buffer reaction (98 µl NADP Cycling Buffer, 2 µl NADP Cycling Enzyme) and incubated 5 minutes at room temperature to convert NADP$^+$ to NADPH. Then, 10 µl of NADPH Developer was added to each well and incubated for 2 hours at room temperature. The absorbance at 450 nm was measured using a Fluoroskan Ascent FL (Thermo Fisher).

NADPt and NADPH concentration was determined using a NADPH standard curve (0-100 pmol/well). NADP$^+$ concentration was calculated from the formula

$$\text{NADPt} - \text{NADPH} = \text{NADP}^+$$

18. *de novo* LIPOGENESIS FLUX MEASUREMENT

To measure the flux of the *de novo* lipogenesis (DNL), a previously reported protocol (Tabernero *et al.,* 1993) with some modifications was used. This method determines the DNL flux by determining the incorporation of ^{14}C in the total lipidic fraction. To do so, astrocytes were seeded in 6 wells plate. At DIV15, medium was replaced by KRPG in the presence of 3 µCi/ml of D-[6-^{14}C]-glucose

and cells were incubated in a thermostatic orbital shaker at 37ºC for 3 hours. After the incubation period, cells were washed twice with PBS, recollected and centrifuged at 500 *g* for 5 minutes. The supernatant was discarded and the pellet was re-suspended in 500 µl of a mixture chloroform/methanol (2:1, v/v) and incubated at -20ºC for 16 hours. Subsequently, 250 µl of 0.3% (w/v) NaCl saturated with chloroform were added, the samples were centrifuged at 1,500 *g* for 15 minutes and the aqueous phase, containing the cellular hydro soluble components, was discarded. Later, this same process was repeated, this time using 250 µl of 0.3% (w/v) NaCl saturated with chloroform and 180 µl of methanol. The resulting chloroformic phase was passed to a new tube. Every step was performed at 4ºC. An aliquot of 50 µl of the chloroformic phase containing the lipid fraction, was placed in a vial containing Optiphase HiSafe III (PerkinElmer) scintillating liquid, vortexed at maximum speed for 20 seconds and left to equilibrate overnight. The following day, counts per minute was measured using a Tri-Carb 4810 TR (PerkinElmer) liquid scintillating analyser and results were expressed as nmol of glucose incorporated in lipids per hour and per mg protein.

19. STATISTICAL ANALYSIS

All measurements were carried out at least in three different culture preparations or animals, and the results were expressed as the mean values ± SEM (Standard Error of the Mean). For the comparison between two groups of values, the statistical analysis of the results was performed by the Student's *t* test. The statistical analysis was performing using the SPSS software. In all cases, $p<0.05$ was considered significant.

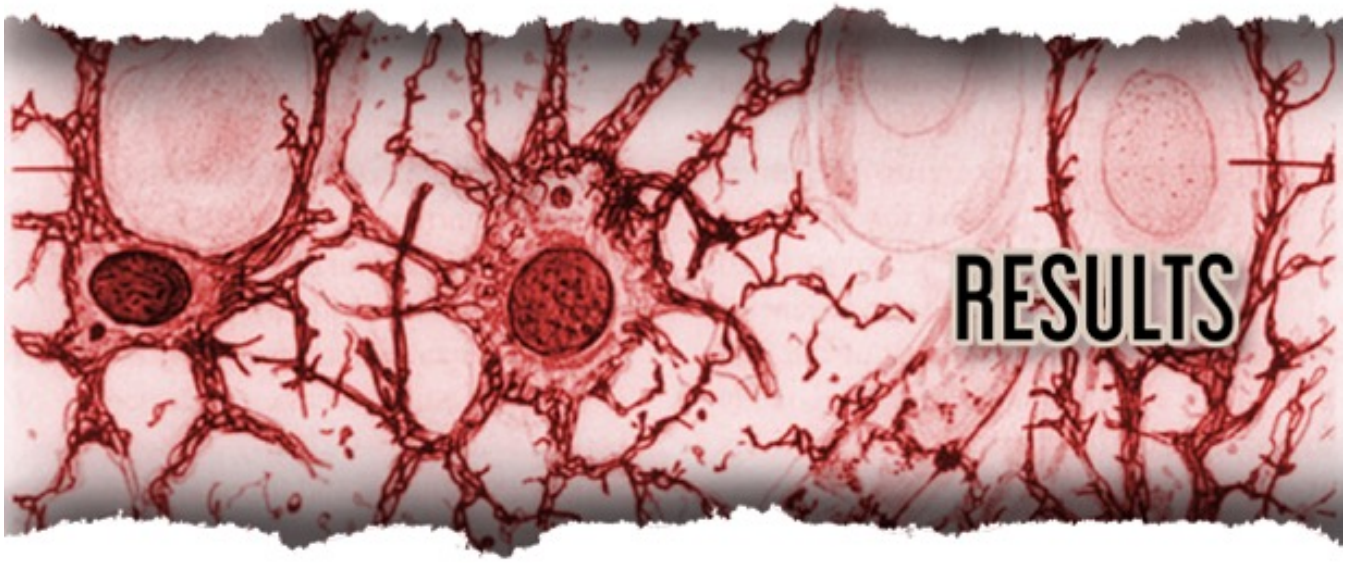
RESULTS

1. mCAT expression down-modulates endogenous mROS in MEFs

Astrocytes, despite their major antioxidant defenses, produce higher mitochondrial reactive oxygen species (mROS) compared with neurons under basal conditions (Lopez-Fabuel *et al*., 2016). The vast majority of studies on ROS-mediated cell signalling have used a strategy based on increasing ROS, either by exogenous or endogenously-supplied ROS. However, this approach might mask the beneficial effects of mROS. In this work the alternative approach to down-modulate mROS abundance specifically is used.

Several transgenic mouse models able to down-modulate mROS have been generated in the last decades. Nevertheless, every model presents a major disadvantage. The overexpression of mitochondrial superoxide dismutase (MnSOD) efficiently decrease the amount of superoxide, but it increases the concentration of hydrogen peroxide (Chen *et al*., 1998). Down-modulation of endogenous mitochondrial hydrogen peroxide has been achieved through the overexpression of peroxiredoxin-3 (Matsushima *et al*., 2006). The peroxiredoxin/thioredoxin complex is a very efficient system to convert hydrogen peroxide into water. However, to regenerate reduced peroxiredoxin, NADPH is required (Patenaude *et al*., 2005). The consumption of reducing equivalents will thus modify the NAPDH/$NADP^+$ ratio, changing the redox state that could alter cellular metabolism. Recently, it was demonstrated that the expression of a mitochondrial form of the glutamate-cysteine ligase (mGCL) down-modulates mROS (Quintana-Cabrera *et al*., 2012). mGCL directs the biosynthesis of γ-glutamylcysteine (γ-GC, the immediate glutathione precursor) to the mitochondria, where it efficiently detoxifies mROS acting as glutathione peroxidase-1 cofactor (Quintana-Cabrera *et al*., 2012). However, it consumes ATP, cysteine and glutamate, interfering in cellular metabolism. A clean manner to down-modulate mROS is the expression of a mitochondrial form of catalase (mCAT). A mCAT mouse model has been generated (Schriner *et al*., 2005). However, this mCAT model was generated by non site-directed insertion of the

construct, thus likely affecting the expression of other genes. Furthermore, this technique does not allow to control the number of copies inserted.

Accordingly, we aimed to generate a new mCAT mouse by insertion of the construct in the *Rosa26* locus of C57Bl/6 embryonic stem cells by homologous recombination.

Preliminary studies were performed in immortalized MEFs transfected with the pIRES2eGFP-mCAT (henceforth mCAT) or the empty plasmid, in order to ascertain the correct expression of the construct. The data obtained show that cells transfected with mCAT express the HA tag (**Figure 1A**), and higher catalase abundance (**Figure 1B**) compared to MEFs transfected with the empty plasmid.

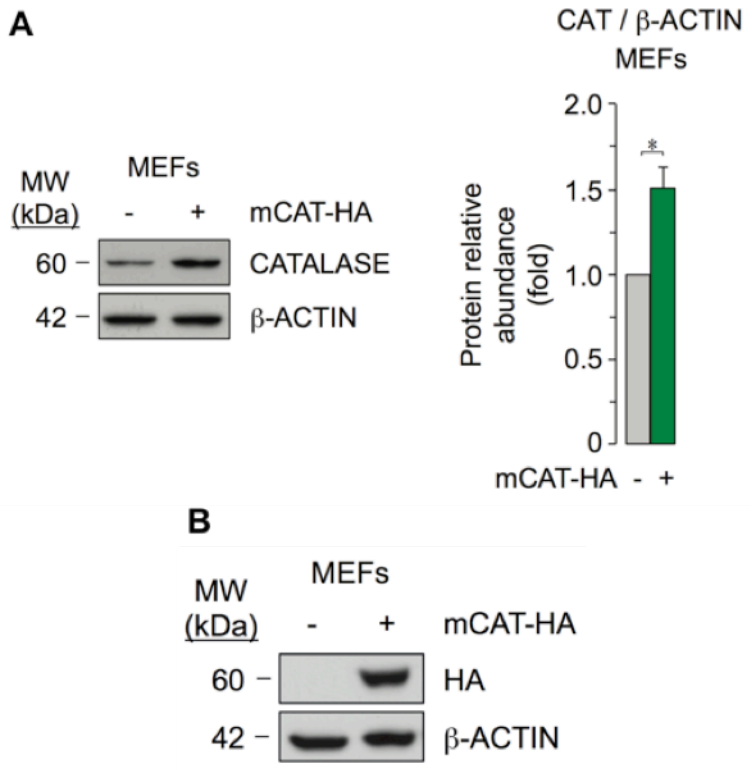

Figure 1: HA occurrence and catalase abundance in transfected MEFs. Immunoblot revealed that MEFs transfected with mCAT show increased abundance of catalase **(A)** and express the HA tag **(B)** compared to the empty plasmid. β-Actin was used as loading control. Data are expressed as mean ± S.E.M.; **p*<0.05 Student's *t*-test; n=3 independent experiments.

Next, with the aim to establish whether mCAT is able to detoxify hydrogen peroxide, the functionality of the enzyme was investigated. The catalytic activity of mCAT was assessed in isolated mitochondria in presence of different concentrations of exogenous hydrogen peroxide. As shown in **Figure 2**, mitochondria isolated from MEFs expressing mCAT neutralize exogenous hydrogen peroxide faster than cells transfected with the empty plasmid. Analyzing these results, it seems that mCAT is not able to down-modulate endogenous mROS, considering that in absence of exogenous hydrogen peroxide there are no differences between mitochondria expressing mCAT and the empty plasmid. However, the colorimetric method used to measure mCAT activity is not sensitive enough to detect endogenous mROS levels.

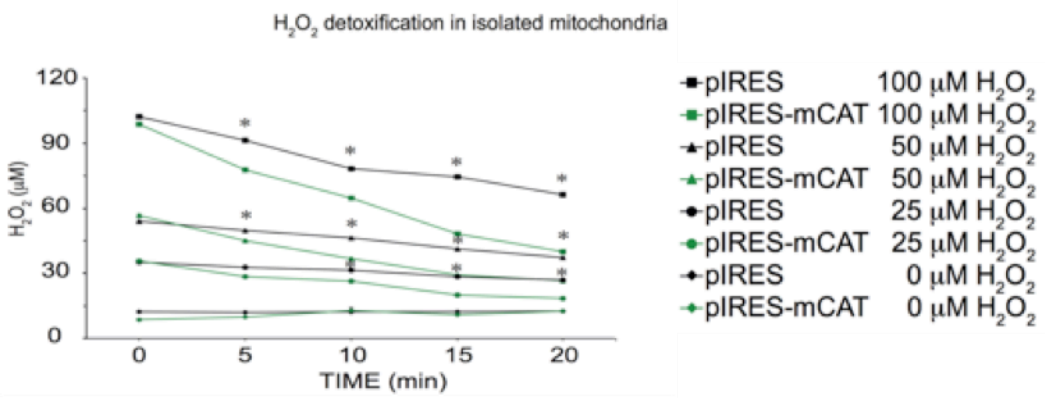

Figure 2: mCAT expression increases mitochondrial hydrogen peroxide detoxification in MEFs. Incubation of isolated mitochondria with different concentrations of exogenous hydrogen peroxide for different time period shows that mCAT expression increases significantly the rate of hydrogen peroxide neutralization at all concentration used. In the absence of exogenous hydrogen peroxide, there were no differences between mitochondria expressing mCAT and the empty plasmid. Data are expressed as mean ± S.E.M.; *p<0.05 Student's t-test; n=3 independent experiments.

The release rate of mROS in basal conditions was then assessed using the Amplex Red, a non-fluorescent probe that is selectively oxidized by extracellular hydrogen peroxide to the fluorescent molecule resorufin in presence of the horseradish peroxidase. This assay is very sensitive and allows to detect hydrogen peroxide in the picomolar range (Mishin *et al*., 2010; Mohanty *et al*., 1997). First, the hydrogen peroxide release rate was measured in mitochondria isolated from

transfected MEFs. As shown in **Figure 3**, mitochondria that express mCAT produce lower hydrogen peroxide release rate compared to the empty plasmid. Considering that hydrogen peroxide diffuses through biological membranes (Han *et al*., 2003), its mitochondrial production may affect the rest of the cell. As illustrated in **Figure 3**, the expression of mCAT down-modulates hydrogen peroxide release rate from whole cells too. Hence, mCAT is functional and its expression in MEFs is sufficient to down-modulate endogenous levels of mROS.

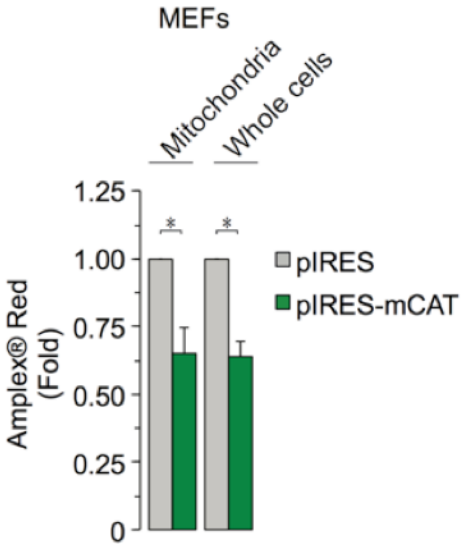

Figure 3: mCAT expression down-modulates endogenous mROS and ROS levels in transfected MEFs. Mitochondria and intact MEFs expressing mCAT show a ~0.4 fold lower hydrogen peroxide release rate when compared to the empty plasmid. Data are expressed as mean ± S.E.M.; *p<0.05 Student's t-test; n=3 independent experiments.

2. Endogenous mROS modulate NRF2 abundance and activity in immortalized MEFs

The cellular abundance and the consequent nuclear translocation of NRF2 is mainly controlled by the complex formed by the redox sensitive protein KEAP1 and Cul3, which binds and ubiquitinates NRF2 for its proteasomal degradation (Itoh *et al*., 1999). Oxidation of three Cys residues on KEAP1 causes a conformational change on the KEAP1-Cul3 complex that does not allow the

ubiquitination and recycling of the complex (Baird *et al*., 2013). In this situation, *de novo* synthesized NRF2 can accumulate and translocate to the nucleus, where it up-regulates the transcription of its target genes (Baird *et al*., 2013).

With the aim to investigate whether endogenous mROS are sufficient to activate the NRF2 pathway, NRF2 protein abundance was measured by immunoblot. As shown in **Figure 4A**, MEFs expressing mCAT express lower NRF2 levels compared to the empty plasmid.

Afterwards, we aimed to ascertain whether NRF2 down-modulation affected the expression of antioxidant genes by analyzing the mRNA levels of three of its target genes. Using *β-actin* as housekeeping gene, the expression of the glutamate-cysteine ligase catalytic subunit (*Gclc*), heme oxygenase 1 (*Ho-1*) and NADPH quinone dehydrogenase 1 (*Nqo1*) were measured by RT-qPCR. As shown in **Figure 4B** the levels of *Gclc*, *Ho-1*, and *Nqo1* were 18%, 30% and 44% lower in MEFs transfected with mCAT compared to the empty plasmid, respectively.

These results indicate that endogenous mROS modulate the NRF2 protein abundance and the transcription of some of its target genes in MEFs.

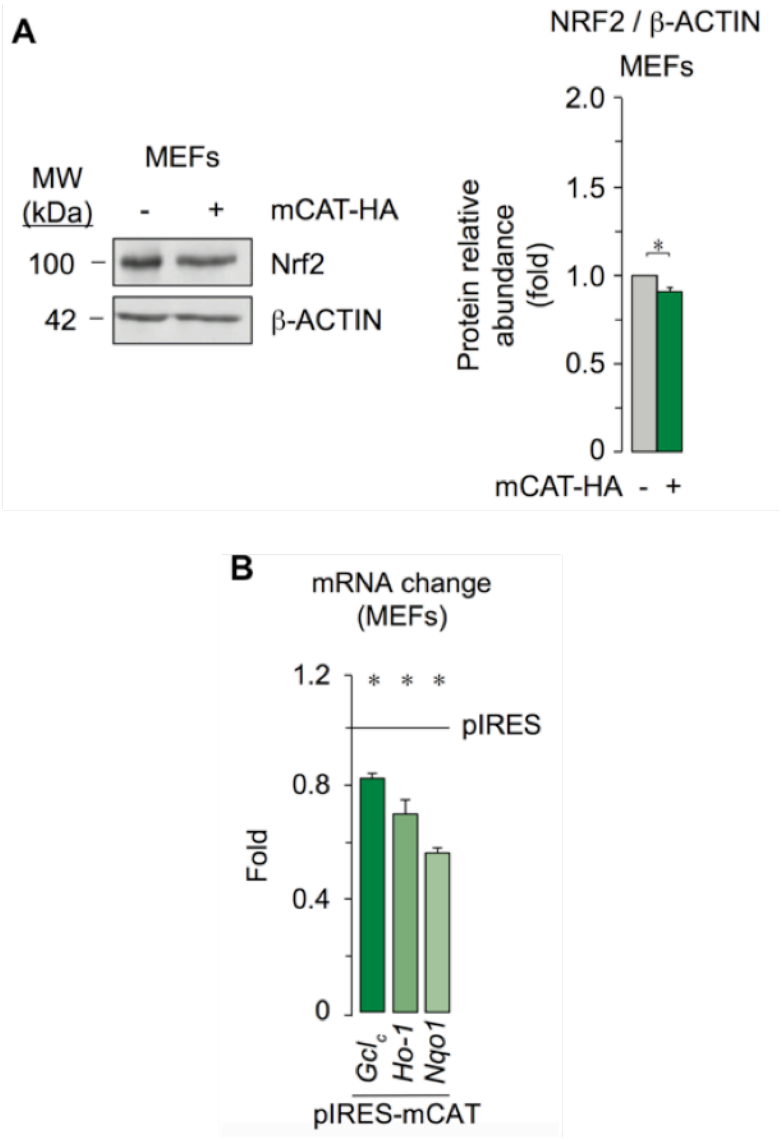

Figure 4: mROS modulate NRF2 abundance and its transcriptional activity in MEFs. (A) mCAT expression decreases NRF2 abundance in MEFs. β-Actin was used as loading control. **(B)** mRNA levels of *Gcl*$_c$, *Ho-1* and *Nqo1* were significantly decreased in MEFs expressing mCAT when compared to the empty plasmid. *β-actin* was used as housekeeping gene. Data are expressed as mean ± S.E.M.; **p*<0.05 Student's *t*-test; n=3 independent experiments.

3. mCAT expression down-modulates physiological endogenous mROS in primary astrocytes

In light of the preliminary data obtained in immortalized MEFs, primary astrocytes were transfected with mCAT in order to ascertain whether its expression down-modulates endogenous mROS in primary glial cells too.

Astrocytes transfected with mCAT show the HA tag, indicating the correct mCAT expression (**Figure 5A**). Considering that in primary astrocytes the efficiency of transfection is low (~30% of cells were transfected, compared to >70% MEFs transfected), cells expressing mCAT slightly decrease hydrogen peroxide release rate (~13%) compared to the empty plasmid (**Figure 5B**). Thus, the expression of mCAT down-modulates endogenous mROS levels in primary astrocytes.

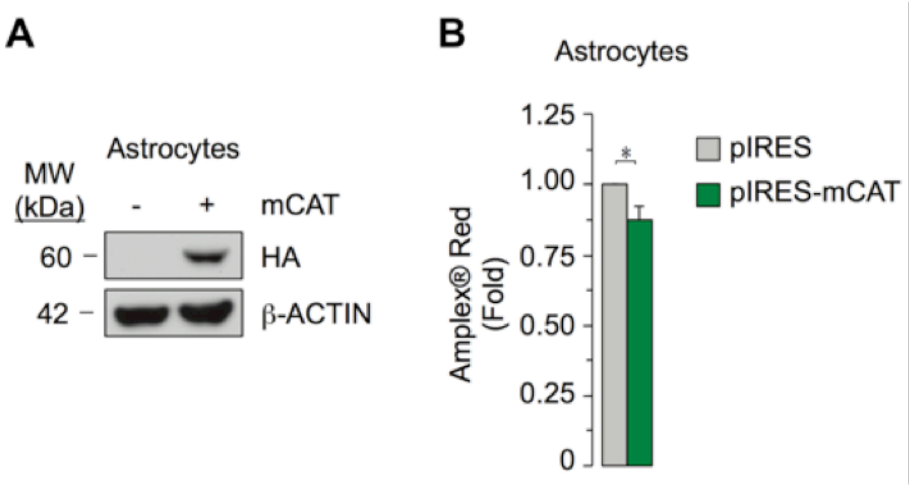

Figure 5: HA occurrence and ROS levels in transfected primary astrocytes. Primary astrocytes were transfected 24h before the experiments. **(A)** Immunoblot revealed that primary astrocytes transfected with mCAT express the HA tag. β-Actin was used as loading control. **(B)** Hydrogen peroxide production was lower in astrocytes expressing mCAT when compared to the empty plasmid. Data are expressed as mean ± S.E.M.; **p*<0.05 Student's *t*-test; n=3 independent experiments.

4. Generation of constitutive +/mCAT mouse

Considering the preliminary results in transfected immortalized MEFs and primary astrocytes, we generated the Cre recombinase-inducible ROSA26-floxed knock-in mouse harboring the floxed-mCAT by homologous recombination.

In order to express mCAT ubiquitously, $mCAT^{floxed/+}$ mice were crossbred with (CMV)-Cre recombinase mice under a C57Bl/6 background, which yielded the $C57Bl6^{+/mCAT}$ mouse line (henceforth mCAT). The offspring was genotyped (**Figure 6**) and used to obtain +/mCAT immortalized MEFs and primary astrocytes.

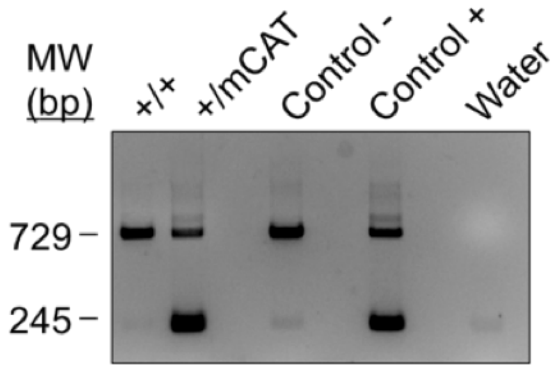

Figure 6: Example of a PCR. The genotype of the mice was determined by PCR. Wild type mice present only one band at 729 bp, while for the mCAT animals an additional band at 245 bp was detected. As controls, DNA from the tail of progenitor mice was used.

5. mCAT constitutive expression in MEFs down-modulates hydrogen peroxide release

In order to confirm the correct expression and the sub-cellular localization of mCAT construct, the occurrence of HA tag was evaluated in MEFs by immunoblot. First of all, detection of the HA tag was performed in the whole extract obtained from immortalized MEFs (**Figure 7A**). The results confirm that +/mCAT MEFs express the HA tag, while WT (or +/+) do not. Next, mitochondrial localization of the mCAT was confirmed. After a sub-cellular fractionation, HA tag detection was carried out in the cytosolic and in the mitochondrial fractions of MEFs (**Figure 7B**). As expected, only mitochondrial fraction obtained from +/mCAT MEFs expresses the HA tag.

The following step was to confirm that the constitutive expression of mCAT down-modulates endogenous ROS levels. Using the Amplex Red probe, hydrogen peroxide release rate from intact MEFs was measured. As shown in **Figure 7C**, +/mCAT MEFs released hydrogen peroxide 43% slower than WT.

These results confirm that mCAT is correctly localized in the mitochondria of +/mCAT MEFs and its constitutive expression down-modulates endogenous release of ROS.

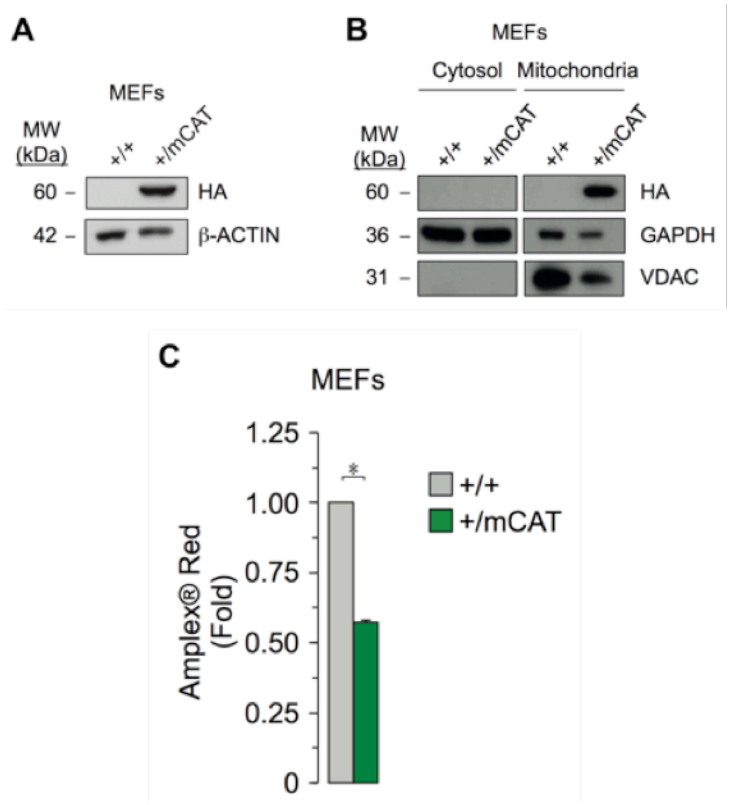

Figure 7: Constitutive mCAT expression decreases endogenous ROS release in MEFs. Expression of HA tag in MEFs that constitutively express mCAT was assessed by immunoblot in **(A)** whole cells and **(B)** cytosolic and mitochondrial fractions. HA tag was detected only in the +/mCAT MEFs and localized only in the +/mCAT mitochondria. β-Actin was used as loading control for the whole cells extract; GAPDH was used as loading control for the cytosolic fraction; VDAC was used as loading control for the mitochondrial fraction. **(C)** Intact cells expressing constitutively mCAT showed a decreased hydrogen peroxide production when compared to WT. Data are expressed as mean ± S.E.M.; **p*<0.05 Student's *t*-test; n=3 independent experiments.

6. mCAT constitutive expression in primary astrocytes

In light of the previous results confirming the correct expression and activity of mCAT in MEFs, the occurrence of mCAT was confirmed in primary astrocytes. First, the expression of HA tag and the abundance of catalase were detected by immunoblot in whole cell extracts. As expected, +/mCAT astrocytes showed higher (~6 fold) catalase abundance compared to the WT (**Figure 8A**) and they expressed the HA tag (**Figure 8B**). Subsequently, the mitochondrial localization of mCAT was confirmed. After a subcellular fractionation, HA tag was detected in mitochondria isolated from +/mCAT astrocytes (**Figure 8C**). However, a slight

band corresponding to the HA tag was detected also in the cytoplasmic compartment of +/mCAT astrocytes, likely reflecting the newly synthesized protein.

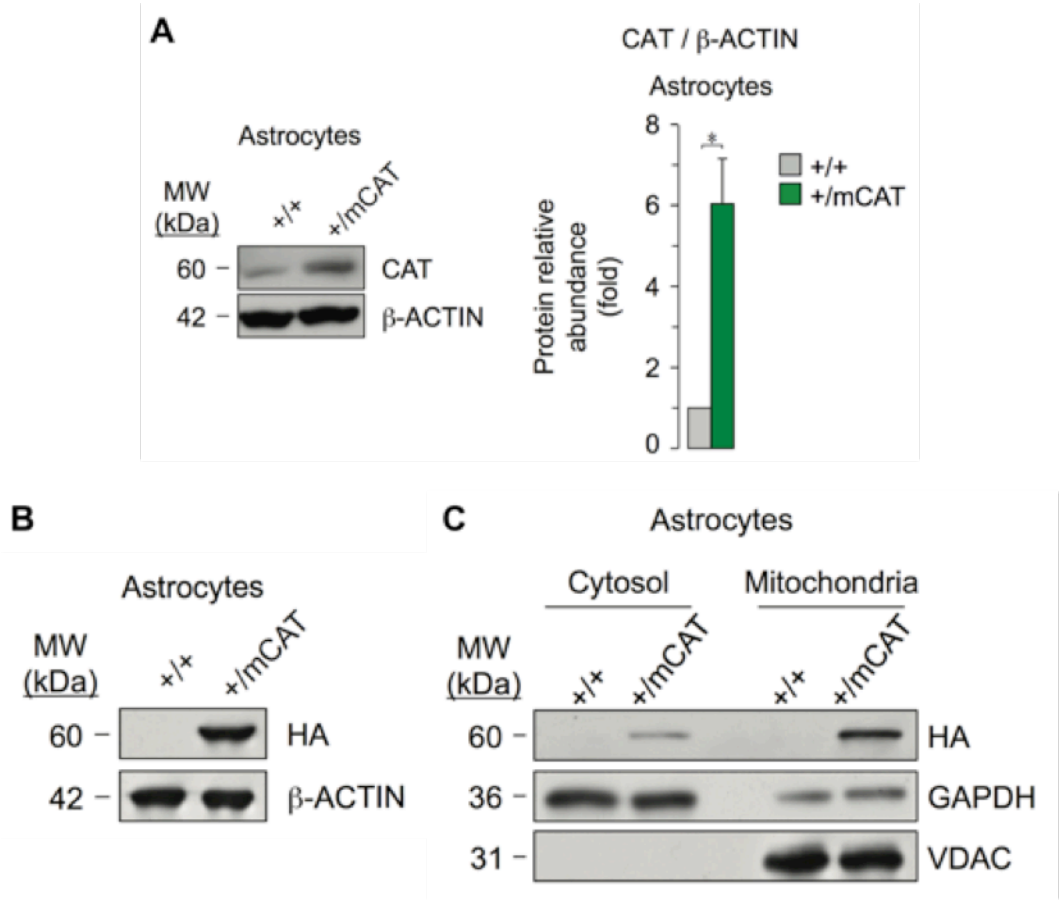

Figure 8: HA occurrence and catalase abundance in primary astrocytes. Immunoblot revealed that primary +/mCAT astrocytes show increased levels of catalase when compared to WT **(A)** and expressed the HA tag **(B)**. After a subcellular fractionation, mitochondrial localization of mCAT was evaluated detecting the HA tag by immunoblot **(C)**. β-Actin was used as loading control of the whole cell extract; GAPDH was used as loading control of the cytosolic fraction; VDAC was used as loading control of the mitochondrial fraction. Data are expressed as mean ± S.E.M.; *p<0.05 Student's t-test; n=3 independent experiments.

Mitochondrial localization of mCAT in primary astrocytes was further confirmed by immunofluorescence by confocal microscopy. To do so, heat shock protein-60 (HSP-60) was used as mitochondrial marker. As expected, +/mCAT astrocytes express the HA tag, which co-localizes with HSP-60 (**Figure 9**). In contrast, WT astrocytes did not express HA.

Altogether, these results confirm that mCAT is correctly expressed in the mitochondria of +/mCAT astrocytes.

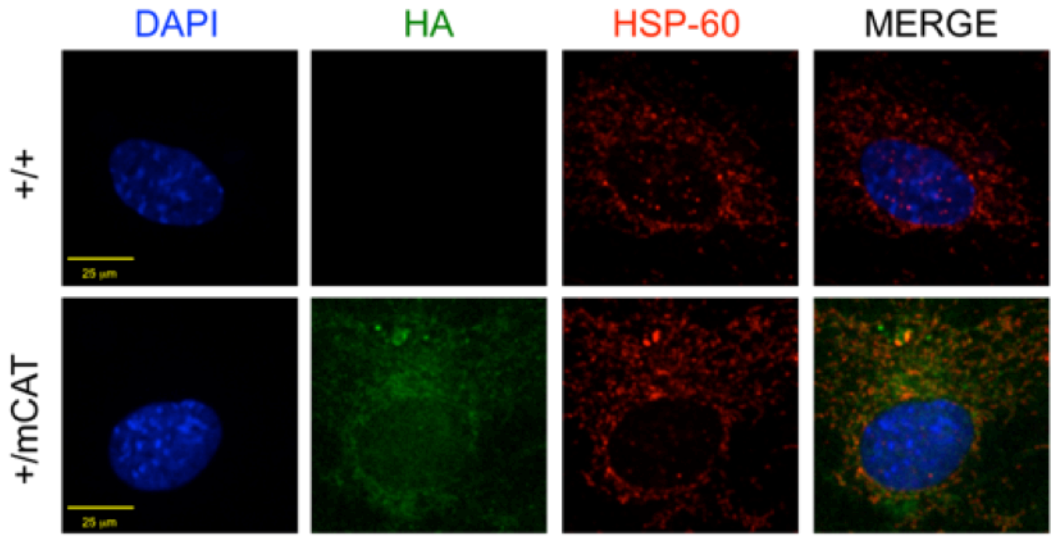

Figure 9: HA tag co-localizes with mitochondria in +/mCAT astrocytes. Confocal microscopy images revealed that +/mCAT astrocytes express the HA tag which co-localizes with the mitochondrial protein HSP-60.

7. Constitutive expression of mCAT efficiently detoxifies hydrogen peroxide and down-modulates endogenous ROS in primary astrocytes

The following step was to confirm the functionality of mCAT and to corroborate whether its constitutive expression is sufficient to down-modulate endogenous mROS in primary astrocytes.

Catalytic activity of mCAT was measured in mitochondria isolated from WT and +/mCAT primary astrocytes incubated with different concentrations of exogenous hydrogen peroxide. The results shown in **Figure 10** demonstrate that mitochondria expressing mCAT neutralize exogenous hydrogen peroxide faster than WT cells. In the firsts 5 minutes of the assay, mCAT neutralized half of the exogenous hydrogen peroxide. In addition, after 20 minutes, the totality of exogenous hydrogen peroxide was completely neutralized by mCAT at all

concentrations tested. Nevertheless, as in transfected MEFs, it seems that according to this experiment, mCAT is not able to down-modulate ROS when no hydrogen peroxide was added.

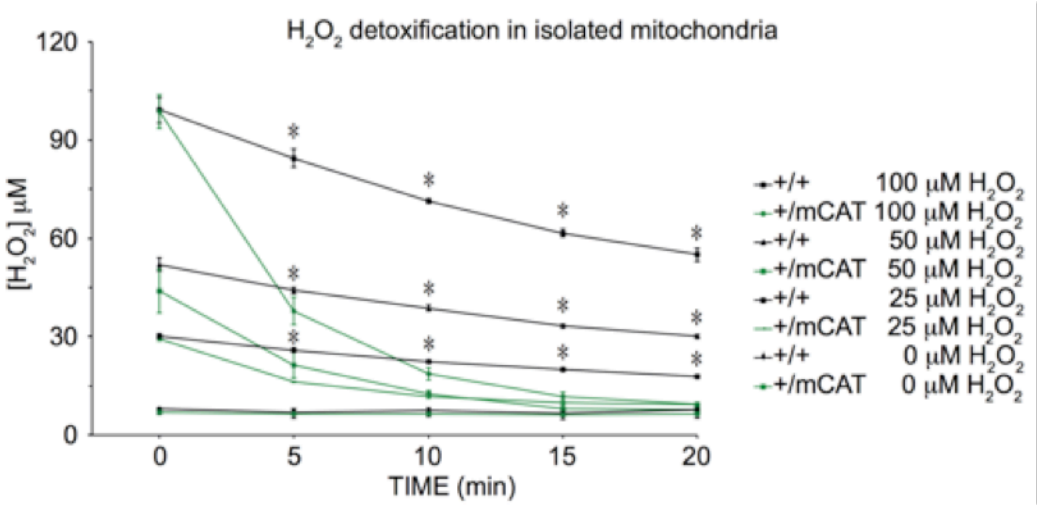

Figure 10: Constitutive mCAT expression increases mitochondrial hydrogen peroxide detoxification in primary astrocytes. Incubation of isolated mitochondria with different concentrations of exogenous hydrogen peroxide for different time periods shows that mCAT constitutive expression increases significantly the rate of hydrogen peroxide neutralization at all concentration used. In the absence of exogenous hydrogen peroxide, there were no differences between mitochondria expressing mCAT and WT. Data are expressed as mean ± S.E.M.; **p*<0.05 Student's *t*-test; n=3 independent experiments.

Accordingly, we next used two more sensitive probes, namely the Amplex Red and the MitoSox.

Hydrogen peroxide analysis from isolated mitochondria and intact astrocytes was first performed using the Amplex Red dye. The result represented in **Figure 11A** indicates that, under basal conditions, both +/mCAT mitochondria and intact astrocytes release hydrogen peroxide slower than WT. Next, MitoSox Probe was used. This mROS-sensitive probe enters the mitochondria depending on the mitochondrial membrane potential ($\Delta\Psi_m$), and the oxidized product is highly fluorescent. Differences in the $\Delta\Psi_m$ may lead to a different accumulation of the MitoSox in the mitochondria. Hence, it is necessary to disregard any difference in the $\Delta\Psi_m$ to correctly analyze and interpret the MitoSox results. Using the DilC1(5) probe, $\Delta\Psi_m$ was measured by flow cytometry and the results show that

there are no significant differences between WT and +/mCAT astrocytes (**Figure 11B**). Subsequently, MitoSox fluorescence was measured and the result indicates that +/mCAT astrocytes present a ~20% lower amount of mROS compared to WT (**Figure 11C**).

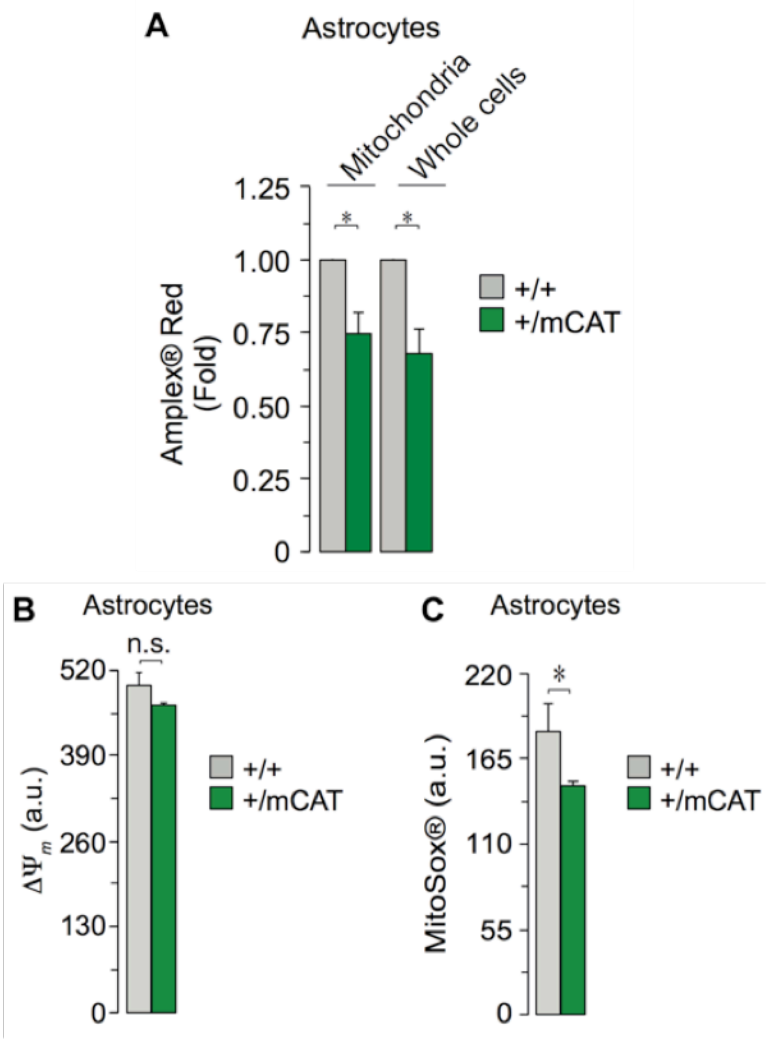

Figure 11: Constitutive mCAT expression down-modulates endogenous mROS and ROS in primary astrocytes. (A) Intact cells and isolated mitochondria constitutively expressing mCAT release hydrogen peroxide slower when compared to WT. **(B)** Assessment of $\Delta\Psi_m$ was performed by flow cytometry. WT and +/mCAT astrocytes do not show significant differences. **(C)** mROS measurement was performed by flow cytometry using the MitoSox Red dye. +/mCAT astrocytes present lower mROS when compared to WT. Data are expressed as mean ± S.E.M.; **p*<0.05 Student's *t*-test; n=3 independent experiments.

Altogether these results further indicate that mCAT is efficient at neutralizing exogenous hydrogen peroxide, and its constitutive expression in primary

astrocytes is sufficient to down-modulate endogenous mROS. Furthermore, these changes in the redox environment in glial cells do not affect $\Delta\Psi_m$.

8. Down-modulation of endogenous mROS does not affect astrocytic survival

Given that ROS modulate apoptosis (Circu and Aw, 2010), it was investigated whether the constitutive expression of mCAT in primary astrocytes exerted any effect on cellular survival. To do so, the activity of the enzyme caspase-3 (CSP-3), an effector of apoptosis (Elmore, 2007), was used. CSP-3 activity was measured in primary astrocytes under basal conditions and after a 4 hours treatment with 100 μM etoposide, an apoptotic inducer. The results obtained indicate that under basal conditions, mCAT constitutive expression does not affect astrocytic survival (**Figure 12**). The treatment with etoposide increased ~3.5 fold the CSP-3 activity, but no differences between WT and +/mCAT astrocytes were observed. Taken together, these results indicate that down-modulation of endogenous mROS has no effect on astrocytic survival, both under basal conditions or after an apoptotic stimulus.

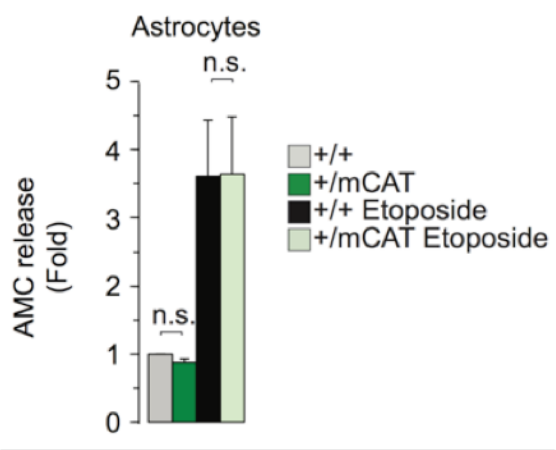

Figure 12: Down-modulation of endogenous mROS does not affect astrocytic survival. Activity of CSP-3 was used as apoptotic marker. Under basal conditions, no differences were observed between WT and +/mCAT astrocytes. After a 4h treatment with 100 μM etoposide, activity of CSP-3 was increased ~3.5 fold, but still no differences between the two genotypes were detected. Data are expressed as mean ± S.E.M.; n.s $p>0.05$ Student's *t*-test; n=3 independent experiments.

9. Endogenous mROS modulate nuclear accumulation of NRF2 in primary astrocytes and *in vivo*

In order to investigate whether endogenous mROS modulate the NRF2 nuclear accumulation in astrocytes, a subcellular fractionation was performed. NRF2 abundance was detected by immunoblot in the cytosolic and in the nuclear fraction of primary astrocytes. As shown in **Figure 13**, nuclei obtained from +/mCAT astrocytes show lower NRF2 abundance compared to the WT, whereas no differences were found in the cytosolic compartment.

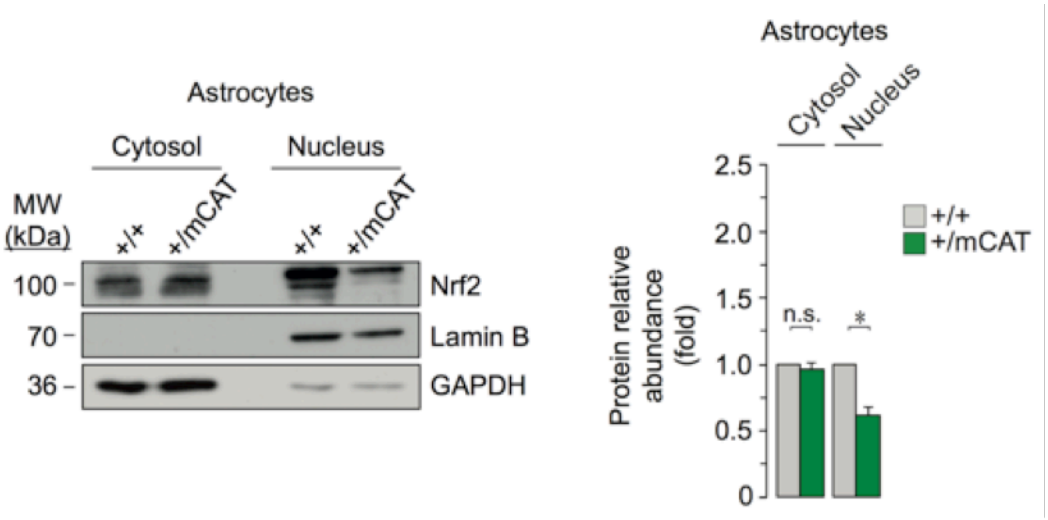

Figure 13: Down-modulation of endogenous mROS decreases NRF2 nuclear accumulation in primary astrocytes. Nucleus isolated from +/mCAT astrocytes showed a lower nuclear NRF2 accumulation. Lamin B was used as loading control of the nuclear fraction. GAPDH was used as loading control of the cytosolic fraction. Data are expressed as mean ± S.E.M.; **p*<0.05, n.s p>0.05 Student's *t*-test; n=3 independent experiments.

This result was further confirmed by immunofluorescence. As illustrated in **Figure 14**, WT astrocytes show higher nuclear abundance (~17%) of NRF2 compared to mCAT cells, as shown by Cy2-labeled NRF2 co-localization with nuclear staining DAPI.

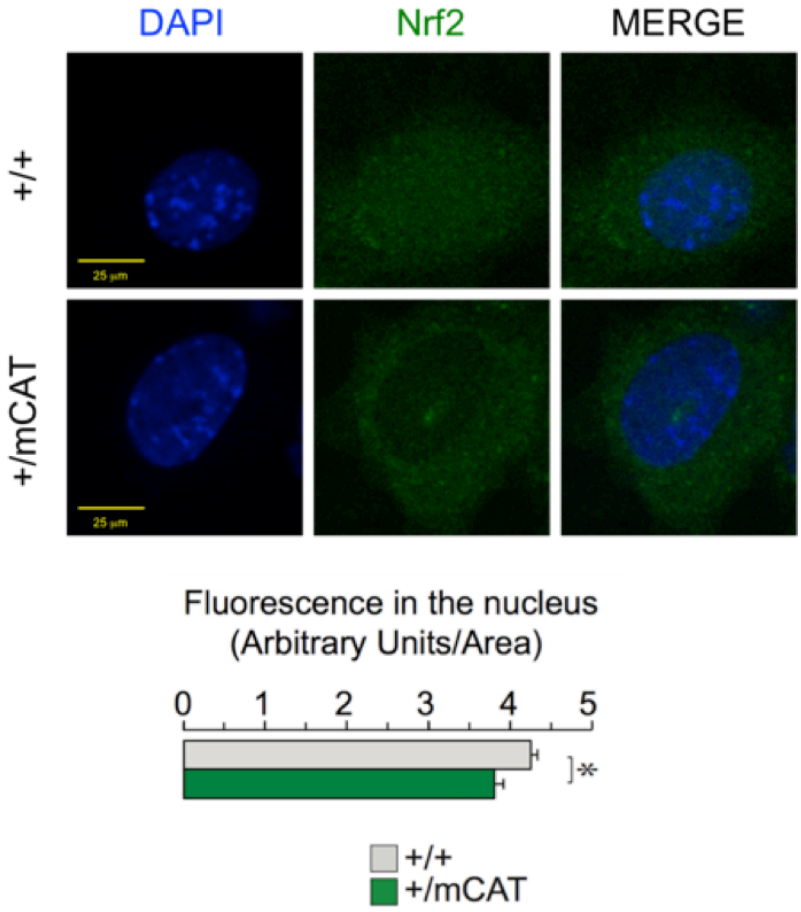

Figure 14: mROS-weakened astrocytes show decreased NRF2 nuclear accumulation. Confocal microscopy images revealed that +/mCAT astrocytes present lower NRF2 co-localization with DAPI staining when compared to WT. Quantification of nuclear fluorescence was carried out in 120 cells. Data are expressed as mean ± S.E.M.; **p*<0.05 Student's *t*-test; n=3 independent experiments.

Next, NRF2 levels were evaluated in the cytosolic and nuclear compartments of the brain, heart, liver and kidney obtained from WT or +/mCAT mice. Immunoblot revealed that brain from +/mCAT mice show lower nuclear and higher cytosolic abundance of NRF2 compared to WT (**Figure 15A**). a similar result was obtained in the heart, although the differences were less evident (**Figure 15B**). The hepatic cytosolic compartment did not show differences in NRF2 abundance, while a decrease was found in the nuclei of +/mCAT mice (**Figure 15C**). No differences were detected in the kidney (**Figure 15D**).

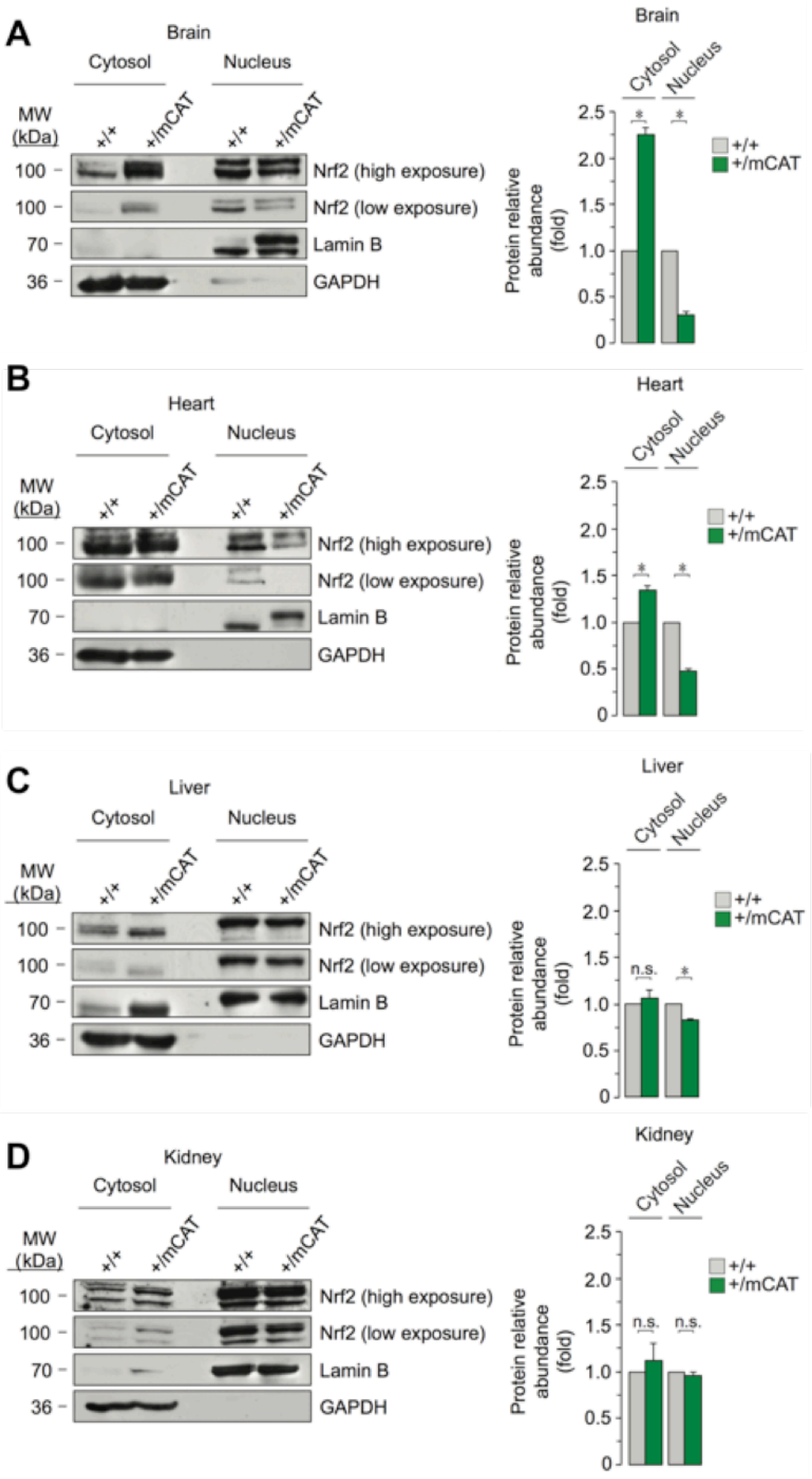
A
Brain
Cytosol
Nucleus
MW (kDa)
+/+
+/mCAT
+/+
+/mCAT
100
100
70
36
Nrf2 (high exposure)
Nrf2 (low exposure)
Lamin B
GAPDH
Brain
Cytosol
Nucleus
Protein relative abundance (fold)
2.5
2.0
1.5
1.0
0.5
0
*
*
+/+
+/mCAT
B
Heart
Cytosol
Nucleus
MW (kDa)
+/+
+/mCAT
+/+
+/mCAT
100
100
70
36
Nrf2 (high exposure)
Nrf2 (low exposure)
Lamin B
GAPDH
Heart
Cytosol
Nucleus
Protein relative abundance (fold)
2.5
2.0
1.5
1.0
0.5
0
*
*
+/+
+/mCAT
C
Liver
Cytosol
Nucleus
MW (kDa)
+/+
+/mCAT
+/+
+/mCAT
100
100
70
36
Nrf2 (high exposure)
Nrf2 (low exposure)
Lamin B
GAPDH
Liver
Cytosol
Nucleus
Protein relative abundance (fold)
2.5
2.0
1.5
1.0
0.5
0
n.s.
*
+/+
+/mCAT
D
Kidney
Cytosol
Nucleus
MW (kDa)
+/+
+/mCAT
+/+
+/mCAT
100
100
70
36
Nrf2 (high exposure)
Nrf2 (low exposure)
Lamin B
GAPDH
Kidney
Cytosol
Nucleus
Protein relative abundance (fold)
2.5
2.0
1.5
1.0
0.5
0
n.s.
n.s.
+/+
+/mCAT

Figure 15: Constitutive mCAT expression *in vivo* modulates NRF2 subcellular localization. Immunoblot from *in vivo* samples reveals different cytosolic and nuclear NRF2 abundance. Cerebral **(A)** and cardiac **(B)** samples revealed higher cytosolic and lower nuclear NRF2 abundance in +/mCAT mice when compared to WT. The hepatic samples **(C)** show no differences in the cytosolic compartment, however NRF2 nuclear accumulation decreased in +/mCAT mice. Kidney **(D)** shows no differences of NRF2 abundance. Data are expressed as mean ± S.E.M.; **p*<0.05, n.s >0.05 Student's *t*-test; n=2 independent experiments.

These results show that down-modulation of physiological endogenous mROS in primary astrocytes leads to a decrease in the nuclear accumulation of NRF2. In addition, they suggest that mCAT is more efficient at decreasing physiological endogenous mROS in the brain and heart than in the liver and kidney.

10. Endogenous mROS modulate NRF2 functional activity in primary astrocytes

To investigate whether the decreased nuclear localization of NRF2 in +/mCAT astrocytes could affect its transcriptional activity, the mRNA levels of several NRF2 target genes were measured by RT-qPCR. The genes chosen were NADPH quinone dehydrogenase 1 (*Nqo1*), glutamate-cysteine ligase catalytic subunit (Gcl_c), glutathione peroxidase-2 (*Gpx2*), heme oxygenase 1 (*Ho-1*), thioredoxin-1 (*Trx1*), nuclear factor (erythroid-derived-2)-like 2 (*Nrf2*), peroxiredoxin-1 (*Prdx1*), 6-phosphogluconate dehydrogenase (*6pgd*) and glucose-6-phosphate dehydrogenase (*G6pd*). The firsts seven genes analyzed, had decreased mRNA levels in mCAT astrocytes, although the *Prdx1* not in a significant manner (**Figure 16**). Surprisingly, the transcription of *6pgd* and *G6pd* genes were up-regulated in mROS-weakened astrocytes, suggesting the occurrence of another mechanism that modulates their transcription.

Taken together, these results illustrate that endogenous mROS modulate the transcription levels of several NRF2 target genes.

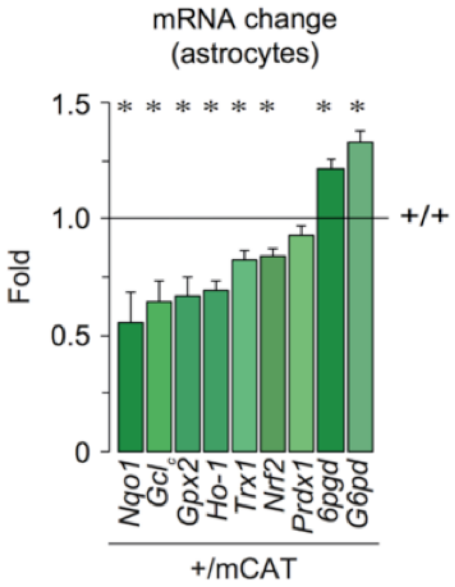

Figure 16: Endogenous mROS modulate the transcription of several NRF2 target genes. Expression of several NRF2 target genes was evaluated by RT-qPCR using *β-actin* as housekeeping gene. Constitutive expression of mCAT leads to a decreased expression of several NRF2 target genes (*Nqo1*, Gcl_c, *Gpx2*, *Ho-1*, *Trx1*, *Nrf2*, *Prdx1*) and, surprisingly, a significant increase of *6pgd* and *G6pd* genes in +/mCAT astrocytes compared with WT. *Nqo1*: NADPH quinone dehydrogenase 1; Gcl_c: glutamate-cysteine ligase catalytic subunit; *Gpx2*: glutathione peroxidase-2; *Ho-1*: heme oxygenase 1; *Trx1*: thioredoxin-1; *Nrf2*: nuclear factor (erythroid-derived-2)-like 2; *Prdx1*: peroxiredoxin-1; *6pgd*: 6-phoshogluconate dehydrogenase; *G6pd*: glucose-6-phosphate dehydrogenase. Data are expressed as mean ± S.E.M.; **p*<0.05 Student's *t*-test; n=3 independent experiments.

11. Down-modulation of endogenous mROS increases the abundance of pentose phosphate pathway (PPP)-related enzymes

Glucose-6-phosphate dehydrogenase (G6PD) is the enzyme that catalyses the first and rate limiting step of the pentose phosphate pathway (PPP). In order to investigate whether the increased transcription of the *G6pd* gene leads to an increase of the G6PD protein levels, its abundance was studied by immunoblotting. As shown in **Figure 17A**, +/mCAT astrocytes express higher G6PD abundance compared to WT, which is coherent with the previously data obtained by the mRNA analysis. In addition, abundance of 6-phosphogluconate dehydrogenase (6PGD) was evaluated. 6PGD is the third enzyme involved in the

oxidative branch of the PPP, where it catalyses the decarboxylation of 6-phosphogluconate to ribulose-5-phosphate. This enzyme is fundamental in maintaining cellular homeostasis, because together with G6PD, they are the major producers of cytosolic NADPH (Wamelink *et al*., 2008). This co-enzyme plays a key role in the glutathione (GSH) homeostasis and lipogenesis by supplying the reduced equivalents necessary to reduce GSSG to GSH and for the *de novo* synthesis of lipids (Wamelink *et al*., 2008). In +/mCAT astrocytes, protein levels of 6PGD are higher than in WT (**Figure 17B**).

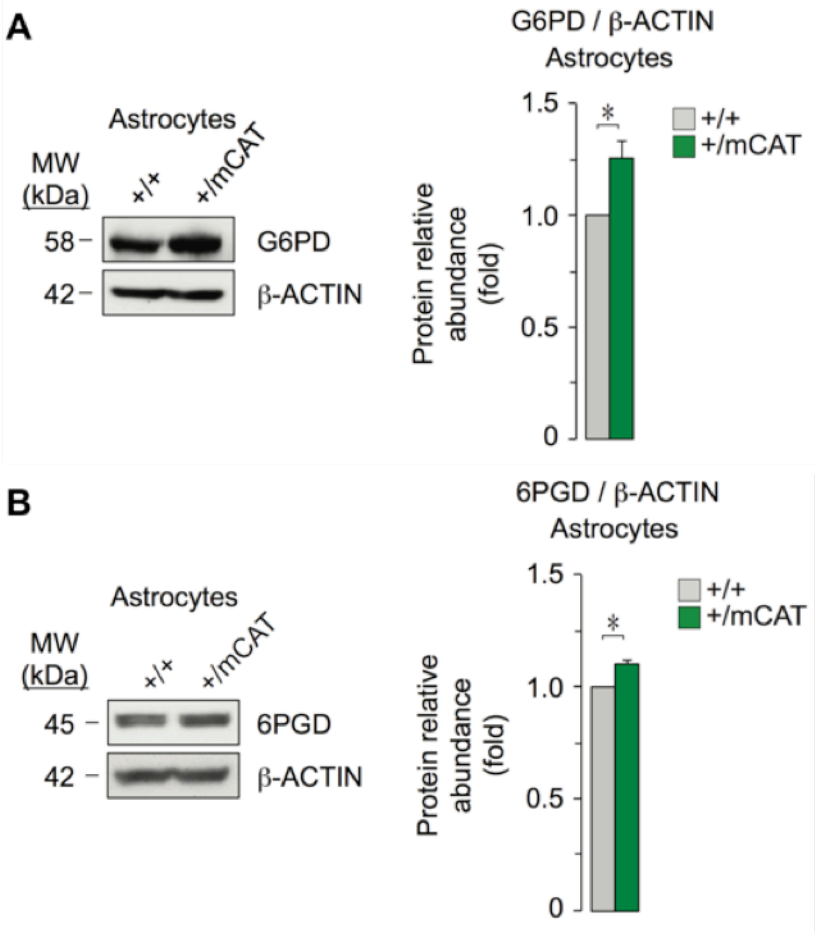

Figure 17: Endogenous mROS down-modulation increases G6PD and 6PGD abundance in primary astrocytes. Immunoblot showed that mROS-weakened astrocytes present higher G6PD (**A**) and 6PGD (**B**) abundance when compared to WT. β-Actin was used as loading control. Data are expressed as mean ± S.E.M.; **p*<0.05 Student's *t*-test; n=3 independent experiments.

12. Down-modulation of endogenous mROS increases miR-1 and miR-206 expression in astrocytes

Recently, an alternative regulation of the transcription of several PPP-related genes was discovered (Singh *et al*., 2013). This mechanism involves the histone deacetylase HDAC4, which accumulates in the nucleus when the two cysteine residues, Cys-667 and Cys-669, are in their reduced state (Ago *et al*., 2008). In this manner, HDAC4 represses the transcription of two microRNAs, miR-1 and miR-206, which degrade the newly synthesized mRNA of several PPP-related genes and HDAC4 itself (Singh *et al*., 2013).

The increased *G6pd* and *6pgd* mRNA levels that we observed are compatible with this mechanism. The results obtained so far show that +/mCAT astrocytes present lower ROS amount under basal conditions compared to the WT. In this less oxidant environment, HDAC4 cysteine resideus could be in their reduced state. In this scenario, HDAC4 would be localized in the nucleus repressing the transcription of miR-1 and miR-206, hence stabilizing G6PD and 6PGD mRNA. To investigate whether down-modulation of endogenous mROS in primary astrocytes regulates the subcellular localization of HDAC4, its abundance in whole cells and in the nuclear fraction was evaluated by immunoblotting. Both in whole cell extract (**Figure 18A**) and in the nuclear compartment (**Figure 18B**), +/mCAT astrocytes showed higher HDAC4 abundance compared to WT.

Subsequently, miR-1 and miR-206 abundances were evaluated by RT-qPCR. The data obtained show that +/mCAT astrocytes express 15% and 30% less miR-1 and miR-206 abundances, respectively, compared to WT (**Figure 18C**). This result is consistent with the higher nuclear localization of HDAC4 in +/mCAT astrocytes and it could explain the higher levels of G6PD, 6PGD and HDAC4 in mROS-weakened astrocytes.

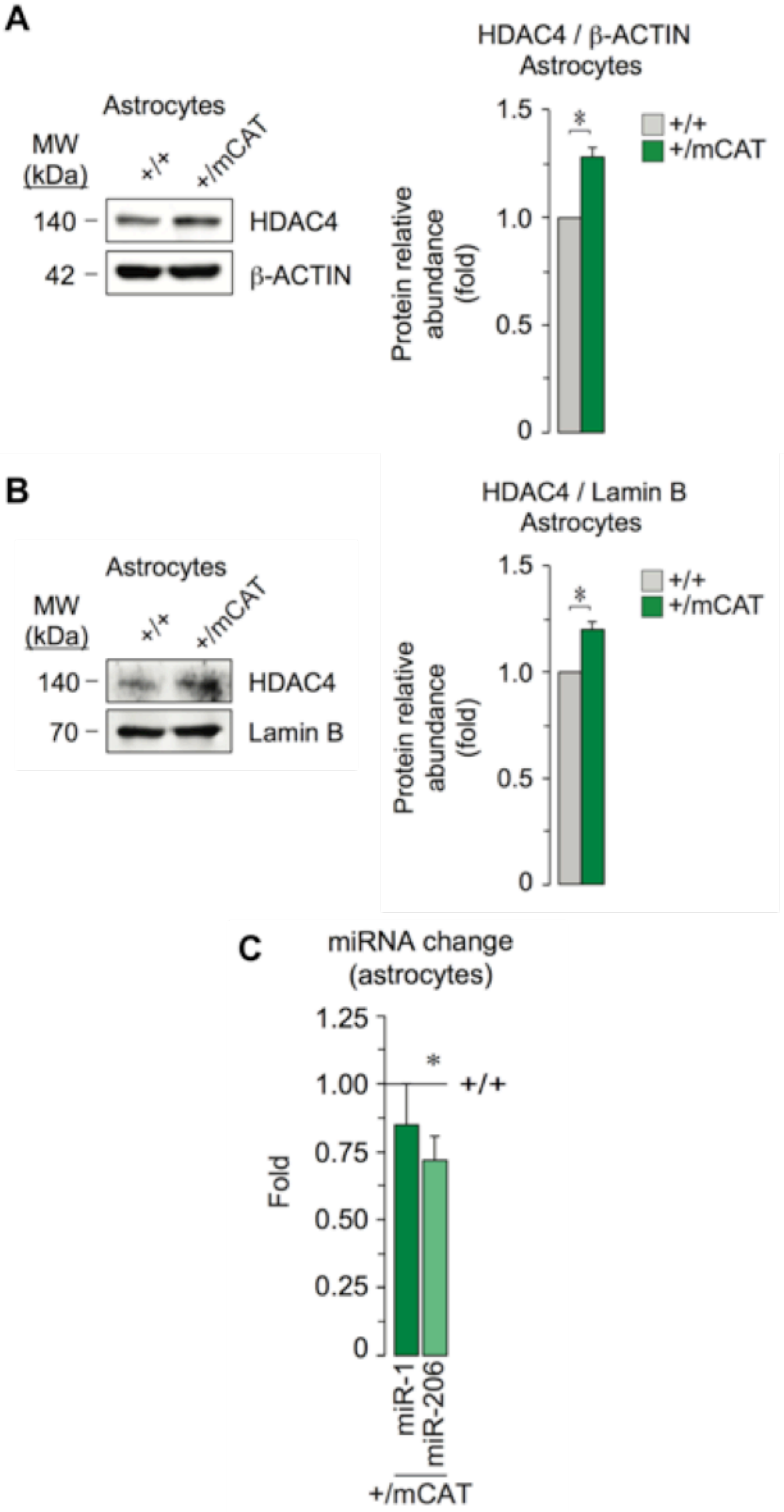

Figure 18: Endogenous mROS down-modulation increases HDAC4 abundance and decreases miR-1 and miR-206 expression. Immunoblot revealed that +/mCAT astrocytes express higher HDAC4 abundance both in whole cells **(A)** and in the nuclear fraction **(B)** when compared to WT. **(C)** RT-qPCR shows that mROS-weakened astrocytes express 15% and 30% less miR-1 and miR-206 respectively, when compared to WT. β-Actin was used as loading control for whole cells; lamin B was used as loading control for the nuclear compartment; mmu-miR-202 was used as endogenous control. Data are expressed as mean ± S.E.M.; *p<0.05 Student's t-test; n=3 independent experiments.

13. Down-modulation of endogenous mROS increases glucose flux through PPP

In light of these results, the flux of glucose through the PPP was measured following a protocol optimized in our laboratory (Rodriguez-Rodriguez *et al*., 2013). To do so, intact primary astrocytes were incubated in the presence of D-[1-^{14}C]-glucose or D-[6-^{14}C]-glucose, and the $^{14}CO_2$ released was quantitatively trapped and measured. $^{14}CO_2$ released from D-[1-^{14}C]-glucose reflects 6-phosphogluconate decarboxylation by 6PGD plus acetyl-CoA decarboxylation at isocitrate dehydrogenase and α-ketoglurate dehydrogenase of the tricarboxilic acid (TCA). However, $^{14}CO_2$ released from D-[6-^{14}C]-glucose reflects acetyl-CoA decarboxylation at isocitrate dehydrogenase and α-ketoglurate dehydrogenase. Thus, the difference between $^{14}CO_2$ released from D-[1-^{14}C]-glucose and that from D-[6-^{14}C]-glucose is used to estimate glucose oxidized through the PPP. As shown in **Figure 19**, mCAT astrocytes show a 40% increase in the flux of glucose oxidized through the PPP when compared to WT cells.

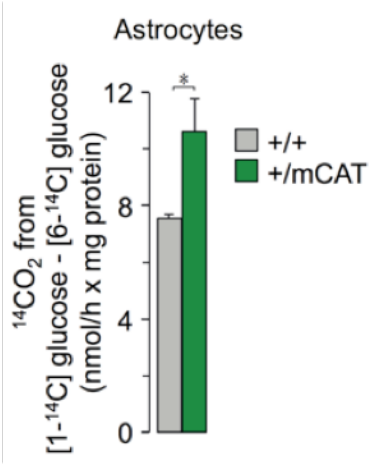

Figure 19: Glucose flux through the oxidative branch of the PPP is increased by the down-modulation of endogenous mROS. PPP rate was evaluated incubating intact astrocytes with radiolabelled glucose. mROS-weakened astrocytes showed a 40% increase of glucose oxidation *via* the PPP when compared to WT. Data are expressed as mean ± S.E.M.; **p*<0.05 Student's *t*-test; n=3 independent experiments.

A major function of PPP is to regenerate NADPH necessary for redox homeostasis and anabolic pathways (Wamelink *et al*., 2008). Given that down-

modulation of astrocytic mROS increases the protein levels of G6PD and 6PGD, and increases the rate of the PPP, the NAPDH/NADP$^+$ ratio was measured. Surprisingly, mROS-weakened astrocytes showed decreased NADPH/NADP$^+$ ratio compared to WT (**Figure 20A**). One possible explanation is that +/mCAT astrocytes consume more NADPH compared to WT. Since lipid synthesis consumes NADPH (Wamelink *et al.*, 2008), the *de novo* lipogenesis was measured. Intact astrocytes were incubated with D-[6-^{14}C]-glucose for 3 hours, the lipid fraction was extracted and the radioactivity quantified. As shown in **Figure 20B**, the constitutive expression of mCAT does not alter the rate of the *de novo* lipogenesis in primary astrocytes. These results suggest that mROS deficient astrocytes consume more NADPH compared to WT, although these reducing equivalents do not seem to be used for the *de novo* lipogenesis.

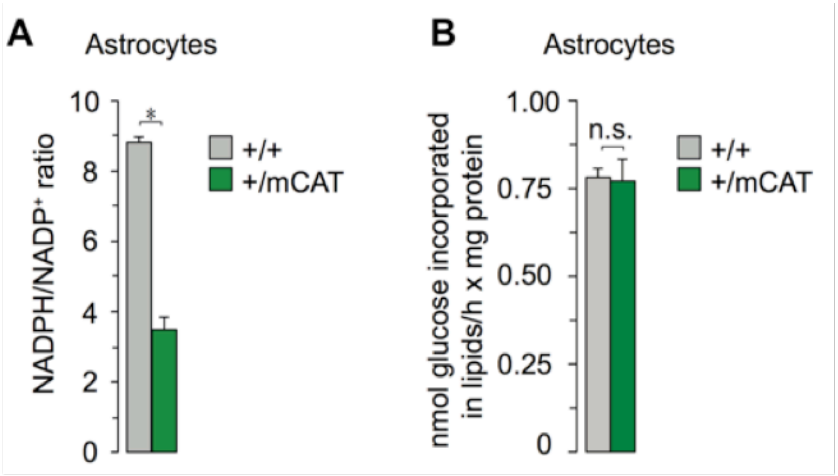

Figure 20: Endogenous mROS down-modulation decreases the NADPH/NADP$^+$ ratio, however it does not affect the *de novo* lipogenesis rate. mROS-weakened astrocytes showed a significant decrease of the NADPH/NADP$^+$ ratio (**A**) compared to WT, which does not affect the rate of *de novo* lipogenesis (**B**). Data are expressed as mean ± S.E.M.; *p<0.05 Student's t-test; n=3 independent experiments.

14. Endogenous mROS modulate extracellular superoxide production in primary astrocytes

Recent evidences show that G6PD is found in close proximity with the ROS producer enzymes NADPH-oxidases (NOX) (Yang *et al.,* 2016). This enzyme

family uses NADPH to produce superoxide or hydrogen peroxide, depending on the isoform. The interaction between G6PD (one of the major cytoplasmic NADPH producers) and NOXs may modulate downstream transduction signals. In addition, it was recently reported that NRF2 represses the expression of NOX2, while enhances NOX4 expression (Kovac *et al*., 2015; Wei *et al*., 2016), although the mechanism is unknown. Considering that +/mCAT astrocytes show lower NRF2 activity and more NADPH consumption compared to WT, the mRNA levels of NOX-1, -2, -4 were evaluated. The data obtained illustrate that +/mCAT astrocytes express higher levels of NOX1 and NOX2 mRNA (46% and 51%, respectively), while a decreased levels of NOX4 when compared with WT (**Figure 21A**). Considering that NOX1 and -2 produce extracellular superoxide, whereas NOX4 produces hydrogen peroxide, the extracellular superoxide release was determined. To do so, intact astrocytes were incubated with oxidized cytochrome c, which is reduced by superoxide. The reduced form of cytochrome c absorbs light at 550 nm, allowing its detection. As shown in **Figure 21B**, +/mCAT astrocytes release 20% more superoxide compared to WT. These results indicate that down-modulation of endogenous mROS in primary astrocytes increases the expression of NOX1 and NOX2, but decreases the levels of NOX4. This increase of the two NOX isoforms responsible for extracellular superoxide production is compatible with the observed increase of extracellular superoxide. Furthermore, the increase of NOX1 and NOX2 is consistent with the increased NADPH consumption observed in +/mCAT astrocytes. Nevertheless, the mechanism responsible of the increase of NOX1 and -2 and the decrease of NOX4 is still elusive.

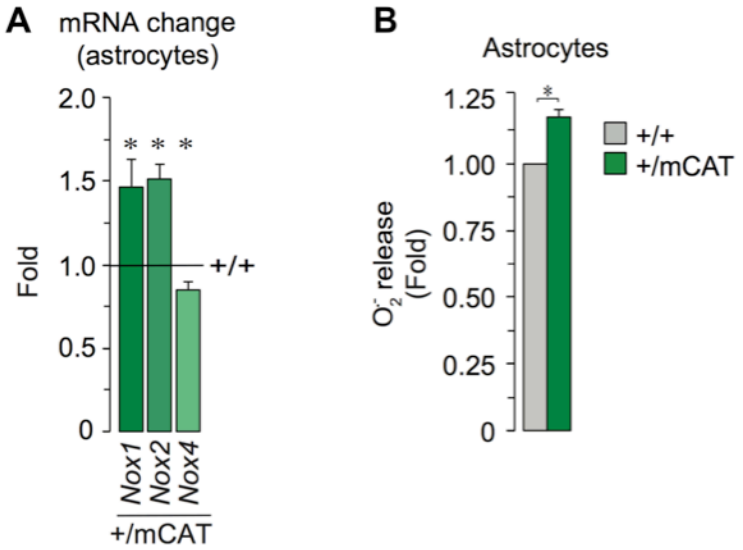

Figure 21: Endogenous mROS down-modulation modulate NOX expression and increased superoxide release. mROS-weakened astrocytes showed an increase of the NOX-1 and -2 expression, whereas a NOX-4 decrease (**A**) when compared to WT, which increase production of extracellular superoxide (**B**). Data are expressed as mean ± S.E.M.; **p*<0.05 Student's *t*-test; n=3 independent experiments.

15. Rescue of the NRF2 levels decreases extracellular superoxide release by primary astrocytes

In order to corroborate that NRF2 deficiency leads to an increase in extracellular superoxide release through NOX1 and -2 activities, +/mCAT astrocytes were transfected with a constitutively active form of NRF2. This construct encodes for a NRF2 protein which directly translocates to the nucleus and up-regulates the transcription of its target genes. The plasmid was previously designed and validated in our laboratory (Jimenez-Blasco *et al*., 2015). The construct contains the human NRF2 sequence (1817 bp, access number NM_006164.3) fused at the 5' end with the green fluorescent protein (GFP). To obtain the phosphomimetic form (NRF2 PM), three residues (Thr395, Ser433 and Thr439) were substituted by aspartate by site-directed mutagenesis (Jimenez-Blasco *et al*., 2015). The resulting phosphomimetic NRF2 (NRF2 PM) accumulates and translocates to the nucleus of transfected cells (Jimenez-Blasco *et al*., 2015). We first confirmed the correct NRF2 expression by RT-qPCR and immunoblotting. As shown in **Figure**

22A, +/mCAT astrocytes transfected with NRF2 PM express ~35-fold higher *Nrf2* mRNA abundance compared to the empty plasmid. Immunoblot analysis revealed two bands of NRF2, namely the constitutive (with a molecular weight of 100 kDa) and the phosphomimetic, which is detected at 130 kDa. As expected, only astrocytes transfected with NRF2 PM showed two bands (**Figure 22B**).

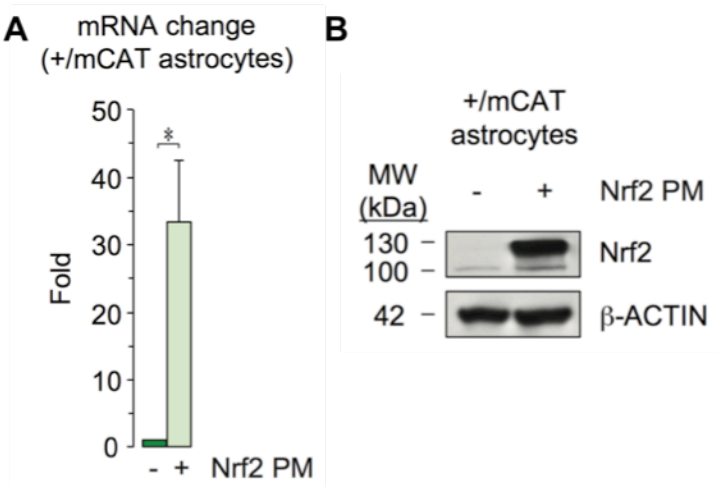

Figure 22: NRF2 PM expression increased NRF2 abundance in +/mCAT astrocytes. (A) mRNA levels of NRF2 were measured by RT-qPCR using *β-actin* as housekeeping gene. mCAT astrocytes transfected with NRF2 PM show a ~35-fold higher *Nrf2* expression when compared to the empty plasmid. **(B)** NRF2 protein abundance was evaluated by immunoblot. +/mCAT astrocytes transfected with NRF2 PM show a slightly increase of consitutive NRF2, as shown by the 100 kDa band, and they expressed an additional band at 130 kDa, corresponding to NRF2 PM, when compared to the empty plasmid. β-Actin was used as loading control. Data are expressed as mean ± S.E.M.; **p*<0.05 Student's *t*-test; n=3 independent experiments.

Subsequently, the mRNA levels of NOX1, -2 and -4 were measured in +/mCAT astrocytes transfected with NRF2 PM. The data obtained show that the transfection of +/mCAT astrocytes with NRF2 PM completely rescued the mRNA levels of NOX1, -2 and -4 compared with WT cells transfected with the empty plasmid (**Figure 23A**). Next, extracellular superoxide release was measured in order to ascertain whether NRF2 PM expression was sufficient to restore the basal values. As illustrated in **Figure 23B**, +/mCAT astrocytes released a 10% more extracellular superoxide compared to WT cells when transfected with the empty plasmid. However, no differences were found when +/mCAT cells were trasfected with NRF2 PM versus WT cells transfected with the empty plasmid. Taken

together, these results confirm that NRF2 represses the expression of NOX1 and -2, while it increases NOX4 in primary astrocytes. Furthermore, the rescue of NRF2 levels in +/mCAT glial cells restores basal release of extracellular superoxide, suggesting that mROS modulate extracellular ROS release through an NRF2-mediated mechanism.

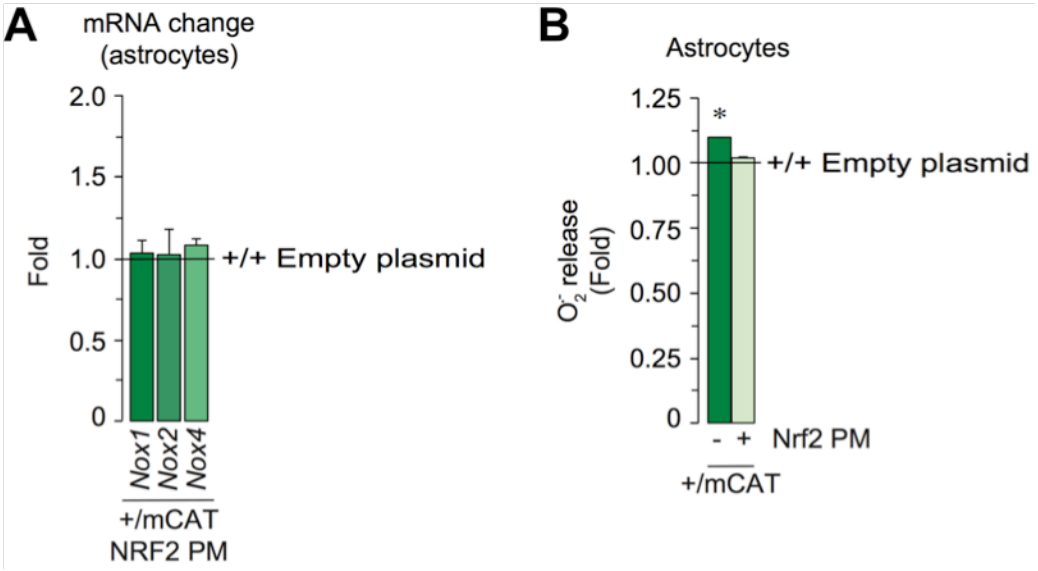

Figure 23: NRF2 PM expression in +/mCAT astrocytes restores basal expression of NOXs and extracellular superoxide release. mROS-weakened astrocytes expressing NRF2 PM show no differences of NOX1, -2 and -4 mRNA levels **(A)** and extracellular superoxide release **(B)** when compared with WT astrocytes transfected with the empty plasmid. *β-actin* was used as housekeeping gene. Data are expressed as mean ± S.E.M.; **p*<0.05 Student's *t*-test; n=3 independent experiments.

16. Endogenous mROS modulate glutathione abundance in primary astrocytes *via* NRF2

Glutathione (GSH), the most abundant thiol-containing antioxidant, is synthesized in two consecutive ATP-requiring steps, namely γ-glutamate cysteine ligase (GCL) and glutathione synthase (GS), respectively (Dringen, 2000). The first step is the rate limiting, hence the expression and activity of GCL control the synthesis GSH. Down-modulation of endogenous mROS in astrocytes led to a decreased expression of the Gcl_c gene (**Figure 16**). In order to investigate whether this

decreased Gcl_c transcription leads to a lower GSH synthesis in mROS-weakened astrocytes, GCL protein and the total GSH abundances were evaluated. Immunoblotting showed decreased GCL abundance in +/mCAT astrocytes compared to WT (**Figure 24A**). As expected, +/mCAT astrocytes showed a decrease (20%) of GSH concentration (**Figure 24B**).

In order to investigate whether astrocytic mROS modulate GSH abundance through the NRF2 pathway, +/mCAT astrocytes were transfected with NRF2 PM. As expected, the expression of NRF2 PM increase GCL protein abundance in +/mCAT astrocytes (**Figure 24C**). Subsequently, total GSH concentration was measured. Consistent with the GCL increase, +/mCAT astrocytes transfected with NRF2 PM showed higher total GSH concentration (**Figure 24D**).

Taken together, these results suggest that astrocytic endogenous mROS modulate GCL and GSH abundances *via* NRF2.

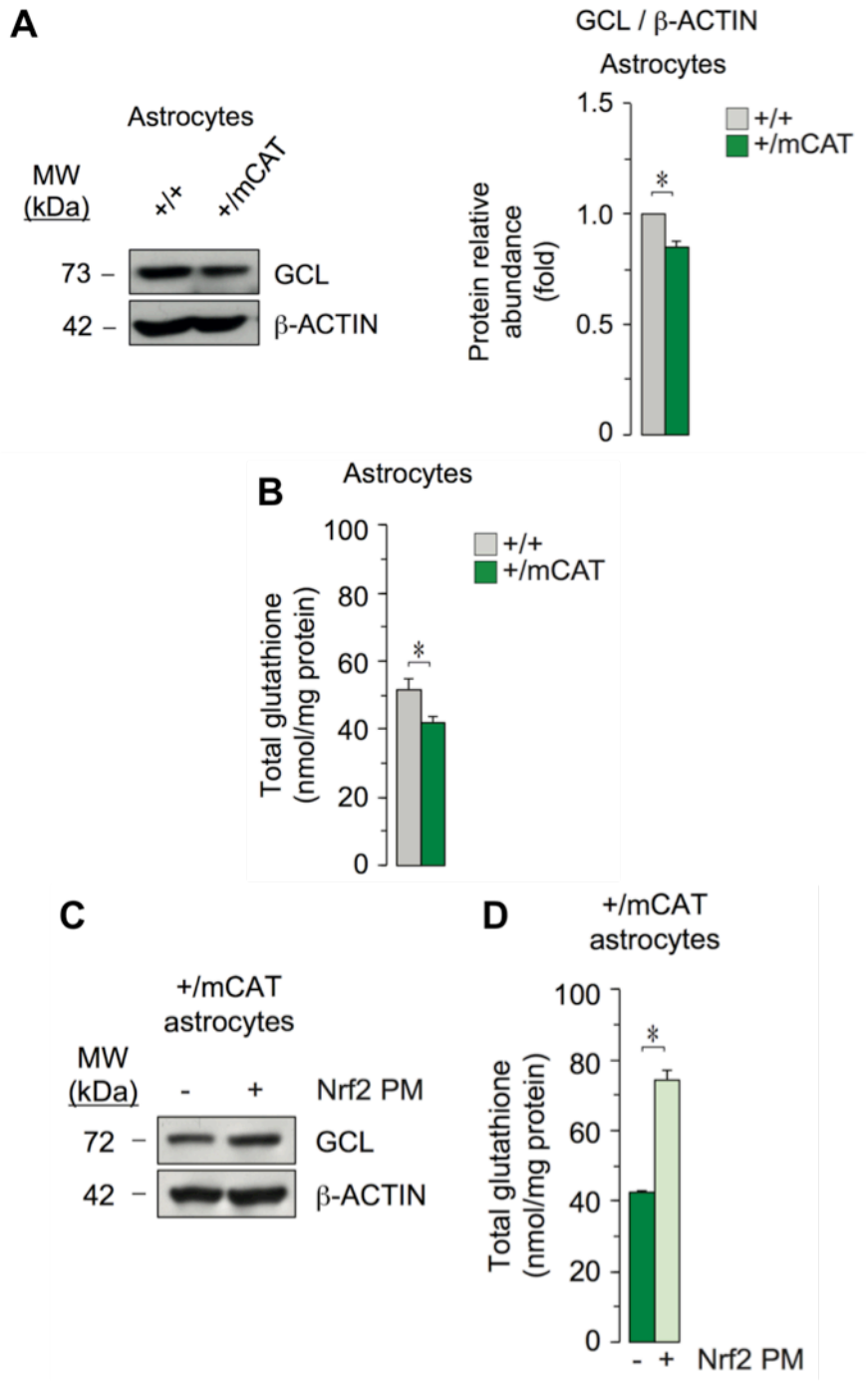

Figure 24: mROS modulate GSH synthesis through the NRF2 pathway. (A) Immunoblot showed that +/mCAT astrocytes express lower GCL levels when compared to WT. **(B)** Measurement of GSH concentration showed that mROS-weakened astrocytes present a 20% decrease in total GSH when compared to WT. Transfection of mROS-weakened astrocytes with NRF2 PM increases GCL abundance **(C)** and GSH concentration **(D),** when compared to the empty plasmid. β-Actin was used as loading control. Data are expressed as mean ± S.E.M.; **p*<0.05 Student's *t*-test; n=3 independent experiments.

17. Neurons co-cultured with mROS-weakened astrocytes show less antioxidant defenses, and higher ROS release and apoptosis

Previous works (Bolaños *et al*., 1996; Diaz-Hernandez *et al*., 2005; Dringen *et* al., 1999) demonstrated that neurons depend on astrocytic supply of precursors for the *de novo* synthesis of GSH. Furthermore, it has been demonstrated that the increase of astrocytic NRF2 activity, increases GSH synthesis and export from glial cells (Jimenez-Blasco *et al*., 2015). In order to investigate whether down-modulation of astrocytic endogenous mROS is deleterious for neurons, astrocyte-neuron co-cultures were performed. To do so, astrocytes were plated in inserts with a semi-permeable membrane, while neurons were seeded in a multiwell plate. After three days, astrocytes-containing inserts were placed above neurons and co-cultured for four more days. Subsequently, inserts containing astrocytes were discarded and GSH concentration and hydrogen peroxide release were measured in neurons.

As indicated in the **Figure 25A**, neurons co-cultured with +/mCAT astrocytes show a 27% decrease in total GSH concentration compared to neurons co-cultured with WT astrocytes. With the aim to ascertain whether this GSH deficit disrupts neuronal redox homeostasis, hydrogen peroxide was measured. As shown in **Figure 25B**, neurons had higher hydrogen peroxide production when co-cultured with mROS-weakened astrocytes. Taken together, these data confirm the importance of the GSH precursors supply from neighbour astrocytes for neuronal homeostasis. In addition, they strongly suggest that down-modulation of astrocytic endogenous mROS disrupt neuronal redox homeostasis.

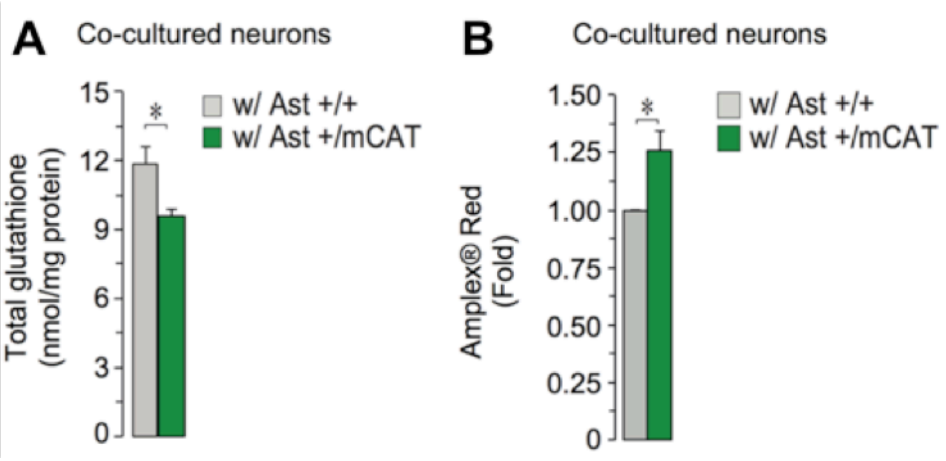

Figure 25: Neurons co-cultured with mROS-weakened astrocytes show lower antioxidant defences and increased ROS levels. Incubation of neurons with +/mCAT astrocytes for four days decreases neuronal GSH pool **(A)** and leads to an increase of the hydrogen peroxide release rate **(B)** when compared to neurons co-cultured with WT astrocytes. Data are expressed as mean ± S.E.M.; **p*<0.05 Student's *t*-test; n=3 independent experiments.

To investigate whether disruption of neuronal redox homeostasis affects survival, the abundance of the active form CSP-3 and its activity were evaluated as markers of apoptosis. Once discarded the inserts, the abundance of the 17 kDa CSP-3 cleaved active fragment was detected. Immunoblot show that neurons express higher active CSP-3 when co-cultured with mCAT astrocytes under basal conditions (**Figure 26A**). This result was further confirmed by the measurement of CSP-3 activity, which was evaluated in co-cultured neurons under basal conditions or after a 4 hours treatment with 100 μM etoposide. AMC release, a marker of CSP-3 activity, was higher in neurons co-cultured with mROS-weakened astrocytes in basal conditions (**Figure 26B**). After a 4 hours treatment with etoposide, CSP-3 activity was significantly increased in neurons; however, as shown in **Figure 26B**, the increase was higher in neurons co-cultured with mROS-weakened astrocytes compared with neurons co-cultured with WT astrocytes. These data suggest an increased vulnerability of neurons co-cultured with mROS-weakened astrocytes. In addition to the CSP-3 activity, $\Delta\Psi_m$ was evaluated as a marker of mitochondrial stress. The data obtained using the DilC1(5) dye show no differences in $\Delta\Psi_m$ in neurons co-cultured with WT or mCAT astrocytes (**Figure 26C**). Taken together, these results indicate that down-

modulation of astrocytic endogenous mROS is deleterious for the neighbour neurons, although neuronal $\Delta\Psi_m$ is unaffected.

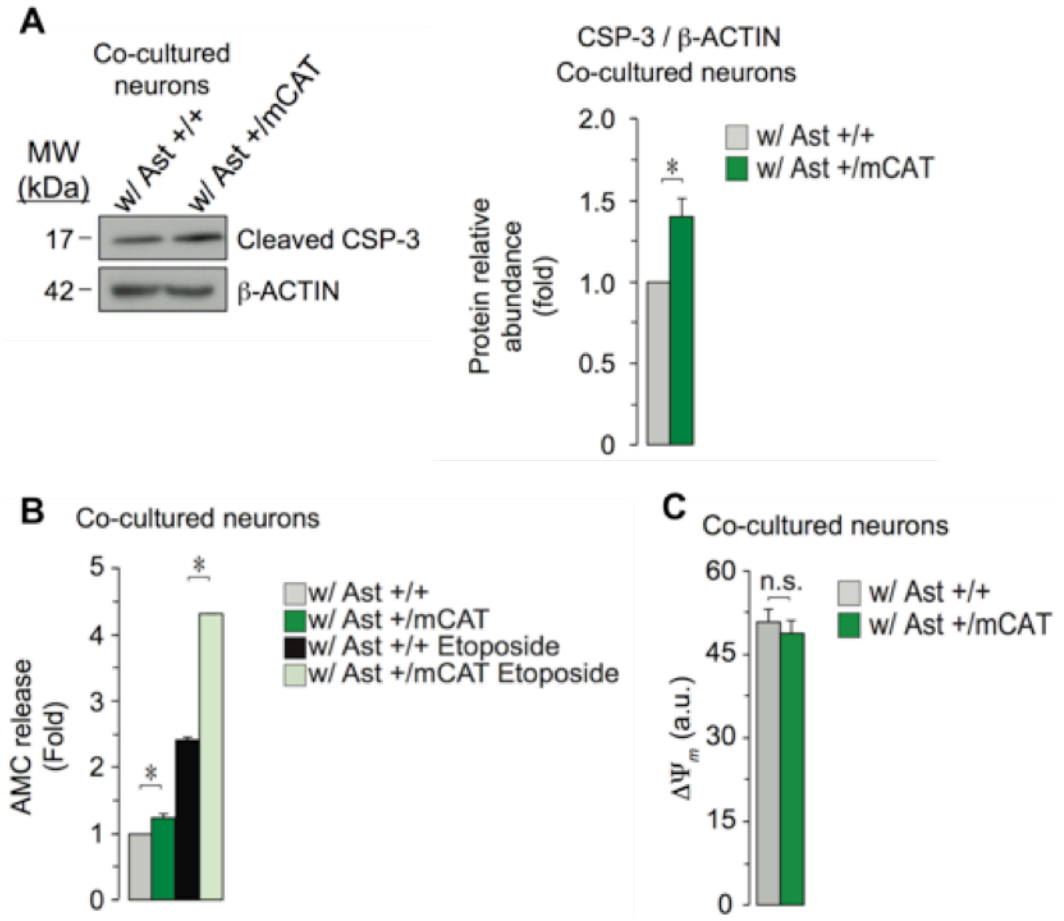

Figure 26: Neurons co-cultured with mROS-weakened astrocytes show higher apoptosis and unaffected mitochondrial membrane potential. (A) Immunoblot showed that, under basal conditions, co-culture of neurons with mROS-weakened astrocytes increases the abundance of the active fragment of CSP-3. β-Actin was used as loading control. **(B)** Incubation of neurons with mCAT astrocytes for four days shows a ~0.5 fold and ~1.7 fold higher CSP-3 activation under basal condition and after a 4h treatment with 100 μM etoposide, respectively, compared to neurons co-cultured with WT astrocytes. **(C)** Neuronal $\Delta\Psi_m$ was unaffected by the presence of +/mCAT astrocytes. Data are expressed as mean ± S.E.M.; *p<0.05, n.s. p>0.05 Student's t-test; n=3 independent experiments

18. Expression of NRF2 PM in mCAT astrocytes rescues the antioxidant defenses and survival of neurons

To investigate whether astrocytic mROS modulate the neuronal redox homeostasis and survival *via* the NRF2 pathway, neurons were co-cultured with +/mCAT astrocytes previously transfected with NRF2 PM or with the empty plasmid. To do so, astrocytes were transfected at DIV11. On the following day, the inserts were washed, the medium replaced, and cells were co-cultured for three days. After this period, the inserts were discarded and total GSH concentration, hydrogen peroxide release and CSP-3 activity were measured in neurons. As previously reported, treatments that increase astrocytic GSH enhance neuronal GSH (Dringen *et al*., 2015; Jimenez-Blasco *et al*., 2015). With the aim to investigate whether NRF2 PM rescues neuronal GSH pool, total GSH concentration was measured in co-cultured neurons. As illustrated in **Figure 27A**, neurons co-cultured with +/mCAT astrocytes previously transfected with NRF2 PM showed higher levels of GSH, reaching the values of neurons co-cultured with WT astrocytes (**Figure 25A**). Next, hydrogen peroxide release was measured. As depicted in **Figure 27B**, neurons co-cultured with mROS-weakened astrocytes, previously transfected with NRF2 PM, showed a ~40% decreased in hydrogen peroxide release when compared to neurons co-cultured with +/mCAT astrocytes transfected with the empty plasmid. Finally, to test whether astrocytic NRF2 PM expression rescues neuronal death, the activity of CSP-3 was evaluated. **Figure 27C** illustrates that neurons co-cultured with mROS-weakened astrocytes expressing NRF2 PM had lower CSP-3 activity compared to neurons co-cultured with astrocytes transfected with the empty plasmid.

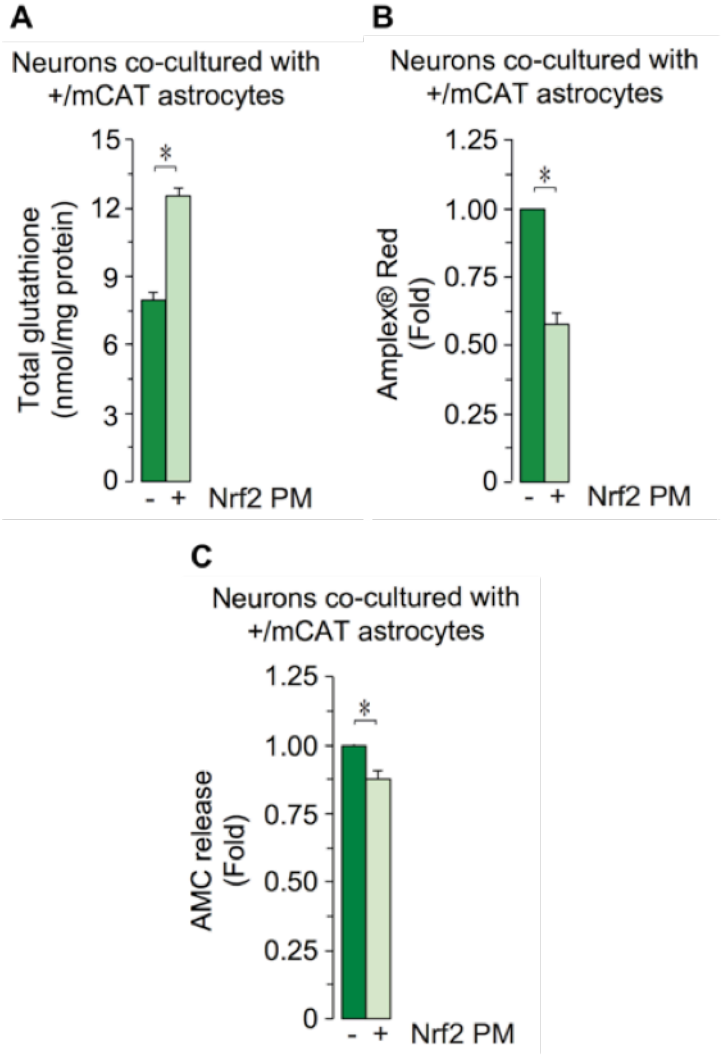

Figure 27: NRF2 PM expression in mROS-weakened astrocytes rescued antioxidant defences and survival of co-cultured neurons. (A) Neurons incubated for 3 days with +/mCAT astrocytes expressing NRF2 PM rescued their GSH pool and their hydrogen peroxide release **(B)**. In addition, a slightly but significant increase of neuronal viability **(C)** was found in neurons co-cultured with +/mCAT astrocytes expressing NRF2 PM. Data are expressed as mean ± S.E.M.; **p*<0.05 Student's *t*-test; n=3 independent experiments.

Taken together, these results are consistent with previous work from our laboratory (Jimenez-Blasco *et al*., 2015) which demonstrates that the increase of the astrocytic NRF2 pathway leads to a boost of neuronal antioxidant defences and survival. In addition, they strongly suggest that endogenous astrocytic mROS modulate redox homeostasis and increase viability of neurons through the NRF2 pathway.

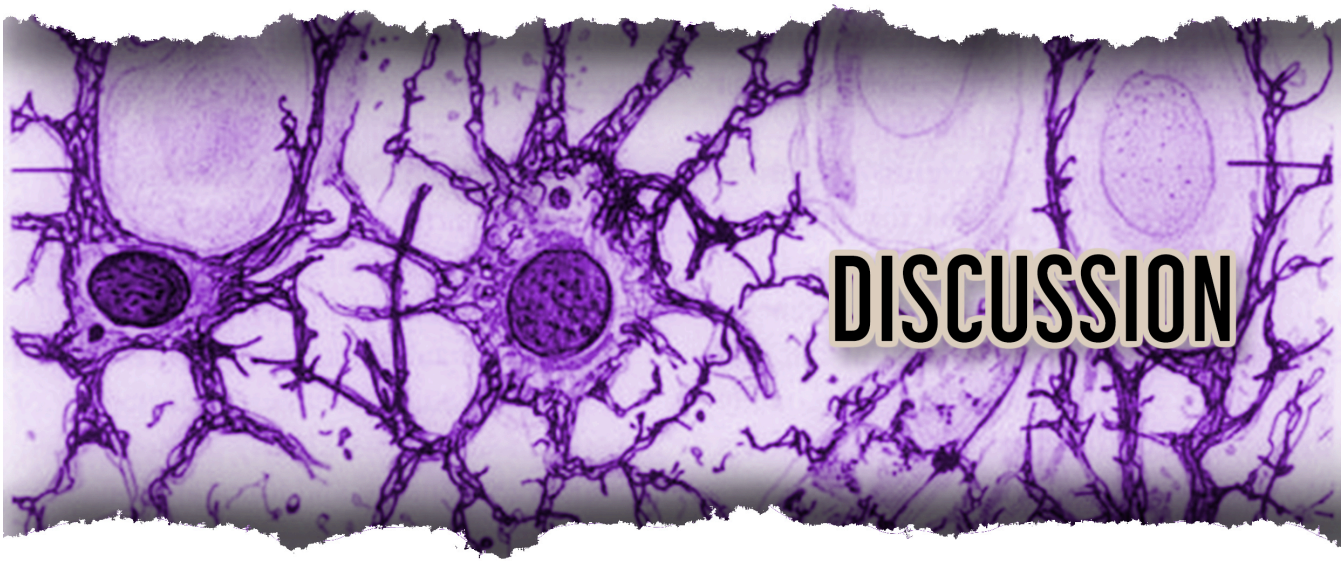
DISCUSSION

1. Expression of a mitochondrial form of catalase allows to investigate physiological roles of mROS

Traditionally, ROS have been associated with oxidative stress and human diseases. However, given that clinical trials based on antioxidants have not been conclusive (Halliwell 2013; Heyland *et al*., 2013; Kamat *et al*., 2008; Snow *et al*., 2010), the pathological role of ROS is questioned.

To investigate the functions of ROS, the majority of studies have used strategies based on increasing ROS, either by exogenously or endogenously supplied ROS. However, this approach could mask the beneficial roles of endogenous ROS. Here, we implemented an alternative approach aimed to down-modulate endogenous mROS. Several mouse models designed to down-modulate endogenous mROS have already been described. However, they have side effects on metabolism (Chen *et al*., 1998; Matsushima *et al*., 2006; Quintana-Cabrera *et al*., 2012). The strategy used in this work to down-modulate endogenous mROS based on the expression of a mitochondrial form of catalase, which neutralizes hydrogen peroxide with minimal effect on metabolism. In fact, a mCAT mouse model has been previously described (Schriner *et al*., 2005). However, the conventional microinjection technique used to generate that model has two major drawbacks, namely a non site-directed insertion of the DNA construct and the impossibility to control the numbers of copies inserted. Hence, whether the effects observed are due to mCAT activity or to any unknown effect caused by gene expression disruption is uncertain.

Accordingly, we generated a new mCAT mouse model in order to investigate the physiological roles of mROS. The mCAT construct was inserted in the *Rosa26* locus of C57Bl/6 of embryonic stem cells by homologous recombination. This technique inserts only one copy of the mCAT construct in a defined and safe locus. Furthermore, the model was generated based on the Cre-LoxP strategy, which allows controlling the *in vivo* mCAT expression in a tissue specific and time-controlled manner.

The results obtained in this work show that the newly generated mCAT mouse model is able to down-modulate endogenous mROS in primary astrocytes. Therefore, this is useful to investigate the biological roles of astrocytic mROS.

Moreover, the mCAT floxed mouse model could be used to study the involvement of mROS in any tissue both in physiological and pathological circumstances.

2. Endogenous mROS modulate redox homeostasis in primary astrocytes *via* the NRF2 pathway

The NRF2 pathway is essential for redox homeostasis in the brain. However, its activity differs between the two most abundant cell types, neurons and astrocytes. Neurons show a repressed antioxidant defences because of the continuous NRF2 protein destabilization (Bell *et al*., 2015; Jimenez-Blasco *et al*., 2015). In contrast, NRF2 is highly stable in astrocytes, which explains their robust antioxidant defences (Habas *et al*., 2013; Jimenez-Blasco *et al*., 2015). Nevertheless, the mechanism whereas astrocytic NRF2 is stabilized is still elusive. In this context, a recent study demonstrated that astrocytes produce severalfold higher mROS than neurons under basal conditions (Lopez-Fabuel *et al*., 2016). The physiological roles of these glial mROS production are, however, elusive.

The results obtained in this work demonstrate that endogenous mROS in astrocytes maintain high the levels of NRF2 activation. Accordingly, high levels of NRF2 activity promote the expression of antioxidant systems that contribute to keep the robust antioxidant machinery of astrocytes. On the other hand, NRF2 modulates the expression of the ROS-producer enzymes NADPH-oxidases in astrocytes. In particular, NRF2 represses the expression of NOX-1 and -2 and enhance NOX-4 expression, in good agreement with previous works (Kovac *et al*., 2015; Wei *et al*., 2016). The mechanism(s) whereby NRF2 modulates NOXs expression is unknown. It is tempting to speculate that the increase in extracellular superoxide production observed in mROS-weakened astrocytes could be a redox signal for neighbour neurons, indicating a altered astrocytic metabolism.

To the best of our knowledge, this is the first evidence that endogenous mROS modulates the redox homeostasis *via* the NRF2 pathway in astrocytes.

Furthermore, considering that mCAT expression in brain, liver and heart decreases NRF2 nuclear abundance, our data strongly suggest that endogenous mROS modulate this pathway *in vivo*.

3. Endogenous mROS modulate glucose flux through the pentose phosphate pathway (PPP)

PPP is a metabolic pathway, a function of which in the adult brain is regenerating NADPH to contribute to cellular redox homeostasis. The data presented in this work show that down-modulation of endogenous mROS in astrocytes enhances the flux of glucose through the PPP. These data are in apparent contradiction with the widely-held notion that ROS activate PPP activity (Stincone *et al*., 2015). Thus, ROS, by activating NRF2, promote *G6pd* and *6pgd* expression (Hayes and Dinkova-Kostova, 2014). However, in another work it has been shown that NRF2 modulates the expression of PPP-related genes *via* an indirect mechanism involving epigenetic modifications (Singh *et al*., 2013).

Here, we show that mROS-weakened astrocytes show a decreased NRF2 activity despite enhanced transcription of PPP-related genes. Our data suggest that mROS modulate the expression of G6PD and 6PGD by promoting nuclear localization of HDAC4, which represses the expression of miR-206. This miRNA targets G6PD and 6PGD mRNAs for degradation, leading to decreased protein levels.

Altogether, these results demonstrate that endogenous mROS can modulate glucose metabolism in astrocytes. The suggested epigenetic mechanism is coherent with the study of Singh *et al*. (2013) and further demonstrate that *G6pd* and *6pgd* are not direct NRF2 target genes. It will be very interesting to investigate if other metabolic pathways are also affected in mROS-weakened astrocytes, in order to have a better view on the role of mROS in the regulation of cell metabolism.

4. Endogenous mROS are neuroprotective

Oxidative stress is a hallmark of several neurodegenerative diseases. Accordingly,

ROS have always been considered as harmful species. However, the fact that astrocytes produce a considerable high amount of mROS (Lopez-Fabuel *et al*., 2016), strongly suggests a physiological function of these mROS.

Astrocytes protect co-cultured neurons from oxidative insults (Bélanger and Magistretti, 2009; Dringen, 2000; Wilson, 1997) by increasing the antioxidant defences through the supply of GSH precursors (Bolaños *et al*., 1996; Dringen *et al*., 1997). This phenomenon, which has been named as the astrocyte-neuron glutathione shuttle (Bolaños, 2016), is maintained by constitutively activation of NRF2 in astrocytes (Jimenez-Blasco *et al*., 2015). In fact, the notion that NRF2 activation in astrocytes increases neuronal survival against an oxidative insult is a well known phenomenon, both *in vitro* (Jakel *et al*., 2007; Jimenez-Blasco *et al*., 2015; Shih *et al*., 2003) and in rodent models of neurodegenerative diseases (Chen *et al.*, 2009; Vargas *et al*., 2008). However, in these studies, astrocytic NRF2 activity was artificially increased by protein overexpression or pharmacological activation. Here, we further demonstrate that endogenous mROS play a major role at activating NRF2 in astrocytes, and through this mechanism exerts neuroprotection. A previous study suggested that subtoxic levels of astrocytic hydrogen peroxide failed to activate NRF2 and triggers NRF2-independent processes that protected co-cultured neurons (Haskew-Layton *et al*., 2010). However, these conclusions were questioned on the basis of the experimental design, which did not use appropriate techniques to evaluate astrocytic NRF2 activation (Bell *et al*., 2011). Moreover, subtoxic doses of hydrogen peroxide activated NRF2 in astrocytes (Bell *et al*., 2011). Whilst these data are in agreement with our results, the dose of hydrogen peroxide tested were ~16 fold-higher than the physiological levels that we measured in primary astrocytes in our laboratory (Lopez-Fabuel *et al*., 2016). We therefore believe that, even at subtoxic concentrations of hydrogen peroxide, an aberrant redox signal might contribute to masking the neuroprotective role of endogenous astrocytic mROS.

It should to be noted that rescue of NRF2 levels in mROS-weakened astrocytes only partially restored the survival of co-cultured neurons. These data suggest that endogenous mROS may modulate neuroprotective pathways besides NRF2.

Whether glycolysis, a fundamental metabolic route in the metabolic interactions between astrocytes and neurons (Pellerin and Magistretti, 1994), is affected in mROS-weakened astrocytes is an interessant possibility worth studying.

The data obtained in this work further confirm that endogenous mROS play fundamental roles in maintaining cellular homeostasis, as observed in different tissues (Puente *et al*., 2014; Zhou *et al*., 2016). To the best of our knowledge, this work demonstrates for the first time that endogenous astrocytic mROS have a neuroprotective role. Furthermore, it can be speculated that clinical trials based on antioxidant strategy in patients suffering neurological disorders failed because antioxidants scavenge ROS unspecifically across the brain cell. We propose that this approach could be more beneficious if decreasing ROS specifically in neurons, and not in astrocytes that we show ROS are neuroprotective. These considerations should be taken into account for the design of new antioxidant therapies in the future.

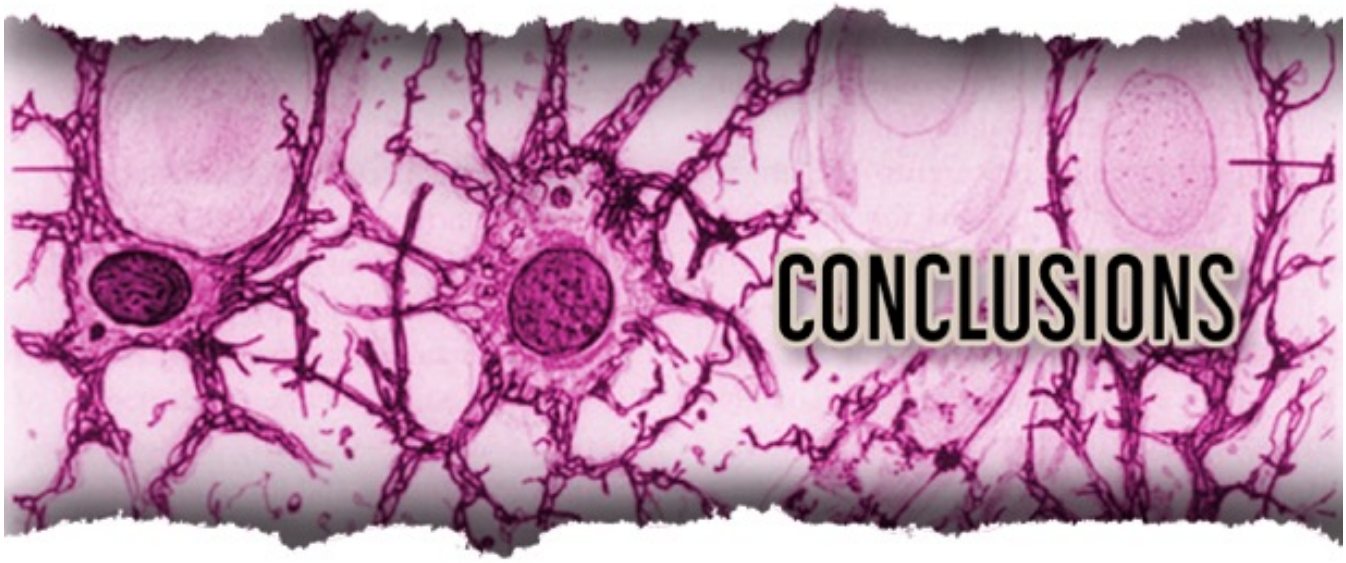
CONCLUSIONS

In the light of the results presented in this Thesis, we have achieved the following conclusions:

1. Here, we have partially characterized a novel mouse model conditionally expressing a mitochondrial-tagged isoform of catalase (mitoCatalase or mCAT) cDNA. This model was designed by our group, and externally generated specifically for this project, by targeted insertion of the mCAT sequence within the *Rosa26* locus *via* homologous recombination in embryonic stem cells from C57Bl/6 mouse strain. The insertion was achieved such that in the resulting model the expression of the mCAT cDNA is under the control of the ubiquitous CAG promoter. A floxed (loxP flanked) transcriptional STOP cassette was incorporated between the mCAT sequence and the CAG promoter to allow the expression of the resulting transgene to be dependent upon the Cre recombinase ($mCAT^{floxed/+}$). By breeding $mCAT^{floxed/+}$ with the C57Bl/6 mice expressing Cre recombinase, it was obtained mice ubiquitously expressing mCAT (mCAT mouse).

2. Cortical astrocytes in primary culture obtained from the mCAT mouse show a significant reduction in the production of endogenous (basal) mitochondrial reactive oxygen species (mROS). Taking advantage of this system, we show that endogenous mROS control the expression of antioxidant genes by up-regulating the activity of the nuclear factor (erythroid-derived 2)-like 2 (NRF2) transcriptional factor in astrocytes. In turn, NRF2 represses the production of extracellular ROS, likely by down-modulating NADPH-dependent oxidases (NOXs) types -1 (NOX1) and -2 (NOX2).

3. Using cortical astrocytes in primary culture obtained from the mCAT mouse, we show that endogenous mROS regulates glucose oxidation through the pentose phosphate pathway (PPP). Thus, down-modulation of

endogenous mROS enhanced PPP activity through a mechanism likely mediated by the reduction of the redox-sensitive histone deacetylase HDAC4. When reduced, HDAC4 is constitutively active in the nucleus, where it represses the expression of miR-1 and miR-206, which in turn represses the mRNA abundances of G6PD and 6PGD. We show that mROS lowers the occurrence of HDAC4 in the nucleus, which leads to decreased miR-1 and miR206 abundances and enhanced G6PD and 6PGD expression and PPP activity. Therefore, in astrocytes, mROS keeps partially repressed the PPP activity thus representing, to the best of our knowledge, the first evidence connecting endogenous mROS production with the regulation of glucose metabolism.

4. In experiments in which mCAT-derived astrocytes were co-cultured with wild type neurons, we show that mROS in astrocytes affects the redox status and survival of neurons. Thus, we show that endogenous mROS in astrocytes, by keeping NRF2 active, contributes to the sustaining of total glutathione abundance in neighbour neurons. Moreover, through this mechanism, we show that mROS in astrocytes supports neuronal survival.


RESUMEN EN ESPAÑOL

1. INTRODUCCIÓN

La aparición del oxígeno en la atmósfera de la Tierra fue un evento crucial que promovió la evolución de los organismos aeróbicos, capaces de producir energía de una manera muy eficiente. Una de las consecuencias de esta mejora fue la aparición de nuevas moléculas reactivas derivadas del oxígeno denominadas especies reactivas de oxígeno (ROS, del inglés *Reactive Oxygen Species*).

Los ROS incluyen, principalmente, anión superóxido ($O_2^{\bullet-}$), peróxido de hidrógeno (H_2O_2) y radical hidroxilo ($^{\bullet}OH$). Estas especies presentan mayor reactividad química respecto al oxígeno y son capaces de desencadenar procesos tanto fisiológicos como patológicos. En condiciones normales, el nivel de los ROS celulares es constante en un equilibrio dinámico, y este equilibrio se modula mediante procesos celulares que producen y eliminan ROS (Zhang *et al*., 2016). Sin embargo, bajo ciertas circunstancias, la tasa de producción de ROS excede la capacidad de los sistemas antioxidantes para eliminarlos. Este exceso de ROS, comúnmente llamado estrés oxidativo o estrés redox, lleva a la oxidación de proteínas, ácidos nucleicos y lípidos (Poyton *et al*., 2009; Temple *et al*., 2005). De hecho, en las muestras cerebrales *post mortem* de enfermedades neurológicas se han encontrado huellas de estrés oxidativo en las áreas cerebrales dañadas (Cannon and Greenamyre 2013; Federico *et al*., 2012). Por lo tanto, el estrés oxidativo parece estar asociado a las enfermedades neurodegenerativas. Sin embargo, los ensayos clínicos basados en una estrategia antioxidante realizados hasta ahora en pacientes que padecen enfermedades neurodegenerativas no han sido fructíferos (Halliwell 2013; Heyland *et al*., 2013; Kamat *et al*., 2008; Snow *et al*., 2010), lo que podría sugerir que el exceso de ROS no tiene un papel patológico. Por el contrario, la idea de que los ROS modulan fisiológicamente vías de supervivencia ha recibido, sin embargo, poca o ninguna atención.

Varios orgánulos dentro de la célula pueden generar ROS fisiológicamente. Estos incluyen las mitocondrias, el retículo endoplásmico y los peroxisomas. Además, varias enzimas, incluidas oxidasas y oxigenasas, generan ROS como parte de sus ciclos de reacción (Holmström and Finkel, 2014). Asimismo, la generación de

ROS es específica de especie, célula y tejido, y también depende del estado fisiopatológico de las células. Por estas razones, la identificación de la principal fuente intracelular de los ROS es compleja.

Dentro del sistema nervioso central, las neuronas y los astrocitos, los dos tipos de células más abundantes en el cerebro, presentan un patrón diferencial de producción de los ROS mitocondriales (mROS), siendo las células gliales las que producen más mROS (López-Fabuel *et al*., 2016). Sin embargo, el papel fisiológico de esta producción de mROS por parte de los astrocitos aún se desconoce.

Tradicionalmente, los ROS se consideran como especies no reguladas y nocivas, con dianas intracelulares aleatorias. Aunque este aspecto inespecífico, aleatorio y dañino de la biología de los ROS persiste, un creciente número de evidencias ahora sugiere que los ROS actúan como moléculas de señalización en varios procesos fisiológicos (D'Autréaux and Toledano, 2007; Holmström and Finkel, 2014; Wang and Hai, 2016). Sin embargo, esta visión no está libre de controversia. Las especies reactivas de oxígeno, en particular el peróxido de hidrogeno, son segundos mensajeros capaces de modular rutas involucradas en la transcripción nuclear, diferenciación celular, muerte celular y envejecimiento, entre otros. Cabe destacar la importancia del factor de transcripción nuclear NRF2 [nuclear factor (erythroid-derived-2)-like 2], el principal regulador de la respuesta antioxidante que está modulado por ROS. En condiciones basales, los niveles de NRF2 se mantienen bajos gracias a su degradación por parte del proteosoma mediada por el complejo formado por KEAP1 (Kelch-like ECH-associated protein 1) y CUL3 (Cullin 3) (Kobayashi *et al*., 2004). Actuando como un sensor de estrés redox, KEAP1 presenta múltiples tioles, cuya modificación lleva a un cambio conformacional de KEAP1 que conduce a la acumulación nuclear de NRF2 (Taguchi *et al*., 2011). Una vez en el núcleo, NRF2 promueve la transcripción de una plétora de genes implicados en la respuesta a diferentes tipos de estrés celulares (Taguchi *et al*., 2011). La ruta de NRF2 tiene un papel crucial en el cerebro, debido al hecho de que modula la transcripción de todas las enzimas involucradas en la homeostasis del glutatión, fundamental para mantener el estado redox de las neuronas. En el cerebro, los astrocitos son el reservorio principal de

GSH, mientras que las neuronas dependen del suministro de precursores de GSH por parte de las células gliales para sintetizarlo (Bolaños, 2016). Además de la regulación positiva de las defensas antioxidantes, recientemente se ha descubierto que NRF2 modula la homeostasis redox modulando la expresión de las NADPH oxidasas (NOXs), enzimas productores de ROS. La actividad de NRF2 reprime la expresión de la NOX2, mientras que aumenta la expresión de NOX4 (Kovac *et al*., 2015; Wei *et al*., 2016), aunque los mecanismos aún se desconocen. Estos enzimas producen ROS utilizando equivalentes reductores procedentes de NADPH, producidos mayoritariamente en la vía de las pentosas fosfato (PPP) gracias a la acción de la glucosa-6-fosfato deshidrogenasa (G6PD) y la 6-fosfogluconato deshidrogenasa (6PGD) (Wamelink, *et al*., 2008). Esta ruta oxida la glucosa para producir ribosa-5-fosfato, necesaria para la síntesis de ácidos nucleicos, así como para regenerar NADPH para mantener la homeostasis redox y para ciertos procesos anabólicos (Riganti *et al*., 2012).

2. HIPÓTESIS

Los ROS han estado tradicionalmente asociados a situaciones de estrés redox e involucrados en la etiología de las patologías humanas, incluidas las enfermedades neurodegenerativas. Aunque los tratamientos con antioxidantes en modelos *in vitro* e *in vivo* de enfermedades neurodegenerativas han demostrado protección neuronal, la traslación a humanos no ha sido concluyente (Halliwell, 2013; Heyland *et al*., 2013; Kamat *et al*., 2008; Snow *et al*., 2010), lo que cuestiona el papel patológico de los ROS.

Resultados recientes de nuestro laboratorio muestran que, en condiciones basales, los astrocitos producen más ROS mitocondriales (mROS) en comparación con las neuronas (López-Fabuel *et al*., 2016). Esto parece ser una paradoja, considerando que los astrocitos expresan una robusta maquinaria antioxidante, gracias a una elevada actividad de la ruta NRF2, en comparación con las neuronas (Jimenez-Blasco *et al*., 2015). Además, los astrocitos sustentan las defensas antioxidantes de las neuronas proporcionándoles los precursores del glutatión (GSH), gracias a

la acción de NRF2 en los astrocitos. Sin embargo, los mecanismos responsables de la alta actividad de la vía de NRF2 en los astrocitos aún se desconocen.

Con estos antecedentes, nuestra hipótesis es que los mROS endógenos mantienen activa la ruta de NRF2 en los astrocitos contribuyendo a la supervivencia neuronal.

3. OBJETIVOS

Para abordar la hipótesis mencionada, nos hemos planteado los siguientes objetivos:

1. Generar un modelo de ratón capaz de disminuir los niveles de mROS endógenos en astrocitos.

2. Estudiar si los mROS endógenos modulan la homeostasis redox en los astrocitos.

3. Estudiar si los mROS astrocíticos modulan la homeostasis redox y la supervivencia de las neuronas.

4. RESULTADOS

1. Generación del ratón +/mCAT constitutivo

Teniendo en cuenta los resultados preliminares en MEFs inmortalizados y astrocitos primarios transfectados, se generó el ratón inducible mitocatalasa ($mCAT^{floxed/+}$), insertando la construcción mCAT en el locus Rosa 26 de células madre embrionarias de ratón con fondo C57Bl/6 por recombinación homóloga. Además, entre el fuerte promotor CAG y la mCAT, se insertó un *cassette* con la señal STOP floxeado.

Con el fin de expresar mCAT de forma ubicua, los ratones $mCAT^{floxed/+}$ se cruzaron con ratones (CMV)-Cre recombinasa bajo un fondo C57Bl/6, lo que produjo la línea de ratón $C57Bl6^{+/mCAT}$ (en adelante mCAT). La descendencia se genotipó (**Figura 1**) y se utilizó para obtener astrocitos primarios +/mCAT.

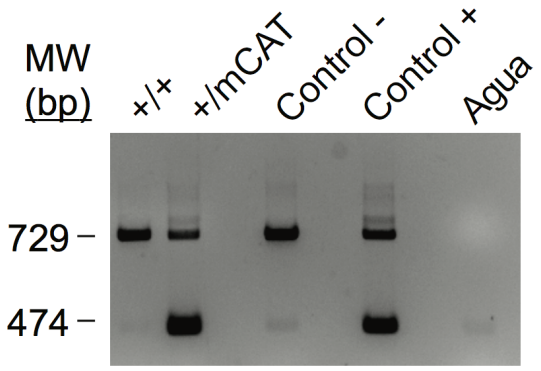

Figura 1: Ejemplo de un gel de PCR. El genotipo de los ratones fue determinado por PCR. Los animales wild type presentan sólo una banda a 729 bp, mientras que en los mCAT aparece una banda adicional a 245 bp. Como controles se utilizó DNA procedente de la cola de los ratones parentales.

2. Expresión constitutiva de la mCAT en los astrocitos primarios

La presencia de la mCAT se confirmó en los astrocitos primarios. Primero, la expresión del epítopo HA y la abundancia de la catalasa se detectaron mediante transferencia de tipo Western en extractos de células enteras. Como era de

esperar, los astrocitos +/mCAT mostraron una mayor abundancia de la catalasa, de unas 6 veces, en comparación con los WT (**Figura 2A**) y expresaron el epítopo HA (**Figura 2B**). Posteriormente, se confirmó la localización mitocondrial de la mCAT. Así, después de un fraccionamiento subcelular, se detectó HA en las mitocondrias aisladas de los astrocitos +/mCAT (**Figura 2C**). Sin embargo, se detectó también una pequeña banda correspondiente a HA en el compartimento citosólico de los astrocitos +/mCAT, lo que probablemente refleja la proteína recién sintetizada. En conjunto, estos resultados confirman que la mCAT se expresa correctamente en las mitocondrias de los astrocitos +/mCAT.

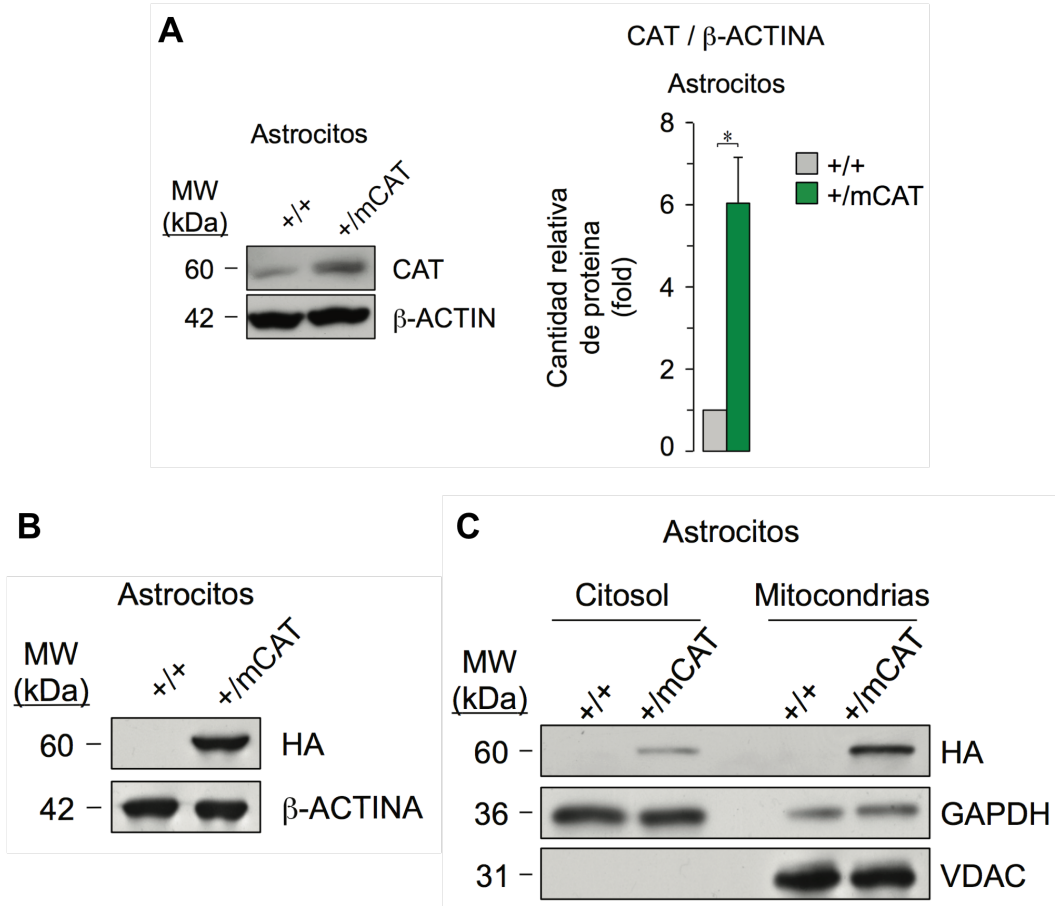

Figura 2: Presencia del epítopo HA y abundancia de la catalasa en astrocitos primarios. El análisis de la transferencia de Western reveló que los astrocitos +/mCAT tienen niveles más altos de catalasa respecto a los WT **(A)** y presentan HA **(B)**. Después de un fraccionamiento subcelular, la localización mitocondrial de HA se analizó mediante transferencia de Western (**C**). Se utilizó β-actina como control de carga del extracto total, GAPDH como control de carga citosólico y VDAC como control de carga mitocondrial. Los datos son expresados como la media ± SEM; *p<0,05 test *t*-Student; n=3 experimentos independientes.

3. La mCAT constitutiva destoxifica eficientemente el peróxido de hidrogeno y disminuye los niveles de los ROS endógenos en los astrocitos primarios

El siguiente paso fue confirmar la funcionalidad de la mCAT y corroborar si su expresión constitutiva es suficiente para disminuir los niveles de mROS endógenos en astrocitos primarios.

La actividad catalítica de la mCAT se midió en mitocondrias aisladas de astrocitos primarios WT y +/mCAT incubados con diferentes concentraciones de peróxido de hidrogeno exógeno. Los resultados mostrados en la **Figura 3** demuestran que las mitocondrias que expresan mCAT neutralizan el peróxido de hidrógeno exógeno más rápidamente que las células WT. Después de 20 minutos, la totalidad del peróxido de hidrógeno exógeno se neutralizó por completo mediante la acción de la mCAT a todas las concentraciones de peroxido de hidrogeno utilizadas. No obstante, parece que la mCAT no es capaz de disminuir los noveles de los ROS en ausencia de peróxido de hidrógeno. En este sentido, hay que tener en cuenta que el método colorimétrico utilizado para medir la actividad de la mCAT no es muy sensible.

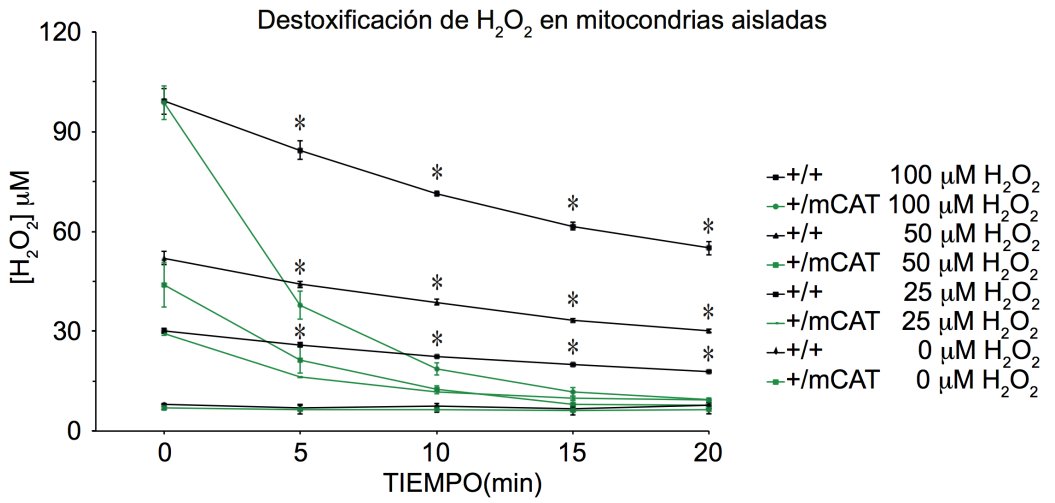

Figura 3: La expresión constitutiva de la mCAT aumenta la destoxificación mitocondrial del peróxido de hidrogeno en astrocitos primarios. La incubación de mitocondrias aisladas con diferentes concentraciones de peróxido de hidrogeno exógeno durante diferentes tiempos mostró que la expresión constitutiva de la mCAT aumenta de manera significativa la velocidad de destoxificación del peróxido de hidrogeno a todas las concentraciones testadas. En ausencia de peróxido de hidrogeno, no se han encontrado diferencias entre las mitocondrias que expresan la mCAT y los WT. Los datos son expresados como la media ± SEM; *p<0,05 test *t*-Student; n=3 experimentos independientes.

Por esta razón, se utilizaron dos sondas más sensibles: Amplex Red y MitoSox. Se midió la liberación de peróxido de hidrógeno por parte de las mitocondrias aisladas y de los astrocitos intactos con la sonda Amplex Red. El resultado mostrado en la **Figura 4A** indica que, en condiciones basales, tanto las mitocondrias +/mCAT como los astrocitos intactos liberan menos peróxido de hidrógeno respecto a los WT. A continuación, se utilizó la sonda MitoSox. Esta sonda sensible a mROS penetra en la mitocondria en función del potencial de membrana mitocondrial ($\Delta\psi_m$), por lo que diferencias en $\Delta\psi_m$ podrían alterar la acumulación mitocondrial de MitoSox. Por lo tanto, es necesario monitorizar $\Delta\psi_m$. Usando la sonda DilC1(5), $\Delta\psi_m$ se determinó por citometría de flujo y los resultados demuestran ausencia de diferencias significativas entre astrocitos WT y +/mCAT (**Figura 4B**). Posteriormente, se midió la fluorescencia de MitoSox y el resultado indica que los astrocitos +/mCAT presentan una menor abundancia de mROS (~20%) en comparación con los WT (**Figura 4C**).

En conjunto, estos resultados muestran que mCAT eficientemente neutraliza el peróxido de hidrógeno exógeno, y que su expresión constitutiva en astrocitos primarios es suficiente para disminuir los niveles de los mROS endógenos. Además, estos cambios en el entorno redox en las células gliales no afectan al $\Delta\psi_m$.

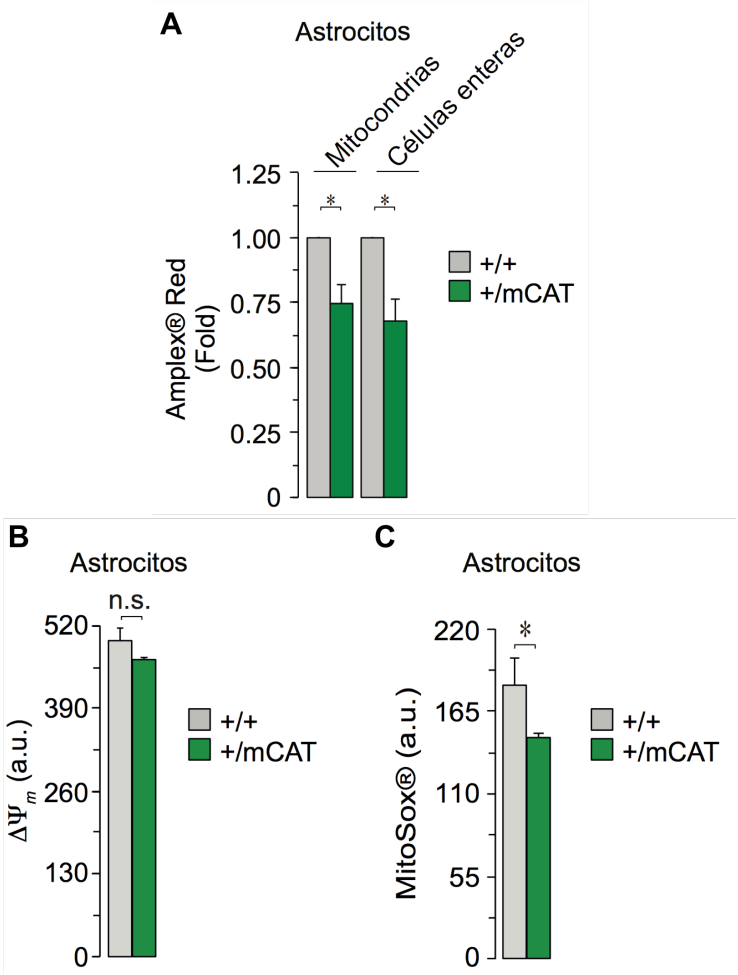

Figura 4: La expresión constitutiva de la mCAT disminuye los niveles de mROS y ROS endógenos en astrocitos primarios. (A) Células enteras y mitocondrias aisladas que expresan constitutivamente la mCAT liberan menos peróxido de hidrogeno respecto a los WT. **(B)** La medición del $\Delta\psi_m$ ha sido analizado mediante citometría de flujo. No se encontraron diferencias entre los astrocitos WT y +/mCAT. (**C**) El análisis de los mROS ha sido realizado por citometrá de flujo utilizando la sonda MitoSox Red. Los astrocitos +/mCAT tienen menos mROS respecto a los WT. Los datos son expresados como la media ± SEM; *p<0,05 test *t*-Student; n=3 experimentos independientes.

4. Los mROS endógenos modulan la acumulación nuclear y la actividad funcional de NRF2 en astrocitos primarios

Para investigar si los mROS endógenos modulan la acumulación nuclear de NRF2 en astrocitos, realizamos fraccionamiento subcelular y la abundancia de NRF2 se detectó mediante transferencia tipo Western en las fracciones citosólica y nuclear. Como se muestra en la **Figura 5A**, los núcleos obtenidos a partir de astrocitos +/mCAT presentan una menor abundancia de NRF2 en comparación con los WT, mientras que no se encontraron diferencias en el compartimento citosólico.

Para investigar si la disminución de la localización nuclear de NRF2 en astrocitos +/mCAT podría afectar a su actividad transcripcional, los niveles de mRNA de varios genes diana de NRF2 se midieron mediante RT-qPCR. Los genes elegidos fueron NADPH-quinona deshidrogenasa 1 (*Nqo1*), glutamato-cisteína ligasa subunidad catalítica (Gcl_c), glutatión peroxidasa-2 (*Gpx2*), hemo-oxigenasa 1 (*Ho-1*), tiorredoxina-1 (*Trx1*), nuclear factor (erythroid-derived-2)-like 2 (*Nrf2*), peroxiredoxina-1 (*Prdx1*), 6-fosfogluconato deshidrogenasa (*6pgd*) y glucosa-6-fosfato deshidrogenasa (*G6pd*). Los primeros siete genes analizados mostraron menores niveles de mRNA en astrocitos mCAT, aunque *Prdx1* no de manera significativa (**Figura 5B**). Sorprendentemente, la abundancia de los transcritos de los genes *6pgd* y *G6pd* era superior en astrocitos +/mCAT, lo que sugiere la existencia de un mecanismo particular de control de su expresión.

En conjunto, estos resultados muestran que los mROS endógenos modulan la acumulación nuclear de NRF2 y de los niveles de mRNA de varios de sus genes diana.

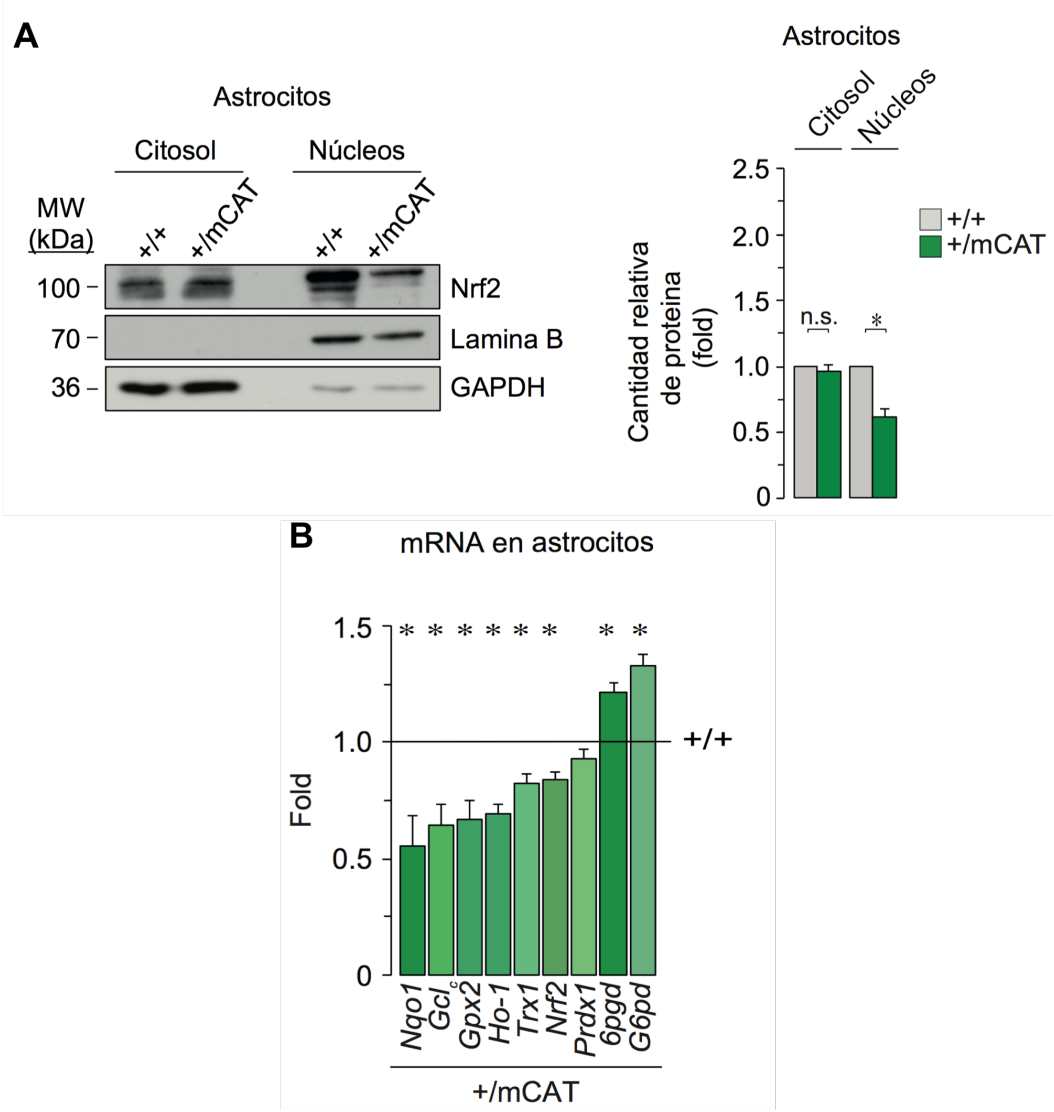

Figura 5: La disminución de los mROS endógenos modula la acumulación nuclear de NRF2 y su actividad. (A) Los núcleos aislados de los astrocitos +/mCAT mostraron una menor acumulación nuclear de NRF2. Se utilizó GAPDH como control de carga citosólica y Lamina B como control de carga nuclear. **(B)** La expresión de varios genes diana de NRF2 se evaluó por RT-qPCR. Se utilizó *β-actina* como housekeeping gene. Los datos son expresados como la media ± SEM; *p<0,05 test *t*-Student; n=3 experimentos independientes.

5. La disminución de los niveles de mROS endógenos aumenta la abundancia de los enzimas de la PPP

La glucosa-6-fosfato deshidrogenasa (G6PD) cataliza el primer paso limitante de la vía de las pentosas fosfato (PPP). Con el fin de investigar si el aumento de la transcripción del gen *G6pd* conlleva un aumento de la proteína G6PD, se estudió

su abundancia mediante transferencia tipo Western. Como se muestra en la **Figura 6A**, los astrocitos +/mCAT expresan una mayor abundancia de G6PD en comparación con los WT. Además, se evaluó la abundancia de 6-fosfogluconato deshidrogenasa (6PGD). La 6PGD cataliza la tercera reacción de la fase oxidativa del PPP, consistente en la descarboxilación del 6-fosfogluconato formando ribulosa-5-fosfato. Este enzima es fundamental en el mantenimiento de la homeostasis redox celular, porque junto con G6PD, es el principal sistema regenerador del NADPH citosólico (Wamelink *et al*., 2008). Este coenzima juega un papel clave en la homeostasis del glutatión (GSH) al suministrar los equivalentes reductores necesarios para reducir GSSG a GSH (Wamelink *et al*., 2008). En astrocitos +/mCAT, los niveles de proteína de 6PGD son más altos que en los WT (**Figura 6B**).

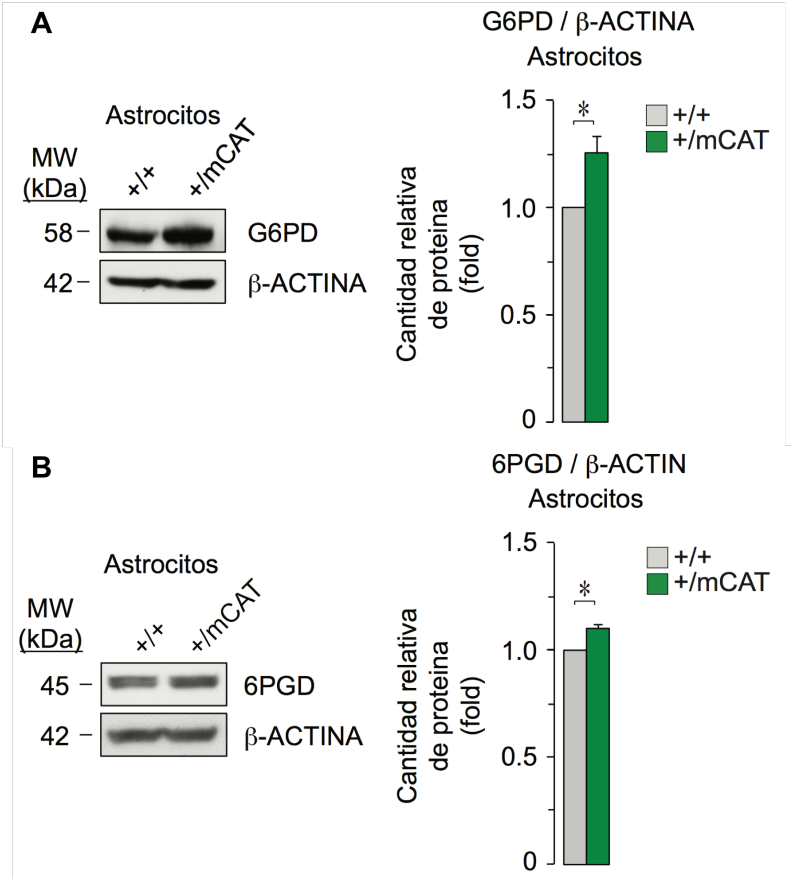

Figura 6: La disminución de los mROS endógenos aumenta la abundancia de G6PD y 6PGD en astrocitos primarios. El análisis de la transferencia de Western mostró que los astrocitos +/mCAT tienen una mayor abundancia de G6PD **(A)** y 6PGD **(B)** respecto a los WT. Se utilizó β−Actina como control de carga. Los datos son expresados como la media ± SEM; *p<0,05 test *t*-Student; n=3 experimentos independientes.

6. La disminución de los niveles de los mROS endógenos aumenta la expresión de miR-1 y miR-206

Recientemente se ha puesto de manifiesto un mecanismo de regulación alternativa de la transcripción de varios genes relacionados con la vía PPP (Singh *et al*., 2013). Este mecanismo está mediado por la histona deacetilasa HDAC4, que se acumula en el núcleo cuando los dos residuos de cisteína, Cys-667 y Cys-669, están en su estado reducido (Ago *et al*., 2008). De esta manera, HDAC4 reprime la transcripción de dos microRNA, miR-1 y miR-206, los cuales degradan el mRNA recién sintetizado de varios genes relacionados con la vía PPP, además del propio HDAC4 (Singh *et al*., 2013).

El aumento de los niveles de los mRNA de *G6pd* y *6pgd* que hemos observado es compatible con este mecanismo. Puesto que los astrocitos +/mCAT presentan un entorno menos oxidante, los residuos de cisteína de HDAC4 podrían estar en su estado reducido. De ser así, HDAC4 estaría localizado en el núcleo reprimiendo la transcripción de miR-1 y miR-206, lo que conllevaría una estabilización de los mRNA de G6PD y 6PGD. Para dilucidar esta hipótesis, la abundancia de HDAC4 en la fracción nuclear se evaluó mediante transferencia tipo western. Los resultados revelan que la abundancia de HDAC4 en el núcleo es mayor en los astrocitos +/mCAT que en los WT (**Figura 7A**). Para confirmar estos resultados, evaluamos las abundancias de los miR-1 y 206 mediante RT-qPCR. Los datos obtenidos muestran que las abundancias de los miR-1 y 206 en los astrocitos +/mCAT son un 15% y un 30% menores que las de los WT, respectivamente (**Figura 7B**).

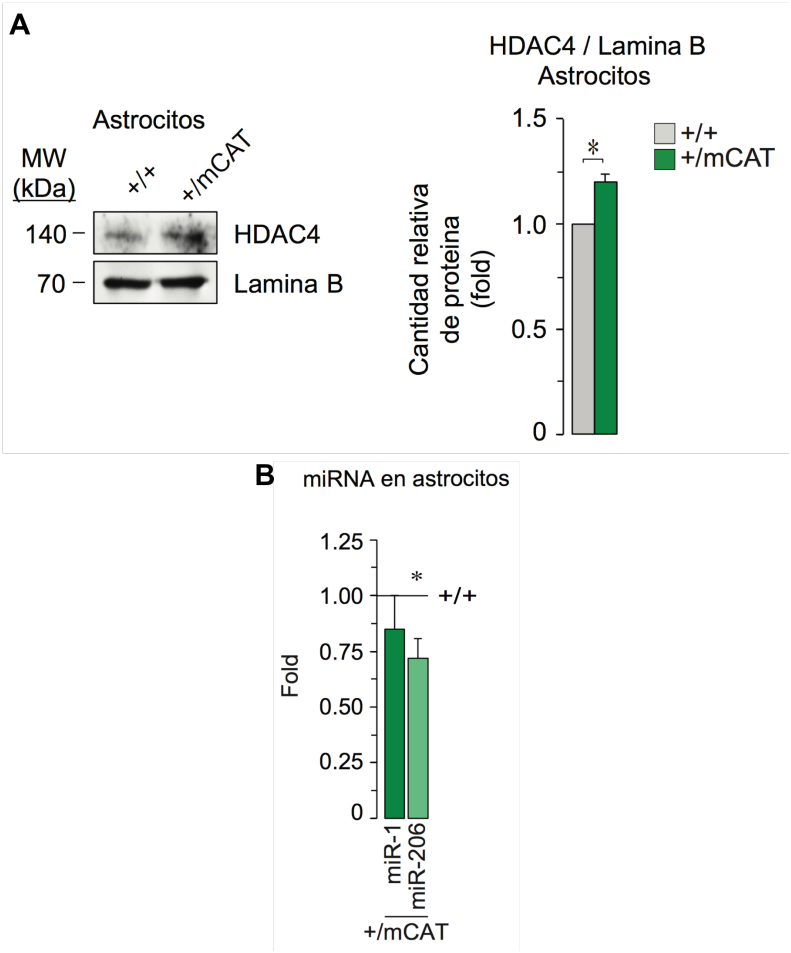

Figura 7: La disminución de los mROS endógenos aumenta la abundancia nuclear de HDAC4 y disminuye la expresión de miR-1 y miR-206. El análisis de la transferencia tipo Western mostró que los astrocitos +/mCAT presentan una mayor abundancia nuclear de HDAC4 **(A)** respecto a los WT. Se utilizó Lamina B como control de carga nuclear. **(B)** El análisis por RT-qPCR reveló que los astrocitos +/mCAT expresan menos miR-1 y miR-206 respecto a los WT. Se utilizó miR-202 como control interno. Los datos son expresados como la media ± SEM; *p<0,05 test *t*-Student; n=3 experimentos independientes.

7. La disminución de los niveles de los mROS endógenos aumenta el flujo de glucosa hacia la PPP

Con objeto de dilucidar si los incrementos en las abundancias de mRNA y proteína de G6PD y 6PGD correlacionan con un aumento en el flujo de glucosa a través del PPP, a continuación determinamos la velocidad de esta vía metabólica utilizando un protocolo optimizado en nuestro laboratorio (Rodríguez-Rodríguez *et al*., 2013). Como se muestra en la **Figura 8A**, el flujo de glucosa oxidada a través de la vía PPP es un 40% mayor en los astrocitos mCAT que en los WT.

Una de las funciones principales de la vía PPP es la regeneración del NADPH necesario para mantener la homeostasis redox y otras vías anabólicas (Wamelink *et al*., 2008). Dado que la disminución de los mROS astrocíticos aumenta los niveles de G6PD y 6PGD junto con la tasa de PPP, se midió la razón NAPDH/NADP$^+$. Sorprendentemente, los astrocitos +/mCAT mostraron una razón NAPDH/NADP$^+$ menor qua la de los WT (**Figura 8B**). Este resultado se podría explicar por un mayor consumo de NADPH en los astrocitos +/mCAT,

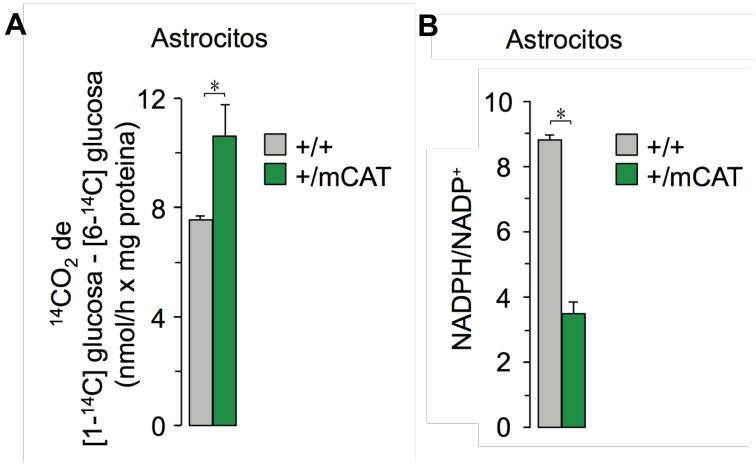

Figura 8: La disminución de los mROS endógenos aumenta flujo de la glucosa oxidada a través de la PPP. (A) El flujo de la PPP fue evaluado incubando los astrocitos con glucosa marcada radioactivamente. Las células +/mCAT mostraron un incremento de la oxidación de la glucosa a través de la PPP respecto a los WT. Sin embargo, los astrocitos +/mCAT presentan una menor razón NADPH/NADP$^+$ comparados con los WT **(B)**. Los datos son expresados como la media ± SEM; *p<0,05 test *t*-Student; n=3 experimentos independientes.

entre otras posibles razones.

8. Los mROS endógenos modulan la producción de superóxido extracelular en los astrocitos

En estudios muy recientes se ha observado que la G6PD se encuentra muy próxima a los enzimas productores de ROS, NADPH-oxidasas (NOX) (Yang *et al*., 2016). Esta familia de enzimas utiliza NADPH para producir superóxido o, según la isoforma, peróxido de hidrógeno. Además, recientemente se ha demostrado que NRF2 reprime la expresión de NOX2, mientras que aumenta la expresión de NOX4 (Kovac *et al*., 2015; Wei *et al*., 2016), aunque se desconoce

el mecanismo. Considerando que los astrocitos +/mCAT muestran una menor actividad de NRF2 y, probablemente, más consumo de NADPH en comparación con los WT, decidimos evaluar los niveles de mRNA de NOX1, -2, -4. Los datos obtenidos ilustran que los astrocitos +/mCAT expresan niveles más altos de mRNA de NOX1 y NOX2 (46% y 51%, respectivamente), mientras que disminuyen los niveles de NOX4 en comparación con los WT (**Figura 9A**). Teniendo en cuenta que NOX1 y -2 producen superóxido extracelular, mientras que NOX4 produce peróxido de hidrógeno, se determinó la liberación de superóxido extracelular. Como se muestra en la **Figura 9B**, los astrocitos +/mCAT liberan un 20% más de superóxido extracelular en comparación con los WT. Estos resultados indican que la disminución de los mROS endógenos en astrocitos primarios aumenta la expresión de NOX1 y NOX2, pero disminuye los niveles de NOX4. Este aumento de las dos isoformas de NOX responsables de la producción de superóxido extracelular es compatible con el aumento observado de este ROS. Además, el aumento de NOX1 y NOX2 es consistente con el aumento en el consumo de NADPH observado en los astrocitos +/mCAT. Sin embargo, se desconoce el mecanismo responsable del aumento de NOX1 y -2 y la disminución de NOX4.

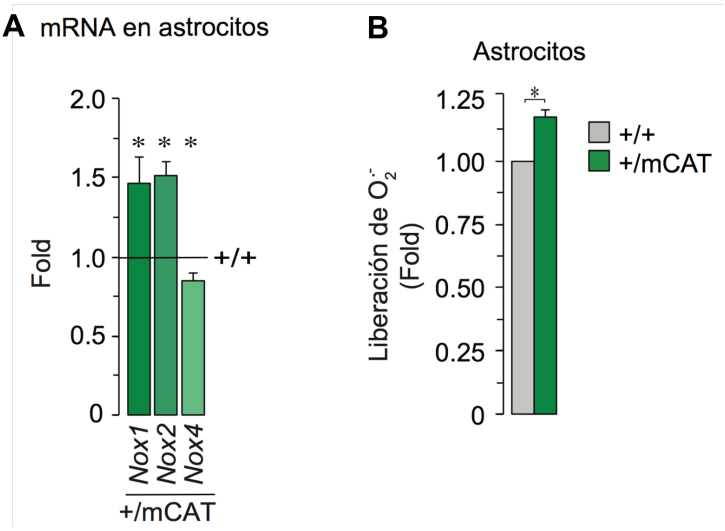

Figura 9: Los mROS endógenos modulan la expresión de las NOXs y la liberación del superóxido extracelular. Los astrocitos +/mCAT presentan una mayor expresión de las NOX-1 y -2, mientras una disminución de la NOX-4 respecto a los WT **(A)**, lo que lleva a un aumento de la liberación del superóxido extracelular **(B)**. Los datos son expresados como la media ± SEM; *p<0,05 test *t*-Student; n=3 experimentos independientes.

9. El rescate de los niveles de NRF2 disminuye la liberación de superóxido en los astrocitos

Con el fin de corroborar que la deficiencia de NRF2 conduce a un aumento en la liberación de superóxido extracelular a través de la actividad de las NOX1 y -2, los astrocitos +/mCAT se transfectaron con un cDNA codificante para una forma fosfomimética de NRF2 (NRF2 PM). Esta isoforma de NRF2 se transloca directamente al núcleo e incrementa la transcripción de sus genes diana. El plásmido se diseñó y se validó previamente en nuestro laboratorio (Jimenez-Blasco *et al*., 2015).

Primero confirmamos la correcta expresión de NRF2 mediante RT-qPCR y transferencia de tipo Western. Como se muestra en la **Figura 10A**, los astrocitos +/mCAT transfectados con NRF2 PM expresan unas 35 veces más mRNA de Nrf2 en comparación con el plásmido vacío. La transferencia de tipo Western reveló dos bandas de NRF2, concretamente la constitutiva (con un peso molecular de 100 kDa) y la fosfomimética, que se detecta a 130 kDa. Como era esperable,

sólo los astrocitos transfectados con NRF2 PM mostraron dos bandas (**Figura 10B**).

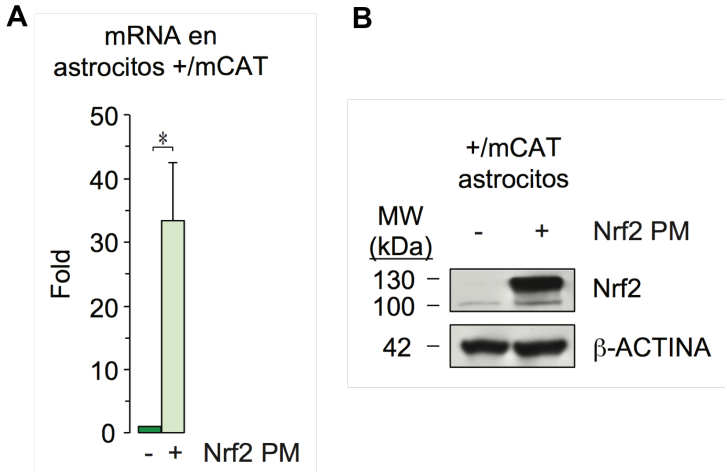

Figura 10: La expresión de NRF2 PM aumenta la abundancia de NRF2 en los astrocitos +/mCAT. (A) Se midieron los niveles de expresión de *Nrf2* mediante RT-qPCR, utilizando *β-actina* como housekeeping gene. Los astrocitos +/mCAT transfectados con NRF2 PM muestran una expresión ~35 veces mayor respecto a las células transfectadas con el plásmido vacío. **(B)** El análisis de la transferencia tipo Western mostró que los astrocitos +/mCAT transfectados con NRF2 PM tienen un pequeño incremento de la expresión de la forma constitutiva de NRF2, como se aprecia en la banda de 100 kDa, y expresan una banda adicional a 130 kDa que corresponde a NRF2 PM, respecto a las células transfectadas con el plásmido vacío. Los datos son expresados como la media ± SEM; *p<0,05 test *t*-Student; n=3 experimentos independientes.

Posteriormente, los niveles de mRNA de NOX1, -2 y -4 se midieron en astrocitos +/mCAT transfectados con NRF2 PM. Los datos obtenidos muestran que la transfección de astrocitos +/mCAT con NRF2 PM restableció los niveles de mRNA de NOX1, -2 y -4 en comparación con las células WT transfectadas con el plásmido vacío (**Figura 11A**). A continuación, se midió la liberación de superóxido extracelular con el fin de determinar si la expresión de NRF2 PM era suficiente para restablecer los valores basales. Como se ilustra en la **Figura 11B**, los astrocitos +/mCAT liberaron un 10% más de superóxido extracelular en comparación con las células WT cuando se transfectaron con el plásmido vacío. Sin embargo, no se encontraron diferencias entre las células +/mCAT transfectadas con NRF2 PM frente a las células WT transfectadas con el plásmido vacío. En conjunto, estos resultados confirman que NRF2 reprime la expresión de NOX1 y -2, mientras que aumenta NOX4 en astrocitos. Además, el rescate de los

niveles de NRF2 en los astrocitos +/mCAT restaura la liberación basal de superóxido extracelular, lo cual sugiere que los mROS modulan la liberación de ROS extracelular a través de un mecanismo mediado por NRF2.

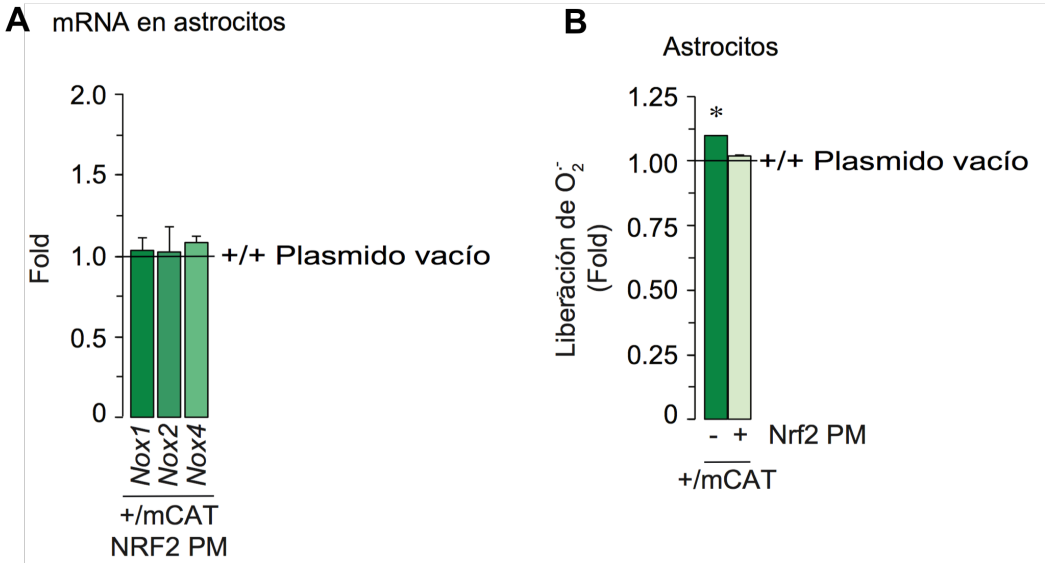

Figura 11: La transfección de los astrocitos +/mCAT con NRF2 PM restablece la expresión basal de las NOXs y la liberación del superóxido. Los astrocitos +/mCAT que expresan NRF2 PM no muestran diferencia en la expresión de NOX1, -2 y -4 **(A)** ni en la liberación de superóxido extracelular **(B)** respecto a los WT transfectado con plásmido vacío. Se utilizó *β-actina* como housekeeping gene. Los datos son expresados como la media ± SEM; *p<0,05 test *t*-Student; n=3 experimentos independientes.

10. Los mROS endógenos modulan la abundancia del glutatión en astrocitos primarios a través de la vía NRF2

El glutatión (GSH) se sintetiza en dos pasos consecutivos, ATP-dependientes, catalizados por la glutamato cisteína ligasa (GCL) y glutatión sintasa (GS), respectivamente (Dringen, 2000). El primer paso es el limitante, razón por la cual la expresión y actividad de GCL controlan la síntesis de GSH. La disminución de los mROS endógenos en astrocitos conlleva una menor expresión del gen Gcl_c (**Figura 5B**). Con el fin de investigar si esta disminución de la transcripción del gen Gcl_c conduce a una menor síntesis de GSH en astrocitos +/mCAT, se evaluaron las abundancias de la proteína GCL y de GSH total. La transferencia de tipo Western mostró una disminución de la abundancia de la GCL en astrocitos +/mCAT en comparación con los WT (**Figura 12A**). Como era esperable, los

astrocitos +/mCAT mostraron una disminución (20%) de la concentración de GSH (**Figura 12B**).

Con el fin de investigar si los mROS astrocíticos modulan la abundancia de GSH a través de la ruta NRF2, los astrocitos +/mCAT se transfectaron con NRF2 PM. Como se observa en la **Figura 12C**, la expresión de NRF2 PM aumenta la abundancia de la proteína GCL en astrocitos +/mCAT. Posteriormente se midió la concentración total de GSH. Coherentemente con el aumento de la GCL, los astrocitos +/mCAT transfectados con NRF2 PM mostraron una concentración de GSH total mayor (**Figura 12D**). En conjunto, estos resultados sugieren que los mROS endógenos astrocíticos modulan las abundancias de GCL y GSH a través de NRF2.

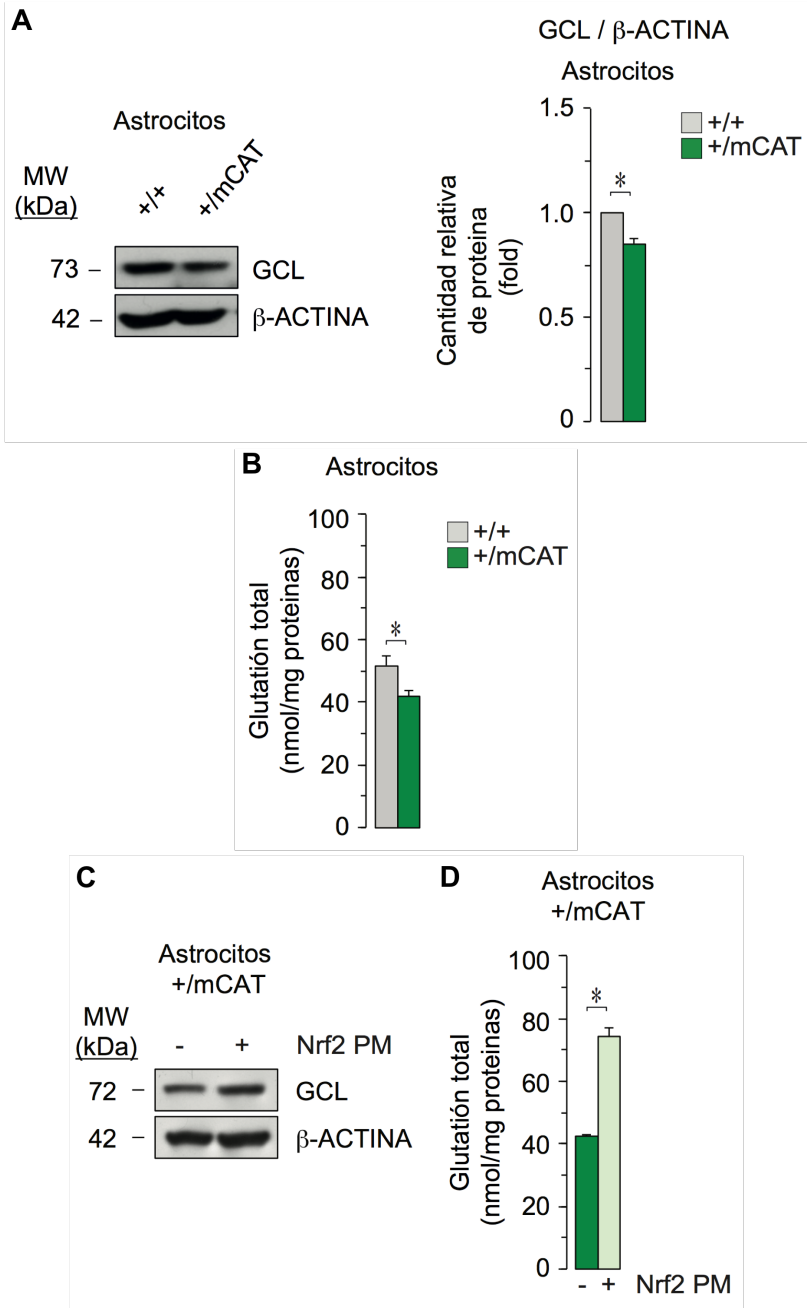

Figura 12: Los mROS endógenos modulan la síntesis del GSH a través de la vía NRF2. (A) El análisis de la transferencia de tipo Western muestra que los astrocitos expresan una menor cantidad de GCL respecto a los WT. **(B)** La medición de los niveles de glutatión mostró que los astrocitos +/mCAT tienen una menor cantidad de GSH respecto a los WT. La transfección de los astrocitos +/mCAT con NRF2 PM aumenta la abundancia de la GCL **(C)** y la concentración de GSH **(D)** respecto al plásmido vacío. Se utilizó β-Actina como control de carga. Los datos son expresados como la media ± SEM; *p<0,05 test *t*-Student; n=3 experimentos independientes.

11. Las neuronas co-cultivadas con astrocitos +/mCAT presentan menos defensas antioxidantes, un aumento de la liberación de ROS y más apoptosis

Con el fin de investigar si la disminución de los mROS endógenos astrocíticos altera la homeostasis redox y supervivencia de las neuronas, se realizaron co-cultivos de astrocitos y neuronas. Como se presenta en la **Figura 13A**, las neuronas co-cultivadas con astrocitos +/mCAT muestran una disminución del 27% en la concentración total de GSH en comparación con las neuronas co-cultivadas con astrocitos WT. Con el objetivo de determinar si este déficit de GSH altera la homeostasis redox neuronal, se midió el peróxido de hidrógeno. Como aparece en la **Figura 13B**, las neuronas produjeron más peróxido de hidrógeno cuando se co-cultivaron con astrocitos +/mCAT. Para averiguar si estos cambios en las defensas antioxidantes afectan a la supervivencia neuronal, se midió la actividad de la caspasa-3 (CSP-3) como marcador de apoptosis en neuronas co-cultivadas en condiciones basales o tras un tratamiento con 100 μM de etopósido, un activador de la apoptosis. La liberación de AMC, marcador de la actividad de la CSP-3, fue mayor en neuronas co-cultivadas con astrocitos +/mCAT en condiciones basales (**Figura 13C**). Después de un tratamiento de 4 horas con etopósido, la actividad de CSP-3 aumentó significativamente en las neuronas; sin embargo, como se muestra en la **Figura 13C**, el aumento fue mayor en neuronas co-cultivadas con astrocitos +/mCAT en comparación con neuronas co-cultivadas con astrocitos WT.

En conjunto, estos datos confirman la importancia del suministro de precursores de GSH de los astrocitos para la homeostasis neuronal. Además, sugieren que la disminución de los niveles de mROS endógenos astrocíticos altera la homeostasis redox y disminuye la supervivencia de las neuronas.

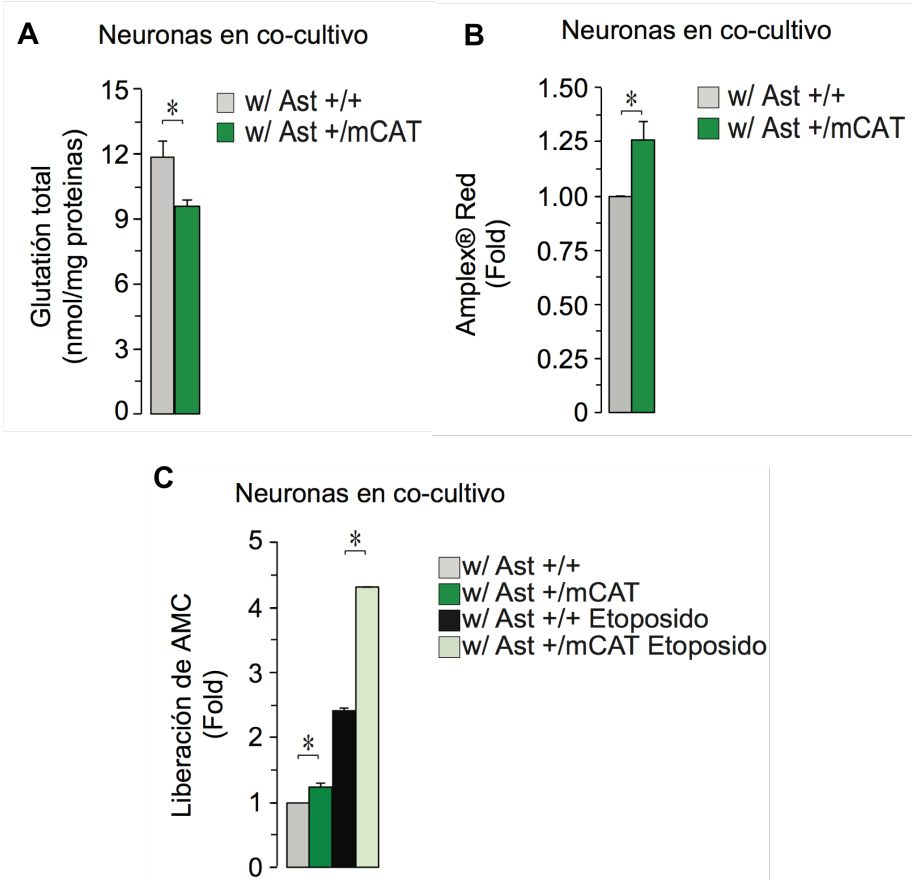

Figura 13: Las neuronas co-cultivadas con astrocitos +/mCAT muestran una disminución en las defensas antioxidantes y una incrementada liberación de ROS y apoptosis. La incubación de las neuronas con astrocitos +/mCAT durante 4 días disminuye el pool neuronal de GSH **(A)**, lo que lleva a un aumento de la liberación de ROS **(B)** y a una mayor activación apoptótica respecto a las neuronas co-cultivadas con astrocitos WT. Los datos son expresados como la media ± SEM; *p<0,05 test *t*-Student; n=3 experimentos independientes.

12. La expresión de NRF2 PM en los astrocitos +/mCAT restablece las defensas antioxidantes y la supervivencia de las neuronas

Para investigar si los mROS astrocíticos modulan la homeostasis redox y la supervivencia neuronal a través de la ruta NRF2, se co-cultivaron las neuronas con astrocitos +/mCAT previamente transfectados con NRF2 PM o con el plásmido vacío. Posteriormente se determinaron la concentración total de GSH, la liberación de peróxido de hidrógeno y la actividad de CSP-3 en las neuronas.

Como se ilustra en la **Figura 14A**, las neuronas co-cultivadas con astrocitos +/mCAT previamente transfectados con NRF2 PM mostraron niveles más altos de GSH, alcanzando los valores de neuronas co-cultivadas con astrocitos WT (**Figura 13A**). A continuación se midió la liberación de peróxido de hidrógeno y, tal como se representa en la **Figura 14B**, las neuronas co-cultivadas con astrocitos +/mCAT, previamente transfectadas con NRF2 PM, mostraron una disminución del ~40% en la liberación de peróxido de hidrógeno respecto a las neuronas co-cultivadas con astrocitos +/mCAT transfectados con el plásmido vacío. Finalmente, para corroborar si la expresión de NRF2 PM en los astrocitos rescata la muerte neuronal, se evaluó la actividad de CSP-3. La **Figura 14C** muestra que las neuronas co-cultivadas con astrocitos +/mCAT que expresan NRF2 PM tenían una menor actividad de CSP-3 en comparación con las neuronas co-cultivadas con astrocitos transfectados con el plásmido vacío.

En conjunto, estos resultados son consistentes con el trabajo previo de nuestro laboratorio (Jimenez-Blasco *et al*., 2015) que demuestra que el aumento de la vía NRF2 en los astrocitos lleva a un aumento de las defensas antioxidantes y de la supervivencia neuronales. Además, nuestros datos demuestran que los mROS astrocíticos endógenos modulan la homeostasis redox y aumentan la viabilidad de las neuronas a través de la ruta NRF2.

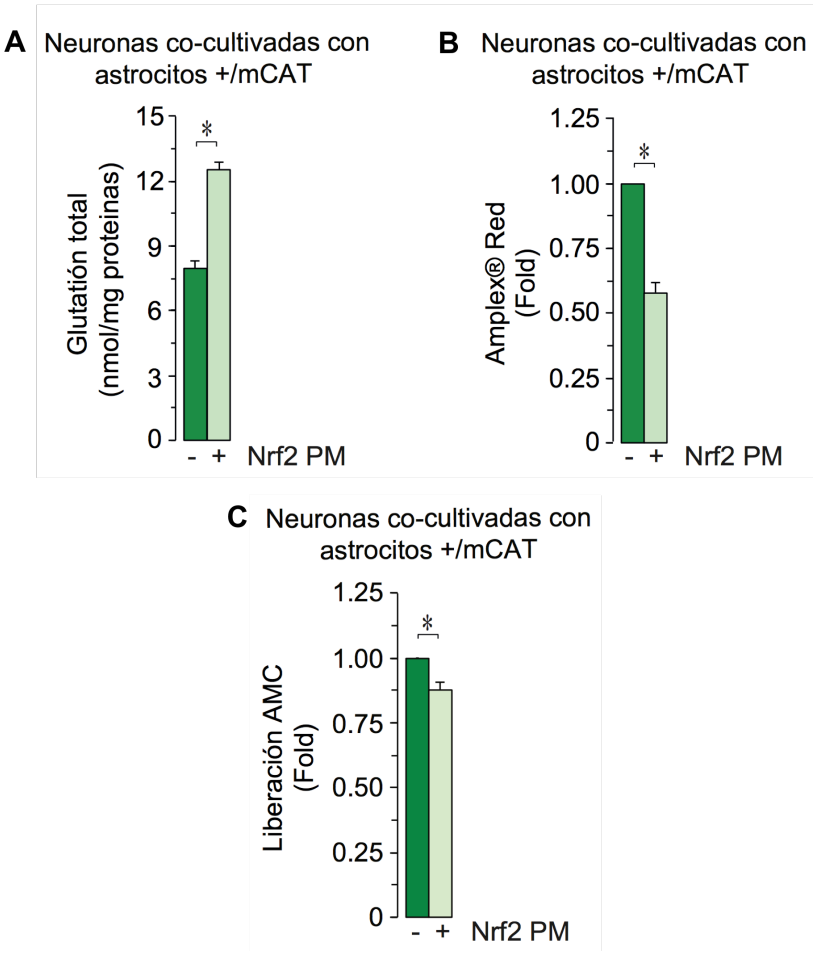

Figura 14: La expresión de NRF2 PM en los astrocitos +/mCAT restablece las defensas antioxidantes y la supervivencia de las neuronas co-cultivadas. La expresión de NRF2 PM en los astrocitos +/mCAT restablece los niveles de GSH **(A)** y disminuye la liberación de ROS **(B)** por parte de las neuronas co-cultivadas, respecto al plásmido vacío. Además, se incrementa levemente, pero de manera significativa, la viabilidad neuronal tras el co-cultivo de las neuronas con los astrocitos +/mCAT que expresan NRF2 PM comparado con el plásmido vacío. Los datos son expresados como la media ± SEM; *p<0,05 test *t*-Student; n=3 experimentos independientes.

5. DISCUSIÓN

La expresión de una forma mitocondrial de la catalasa permite estudiar el papel fisiológico de los mROS

Tradicionalmente, el exceso de ROS ha sido asociado a estrés oxidativo y enfermedades humanas. Sin embargo, los ensayos clínicos basados en antioxidantes no han sido concluyentes (Halliwell, 2013; Heyland *et al*., 2013;

Kamat *et al*., 2008; Snow *et al*., 2010), lo que cuestiona un papel patológico para los ROS.

Por otro lado, para investigar las funciones de los ROS, la mayoría de los estudios anteriores utilizan estrategias basadas en su aumento, ya sea por vías exógenas o endógenas. Sin embargo, este enfoque podría enmascarar los papeles beneficiosos de los ROS endógenos. En este trabajo, presentamos un enfoque alternativo consistente en la disminución de los niveles de mROS endógenos. Varios modelos de ratones diseñados con este fin ya han sido descritos. Sin embargo, tienen efectos secundarios sobre el metabolismo (Chen *et al*., 1998; Matsushima *et al*., 2006; Quintana-Cabrera *et al*., 2012). La estrategia utilizada en este trabajo para disminuir los mROS endógenos está basada en la expresión de una forma mitocondrial de la catalasa, la cual neutraliza el peróxido de hidrógeno con un efecto mínimo sobre metabolismo. De hecho, se ha descrito previamente un modelo de ratón mCAT (Schriner *et al*., 2005). Sin embargo, la técnica de microinyección convencional utilizada para generar ese modelo tiene dos inconvenientes principales: una inserción del constructo de DNA no dirigida y la imposibilidad de controlar el número de copias insertadas. Por lo tanto, es incierto si los efectos observados se deben a la actividad de mCAT o a cualquier efecto desconocido causado por la alteración de la expresión génica.

En consecuencia, diseñamos un modelo de ratón mCAT para investigar los papeles fisiológicos de los mROS. La construcción mCAT se insertó en el locus *Rosa26* de células madre embrionarias de ratón con fondo C57Bl/6 mediante recombinación homóloga. Esta técnica inserta sólo una copia de la construcción mCAT en un locus definido. Además, el modelo se generó basado en la estrategia Cre-LoxP, que permite controlar la expresión de mCAT *in vivo* de una manera específica del tejido y controlada por tiempo.

Los resultados obtenidos en este trabajo muestran que este modelo de ratón mCAT es capaz de disminuir los niveles de los mROS endógenos enlos astrocitos primarios. Por lo tanto, parece útil para investigar las funciones biológicas de los mROS astrocíticos.

Los mROS endógenos modulan la homeostasis redox en los astrocitos primarios a través de la vía NRF2

La ruta NRF2 es esencial para la homeostasis redox en el cerebro. Sin embargo, su actividad difiere entre los dos tipos de células más abundantes, neuronas y astrocitos. Las neuronas muestran las defensas antioxidantes reprimidas debido a la desestabilización continua de la proteína NRF2 (Bell *et al*., 2015; Jiménez-Blasco *et al*., 2015). Por el contrario, NRF2 es altamente estable en los astrocitos, lo que explica sus robustas defensas antioxidantes (Habas *et al*., 2013; Jiménez-Blasco *et al*., 2015). No obstante, aún se desconoce el mecanismo según el cual NRF2 se estabiliza en astrocitos. En este contexto, un estudio reciente demostró que los astrocitos producen más mROS que las neuronas en condiciones basales (López-Fabuel *et al*., 2016). Sin embargo, las funciones fisiológicas de esta producción glial de mROS no se conocen.

Los resultados obtenidos en este trabajo demuestran que los mROS endógenos en los astrocitos mantienen altos los niveles de activación de NRF2, promoviendo la expresión de sistemas antioxidantes que así contribuyen a mantener su robusta maquinaria antioxidante. Por otro lado, NRF2 modula la expresión de los enzimas productores de ROS, NADPH-oxidasas, en astrocitos. En particular, NRF2 reprime la expresión de NOX-1 y -2 y aumenta la expresión de NOX-4, de acuerdo con trabajos previos (Kovac *et al*., 2015; Wei *et al*., 2016). El mecanismo (s) conforme al cual NRF2 modula la expresión de las NOXs es desconocido. Se puede especular que el aumento en la producción de superóxido extracelular observado en los astrocitos que contienen menos mROS podría ser una señal redox para las neuronas vecinas, lo que indicaría una alteración del metabolismo astrocítico.

Hasta donde sabemos, ésta es la primera evidencia de que los mROS endógenos modulan la homeostasis redox a través de la ruta NRF2 en los astrocitos.

Los mROS endógenos modulan el flujo de la glucosa hacia la PPP

La PPP es una ruta metabólica cuya función principal en el cerebro adulto es regenerar NADPH para contribuir a la homeostasis redox celular. Los datos presentados en este trabajo muestran que la disminución de los mROS endógenos en astrocitos aumenta el flujo de la glucosa a través de la vía PPP. Estos datos están en aparente contradicción con la noción ampliamente difundida de que los ROS, al activar NRF2, promueven la expresión de *G6pd* y *6pgd* aumentando la actividad de la PPP (Hayes and Dinkova-Kostova, 2014; Stincone *et al*., 2015). Sin embargo, se ha demostrado que NRF2 modula la expresión de genes relacionados con la vía PPP a través de un mecanismo indirecto involucrando modificaciones epigenéticas (Singh *et al*., 2013).

En este trabajo mostramos que los astrocitos que presentan menos mROS muestran una actividad NRF2 disminuida a pesar de la aumentada transcripción de genes relacionados con la vía PPP. Nuestros datos sugieren que los mROS modulan la expresión de G6PD y 6PGD al promover la localización nuclear de HDAC4, que reprime la expresión de miR-206. Este miRNA se une a los mRNAs G6PD y 6PGD para su degradación, lo que lleva a la disminución de los niveles de proteína.

En conjunto, estos resultados demuestran que los mROS endógenos pueden modular el metabolismo de la glucosa en los astrocitos. El mecanismo epigenético sugerido es coherente con el estudio de Singh *et al*. (2013) y demuestra una vez más que *G6pd* y *6pgd* no son genes diana de NRF2. Sería muy interesante investigar si otras vías metabólicas también se ven afectadas en los astrocitos +/mCAT, con el fin de tener una visión más amplia del papel de los mROS en la regulación del metabolismo celular.

Los mROS endógenos son neuroprotectores

El estrés oxidativo es una característica distintiva de varias enfermedades neurodegenerativas. Así, los ROS han sido siempre considerados como especies dañinas. Sin embargo, el hecho de que los astrocitos produzcan una cantidad considerable de mROS (López-Fabuel *et al*., 2016) sugiere una función fisiológica de estos mROS.

Los astrocitos protegen a las neuronas co-cultivadas de los daños oxidativos (Bélanger and Magistretti, 2009; Dringen, 2000; Wilson, 1997) al aumentar las defensas antioxidantes a través del suministro de precursores de GSH (Bolaños *et al*., 1996; Dringen *et al*., 1997). Este fenómeno, que ha sido denominado lanzadera de glutatión astrocito-neurona (Bolaños, 2016), se mantiene mediante la activación constitutiva de NRF2 en astrocitos (Jimenez-Blasco *et al*., 2015). De hecho, la idea de que la activación de NRF2 en los astrocitos aumenta la supervivencia neuronal frente a un daño oxidativo es un fenómeno bien conocido, tanto *in vitro* (Jakel *et al*., 2007; Jiménez-Blasco *et al*., 2015; Shih *et al*., 2003) como en modelos animales de enfermedades neurodegenerativas (Chen *et al*., 2009; Vargas et al., 2008). Sin embargo, en estos estudios, la actividad de NRF2 en astrocitos se vio aumentada artificialmente por su sobreexpresión o su activación farmacológica. En este trabajo, demostramos que los mROS endógenos juegan un papel importante en la activación de NRF2 en astrocitos, y a través de este mecanismo ejercen neuroprotección. Un estudio previo sugirió que niveles subtóxicos de peróxido de hidrógeno astrocítico no activan NRF2 y desencadenan procesos independientes de NRF2 que protegen las neuronas co-cultivadas (Haskew-Layton *et al*., 2010). Sin embargo, estas conclusiones fueron cuestionadas (Bell *et al*., 2011). Además, las dosis subtóxicas de peróxido de hidrógeno utilizadas activan NRF2 en astrocitos (Bell *et al*., 2011). Si bien estos datos concuerdan con nuestros resultados, la dosis de peróxido de hidrógeno probada fue unas 16 veces mayor que los niveles fisiológicos que observamos en astrocitos en nuestro laboratorio (López-Fabuel *et al*., 2016). Por lo tanto, creemos que incluso utilizando concentraciones subtóxicas de peróxido de hidrógeno, se podría desencadenar una señal redox aberrante que podría enmascarar el papel neuroprotector de los mROS astrocíticos endógenos.

Cabe destacar que el rescate de los niveles de NRF2 en astrocitos mCAT sólo restauró parcialmente la supervivencia de las neuronas co-cultivadas. Estos datos sugieren que los mROS endógenos pueden modular otras rutas neuroprotectoras además de NRF2. Una posibilidad interesante que merece la pena estudiar es si la glucólisis, una ruta metabólica fundamental en las interacciones metabólicas entre

los astrocitos y las neuronas (Pellerin and Magistretti, 1994), se ve afectada en los astrocitos que presentan menos mROS.

Los datos obtenidos en este trabajo confirman una vez más que los mROS endógenos desempeñan papeles fundamentales en el mantenimiento de la homeostasis celular, como se observa en diferentes tejidos (Puente *et al*., 2014; Zhou *et al*., 2016). Este trabajo demuestra por primera vez que los mROS astrocíticos endógenos tienen un papel neuroprotector. Además, se puede especular que los ensayos clínicos basados en la estrategia antioxidante en pacientes que padecen enfermedades neurológicas no han sido concluyentes debido a que los antioxidantes eliminan los ROS de forma inespecífica en todas las células cerebrales. Proponemos que este enfoque podría ser más beneficioso si se disminuyen los ROS específicamente en las neuronas, y no en los astrocitos que demostramos ser neuroprotectores. Estas consideraciones deben tenerse en cuenta para el diseño de nuevas terapias antioxidantes en el futuro.

6. CONCLUSIONES

A la luz de los resultados presentados en esta Tesis, hemos obtenido las siguientes conclusiones:

1. Hemos caracterizado parcialmente un nuevo modelo de ratón que expresa condicionalmente una isoforma mitocondrial de la catalasa (mitoCatalasa o mCAT). Este modelo ha sido diseñado por nuestro grupo, y se generó externamente y específicamente para este proyecto, mediante la inserción dirigida de la secuencia mCAT en el locus *Rosa26* de células madre embrionarias de la cepa C57Bl/6 de ratón mediante recombinación homóloga. La inserción se logró de tal manera que, en el modelo resultante, la expresión del cDNA de la mCAT está bajo el control del promotor ubicuo CAG. Se insertó un cassete de STOP transcripcional floxeado (flanqueado con loxP) entre la secuencia mCAT y el promotor CAG para permitir que la expresión del transgén resultante dependa de la recombinasa Cre ($mCAT^{floxed/+}$). Al cruzar $mCAT^{floxed/+}$ con los ratones

C57Bl/6 que expresan la recombinasa Cre de forma ubicua, se obtuvieron ratones que expresan constitutivamente la mCAT (ratón mCAT).

2. Los astrocitos corticales primarios obtenidos del ratón mCAT muestran una reducción significativa en la producción de especies reactivas de oxígeno mitocondriales endógenas (basales) (mROS). Aprovechando este sistema, demostramos que los mROS endógenos controlan la expresión de genes antioxidantes mediante la regulación positiva de la actividad de NRF2 [nuclear factor (erythroid-derived 2)-like 2] en los astrocitos. A su vez, NRF2 reprime la producción de ROS extracelulares, reprimiendo la expresión de las NADPH-oxidasas (NOX) tipo -1 (NOX1) y -2 (NOX2).

3. Utilizando astrocitos corticales primarios obtenidos del ratón mCAT, demostramos que los mROS endógenos regulan la oxidación de la glucosa a través de la vía de las pentosas fosfato (PPP). De hecho, la disminución de los mROS endógenos aumentó la actividad de PPP a través de un mecanismo mediado por la reducción de la histona desacetilasa 4 (HDAC4) sensible a ROS. En su estado reducido, HDAC4 es constitutivamente activa en el núcleo, donde reprime la expresión de miR-1 y miR-206, que a su vez reprimen las abundancias de los mRNAs de G6PD y 6PGD. Aquí demostramos que los mROS disminuyen la acumulación de HDAC4 en el núcleo, lo que lleva a la disminución de la abundancia de miR-1 y miR206, y aumenta la expresión de G6PD y 6PGD junto con la actividad de la vía PPP. Por lo tanto, en los astrocitos, los mROS mantienen parcialmente reprimida la actividad de la PPP, representando la primera evidencia que conecta la producción endógena de mROS con la regulación del metabolismo de la glucosa.

4. En experimentos en los que los astrocitos mCAT se co-cultivaron con neuronas WT, mostramos que los mROS de los astrocitos afectan el estado redox y la supervivencia de las neuronas. Así, los mROS endógenos de los astrocitos, al mantener NRF2 activa, contribuyen al mantenimiento de la

abundancia total de glutatión en las neuronas. Además, a través de este mecanismo, los mROS en astrocitos incrementan la supervivencia neuronal.


REFERENCES

Acín-Pérez, R., Fernández-Silva P., Peleato M. L., Pérez-Martos A., and Enriquez J.A. (2008) Respiratory Active Mitochondrial Supercomplexes. *Molecular Cell* 32 (4): 529–39.

Ago, T., Liu T., Zhai P., Chen W., Li H., Molkentin J. D., Vatner S. F., and Sadoshima J. (2008) A Redox-Dependent Pathway for Regulating Class II HDACs and Cardiac Hypertrophy. *Cell* 133 (6): 978–93.

Al-Mehdi A. B., Pastukh V. M., Swiger B. M., Reed D. J., Patel M. R., Bardwell G. C., Pastukh V. V., Alexeyev M. F., and Gillespie M. N. (2012) Perinuclear Mitochondrial Clustering Creates an Oxidant-Rich Nuclear Domain Required for Hypoxia-Induced Transcription. *Science Signaling* 5 (231): ra47.

Almeida, A., Almeida J., Bolaños J. P., and Moncada S. (2001) Different Responses of Astrocytes and Neurons to Nitric Oxide: The Role of Glycolytically Generated ATP in Astrocyte Protection. *Proceedings of the National Academy of Sciences of the United States of America* 98 (26): 15294–99.

Almeida, A., Heales S. J., Bolanos J. P., and Medina J. M. (1998) Glutamate Neurotoxicity Is Associated with Nitric Oxide-Mediated Mitochondrial Dysfunction and Glutathione Depletion. *Brain Research* 790, 209-216.

Almeida, A., Moncada S., and Bolaños J. P. 2004. Nitric Oxide Switches on Glycolysis through the AMP Protein Kinase and 6-Phosphofructo-2-Kinase Pathway. *Nature Cell Biology* 6 (1): 45–51.

Altenhöfer, S., Kleikers P., Radermacher K., Scheurer P., Hermans J., Schiffers P., Ho H., Wingler K., and Schmidt H. H. (2012) The NOX Toolbox: Validating the Role of NADPH Oxidases in Physiology and Disease. *Cellular and Molecular Life Sciences* 69 (14): 2327–43.

Anathy, V., Aesif S. W., Guala A. S., Havermans M., Reynaert N. L., Ho Y. S., Budd R. C., and Janssen-Heininger Y. M. (2009) Redox Amplification of Apoptosis by Caspase-Dependent Cleavage of Glutaredoxin 1 and S-Glutathionylation of Fas. *The Journal of Cell Biology* 184 (2): 241 LP-252.

Andrews, N. C., Erdjument-Bromage H., Davidson M. B., Tempst P., and Orkin S. H. (1993) Erythroid Transcription Factor NF-E2 Is a Haematopoietic-Specific Basic-Leucine Zipper Protein. *Nature* 362 (6422): 722–28.

Baird, L., Llères D., Swift S., and Dinkova-Kostova A. T. (2013) Regulatory Flexibility in the Nrf2-Mediated Stress Response Is Conferred by Conformational Cycling of the Keap1-Nrf2 Protein Complex. *Proceedings of the National Academy of Sciences of the United States of America* 110 (38): 15259–64.

Baizabal, J. M., Furlan-Magaril M., Santa-Olalla J., and Covarrubias L. (2003) Neural Stem Cells in Development and Regenerative Medicine. *Archives of Medical Research* 34 (6): 572–88.

Ballatori, N., Krance S. M., Marchan R., and Hammond C. (2009) Plasma Membrane Glutathione Transporters and Their Roles in Cell Physiology and Pathophysiology. *Molecular Aspects of Medicine*.

Baquer, N. Z., Hothersall J. S., and McLean P. (1988) Function and Regulation of the Pentose Phosphate Pathway in Brain. *Curr Top Cell Regul* 29: 265–89.

Barcia-Vieitez, R., and Ramos-Martínez J. I. (2014) The Regulation of the Oxidative Phase of the Pentose Phosphate Pathway: New Answers to Old Problems. *IUBMB Life* 66 (11): 775–79.

Bélanger, M., Allaman I., and Magistretti P. J. (2011) Brain Energy Metabolism: Focus on Astrocyte-Neuron Metabolic Cooperation. *Cell Metabolism* 14 (6): 724–38.

Bélanger, M., and Magistretti P. J. (2009) The Role of Astroglia in Neuroprotection. *Dialogues in Clinical Neuroscience*.

Belarbi, K., Cuvelier E., Destée A., and Gressier B. (2017) "NADPH Oxidases in Parkinson ' S Disease : A Systematic Review." *Molecular Neurodegeneration*, 1–18.

Bell, E. L., Klimova T. A., Eisenbart J., Moraes C. T., Murphy M. P., Budinger G. R., and Chandel N. S. (2007) The Qo Site of the Mitochondrial Complex III Is Required for the Transduction of Hypoxic Signaling via Reactive Oxygen Species Production. *Journal of Cell Biology* 177 (6): 1029–36.

Bell, K. F., Al-Mubarak B., Martel M. A., McKay S., Wheelan N., Hasel P., Márkus N. M., Baxter P., Deighton R. F., Serio A., Bilican B., Chowdhry S., Meakin P. J., Ashford M. L., Wyllie D. J., Scannevin R. H., Chandran S., Hayes J. D. and Hardingham G. E. (2015) Neuronal Development Is Promoted by Weakened Intrinsic Antioxidant Defences due to Epigenetic Repression of Nrf2. *Nature Communications* 6 (May): 7066.

Bell, K. F., Al-Mubarak B., Fowler J. H., Baxter, P. S., Gupta K., Tsujita T., Chowdhry S., Patani R., Chandran S., Horsburg K., Hayes J. D. and Hardingham G. E. (2011) Mild Oxidative Stress Activates Nrf2 in Astrocytes, Which Contributes to Neuroprotective Ischemic Preconditioning. *Proceedings of the National Academy of Sciences of the United States of America* 108 (1): E1-2-4.

Ben-Yoseph, O., Boxer P. A., and Brian D. Ross. B. D. (1996) Assessment of the Role of the Glutathione and Pentose Phosphate Pathways in the Protection of Primary Cerebrocortical Cultures from Oxidative Stress. *Journal of Neurochemistry* 66 (6).

Bienert, G. P., Møller A. L., Kim A. Kristiansen K. A., Schulz A., Møller I.

M., Schjoerring J. K., and Jahn T. P. (2007) Specific Aquaporins Facilitate the Diffusion of Hydrogen Peroxide across Membranes. *Journal of Biological Chemistry* 282 (2): 1183–92.

Biswas, M., and Chan J. Y. (2010) Role of Nrf1 in Antioxidant Response Element-Mediated Gene Expression and beyond. *Toxicology and Applied Pharmacology*. 244(1):16-20.

Block, K., Gorin Y., and Abboud H. E. (2009) Subcellular Localization of Nox4 and Regulation in Diabetes. *Proceedings of the National Academy of Sciences of the United States of America* 106 (34): 14385–90.

Bolaños, J. P., Heales S. J., Land J. M., and Clark J. B. (1995) Effect of Peroxynitrite on the Mitochondrial Respiratory Chain: Differential Susceptibility of Neurones and Astrocytes in Primary Culture. *Journal of Neurochemistry* 64 (5): 1965–72.

Bolaños, J. P. (2016) Bioenergetics and Redox Adaptations of Astrocytes to Neuronal Activity. *Journal of Neurochemistry* 139: 115–25.

Bolaños, J. P., Heales S. J., Peuchen S., Barker J. E., Land J. M., and Clark J. B. (1996) Nitric Oxide-Mediated Mitochondrial Damage: A Potential Neuroprotective Role for Glutathione. *Free Radical Biology and Medicine* 21 (7): 995–1001.

Boussif, O., Lezoualc'h F., Zanta M. A., Mergny M. D., Scherman D., Demeneix B., and Behr J. P. (1995) A Versatile Vector for Gene and Oligonucleotide Transfer into Cells in Culture and in Vivo: Polyethylenimine. *Proceedings of the National Academy of Sciences of the United States of America* 92 (16): 7297–7301.

Bouzier-Sore, A. K., and Bolaños J. P. (2015) Uncertainties in Pentose-Phosphate Pathway Flux Assessment Underestimate Its Contribution to Neuronal Glucose Consumption: Relevance for Neurodegeneration and Aging." *Frontiers in Aging Neuroscience* 7:1–5.

Brand, M. D. (2010) The Sites and Topology of Mitochondrial Superoxide Production. *Experimental Gerontology* 45 (7–8).

Branda, C. S., and Dymecki S. M. (2004) Talking about a Revolution: The Impact of Site-Specific Recombinases on Genetic Analyses in Mice. *Developmental Cell* 6(1):7-28.

Brooks, P. J. (2002) DNA Repair in Neural Cells: Basic Science and Clinical Implications. *Mutat Res* 509 (1–2): 93–108.

Cambier, D., Rutin J., Alliot F., and Pessac B. (2000) Expression of γ-Glutamyl Transpeptidase in Mouse Perivascular Astrocytes and in a Protoplasmic-like

Astroglial Cell Clone. *Brain Research* 852 (1): 191–97.

Cannon, J. R., and Greenamyre T. J. (2013) Gene-Environment Interactions in Parkinson's Disease: Specific Evidence in Humans and Mammalian Models. *Neurobiology of Disease* 57:38-46.

Chan, J. Y., Han X. L., and Kan Y. W. (1993) Cloning of Nrf1, an NF-E2-Related Transcription Factor, by Genetic Selection in Yeast. *Proceedings of the National Academy of Sciences of the United States of America* 90 (23): 11371–75.

Chandel, N. S., McClintock D. S., Feliciano C. E., Wood T. M., Melendez J. A., Rodriguez A. M., and Schumacker P. T. (2000) Reactive Oxygen Species Generated at Mitochondrial Complex III Stabilize Hypoxia-Inducible Factor-1a During Hypoxia: A Mechanism of O_2 Sensing. *Journal of Biological Chemistry* 275 (33): 25130–38.

Chandel, N. S., Maltepe E., Goldwasser E., Mathieu C. E., Simon M. C., and Schumacker P. T. 1998. Mitochondrial Reactive Oxygen Species Trigger Hypoxia-Induced Transcription. *Proceedings of the National Academy of Sciences of the United States of America* 95 (20): 11715–20.

Chen, J. F., Tao Y., Li J., Deng Z., Yan Z., Xiao X., and Wang D. Z. (2010) microRNA-1 and microRNA-206 Regulate Skeletal Muscle Satellite Cell Proliferation and Differentiation by Repressing Pax7. *Journal of Cell Biology* 190 (5): 867–79.

Chen, P. C., Vargas M. R., Pani A. K., Smeyne R. J., Johnson D. A.,Kan Y. W., and Johnson J. A. (2009) Nrf2-Mediated Neuroprotection in the MPTP Mouse Model of Parkinson's Disease: Critical Role for the Astrocyte. *Proceedings of the National Academy of Sciences of the United States of America* 106 (8): 2933–38.

Chen, Z., Siu B., Ho Y. S., Vincent R., Chua C. C., Hamdy R. C., and Chua B. H. (1998) Overexpression of MnSOD Protects Against Myocardial Ischemia/reperfusion Injury in Transgenic Mice. *Journal of Molecular and Cellular Cardiology* 30 (11): 2281–89.

Chevillard, G., and Blank V. (2011) NFE2L3 (NRF3): The Cinderella of the Cap'n'Collar Transcription Factors. *Cellular and Molecular Life Sciences* 68 (20): 3337–48.

Chinta, S. J., Kumar M. J., Hsu M., Rajagopalan S., Kaur D., Rane A., Nicholls D. G., Choi J., and Andersen J. K. (2007) Inducible Alterations of Glutathione Levels in Adult Dopaminergic Midbrain Neurons Result in Nigrostriatal Degeneration. *The Journal of Neuroscience* 27 (51): 13997-14006.

Chowdhry, S., Zhang Y., McMahon M., Sutherland C., Cuadrado A., and Hayes J. D. (2013) Nrf2 Is Controlled by Two Distinct [Beta]-TrCP Recognition

Motifs in Its Neh6 Domain, One of Which Can Be Modulated by GSK-3 Activity. *Oncogene* 32 (32) 3765–81.
Circu, M. L., and Aw T. Y. (2010) Reactive Oxygen Species, Cellular Redox Systems, and Apoptosis. *Free Radical Biology and Medicine* 48 (6) 749–62.

Coda, D. M., Lingua M. F., Morena D., Foglizzo V., Bersani F., Ala U., Ponzetto C., and Taulli R. (2015) SMYD1 and G6PD Modulation Are Critical Events for miR-206-Mediated Differentiation of Rhabdomyosarcoma. *Cell Cycle* 14 (9): 1389–1402.

D'Autréaux, B., and Toledano M. B. (2007) ROS as Signalling Molecules: Mechanisms That Generate Specificity in ROS Homeostasis. *Nature Reviews Molecular Cell Biology* 8 (10): 813–24.

Dalton, T. P., Chen Y., Schneider S. N., Nebert D. W., and Shertzer H. G. (2004) Genetically Altered Mice to Evaluate Glutathione Homeostasis in Health and Disease. *Free Radical Biology and Medicine* 27(10):1511-26.

DeNicola, G. M., Karreth F. A., Humpton T. J., Gopinathan A., Wei C., Frese K, Mangal D., Yu K. H., Yeo C. J., Calhoun E. S., Scrimieri F., Winter J. M., Hruban R. H., Iacobuzio-Donahue C., Kern S. E., Blair I. A., and Tuveson D. A. (2011) Oncogene-Induced Nrf2 Transcription Promotes ROS Detoxification and Tumorigenesis. *Nature* 475 (7354): 106–9.

Devesa, A., O'Connor J. E., Garciá C., Puertes I. R., and Viña J. R. (1993) Glutathione Metabolism in Primary Astrocyte Cultures: Flow Cytometric Evidence of Heterogeneous Distribution of GSH Content. *Brain Research* 618 (2): 181–89.

Diaz-Hernandez, J. I., Almeida A., Delgado-Esteban M., Fernandez E., and Bolaños J. P. (2005) Knockdown of Glutamate-Cysteine by Ligase by Small Hairpin RNA Reveals That Both Catalytic and Modulatory Subunits Are Essential for the Survival of Primary Neurons. *Journal of Biological Chemistry* 280 (47): 38992–1.

Dimauro, I., Pearson T., Caporossi D., and Jackson M. J. (2012) A Simple Protocol for the Subcellular Fractionation of Skeletal Muscle Cells and Tissue. *BMC Research Notes* 5 (1).

Dinkova-Kostova, A. T., Kostov R. V., and Canning P. (2016) Keap1, the Cysteine-Based Mammalian Intracellular Sensor for Electrophiles and Oxidants. *Archives of Biochemistry and Biophysics* 617:84–93.

Dringen, R., Gutterer J., and Hirrlinger J. (2000) Glutathione Metabolism in Brain: Metabolic Interaction between Astrocytes and Neurons in the Defense against Reactive Oxygen Species. *European Journal of Biochemistry* 267(16):4912-6.

Dringen, R, Hoepken H. H., Minich T., and Ruedig C. (2007) 1.3 Pentose Phosphate Pathway and NADPH Metabolism BT - Handbook of Neurochemistry and Molecular Neurobiology: Brain Energetics. Integration of Molecular and Cellular Processes. In , edited by Abel Lajtha, Gary E Gibson, and Gerald A Dienel, 41–62.

Dringen, R., Kranich O., and Hamprecht B. (1997) The γ-Glutamyl Transpeptidase Inhibitor Activicin Preserves Glutathione Released by Astroglial Cells in Culture. *Neurochem Res* 22 (6): 727–33.

Dringen, R. (2000) Metabolism and Functions of Glutathion in Brain. *Progress in Neurobiology* 62: 33–57.

Dringen, R., Brandmann M., Hohnholt M. C., and Blumrich E. M. (2015) Glutathione-Dependent Detoxification Processes in Astrocytes. *Neurochemical Research* 40 (12): 2570–82.

Dringen, R., Gutterer J. M., Gros C., and Hirrlinger J. (2001) Aminopeptidase N Mediates the Utilization of the GSH Precursor CysGly by Cultured Neurons. *Journal of Neuroscience Research* 66 (5):1003–8.

Dringen, R., and Hamprecht B. (1998) Glutathione Restoration as Indicator for Cellular Metabolism of Astroglial Cells. *Developmental Neuroscience*, 20:401–7.

Dringen, R., Kranich O., and Hamprecht B. (1997) The γ-Glutamyl Transpeptidase Inhibitor Acivicin Preserves Glutathione Released by Astroglial Cells in Culture. *Neurochemical Research* 22 (6): 727–33.

Dringen, R., Kussmaul L., Gutterer J. M., Hirrlinger J., and Hamprecht B. (1999) The Glutathione System of Peroxide Detoxification Is Less Efficient in Neurons than in Astroglial Cells. *Journal of Neurochemistry* 72 (6): 2523–30.

Dringen, R., Pawlowski P. G., and Hirrlinger J. (2005) Peroxide Detoxification by Brain Cells. *Journal of Neuroscience Research*, 79:157–65.

Dringen, R., Pfeiffer B., and Hamprecht B. (1999) Synthesis of the Antioxidant Glutathione in Neurons: Supply by Astrocytes of CysGly as Precursor for Neuronal Glutathione. *The Journal of Neuroscience* 19 (2): 562–69.

Elmore S. (2007) Apoptosis: A Review of Programmed Cell Death. *Toxicologic Pathology* 35 (4): 495–516.

Esteras, N., Dinkova-Kostova A. T., and Abramov A. Y. (2016) Nrf2 Activation in the Treatment of Neurodegenerative Diseases: A Focus on Its Role in Mitochondrial Bioenergetics and Function. *Biological Chemistry* 397 (5): 383–400.

Federico, A., Cardaioli E., Da Pozzo P, Formichi P., Gallus G. N., and Radi

E. (2012) Mitochondria, Oxidative Stress and Neurodegeneration. *Journal of the Neurological Sciences* 322 (1–2):254–62.

Fernandez-Fernandez, S., Almeida A., and Bolaños J. P. (2012) Antioxidant and Bioenergetic Coupling between Neurons and Astrocytes. *Biochemical Journal* 443 (1): 3–11.

Finkel, T. (2000) Redox-Dependent Signal Transduction. *FEBS Letters* 30;476(1-2):52-4.

Finkel, T. (2012) From Sulfenylation to Sulfhydration: What a Thiolate Needs to Tolerate. *Science Signaling* 5 (215): pe10.

Flohé, L., Toppo S., Cozza G., and Ursini F. (2011) A Comparison of Thiol Peroxidase Mechanisms. *Antioxidants & Redox Signaling* 15 (3): 763–80.

Franklin, C.C., Krejsa C. M., Pierce R. H., White C. C., Fausto N., Kavanagh T. J., Chernoff J., Clark E. A., and Krebs E. G. (2002) Caspase-3-Dependent Cleavage of the Glutamate-L-Cysteine Ligase Catalytic Subunit during Apoptotic Cell Death. *The American Journal of Pathology* 160 (5):1887–94.

García-Nogales, P., Almeida A., Fernández E., Medina J. M., and Bolaños J. P. (2003) Induction of Glucose-6-Phosphate Dehydrogenase by Lipopolysaccharide Contributes to Preventing Nitric Oxide-Mediated Glutathione Depletion in Cultured Rat Astrocytes. *Journal of Neurochemistry* 72 (4):1750–58.

Garcia-Ruiz, C., and Fernández-Checa J. C. (2007) Redox Regulation of Hepatocyte Apoptosis. *Journal of Gastroenterology and Hepatology* 22 (s1): S38–42.

Garrido, M., Tereshchenko Y., Zhevtsova Z., Taschenberger G., Bähr M., and Kügler S. (2011) Glutathione Depletion and Overproduction Both Initiate Degeneration of Nigral Dopaminergic Neurons. *Acta Neuropathologica* 121 (4): 475–85.

Giorgio, M., Trinei, M., Migliaccio, E., and Pelicci, P.G. (2007) Hydrogen Peroxide: A Metabolic by-Product or a Common Mediator of Ageing Signals? *Nature Reviews Molecular Cell Biology* 8 (9): 722–28.

Gipp, J. J., Chang C., and Mulcahy R.T. (1992) Cloning and Nucleotide Sequence of a Full-Length cDNA for Human Liver Gamma-Glutamylcysteine Synthetase. *Biochemical and Biophysical Research Communications* 185 (1): 29–35.

Grant, C. M., MacIver F. H., and Dawes I. W. (1997) Glutathione Synthetase Is Dispensable for Growth under Both Normal and Oxidative Stress Conditions in the Yeast Saccharomyces Cerevisiae due to an Accumulation of the Dipeptide Gamma-Glutamylcysteine. *Molecular Biology of the Cell* 8 (9): 1699–1707.

Green, D. R, Galluzzi L., and Kroemer G. (2011) Mitochondria and the Autophagy-Inflammation-Cell Death Axis in Organismal Aging. *Science* 333 (6046): 1109–12.

Griffith, O. W. (1999) Biologic and Pharmacologic Regulation of Mammalian Glutathione Synthesis. *Free Radical Biology and Medicine*, 27:922–35.

Habas, A., Hahn J., Wang X., and Margeta M. (2013) Neuronal Activity Regulates Astrocytic Nrf2 Signaling. *Proceedings of the National Academy of Sciences* 110 (45): 18291–96.

Hak, K. K., Yong S. L., Sivaprasad U., Malhotra A., and Dutta A. (2006) Muscle-Specific microRNA miR-206 Promotes Muscle Differentiation. *Journal of Cell Biology* 174 (5): 677–87.

Halliwell, B. (2013) The Antioxidant Paradox: Less Paradoxical Now? *British Journal of Clinical Pharmacology* 75 (3): 637–44.

Han, D., Canali R., Rettori D., and Kaplowitz N. (2003) Effect of Glutathione Depletion on Sites and Topology of Superoxide and Hydrogen Peroxide Production in Mitochondria. *Molecular Pharmacology* 64 (5): 1136 LP-1144.

Harman, D. (1956) Aging: A Theory Based on Free Radical and Radiation Chemistry. *Journal of Gerontology* 11 (3): 298–300.

Haskew-Layton, R. E., Payappilly J. B., Smirnova N. A., Ma T. C., Chan K. K., Murphy T. H., Guo H., Langley B., Sultana R., Butterfield D. A., Santagata S., Alldred M. J., Gazaryan I. G., Bell G. W., Ginsberg S. D., and Ratan R. R. (2010) Controlled Enzymatic Production of Astrocytic Hydrogen Peroxide Protects Neurons from Oxidative Stress via an Nrf2-Independent Pathway. *Proceedings of the National Academy of Sciences of the United States of America* 107 (40): 17385–90.

Hast, B. E., Goldfarb D., Mulvaney K. M., Hast M. A., Siesser P. F., Yan F., Hayes D. N., and Major M. B. (2013) Proteomic Analysis of Ubiquitin Ligase KEAP1 Reveals Associated Proteins That Inhibit NRF2 Ubiquitination. *Cancer Research* 73 (7): 2199 LP-2210.

Hayes, J. D., and Dinkova-Kostova A. T. (2014) The Nrf2 Regulatory Network Provides an Interface between Redox and Intermediary Metabolism. *Trends in Biochemical Sciences* 39 (4):199–218.

Hayes, J. D., Mcmahon M., Chowdhry S., and Dinkova-Kostova A. T. (2010) Cancer Chemoprevention Mechanisms Mediated Through the Keap1-Nrf2 Pathway. *Antioxidants & Redox Signaling* 13 (11): 1713–48.

Heales, S. J., Bolaños J. P., Land J. M., and Clark J. B. (1994) Trolox Protects

Mitochondrial Complex IV from Nitric Oxide-Mediated Damage in Astrocytes. *Brain Research* 668 (1–2): 243–45.

Hekimi, S., Lapointe J., and Wen Y. (2011) Taking a "Good" Look at Free Radicals in the Aging Process." *Trends in Cell Biology* 21 (10): 569–76.

Herrero-Mendez, A., Almeida A., Fernández E., Maestre C., Moncada S., and Bolaños J. P. (2009) The Bioenergetic and Antioxidant Status of Neurons Is Controlled by Continuous Degradation of a Key Glycolytic Enzyme by APC/C-Cdh1. *Nature Cell Biology* 11 (6): 747–52.

Heyland, D., Muscedere J., Wischmeyer P. E., Cook D., Jones G., Albert M., Elke G., Berger M. M., and Day A. G. (2013) A Randomized Trial of Glutamine and Antioxidants in Critically Ill Patients. *New England Journal of Medicine* 368 (16): 1489–97.

Hirrlinger, J., Schulz J. B., and Dringen R. (2002) Glutathione Release from Cultured Brain Cells: Multidrug Resistance Protein 1 Mediates the Release of GSH from Rat Astroglial Cells. *Journal of Neuroscience Research* 69 (3): 318–26.

Holmgren, A. (1981) Regulation of Ribonucleotide Reductase. *Current Topics in Cellular Regulation* 47–76.

Holmström, K. M., and Finkel T. (2014) Cellular Mechanisms and Physiological Consequences of Redox-Dependent Signalling. *Nature Reviews. Molecular Cell Biology* 15 (6) 411–21.

Hu, R., Saw C. L., Yu R., and Tony Kong A. (2010) Regulation of NF-E2-Related Factor 2 Signaling for Cancer Chemoprevention: Antioxidant Coupled with Antiinflammatory. *Antioxidants & Redox Signaling* 13 (11):1679–98.

Huang, C. S., Anderson M. E., and Meister A. (1993) Amino Acid Sequence and Function of the Light Subunit of Rat Kidney Gamma-Glutamylcysteine Synthetase. *The Journal of Biological Chemistry* 268 (27): 20578–83.

Huang, C. S., Chang L. S., Anderson M. E., and Meister A. (1993) Catalytic and Regulatory Properties of the Heavy Subunit of Rat Kidney Gamma-Glutamylcysteine Synthetase. *Journal of Biological Chemistry* 268 (26): 19675–80.

Huang, Z., Pinto J. T., Deng H, and Richie J. P. (2008) Inhibition of Caspase-3 Activity and Activation by Protein Glutathionylation. *Biochemical Pharmacology* 75 (11): 2234–44.

Hurd, T. R., Prime T. A., Harbour M. E., Lilley K. S., and Murphy M. P. (2007) Detection of Reactive Oxygen Species-Sensitive Thiol Proteins by Redox Difference Gel Electrophoresis: Implications for Mitochondrial Redox Signaling.

The Journal of Biological Chemistry 282 (30):22040–51.

Itoh, K., Wakabayashi N., Katoh Y., Ishii T., Igarashi K., Engel J. D., and Yamamoto M. (1999) Keap1 Represses Nuclear Activation of Antioxidant Responsive Elements by Nrf2 through Binding to the Amino-Terminal Neh2 Domain. *Genes and Development* 13 (1): 76–86.

Jaiswal, A. K. (2004) Nrf2 Signaling in Coordinated Activation of Antioxidant Gene Expression. *Free Radical Biology and Medicine* 15;36(10):1199-207.

Jakel, R. J., Townsend J. A., Kraft A. D., and Johnson J. A. (2007) Nrf2-Mediated Protection against 6-Hydroxydopamine. *Brain Research* 1144 (1): 192–201.

Jimenez-Blasco, D., Santofimia-Castaño P., Gonzalez A., Almeida A., and Bolaños J. P. (2015) Astrocyte NMDA Receptors' Activity Sustains Neuronal Survival through a Cdk5–Nrf2 Pathway. *Cell Death and Differentiation*, 1–13.

Kaelin, W. G., and Ratcliffe P. J. (2008) Oxygen Sensing by Metazoans: The Central Role of the HIF Hydroxylase Pathway. *Molecular Cell* 30(4):393-402.

Kamat, C. D., Gadal S., Mhatre M., Williamson K. S., Pye Q. N., and Hensley K. (2008) Antioxidants in Central Nervous System Diseases: Preclinical Promise and Translational Challenges. *Journal of Alzheimer's Disease* 15 (3): 473–93.

Kang, M. I., Kobayashi A., Wakabayashi N., Kim S. G., and Yamamoto M. (2004) Scaffolding of Keap1 to the Actin Cytoskeleton Controls the Function of Nrf2 as Key Regulator of Cytoprotective Phase 2 Genes. *Proceedings of the National Academy of Sciences of the United States of America* 101 (7): 2046–51.

Katoh, Y., Iida K., Kang M. I., Kobayashi A., Mizukami M., Tong K. I, McMahon M., Hayes J. D., Itoh K., and Yamamoto M. (2005) Evolutionary Conserved N-Terminal Domain of Nrf2 Is Essential for the Keap1-Mediated Degradation of the Protein by Proteasome. *Archives of Biochemistry and Biophysics* 433 (2): 342–50.

Kensler, T. W., and Wakabayashi N. (2010) Nrf2: Friend or Foe for Chemoprevention? *Carcinogenesis* 31 (1): 90–99.

Kletzien, R. F., Harris P. K., and Foellmi L. A. (1994) Glucose-6-Phosphate Dehydrogenase: A 'housekeeping' enzyme Subject to Tissue-Specific Regulation by Hormones, Nutrients, and Oxidant Stress. *The FASEB Journal* 8 (2): 174–81.

Kobayashi, A., Ito E., Toki T., Kogame K., Takahashi S., Igarashi K., Hayashi N., and Yamamoto M. (1999) Molecular Cloning and Functional Characterization of a New Cap'n' Collar Family Transcription Factor Nrf3. *The Journal of Biological Chemistry* 274 (10): 6443–52.

Kobayashi, A., Kang M. I., Okawa H., Ohtsuji M., Zenke Y., Chiba T., Igarashi K., and Yamamoto M. (2004) Oxidative Stress Sensor Keap1 Functions as an Adaptor for Cul3-Based E3 Ligase to Regulate Proteasomal Degradation of Nrf2. *Molecular and Cellular Biology* 24 (16): 7130–39.

Kovac, S., Angelova P. R., Holmström, K. M., Zhang Y., Dinkova-Kostova A. T., and Abramov A. (2015) Nrf2 Regulates ROS Production by Mitochondria and NADPH Oxidase. *Biochimica et Biophysica Acta* 1850 (4): 794–801.

Kranich, O., Dringen R., Sandberg M., and Hamprecht B. (1998) Utilization of Cysteine and Cysteine Precursors for the Synthesis of Glutathione in Astroglial Cultures: Preference for Cystine. *Glia* 22 (1): 11–18.

Kranich, O., Hamprecht B., and Dringen R. (1996) Different Preferences in the Utilization of Amino Acids for Glutathione Synthesis in Cultured Neurons and Astroglial Cells Derived from Rat Brain. *Neuroscience Letters* 219 (3): 211–14.

Kumar, C., Igbaria A., D'Autreaux B., Planson A. G., Junot C., Godat E., Bachhawat A. K., Delaunay-Moisan A., and Toledano M. B. (2011) Glutathione Revisited: A Vital Function in Iron Metabolism and Ancillary Role in Thiol-Redox Control. *The EMBO Journal* 30 (10): 2044–56.

Kwak, M. K., Itoh K., Yamamoto M., and Kensler T. W. (2002) Enhanced Expression of the Transcription Factor Nrf2 by Cancer Chemopreventive Agents: Role of Antioxidant Response Element-like Sequences in the nrf2 Promoter. *Molecular and Cellular Biology* 22 (9):2883–92.

Lambeth, J, D., and Neish A. S. (2014) Nox Enzymes and New Thinking on Reactive Oxygen : A Double-Edged Sword Revisited. *Annu Rev Pathol* 9:119-45.

Lapointe, J., Stepanyan Z., Bigras E., and Hekimi S. (2009) Reversal of the Mitochondrial Phenotype and Slow Development of Oxidative Biomarkers of Aging in Long-Lived Mclk1+/- Mice. *Journal of Biological Chemistry* 284 (30): 20364–74.

Lash, L. H. (2006) Mitochondrial Glutathione Transport: Physiological, Pathological and Toxicological Implications. *Chemico-Biological Interactions* 163 (1–2): 54–67.

Lau, A., Wang X. J., Zhao F., Villeneuve N. F., Wu T., Jiang T., Sun Z., White E., and Zhang D. D. (2010) A Noncanonical Mechanism of Nrf2 Activation by Autophagy Deficiency: Direct Interaction between Keap1 and p62. *Molecular and Cellular Biology* 30 (13): 3275–85.

Lee, J. M., Chan K., Kan Y. W., and Johnson J. A. (2004) Targeted Disruption of Nrf2 Causes Regenerative Immune-Mediated Hemolytic Anemia. *Proceedings of the National Academy of Sciences of the United States of America* 101 (26): 9751–56.

Lee, O. H., Jain A. K., Papusha V., and Jaiswal A. K. (2007) An Auto-Regulatory Loop between Stress Sensors INrf2 and Nrf2 Controls Their Cellular Abundance. *Journal of Biological Chemistry* 282 (50): 36412–20.

Li, Yunbo, Hong Zhu, Kuppunsamy P., Zweier J. L., and Trush M. A. (2016) Mitochondrial Electron Transport Chain-Derived Superoxide Exits Macrophages: Implications for Mononuclear Cell-Mediated Pathophysiological Processes. *Reactive Oxygen Species* 1 (1): 81–97.

Liu, X., Jiang N., Hughes B., Bigras E., Shoubridge E., and Hekimi S. (2005) Evolutionary Conservation of the Clk-1-Dependent Mechanism of Longevity: Loss of mclk1 Increases Cellular Fitness and Lifespan in Mice. *Genes and Development* 19 (20): 2424–34.

Lopez-Fabuel, I., Le Douce J., Logan A., James A. M., Bonvento G., Murphy M. P., Almeida A., and Bolaños J. P. (2016) Complex I Assembly into Supercomplexes Determines Differential Mitochondrial ROS Production in Neurons and Astrocytes. *Proceedings of the National Academy of Sciences of the United States of America* 15;113(46):13063-13068

Loreck, D. J., Galarraga J., Van der Feen J., Phang J. M., Smith B. H., and Cummins C. J. 1987. Regulation of the Pentose Phosphate Pathway in Human Astrocytes and Gliomas. *Metabolic Brain Disease* 2 (1): 31–46.

Lu, S. C. (2009) Regulation of Glutathione Synthesis. *Molecular Aspects of Medicine* 30 (1–2): 42–59.

Lu, S. C. (2013) Glutathione Synthesis. *Biochimica et Biophysica Acta - General Subjects* 1830 (5): 3143–53.

Mächler, P., Wyss M. T., Elsayed M., Stobart J., Gutierrez R., Von Faber-Castell A., Kaelin V., Zuend M., San Martín A., Romero-Gómez I., Baeza-Lehnert F., Lengacher S., Schneider B. L., Aebischer P., Magistretti P. J., Barros L. F., and Weber B. (2016) In Vivo Evidence for a Lactate Gradient from Astrocytes to Neurons. *Cell Metabolism* 23 (1): 94–102.

Malhotra, D., Portales-Casamar E., Singh A., Srivastava S., Arenillas D., Happel C., Shyr C., Shyr C., Wakabayashi N., Kensler T. W., Wasserman W. W., and Biswal S. (2010) Global Mapping of Binding Sites for Nrf2 Identifies Novel Targets in Cell Survival Response through ChIP-Seq Profiling and Network Analysis. *Nucleic Acids Research* 38 (17): 5718–34.

Maranzana, E., Barbero G., Falasca A. I., Lenaz G., and Genova M. L. (2013) Mitochondrial Respiratory Supercomplex Association Limits Production of Reactive Oxygen Species from Complex I. *Antioxidants & Redox Signaling* 19 (13): 1469–80.

Marí, M., Morales A., Colell A., García-Ruiz C., and Fernández-Checa J. C. (2009) Mitochondrial Glutathione, a Key Survival Antioxidant. *Antioxidants & Redox Signaling* 11 (11): 2685–2700.

Matsushima, S., Ide T., Yamato M., Matsusaka H., Hattori F., Ikeuchi M., Kubota T., Sunagawa K., Hasegawa Y., Kurihara T., Oikawa S., Kinugawa S., and Tsutsui H. (2006) Overexpression of Mitochondrial Peroxiredoxin-3 Prevents Left Ventricular Remodeling and Failure after Myocardial Infarction in Mice. *Circulation* 113 (14): 1779–86.

McMahon, M., Thomas N., Itoh K., Yamamoto M., and Hayes J. D. (2004) Redox-Regulated Turnover of Nrf2 Is Determined by at Least Two Separate Protein Domains, the Redox-Sensitive Neh2 Degron and the Redox-Insensitive Neh6 Degron. *The Journal of Biological Chemistry* 279 (30): 31556–67.

McMahon, M., Thomas N., Itoh K., Yamamoto M., and Hayes J. D. (2006) Dimerization of Substrate Adaptors Can Facilitate Cullin-Mediated Ubiquitylation of Proteins by a "tethering" Mechanism: A Two-Site Interaction Model for the Nrf2-Keap1 Complex. *The Journal of Biological Chemistry* 281 (34): 24756–68.

Meister, A. (1988) Glutathione Metabolism and Its Selective Modification. *Journal of Biological Chemistry* 263(33):17205-8.

Meister, A, and Anderson M. E. (1983) "Glutathione." *Annual Review of Biochemistry* 52 (1): 711–60.

Meredith, M. J., and Reed D. J. (1982) Status of the Mitochondrial Pool of Glutathione in the Isolated Hepatocyte. *Journal of Biological Chemistry* 257 (7): 3747–53.

Mesquita, A., Weinberger M., Silva A., Sampaio-Marques B., Almeida B., Leão C., Costa V., Rodrigues F., Burhans W. C., and Ludovico P. (2010) Caloric Restriction or Catalase Inactivation Extends Yeast Chronological Lifespan by Inducing H_2O_2 and Superoxide Dismutase Activity." *Proceedings of the National Academy of Sciences of the United States of America* 107 (34): 15123–28.

Minich, T., Riemer J., Schulz J. B., Wielinga P., Wijnholds J., and Dringen R. (2006) The Multidrug Resistance Protein1 (Mrp1), but Not Mrp5, Mediates Export of Glutathione and Glutathione Disulfide from Brain Astrocytes. *Journal of Neurochemistry* 97 (2): 373–84.

Mishin, V., Gray J. P., Heck D. E., Laskin D. L., and Laskin J. D. (2010) Application of the Amplex Red/horseradish Peroxidase Assay to Measure Hydrogen Peroxide Generation by Recombinant Microsomal Enzymes. *Free Radical Biology and Medicine* 48 (11): 1485–91.

Mockett, R. J., Sohal B. H., and Sohal R. S. (2010) Expression of Multiple

Copies of Mitochondrially Targeted Catalase or Genomic Mn Superoxide Dismutase Transgenes Does Not Extend the Life Span of Drosophila Melanogaster. *Free Radical Biology and Medicine* 49 (12): 2028–31.

Mohanty, J.G., Jaffe J. S., Schulman E. S., and Raible D. G. (1997) A Highly Sensitive Fluorescent Micro-Assay of H_2O_2 Release from Activated Human Leukocytes Using a Dihydroxyphenoxazine Derivative. *Journal of Immunological Methods* 202 (2): 133–41.

Moi, P., Chant K., Asunis I., Cao A., Kant Y. W., and Kan Y. W. (1994) Isolation of NF-E2-Related Factor 2 (Nrf2), a NF-E2-like Basic Leucine Zipper Transcriptional Activator That Binds to the Tandem NF-E2/AP1 Repeat of the F-Globin Locus Control Region. *Genetics* 91 (October): 9926–30.

Motohashi, H., Katsuoka F., Engel J. D., and Yamamoto M. (2004) Small Maf Proteins Serve as Transcriptional Cofactors for Keratinocyte Differentiation in the Keap1–Nrf2 Regulatory Pathway. *Proceedings of the National Academy of Sciences of the United States of America* 101 (17): 6379–84.

Murphy, M. P. (2009) How Mitochondria Produce Reactive Oxygen Species. *Biochemical Journal* 417 (1): 1–13.

Namani, A., Li Y., Wang X. J., and Tang X. (2014) Modulation of NRF2 Signaling Pathway by Nuclear Receptors: Implications for Cancer. *Biochimica et Biophysica Acta (BBA) - Molecular Cell Research* 1843 (9): 1875–85.

Nayernia, Z., and Jaquet V. (2014) New Insights on NOX Enzymes in the Central Nervous System. *Antiox Redox Signal* 20 (17): 2815–38.

Njålsson, R. (2005) Glutathione Synthetase Deficiency. *Cellular and Molecular Life Sciences* 62 (17): 1938–45.

Ohta, T., Iijima K., Miyamoto M., Nakahara I., Tanaka H., Ohtsuji M., Suzuki T., Kobayashi A., Yokota J., Sakiyama T., Shibata T., Yamamoto M., and Hirohashi S. (2008) Loss of Keap1 Function Activates Nrf2 and Provides Advantages for Lung Cancer Cell Growth. *Cancer Research* 68 (5): 1303–9.

Oppenheimer, L., Wellner V. P., Griffith O. W., and Meister A. (1979) Glutathione Synthetase. Purification from Rat Kidney and Mapping of the Substrate Binding Sites. *Journal of Biological Chemistry* 254 (12): 5184–90.

Orr, W. C., and Sohal R. S. (1994) Extension of Life-Span by Overexpression of Superoxide Dismutase and Catalase in Drosophila Melanogaster. *Science* 263 (5150): 1128–30.

Owusu-Ansah, E., and Banerjee U. (2009) Reactive Oxygen Species Prime Drosophila Haematopoietic Progenitors for Differentiation. *Nature* 461 (7263): 537–41.

Pan, Y., Schroeder E. A., Ocampo A., Barrientos, A. and Shadel G. S. (2011) Regulation of Yeast Chronological Life Span by TORC1 via Adaptive Mitochondrial ROS Signaling. *Cell Metabolism* 13 (6): 668–78.

Park, J., Rho H. K., Kim K. H., Choe S. S., Lee Y. S., and Kim J. B. (2005) Overexpression of Glucose-6-Phosphate Dehydrogenase Is Associated with Lipid Dysregulation and Insulin Resistance in Obesity. 25 (12): 5146–57.

Patenaude, A., Murthy M. R. V., and Mirault M. E. 2005. Emerging Roles of Thioredoxin Cycle Enzymes in the Central Nervous System. *Cellular and Molecular Life Sciences*.

Patra, K. C., and Hay N. 2014. The Pentose Phosphate Pathway and Cancer. *Trends in Biochemical Sciences* 39 (8):347–54.

Pellerin, L., and Magistretti P. J. (1994) Glutamate Uptake into Astrocytes Stimulates Aerobic Glycolysis: A Mechanism Coupling Neuronal Activity to Glucose Utilization. *Proceedings of the National Academy of Sciences of the United States of America* 91 (22): 10625–29.

Pellerin, L., and Magistretti P. J. (2012) Sweet Sixteen for ANLS. *Journal of Cerebral Blood Flow and Metabolism* 32 (7): 1152–66.

Pérez, V. I., Van Remmen H., Bokov A., Epstein C. J., Vijg J., and Richardson A. (2009) The Overexpression of Major Antioxidant Enzymes Does Not Extend the Lifespan of Mice. *Aging Cell* 8 (1): 73–75.

Perkins, A., Nelson K. J., Parsonage D., Poole L. B., and Karplus P. A. (2015) Peroxiredoxins: Guardians against Oxidative Stress and Modulators of Peroxide Signaling. *Trends in Biochemical Sciences* 40 (8): 435–45.

Petry, A., Djordjevic T., Weitnauer M., Kietzmann T., Hess J., and Görlach A. (2006) NOX2 and NOX4 Mediate Proliferative Response in Endothelial Cells. *Antioxidants & Redox Signaling* 8 (9–10): 1473–84.

Pi, J., Leung L., Xue P., Wang W., Hou Y., Liu D., Yehuda-Shnaidman E., Lee C., Lau J., Kurtz T. W., and Chan J. Y. (2010) Deficiency in the Nuclear Factor E2-Related Factor-2 Transcription Factor Results in Impaired Adipogenesis and Protects against Diet-Induced Obesity. *The Journal of Biological Chemistry* 285 (12): 9292–9300.

Poyton, R. O., Ball K. A., and Castello P. R. (2009) Mitochondrial Generation of Free Radicals and Hypoxic Signaling. *Trends in Endocrinology and Metabolism* 20(7):332-40.

Puente, B. N., Kimura W., Muralidhar S. A., Moon J., Amatruda J. F., Phelps K. L., Grinsfelder D., Rothermel B. A., Chen R., Garcia J. A., Santos

C. X., Thet S., Mori E., Kinter M. T., Rindler P. M., Zacchigna S., Mukherjee S., Chen D. J., Mahmoud A. I., Giacca M., Rabinovitch P. S., Aroumougame A., Shah A. M., Szweda L. I., and Sadeka H. A. (2014) The Oxygen-Rich Postnatal Environment Induces Cardiomyocyte Cell-Cycle Arrest through DNA Damage Response. *Cell* 157 (3).: 565–79.

Quintana-Cabrera, R., and Bolaños J. P. (2013) Glutathione and γ-Glutamylcysteine in Hydrogen Peroxide Detoxification." *Methods in Enzymology* 527 (January): 129–44.

Quintana-Cabrera, R., Fernandez-Fernandez S., Bobo-Jimenez V., Escobar J., Sastre J., Almeida A., and Bolaños J. P. (2012) γ-Glutamylcysteine Detoxifies Reactive Oxygen Species by Acting as Glutathione Peroxidase-1 Cofactor. *Nature Communications* 3 (January): 718.

Rada, P., Rojo A. I., Chowdhry S., McMahon M., Hayes J. D., and Cuadrado A. (2011) SCF/β-TrCP Promotes Glycogen Synthase Kinase 3-Dependent Degradation of the Nrf2 Transcription Factor in a Keap1-Independent Manner. *Molecular and Cellular Biology* 31 (6): 1121–33.

Rada, P., Rojo A. I., Evrard-Todeschi N., Innamorato N. G., Cotte A., Jaworski T., Tobón-Velasco J. C., Devijiver H., Garcí-Mayoral M. F., Van Leuven F., Hayes J. D., Bertho G., and Cuadrado A. (2012) Structural and Functional Characterization of Nrf2 Degradation by the Glycogen Synthase Kinase 3/β-TrCP Axis." *Molecular and Cellular Biology* 32 (17): 3486–99.

Rice, M. E., and Russo-Menna I. (1997) Differential Compartmentalization of Brain Ascorbate and Glutathione between Neurons and Glia. *Neuroscience* 82 (4): 1213–23.

Richman, P. G., and Meister A. (1975) Regulation of gamma Glutamyl Cysteine Synthetase by Nonallosteric Feedback Inhibition by Glutathione. *Journal of Biological Chemistry* 250 (4): 1422–26.

Riganti, C., Gazzano E., Polimeni M., Aldieri E., and Ghigo D. (2012) The Pentose Phosphate Pathway: An Antioxidant Defense and a Crossroad in Tumor Cell Fate. *Free Radical Biology and Medicine* 53 (3): 421–36.

Rodriguez-Rodriguez, P., Fernandez E., and Bolaños J. P. (2013) Underestimation of the Pentose-Phosphate Pathway in Intact Primary Neurons as Revealed by Metabolic Flux Analysis. *Journal of Cerebral Blood Flow and Metabolism* 33 (12): 1843–45.

Sagara, J., Miura K., and Bannai S. (1993) Maintenance of Neuronal Glutathione by Glial Cells. *Journal of Neurochemistry* 61 (5): 1672–76.

Schaar, C. E., Dues D. J., Spielbauer K. K., Machiela E., Cooper J. F., Senchuk M., Hekimi S., and Van Raamsdonk J. M. (2015) Mitochondrial and

Cytoplasmic ROS Have Opposing Effects on Lifespan. *PLoS Genetics* 11 (2):e1004972.

Schieber, M., and Chandel N. S. (2014) ROS Function in Redox Signaling and Oxidative Stress. *Current Biology* 24 (10): R453–62.

Schriner, S. E., Linford N. J., Martin G. M., Treuting P., Ogburn C. E., M. E., Coskun P. E., Ladiges W., Wolf N., Van Remmen H., Wallace D. C., and Rabonovitch P. S. (2005) Extension of Murine Life Span by Overexpression of Catalase Targeted to Mitochondria. *Science* 308 (5730): 1909–11.

Seelig, G. F., Simondsen R. P., and Meister A. (1984) Reversible Dissociation of γ-Glutamylcysteine Synthetase into Two Subunits." *Journal of Biological Chemistry* 259 (15): 9345–47.

Shibata, T., Kokubu A., Gotoh M., Ojima H., Ohta T., Yamamoto M., and Hirohashi S. (2017) Genetic Alteration of Keap1 Confers Constitutive Nrf2 Activation and Resistance to Chemotherapy in Gallbladder Cancer. *Gastroenterology* 135 (4): 1358–1368.e4.

Shih, A. Y., Johnson D. A., Wong G., Kraft A. D., Jiang L., Erb H., Johnson J. A., and Murphy T. H. (2003) Coordinate Regulation of Glutathione Biosynthesis and Release by Nrf2-Expressing Glia Potently Protects Neurons from Oxidative Stress. *The Journal of Neuroscience* 23 (8): 3394–3406.

Shimizu, N., Matsunami T., and Onishi S. (1960) Histochemical Demonstration of Ascorbic Acid in the Locus Coeruleus of the Mammalian Brain. *Nature* 186 (4723): 479–80.

Singh, A., Boldin-Adamsky S., Thimmulappa R. K., Rath S. K., Ashush H., Coulter J., Blackford A., Goodman S. N., Bunz F., Watson W. H., Gabrielson E., Feinstein E., and Biswal S. (2008) RNAi-Mediated Silencing of Nuclear Factor Erythroid-2-Related Factor 2 Gene Expression in Non-Small Cell Lung Cancer Inhibits Tumor Growth and Increases Efficacy of Chemotherapy. *Cancer Research* 68 (19): 7975–84.

Singh, A., Happel C., Manna S. K., Acquaah-Mensah G., Carrerero J., Kumar S., Nasipuri P., Krausz K. W., Wakabayashi N., Dewi R., Boros L. G., Gonzalez F. J., Gabrielson E., Wong K. K., girnun G., and Biswal S. (2013) Transcription Factor NRF2 Regulates miR-1 and miR-206 to Drive Tumorigenesis. *Journal of Clinical Investigation* 123 (7): 2921–34.

Snow, B. J., Rolfe F. L., Lockhart M. M., Frampton C. M., O'Sullivan J. D., Fung V., Smith R. A., Murphy M. P., Taylor K. M., and Group Protect Study (2010). A Double-Blind, Placebo-Controlled Study to Assess the Mitochondria-Targeted Antioxidant MitoQ as a Disease-Modifying Therapy in Parkinson's Disease. *Mov Disord* 25 (11): 1670–74.

Spence, A. M., Graham M. M., Muzi M., Freeman S. D., Link J. M., J R Grierson J. R., O'Sullivan F., Stein D., Abbott G. L., and Krohn K. A. (1997) Feasibility of Imaging Pentose Cycle Glucose Metabolism in Gliomas with PET: Studies in Rat Brain Tumor Models. *Journal of Nuclear Medicine* 38 (4): 617–24.

Stincone, A., Prigione A., Cramer T., Wamelink M. M., Campbell K., Cheung E., Olin-Sandoval V., Gruning N. M., Kruger A., Tauqeer Alam M., Keller M., Breitenbach M., Brindle K. M., Rabinovitz J. D., and Ralser M. (2015) The Return of Metabolism: Biochemistry and Physiology of the Pentose Phosphate Pathway. *Biological Reviews* 90 (3): 927–63.

Sun, W. M., Huang Z. Z., and Lu S. C. (1996) Regulation of Gamma-Glutamylcysteine Synthetase by Protein Phosphorylation. *The Biochemical Journal* 320 (1): 321–28.

Tabernero, A, Bolaños J. P., and Medina J. M. (1993) Lipogenesis from Lactate in Rat Neurons and Astrocytes in Primary Culture. *The Biochemical Journal* 294 Pt 3 (1 993): 635–38.

Taguchi, K., Motohashi H., and Yamamoto M. (2011) Molecular Mechanisms of the Keap1-Nrf2 Pathway in Stress Response and Cancer Evolution. *Genes to Cells* 16 (2): 123–40.

Temple, M. D., Perrone G. G., and Dawes I. A. (2005) Complex Cellular Responses to Reactive Oxygen Species. *Trends in Cell Biology* 15(6):319-26.

Tietze, F. (1969) Enzymic Method for Quantitative Determination of Nanogram Amounts of Total and Oxidized Glutathione: Applications to Mammalian Blood and Other Tissues. *Analytical Biochemistry* 27 (3): 502–22.

Tong, K. I., Katoh Y., Kusunoki H., Itoh K., Tanaka T., and Yamamoto M. (2006) Keap1 Recruits Neh2 through Binding to ETGE and DLG Motifs: Characterization of the Two-Site Molecular Recognition Model. *Molecular and Cellular Biology* 26 (8): 2887–2900.

Vargas, M. R., Johnson D. A., Sirkis D. W., Messing A., and. Johnson J. A. (2008) Nrf2 Activation in Astrocytes Protects against Neurodegeneration in Mouse Models of Familial Amyotrophic Lateral Sclerosis. *Journal of Neuroscience* 28 (50): 13574–81.

Vargas, M. R., and Johnson J. A. (2009) The Nrf2-ARE Cytoprotective Pathway in Astrocytes."*Expert Rev Mol Med* 11 (June): e17.

Venugopal, R., and Jaiswal A. K. (1998) Nrf2 and Nrf1 in Association with Jun Proteins Regulate Antioxidant Response Element-Mediated Expression and Coordinated Induction of Genes Encoding Detoxifying Enzymes. *Oncogene* 17 (24): 3145–56.

Wakabayashi, N., Itoh K., Wakabayashi J., Motohashi H., Noda S.,

Takahashi S., Imakado S., Kotsuji T., Otsuka F., Roop D. R., harada T., Engel J. D., and Yamamoto M. (2003) Keap1-Null Mutation Leads to Postnatal Lethality due to Constitutive Nrf2 Activation. *Nature Genetics* 35 (3): 238–45.

Wamelink, M. M., Struys E. A., and Jakobs C. (2008) The Biochemistry, Metabolism and Inherited Defects of the Pentose Phosphate Pathway: A Review. *Journal of Inherited Metabolic Disease* 31 (6): 703–17.

Wang, H., Liu K., Geng M., Gao P., Wu X., Hai Y., Li Y., Li Y., Luo L., Hayes J. D., Wang X. J., and Tang X. (2013) RXRα Inhibits the NRF2-ARE Signaling Pathway through a Direct Interaction with the Neh7 Domain of NRF2. *Cancer Research* 73 (10): 3097 LP-3108.

Wang, X., and Hai C. (2016) Novel Insights into Redox System and the Mechanism of Redox Regulation. *Molecular Biology Reports* 43 (7): 607–28.

Wei, Y., Gong J., Xu Z., and Duh E. J. (2016) Nrf2 Promotes Reparative Angiogenesis through Regulation of NADPH Oxidase-2 in Oxygen-Induced Retinopathy. *Free Radical Biology and Medicine* 99: 234–43.

Wilson, J. X. (1997) Antioxidant Defense of the Brain: A Role for Astrocytes. *Canadian Journal of Physiology and Pharmacology* 75 (10–11): 1149–63.

Wu, G., Fang Y. Z., Yang S., Lupton J. R., and Turner N. D. (2004) Glutathione Metabolism and Its Implications for Health. *The Journal of Nutrition* 134 (3): 489–92.

Wu, K. C., Cui J. Y., and Klaassen C. D. (2011) Beneficial Role of Nrf2 in Regulating NADPH Generation and Consumption. *Toxicological Sciences* 123 (2): 590–600.

Xiang, M. J., Namani A., Wu S. J., and Wang X. L. (2014) Nrf2: Bane or Blessing in Cancer? *Journal of Cancer Research and Clinical Oncology* 140 (8): 1251–59.

Yan, N, and Meister A. (1990) Amino Acid Sequence of Rat Kidney G-Glutamylcysteine Synthetase. *J Biol Chem* 265 (3): 1588–93.

Yang, H. C., Wu Y. H., Liu H. Y., Stern A., and Chiu D. T. Y. (2016) What Has Passed Is Prologue: New Cellular and Physiological Roles of G6PD. *Free Radical Research* 5762 (August): 1–58.

Zancai, P., Dal Col J., Piccinin S., Guidoboni M., Cariati R., Rizzo S., Boiocchi M., Maestro R., and Dolcetti R. (2005) Retinoic Acid Stabilizes p27Kip1 in EBV-Immortalized Lymphoblastoid B Cell Lines through Enhanced Proteasome-Dependent Degradation of the p45Skp2 and Cks1 Proteins. *Oncogene* 24 (15): 2483–94.

Zhang, J., Wang X., Vikash V., Ye Q., Wu D., Liu Y, and Dong W. (2016) ROS and ROS-Mediated Cellular Signaling. *Oxidative Medicine and Cellular Longevity* 2016:4350965.

Zhang, P., Singh A., Yegnasubramanian S., Esopi D., Kombairaju P., Bodas M., Wu H., Bova S. G., and Biswal S. (2010) Loss of Kelch-like ECH-Associated Protein 1 Function in Prostate Cancer Cells Causes Chemoresistance and Radioresistance and Promotes Tumor Growth. *Molecular Cancer Therapeutics* 9 (2): 336–46.

Zhou, G., Meng S., Li Y., T. Y. T., and Cooke J. P. 2016. Optimal ROS Signaling Is Critical for Nuclear Reprogramming. *Cell Reports* 15 (5).: 919–25.


ACKNOWLEDGEMENTS

Più di quattro anni sono passati da quando mi sono trasferito a Salamanca con l'obiettivo di diventare Dottorissimo (Dottore lo ero già secondo lo Stato italiano). Questo è stato possibile non solo grazie a me, ma anche grazie alle persone che ho avuto il piacere di conoscere e con cui ho avuto l'onore di collaborare.

Grazie a Juan Pedro, per darmi la possibilità di far parte del tuo gruppo di ricerca. Ogni consiglio, *bronca* e suggerimento che mi hai dato mi ha fatto essere un ricercatore migliore di quello che ero quando sono entrato per la prima volta nel tuo laboratorio.

Grazie a Emilio *Manolo*, sempre disponibile ad aiutarmi per risolvere i miei dubbi e per le chiacchierate su qualsiasi argomento durante le pause caffè.

Grazie ad Ángeles, i tuoi consigli durante questi anni sono stati fondamentali per la riuscita di questo progetto.

Grazie a Gavin, per avermi accolto nel suo laboratorio a Dublino dandomi la possibilità di lavorare per tre mesi in uno dei centri più moderni d'Europa.

Grazie a tutti i compagni di laboratorio. Carlos *el mundano* per il tanto (troppo) tempo passato a compartire cellule, animali, dubbi e incazzature durante questi anni. Dani che con il tuo umorismo e i tuoi outfits sei sempre stato capace di strapparmi un sorriso. Irene per avermi guidato all'inizio della mia avventura in questo laboratorio. Moussa per avermi fatto scoprire limiti della pazienza che non sapevo di avere. Ana *el paibon* con la tua allegria e infinita voglia di festa. Costi che hai portato un po' più di Italia nel laboratorio. Brenda per il tuo entusiasmo così contagioso. Ruben *el mitocondriologo* per i consigli che mi hai dato da quando sei tornato. Carmen, Nuria, Kiara, Lucia, Victor, Eva, Jens e Johann che nonostante il poco tempo passato nel laboratorio siete riusciti a lasciare il segno.

Il PCR Team, composto dalle Monicas (Resch e Carabias), Estefi e Lucia, senza il quale starei ancora genotipando il quarto topo, grazie per occuparsi della gestione degli animali necessari per gli esperimenti. Tutto questo sarebbe stato impossibile senza di voi.

Grazie al laboratorio di Ángeles: Maria, Vero, Cris, Irene, las Rebes, Chustin, Norah, Miguelón, Miguelín, Mary, Emi, Silvia, Marta per l'aiuto in questi anni, il

buon ambiente generato e per i momenti passati fuori dal laboratorio (che nella maggior parte dei casi erano con un cocktail in mano).

Grazie ai Pacos per l'aiuto amministrativo e le chiacchierate mattutine sul calcio, speriamo che dopo quattro anni consecutivi che perdo finali di Champions, arrivi il mio turno.

Rubén e Irene *lynx*, gli unici a parte i nostri laboratori a lavorare con mammiferi in un mondo di *levadurologos*, grazie per i momenti passati tra cultivo, bar ed escape rooms.

Grazie alla TINTIN's family: Jesús, Carmen, Yasmina, Maria, Teodora, Gerard, Lois, Aoife, Nathalie, Michel e Cécile per le trasferte a Dublino e Siena tra pubs irlandesi e feste di contrada.

Grazie a Gerard e Laura per aver reso speciale i tre mesi a Dublino, tra una (eterna) chiacchierata post pranzo e una birra al canale.

Grazie al Añover Vacioplast Salamanca, soprattutto ad Andrés, Chucky, Palotes, Daniel, Mapache, Mario, Bekele, Pablo, Miguel, Boria, Huesines, Popi, Nate, Roberto e Rodri per avermi tenuto un minimo in forma in una squadra dove ciò che più importa sono il *pusse* e il buon ambiente. Il basket è qualcosa di superfluo.

Grazie alla Gatta, che mi riempie di amore incondizionato ogni volta che rientro a casa.

Grazie alla mia famiglia, che nonostante negli ultimi quattro anni ci siamo visti meno di un mese, mi sono sempre stati vicino. È grazie a voi che sono arrivato fin qui.

Grazie a Emilie per avermi seguito in questa avventura *charra*. Grazie per esserci sempre stata ad ascoltare le mie lamentele e sfoghi, a correggere le mie bozze e a rincuorarmi nei momenti tristi. Tu meglio di tutti conosci lo sforzo e i sacrifici fatti per questa Tesi e sai che è anche tua. Adesso non sappiamo quello che ci aspetterà, ma sappiamo che lo affronteremo assieme.

Infine, grazie a me stesso, per non aver mai mollato e aver continuato nonostante le difficoltà. Una volta finito il dottorato, il futuro è ancora più incerto e parafrasando il Sommo poeta:

"(Quasi) *Nel mezzo del cammin di nostra vita,*

mi ritrovai per una selva oscura

ché la diritta via era smarrita."